

THÈSE

En vue de l'obtention du

DOCTORAT DE L'UNIVERSITÉ DE TOULOUSE

Délivré par :

Institut National Polytechnique de Toulouse (Toulouse INP)

Discipline ou spécialité :

Science et Génie des Matériaux

Présentée et soutenue par :

M. ACHRAF BELKHIRI

le mardi 10 mai 2022

Titre :

Controlling glass/matrix interfacial interactions applied to in situ anionic PA6 synthesis for composite manufacturing

---

Ecole doctorale :

Sciences de la Matière (SDM)

Unité de recherche :

Laboratoire de Génie de Productions de l'ENIT (E.N.I.T-L.G.P.)

Directeur(s) de Thèse :

MME VALÉRIE NASSIET

M. OLIVIER DE ALMEIDA

Rapporteurs :

MME ELODIE BOURGEAT-LAMI, UNIVERSITE LYON 1

MME JANNICK DUCHET-RUMEAU, INSA LYON

Membre(s) du jury :

M. MATHIAS DESTARAC, UNIVERSITE TOULOUSE 3, Président

M. FRÉDÉRIC LEONARDI, UNIVERSITE DE PAU ET DES PAYS DE L ADOUR, Membre

M. LAZHAR BENYAHIA, UNIVERSITE DU MANS, Membre

MME FRANCE CHABERT, ECOLE NATIONALE D'INGENIEUR DE TARBES, Membre

MME HÉLÈNE WELEMANE, ECOLE NATIONALE D'INGENIEUR DE TARBES, Invité(e)

MME VALÉRIE NASSIET, ECOLE NATIONALE D'INGENIEUR DE TARBES, Membre

M. NICK VIRGILIO, ECOLE POLYTECHNIQUE DE MONTREAL, Invité(e)

M. OLIVIER DE ALMEIDA, ECOLE NLE SUP DES MINES ALBI CARMAUX, Membre

ACKNOWLEDGEMENTS

This research work was carried out at the Laboratoire Génie de Production (Tarbes, France), the Institut Clément Ader (Albi, France) and Polytechnique Montréal (Canada). It was funded by the Région Occitanie and the Université Fédérale de Toulouse.

First, I would like to thank all the members of the jury for the constructive discussions during the defense. I would like to express my sincere gratitude to Pr. Jannick Duchet-Rumeau and Pr. Elodie Bourgeat-Lami who gave me the honor to review my thesis. I would like to thank Pr. Mathias Destarac who accepted to be the president of the jury. I also warmly thank Pr. Lazhar Benhyahya and Dr. Frédéric Léonardi for examinating my work and participating to the thesis defense.

I would like to express all my gratitude to my thesis directors and supervisors, France, Olivier, Hélène, Nick and Valérie, who allowed me to complete this thesis in the best conditions with all their scientific and human supports. I really appreciated the great confidence and freedom they gave me. I sincerely thank them for all the long and interesting discussions, it was so captivating that I did not see the time pass. Thanks for your help, your kindness and for all the scientific moments that were a real pleasure for me.

My deepest gratitude goes to my parents, Maryem and Allal, who have supported me throughout my career and have given me the strength to achieve my objectives. I would like to express my special gratitude to my wife, Mariem, for her love, patience and unwavering support, especially in difficult times: I love you! Thank you for your presence during the defense that allowed to celebrate this graduation all together. I also think to my brothers, Abderrafi and Youssef, who have always supported me tirelessly. Thank you all for always being there for me.

I would like to thank all the people who helped me daily in the laboratories. Specially, I think to Amandine, Guillaume, Karim and Mathieu. I also warmly thank all the PhD students I met at LGP, ICA and Polytechnique Montreal during my thesis. More generally, thanks to all the staff of the laboratories for the great atmosphere and the good mood every day.

TABLE OF CONTENTS

Introduction **1**

1 An overview of the literature **7**

1.1 Synthesis of PA6 by AROP and properties of resulting matrix 9

1.1.1 Anionic ring opening polymerization (AROP) 10

1.1.2 Factors infuencing polymerization reaction kinetics 12

1.1.3 Characterization of polymerization/crystallization kinetics 15

1.1.4 Characteristics of the synthesized PA6 17

1.1.5 Mechanical properties 21

1.1.6 Conclusion 22

1.2 Glass reinforced anionic PA6 composites 22

1.2.1 Manufacturing glass reinforced composites with an AROP PA6 matrix 22

1.2.2 Mechanical properties of glass reinforced PA6 composites 26

1.2.3 Conclusion 27

1.3 Interaction between glass reinforcements and the reactive system during the synthesis of glass/anionic PA6 composites 28

1.3.1 Interfacial interaction of AROP with raw glass surface 29

1.3.2 Silane treatment (Silanization) 29

1.3.3 Effect of interfacial interaction on composite properties 34

1.3.4 Effect of processing conditions on the interfacial interactions and final properties 36

1.3.5 Conclusion 36

1.4 Glass surface modification with silanes 37

1.4.1 Calcination (dehydroxylation) 37

1.4.2 Surface activation (rehydroxylation) 38

1.4.3 Factors influencing the silane grafting on the surface 39

1.4.4 Reactive silanes 42

1.4.5 Conclusion 43

1.5 Conclusion 44

2 Tailoring the hydroxyl groups density of glass surface for AROP of PA6 **45**

2.1 Materials 47

2.1.1 Reinforcement 47

2.1.2 Reagents for PA6 synthesis and silane . . . 49
2.1.3 Reactive mixture preparation . . . 50
2.2 Characterization of PA6 synthesis by Differential scanning calorimetry (DSC) 51
2.2.1 Sample preparation . . . 51
2.2.2 DSC analysis . . . 51
2.3 Preliminary tests: Influence of the hydroxyl groups density . . . 51
2.3.1 Preliminary Silanization . . . 52
2.4 Control of the hydroxyl groups surface density and adaptation of the silanization process to the anionic PA6 synthesis . . . 55
2.4.1 Analysis techniques . . . 55
2.4.2 Characterization of the surface density of hydroxyl groups on glass particles . . . 57
2.4.3 Comparison of the rehydroxylation protocols . . . 63
2.4.4 Controlling the –OH quantity regenerated during the silanization treatment . . . 64
2.4.5 Polymerization and crystallization kinetics after silane grafting . . . 66
2.5 Conclusion . . . 70

3 Impact of silane interfacial chemistry on the synthesis of anionic PA6 glass reinforced composites 73
3.1 Surface treatments . . . 76
3.1.1 Low chemical interactions . . . 77
3.1.2 Weak bonds . . . 77
3.1.3 Strong bonds . . . 78
3.1.4 Silane grafting . . . 81
3.2 Particle surface characterization . . . 82
3.2.1 FTIR spectroscopy . . . 82
3.2.2 X-ray Photo-electron Spectroscopy . . . 84
3.2.3 Confocal laser scanning microscopy (CLSM) . . . 89
3.2.4 Thermogravimetric Analysis (TGA) . . . 92
3.2.5 Contact angles . . . 94
3.3 Influence of the surface treatment on PA6 polymerization and crystallization 97
3.3.1 Influence on PA6 synthesis kinetics . . . 97
3.3.2 Impact on the conversion degree and crystallization . . . 98
3.3.3 Relationship between surface chemistry of glass particles and polymerization/crystallization kinetics . . . 100
3.4 New reactive treatment synthesis . . . 102
3.4.1 MONOMSILANE synthesis mechanism . . . 103
3.4.2 Procedure for the MONOMSILANE synthesis and grafting . . . 104
3.4.3 Particle surface characterization . . . 104
3.4.4 Contact angle . . . 106

3.4.5 Overview of the monomer grafting on the particle surface 107
3.4.6 Influence of the MONOMSILANE treated particles on PA6 polymerization and crystallization 108
3.5 Conclusion 111

4 Investigation of the properties of anionic PA6 based composites according to glass particles surface treatments 113
4.1 Manufacturing of anionic PA6/glass particles composites 114
4.1.1 Manufacturing specifications 114
4.1.2 Tested process for composites manufacturing 116
4.2 Physical and chemical characteristics 124
4.2.1 TGA 125
4.2.2 DSC 129
4.3 Composite mechanical properties and interface analysis 134
4.3.1 Analysis techniques and experimental conditions 134
4.3.2 Kinematic field measurements 135
4.3.3 Mechanical properties 141
4.3.4 Fracture surfaces analysis 149
4.4 Conclusion 152

Conclusion and perspectives 155

Appendix: Analysis techniques 161

List of Figures 165

List of Tables 171

Résumé étendu 173

Bibliography 195

INTRODUCTION

All efforts on a global scale are focused on reducing energy consumption in response to climate issues and geopolitical instability. In 2017, the Occitanie region has set the goal of becoming the first positive energy region in Europe by 2050. In this way, several sectors such as building construction and transport industries, and agriculture, must reduce their energy consumption. The transport sector is the most critical, since the reduction in energy consumption will have to be reduced by 61 % compared to the current state. All transportation modes, railways, aerospace, automotive and urban vehicles, are concerned by this effort. To achieve this objective, one solution consists in decreasing the weight of materials. Replacing steel and other metals by composite materials made of long carbon or glass fibers embedded in an organic matrix, that are up to 6 times lighter for equivalent rigidity and durability, is a relevant option.

Among composite materials, those with thermoset matrices are generally manufactured at moderate temperatures, from room temperature to slightly above to 180°C for high performance epoxy matrix composites, associated with a low pressure or vacuum in case of infusion processes, or a few bars in Resin Transfer Molding (RTM). Given their low viscosity - 10^{-2} Pa.s -, a large diversity of manufacturing processes offers the possibility to fabricate complex shapes, and reach large production series, smooth surface and high mechanical performance. For instance, RTM is well suited for mass production. It consists in placing stacks of dry fibers layers, or a dry fiber preform, into a mold. The mold cavity is then closed and clamped, and the low-viscosity resin is injected under pressure, chasing the air out through vents, until the mold is filled. The injection phase must guarantee the complete impregnation of the preform. At last, the curing step turns the liquid resin into a solid matrix [1]. The process is well mastered by many companies manufacturing composite parts.

In the coming years, life cycle assessment will probably become mandatory for companies before launching a product. In this framework, the environmental impact of resources will be analyzed throughout the whole product's life, from the raw materials extraction to production, use and disposal. More specifically, material recycling is a fundamental part of such procedure and its consideration has stimulated industrial development to reduce the environmental impact of products. In the special case of composites, the difficulty to recycle thermoset based materials still remains a major problem. As they combine lightening and recycling, thermoplastic composites are thus increasingly chosen. Yet, the manufacturing of thermoplastic matrix composite materials requires the application of

excessive pressures to force the thermoplastics to flow, due to their very high viscosity reaching hundreds of Pa.s. - about 500 bars for injection molding, and 50 bars in hot press consolidation of high performance composites. It also requires heating the materials up to the matrix liquid state, which is comprised between 200°C for conventional thermoplastics, and up to 400 °C for high performance polymers. These processing constraints thus represent a strong limitation for the development of thermoplastic composite materials, and still hinder their generalized application in the industry.

Reactive thermoplastic resins offer a promising option to address these issues. For this new type of polymers, reinforcements are impregnated with a monomer solution prior to *in situ* polymerization into the mold, similarly to thermoset RTM. The low viscosity of precursor mixture allows to use the same equipment as required for thermoset composites at low pressure, less than 10 bars. In addition, reactive thermoplastic resins ensure a good impregnation of the reinforcement combined with a relatively short cycle time. The use of reactive systems can finally improve the fiber/reinforcement adhesion because the polymerization takes place directly around the fibers [2]. However, the interest for this process remains conditioned by the final quality of the composite materials. Obviously, the mechanical properties of the composites depend on each constituent, i.e. the matrix and the reinforcement, as well as the quality of the interfacial adhesion. Indeed, the role of the interface is crucial since the mechanical load must be transferred as a continuum from the matrix to the fibers, the latter being mainly responsible for the stiffness and strength of the composite [3].

Developed about 10 years ago, only a few reactive thermoplastic resins are used until now. The most famous is Elium® from Arkema. It consists in the free radical vinyl polymerization of the methyl methacrylate monomer (MMA) into its polymer, poly(methyl methacrylate) (PMMA), using peroxide catalysts. PMMA-based composites are used in various applications such as wind turbine blades, automotive parts (body or structural parts), construction and sports. Another system has attracted the interest of researchers: polyamide 6 (PA6) obtained by ring opening polymerization of ϵ-caprolactam (ϵ-CL). It has the lowest viscosity among other similar systems and the reaction is particular in that the matrix crystallizes during the polymerization reaction. Moreover, its polymerization is fast and a high conversion degree is reached [2]. This reactive system can be associated to several reinforcing materials to improve their stiffness, such as long carbon or glass fibers, graphene or carbon nanotubes, or any type of fillers [4–6]. Long glass and carbon fibers are the most commonly used reinforcements. Carbon fibers are often chosen for advanced applications as they exhibit the highest stiffness and tensile strength, with a low density. However, their cost is prohibitive and limits their use. In comparison, glass fibers (GF) offer a good compromise between mechanical properties and manufacturing costs, which explains their much wider use in mechanical applications [7].

For anionic PA6/GF composite synthetized by reactive process, the system is composed of ϵ-caprolactam (the monomers), catalyst and activator, which react in contact with the

fibers by anionic ring-opening polymerization (AROP) [2]. The surface of commercial glass fibers is often coated with a sizing. The nature of this sizing and its chemical composition remain poorly documented in the literature, most often due to confidentiality reasons. Among the sizing components, the coupling agent is believed to be primarily responsible for the interfacial adhesion, especially when it interacts with both the matrix and the reinforcements. Whereas industrial coupling agents are typically well suited for most commercial polymeric matrices, surface treatment must still be adapted to fit specific or new polymers. A typical case requiring careful and precise control over surface treatments is for new reactive thermoplastic matrices, in particular anionic PA6. Indeed, an inadequate coupling agent can slow down the polymerization kinetics or even inhibit it and/or affect the crystallization process. Furthermore, the hydroxyl groups naturally present on the glass surface deactivate the catalyst, which also disturbs the polymerization reaction and can ultimately leads to a significant reduction in the synthetized polymer properties. In this case, controlling the GF surface chemistry is crucial because it influences not only the polymerization process, but it also controls the fiber-matrix adhesion at the interface, and therefore the mechanical properties.

Since the combination of PA6 with untreated glass reinforcements is not suitable for AROP, modifying the glass surface is necessary. Despite its fundamental importance and growing commercial interest, the influence of GF surface treatment on the anionic PA6 synthesis is very poorly described and understood in the literature. All of the existing works about the role of the silane coupling agent on the interfacial adhesion between the matrix and fibers, and the resulting improvement in the mechanical behavior, focused on only one type of aminosilane, which is commonly used with conventional polyamides. Moreover, these investigations do not provide a detailed characterization of the reinforcement surface, nor investigate the influence of the surface treatment on the polymerization and crystallization processes themselves. Yet, the kinetics of these two phenomena is crucial during the manufacturing of thermoplastic composites by reactive processing, as it also determines the viscosity and the cycle time. Therefore, the control of the interfacial interaction, through highly controlled and tailored surface treatments in order to improve the synthesis kinetics and the resulting composite properties, requires a very thorough analysis.

Based on this aim, the MOVING project started in 2018 following a call for proposals launched by the Occitanie region, France and the Université Fédérale de Toulouse. The aim of this project is to taylor and control the surface chemistry of GF for the *in situ* polymerization of anionic PA6, which is a current challenge in the manufacturing of such composites. This PhD thesis is a collaboration between three institutes: the Materials and Composite Structures team of Institut Clément Ader (CNRS UMR 5312) at IMT Mines Albi, France, the Mechanics, Materials and Processes department of the Laboratoire Génie de Production at Ecole Nationale d'Ingénieurs de Tarbes (ENIT-INPT), France, and the Department of Chemical Engineering at Polytechnique Montréal, Canada. Three months

were spent in Montréal, half of the three-year duration was spent in each laboratory in Albi and Tarbes.

Developing a glass fiber sizing suitable for anionic PA6 polymerization could offer new and very attractive opportunities for many companies in the Occitanie region. To reach this goal, the objectives were: (i) Tailoring the glass fiber surface chemistry to the reactive thermoplastic matrices; (ii) Understanding the role of sizing on the polymerization and crystallization of reactive PA6; (iii) Quantifying the effect of fiber sizing on the mechanical properties of reactive PA6 composites.

Accordingly, this thesis aims to deepen and broaden the analysis of the surface chemistry of glass reinforcement in order to bring a better understanding regarding anionic PA6 based composites synthesis. This question is all the more important for *in situ* polymerization, where the role of interfacial interactions is amplified, impacting both the fiber-matrix adhesion and the matrix synthesis process. It is therefore important to better control the interactions at the composite interface in order to promote the polymerization and crystallization processes of anionic PA6, and thus to improve the composites overall properties. This work was carried out with glass micro-particles, comparable in size to the diameter of glass fibers, as a model system in order to focus on the interfacial effects, and to avoid the combined influences of fiber length and orientation on the composite properties.

This PhD work was organized according to the following strategy:

- First, monitor and tune the hydroxyl groups surface density on the glass particles in order to enhance and control the synthesis of anionic PA6.
- Next, investigate the grafting process of a silane coupling agent at the particles surface and understand the influence of silane type on the synthesis reaction. This was achieved by comparing different silane-based coupling agents involving different types of interactions (minimum interactions, weak bonds, strong bonds).
- Finally, evaluate the effect of surface treatment on the interface performance and on the resulting macroscopic mechanical properties of composite specimens.

This manuscript is divided into four chapters. Chapter one is a literature review that presents the anionic PA6 synthesis and the main factors influencing the reaction and final properties. A particular attention is given to glass reinforced anionic PA6 composites. As the polymerization proceeds around the reinforcement, different interactions can occur during the synthesis. These interfacial interactions are reported, which allowed to identify the surface treatment compatible with PA6, in particular organosilanes grafting. The various steps and strategies of the glass surface modification by these coupling agents are described as well as their influencing factors.

The second chapter is devoted to the monitoring of the hydroxyl groups surface density on the glass particles. The complete silanization sequence is investigated, and the

influence of calcination time and conditions is studied by ThermoGravimetric Analysis (TGA) and Fourier Transform InfraRed (FTIR) spectroscopy. The impact of the particles surface chemistry on the polymerization and crystallization of the PA6 based composites is evaluated by means of Differential Scanning Calorimetry (DSC).

In the third chapter, different silane-based coupling agents are grafted and compared. The surface of glass particles is characterized using FTIR spectroscopy, X-ray Photoelectron Spectroscopy (XPS), TGA, confocal microscopy and contact angle measurements. Then, glass particles/anionic PA6 composites synthesis is investigated by DSC to evaluate the influence of the coupling agent chemical nature on the polymerization/crystallization kinetics, and the synthetized polymer properties.

In the last chapter, a process was developed to manufacture glass particles reinforced anionic PA6 composites. After determining the physical and chemical properties of the manufactured composites, the effect of reinforcement/matrix interfacial interactions on the mechanical properties was evaluated by tensile tests coupled with digital image correlation.

Finally, a conclusions section summarizes the important findings of this work. Based on these conclusions, several perspectives are proposed to further investigate the role of the reinforcement surface on the anionic polymerization of PA6, and to improve the physical and mechanical properties of the resulting composites.

CHAPTER 1

AN OVERVIEW OF THE LITERATURE

Contents

1.1 Synthesis of PA6 by AROP and properties of resulting matrix **9**

1.1.1 Anionic ring opening polymerization (AROP) 10

1.1.2 Factors infuencing polymerization reaction kinetics 12

1.1.3 Characterization of polymerization/crystallization kinetics 15

1.1.4 Characteristics of the synthesized PA6 17

1.1.5 Mechanical properties 21

1.1.6 Conclusion 22

1.2 Glass reinforced anionic PA6 composites **22**

1.2.1 Manufacturing glass reinforced composites with an AROP PA6 matrix 22

1.2.2 Mechanical properties of glass reinforced PA6 composites 26

1.2.3 Conclusion 27

1.3 Interaction between glass reinforcements and the reactive system during the synthesis of glass/anionic PA6 composites **28**

1.3.1 Interfacial interaction of AROP with raw glass surface 29

1.3.2 Silane treatment (Silanization) 29

1.3.3 Effect of interfacial interaction on composite properties 34

1.3.4 Effect of processing conditions on the interfacial interactions and final properties 36

1.3.5 Conclusion 36

1.4 Glass surface modification with silanes **37**

1.4.1 Calcination (dehydroxylation) 37

1.4.2 Surface activation (rehydroxylation) 38
1.4.3 Factors influencing the silane grafting on the surface 39
1.4.4 Reactive silanes 42
1.4.5 Conclusion 43
1.5 Conclusion **44**

Introduction

This chapter provides a bibliographic review of the synthesis of PA6 by anionic ring-opening polymerization (AROP), its influencing factors and the resulting properties of both the matrix and the associated composite. Surface treatments, in particular silane coating, and the improvements that they provide are also discussed.

1.1 Synthesis of PA6 by AROP and properties of resulting matrix

Polyamide 6 (PA6) has been synthesized since the 1930s. Two ways of synthesizing PA6 exist, both based on the ring opening of ϵ-CL. Figure 1.1 shows the chemical structures of ϵ-caprolactam and PA6.

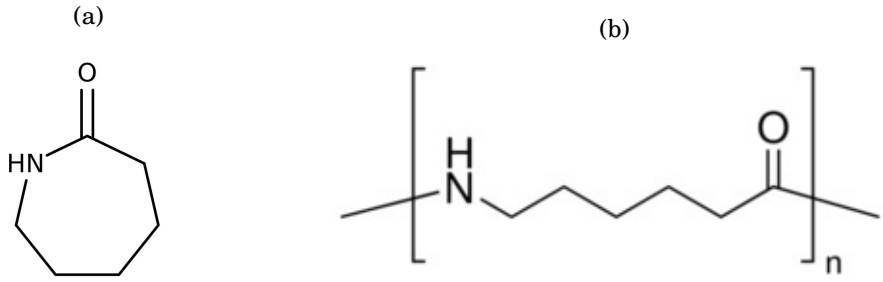

Figure 1.1: Chemical structure of (a) ϵ-caprolactam monomer and (b) polyamide 6

The most commonly used polymerization method is polycondensation. It is based on an amidification reaction of an acid with an amine. The nucleophilic attack of the free doublet of the nitrogen on the electrophilic carbon of the acid function leads to the formation of an amide group and the emission of a water molecule. This reaction is based on three steps: hydrolysis with opening of the ϵ-CL ring, creation of the polymer chain by polycondensation (elimination of water) and finally polymerization by successive addition of the cyclic monomer on the terminal groups of the chain. Thus ϵ-CL is converted into PA6 by polyaddition [8, 9]. This synthesis method is a cheap process but it often requires purification and post-polymerization steps to increase the molar mass or the addition of plasticizers to decrease the polymer viscosity.

The second polymerization reaction for obtaining PA6 is the anionic ring-opening polymerization (AROP) of ϵ-CL. This synthesis reaction has been developed decades ago, but it is only recently that this reaction has received renewed interest as this solution is well suited to the composites manufacturing by reactive process. This study focuses on this latter synthesis method whose reaction mechanisms and influencing factors are detailed hereafter.

1.1.1 Anionic ring opening polymerization (AROP)

1.1.1.1 Reaction mechanism

Anionic ring-opening polymerization involves three main steps: (i) dissociation of the initiator and formation of a lactam anion, (ii) formation of a complex between the catalyst and the activator, which depends on the type of catalyst-activator couple (Section 1.1.2.2), and (iii) polymerization through the lactam anion during which an anion is regenerated after each monomer addition.

Several reaction mechanisms are described in the literature. Van Rijswijk et al. [10] describe the reaction mechanism using hexamethylene-1,6-dicarbamoylcaprolactam as activator and caprolactam magnesium bromide as catalyst (Figure 1.3). The dissociation of the catalyst forms an anion that reacts with the carbonyl of the activator (blocked diisocyanate) by nucleophilic attack. Hashimoto et al. [11] showed that this first attack occurs on the endocyclic carbonyl of the activator because of its higher reactivity. Thus, an imide anion is formed and an hydrogen exchange between the imide anion and the monomer leads to the regeneration of a lactam anion. Hence, the chain growth continues by repetition of the nucleophilic attack on the growth center until consumption of the monomer (Figure 1.2).

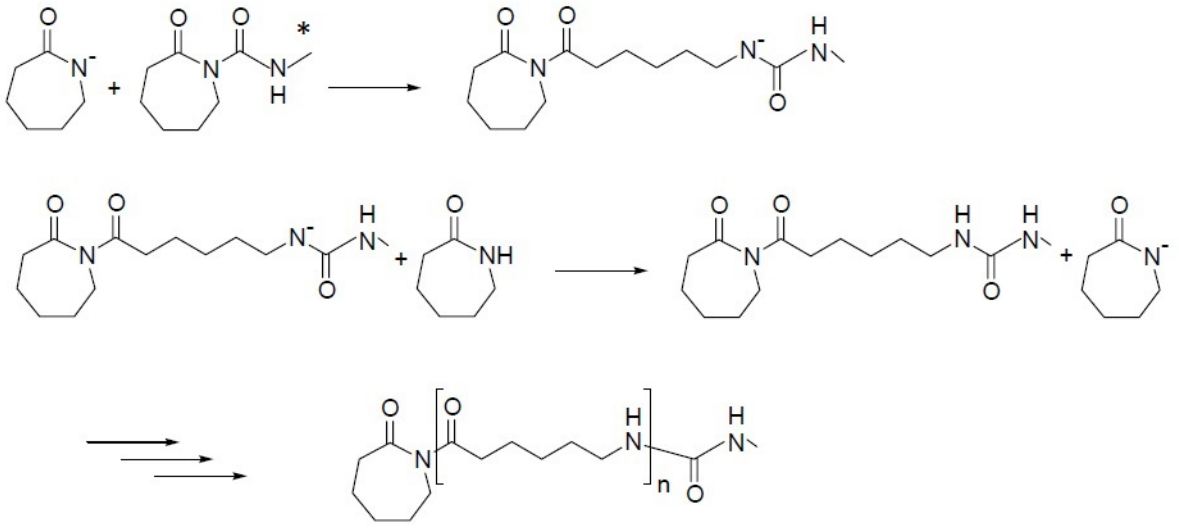

Figure 1.2: Reaction mechanism using hexamethylene-1,6-dicarbamoylcaprolactam as activator and caprolactam magnesium bromide as catalyst [10]

The synthesis temperature is between 130°C and 200°C. The conversion rates can be higher than 97% for reaction times between 3 and 60 min depending on the type of catalyst and activator used and on the concentration of the reagents.

1.1.1.2 Reagents

Anionic ring-opening polymerization can be initiated by using a catalyst, but this polymerization method results in a lag time of synthesis reaction [12]. An activator is therefore

generally added to accelerate the reaction and eliminate the induction time. Accordingly, the polymerization system consists in two additional reagents (catalyst and activator) in addition to the monomer.

Catalyst

Two catalysts are most commonly used in the anionic ring-opening polymerization of ϵ-CL: caprolactam sodium (NaCL) and caprolactam magnesium bromide (MgBrCL). Both products can be purchased from many suppliers such as Sigma-Aldrich (France), Brüggeman Chemical (Germany) and Rhein Chemie (Germany). The chemical structure of the two catalysts is shown in Figure 1.3(d) and 1.3(e). These two catalytic systems are described in several studies [13–15]. During the dissociation of the catalyst, a cation is released and creates a complexation with the activator. This complexation accelerates the polymerization as it favors the dissociation of the lactam anion and the metal cation and promotes the nucleophilic attack [14, 15].

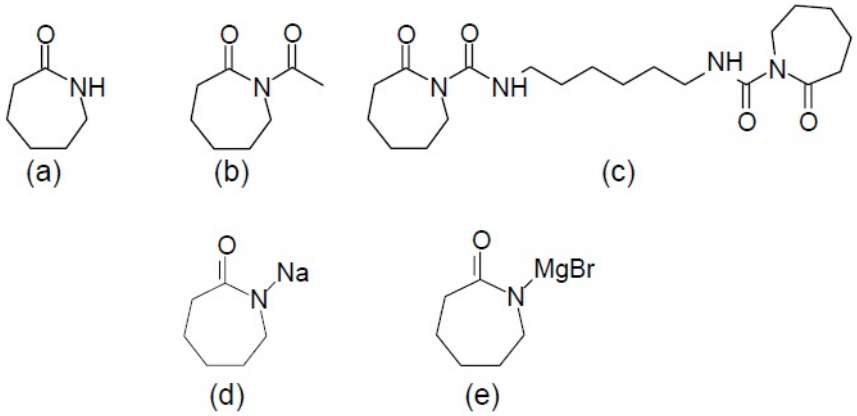

Figure 1.3: Chemical structure of (a) ϵ-caprolactam, (b) N-acetylcaprolactam (N-ACL), (c) hexamethylene-1,6-dicarbamoylcaprolactam (HDCL), (d) caprolactam sodium (NaCL), (e) caprolactam magnesium bromide (MgBrCL) [15]

Activator

Most of the literature studies focus on the anionic polymerization of ϵ-CL using two activators [13–16]. The first one is the monofunctional N-acetylcaprolactam N-ACL ("Activator0", Brüggeman Chemical, Germany) and the second one is the bifunctional hexamethylene-1,6-dicarbamoylcaprolactam HDCL ("C20P", Brüggeman Chemical, Germany). The chemical structure of the activators is shown in Figure 1.3(b) and 1.3(c). A bifunctional activator can lead to a faster polymerization than a monofunctional one because each imide group can initiate chain growth [15].

1.1.1.3 Simultaneous polymerization and crystallization of PA6 chains

PA6 is a semi-crystalline polymer composed of an amorphous phase and an ordered crystalline phase. Typically, polyamides begin to crystallize from the molten state (melting

temperature T_m of around 220°C) upon cooling from 20°C to 30°C below T_m. During the synthesis of PA6 by AROP, polymerization and crystallization therefore occur simultaneously [17]. Indeed, once the polymer chains reach a critical length, the crystallization process begins in the synthesis temperature range (130°C to 180°C) . The crystallization process has an important influence on the viscosity, the conversion rate and the molar weight of polymer chains [17].

Simultaneous polymerization/crystallization induces a strong coupling between the two mechanisms and many studies were aimed at understanding and modelling their interaction [17–20]. Vicard et al. [21] demonstrated that above 170°C both phenomena occur sequentially. Hence, they compared the crystallization process during *in situ* synthesis by AROP to that occurring from the molten state. Figure 1.4(a) shows the crystallization curves from the molten state for different temperatures. The superposition of the crystallization curve at 180°C from the molten state with the crystallization peak of the AROP synthesis curve shows the same crystallization kinetics (Figure 1.4(b)). The same result was obtained for synthesis at 190°C, suggesting that when polymerization and crystallization are decoupled during synthesis at high temperature (>180°C), the crystallization process is similar to the one observed from the molten state.

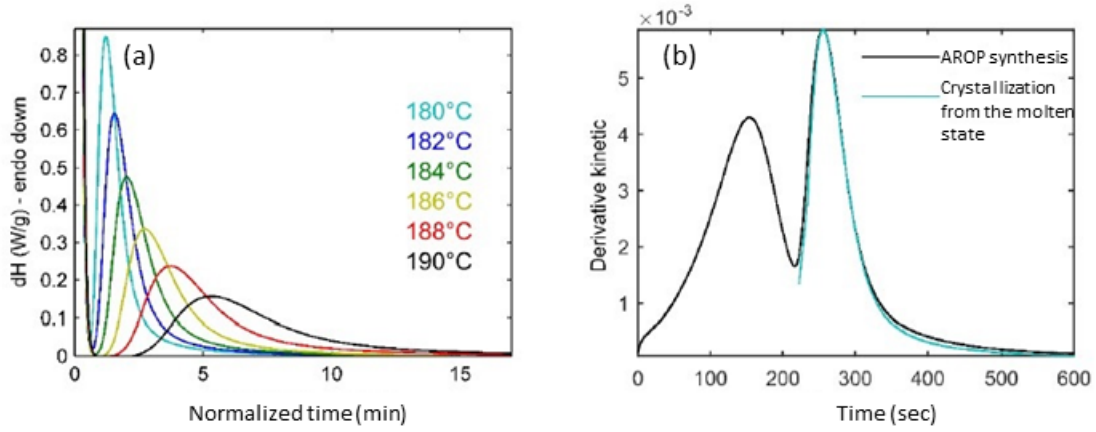

Figure 1.4: (a) Crystallization curves from the molten state for different temperatures, (b) Comparison of crystallization from the molten state at 180°C with that obtained by AROP during isothermal synthesis in DSC at the same temperature (from [21])

1.1.2 Factors infuencing polymerization reaction kinetics

1.1.2.1 Moisture

Moisture may disrupt or inhibit the reaction due to its anionic nature. Khodabakhshi et al. [22] actually showed that the reaction is faster in a dry nitrogen atmosphere. The deactivation mechanism of the catalyst in the presence of water is illustrated in Figure 1.5 where M can be sodium (Na) or magnesium bromide (MgBr). It can be noted that

the reaction system using caprolactam sodium (NaCL) as a catalyst is more sensitive to moisture than caprolactam magnesium bromide (MgBrCL). Therefore, a dry and inert environment is required for ensuring the anionic ring-opening polymerization of ϵ-CL. The reactants should also be stored in an inert environment and necessarily dried prior use.

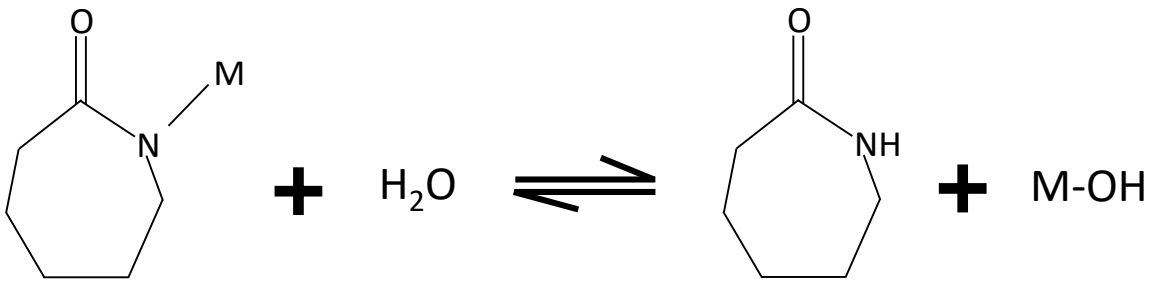

Figure 1.5: Catalyst deactivation by moisture

1.1.2.2 Reagents nature and concentration

The type of reagents has a significant influence on the synthesis kinetics. Indeed, the $MgBr^+$ cation is less electrophilic than Na^+, which results in a higher dissociation rate and therefore faster polymerization kinetics [13, 15, 23].

Moreover, a complex can be formed between the cation released by the catalyst dissociation and the activator, as explained in Section 1.1.1.1. The formation of this complex, which depends on the catalyst-activator couple, influences the synthesis kinetics (Figure 1.6). The MgBrCL/N-ACL and Nacl/HDCL couples can rapidly form a complex, which results in very fast polymerisation kinetics without an initiation period. The NaCL/N-ACL couple do not form a complex, which slows down the reaction kinetics without an initiation period. Finally, the MgBrCL/HDCL couple leads to a late complex formation, which results in an initiation period and a very fast increase of the reaction kinetics.

Several authors have also studied the influence of the catalyst and activator concentration. The quantities used are generally between 0.5-4 mol% for each reagent [8, 13, 15–17, 25]. As shown by Van Rijswijk et al. [15], increasing the MgBrCL catalyst concentration increases the formation of lactam anions, which favors the complex formation and thus accelerates the polymerization (Fig. 1.7(a)). In this case, however, the basicity of the mixture increases, which promotes parasitic reactions and decreases the conversion degree (Fig. 1.7(b)). Increasing the activator concentration also accelerates the polymerization by increasing the number of growth sites (Fig. 1.7(a)).

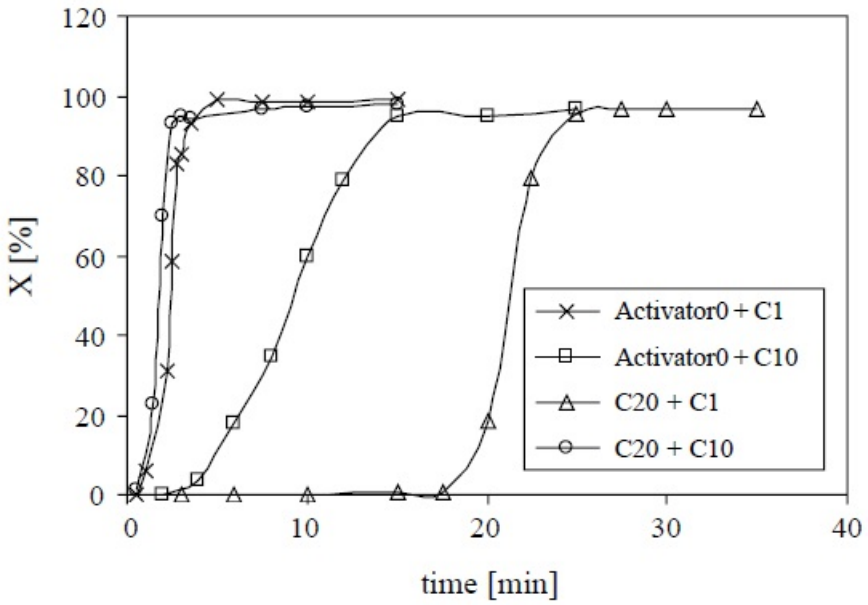

Figure 1.6: Degree of conversion as a function of time for four activator (0.6 mol.%)-catalyst (0.6 mol %) couples synthesized in the same conditions [24]

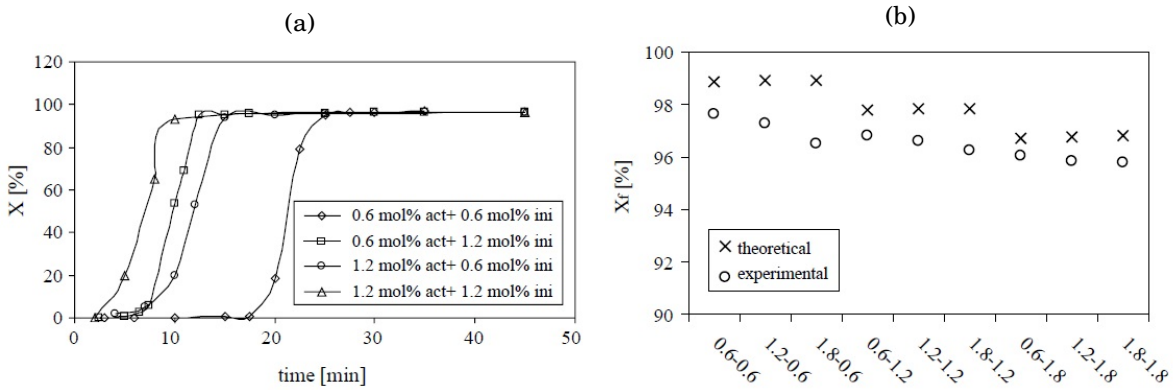

Figure 1.7: (a) Conversion degree as a function of time - Influence of the reagent concentrations on the reaction rate of the MgBrCL/HDCL system at 150°C, (b) Maximum conversion degree as a function of the reagent concentrations of the MgBrCL/HDCL system at 150°C [15]

1.1.2.3 Temperature

As explained in Section 1.1.1.3, polymerization and crystallization occur simultaneously during the synthesis. High synthesis temperature accelerates polymerization (Figure 1.8) and slows down crystallization. Consequently, the conversion degree increases and the crystallinity degree and melting temperature decrease [26]. This is due to the increase of the thermal agitation and the branching rate of the chains. These branching points disturb the formation of the crystals and reduce the crystallinity rate [13, 23, 24]. On the other hand, for low synthesis temperature, the crystallinity degree increases and the active sites are trapped in the crystals before they polymerize. This slows down the reaction and decreases the conversion [11, 16, 23, 25, 26].

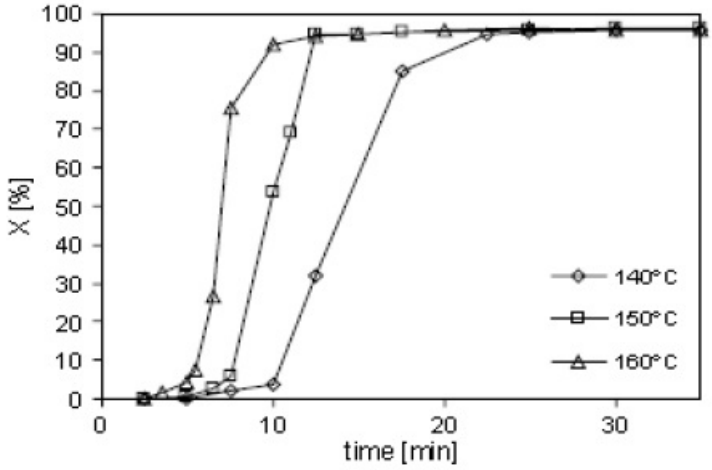

Figure 1.8: Degree of conversion as a function of time at various polymerization temperature [24]

1.1.2.4 Crystallization

The crystallization process can also affect polymerization kinetics when occurring at the early stages of the synthesis reaction. i.e. at low temperature (130-170°C). Since the reactants are excluded from the crystals, the reactive centers are repelled into the amorphous phase between the forming crystal lamellas. Two options are then possible. By repelling the reactants, the crystallization process may in the first case increase the concentration of reactive species in the amorphous phase and therefore accelerate the polymerization reaction. In the second case, the crystallization process can trap the reactive centers in the crystal structures [11, 16, 23, 25, 26], which slows down the polymerization and decreases the conversion rate.

1.1.3 Characterization of polymerization/crystallization kinetics

There are mainly three methods to follow the polymerization and crystallization kinetics during the anionic synthesis of PA6. Due to the strong coupling and simultaneity of both phenomena, their separate characterization remains the main problem for each technique.

1.1.3.1 Monitoring the conversion degree

This technique is based on the measurement of the degree of conversion at different times of the reaction [27–29]. Indeed, PA6 is synthesized under inert atmosphere, then samples are taken and soaked to stop the reaction and the conversion rate of each sample is measured. Yet, a discontinuous monitoring is required for such a method, which makes it difficult to separate the phenomena involved during the synthesis.

1.1.3.2 *In situ* monitoring of temperature in adiabatic reactor

The synthesis kinetics of anionic PA6 can also be studied in adiabatic reactor [30–37]. This technique consists in continuously measuring the increase of the reactive mixture temperature in an isolated adiabatic reactor.

Figure 1.9 shows a typical result of this technique. The slow increase in temperature at the beginning of the curve corresponds to the heating of the mixture. Then, the significant increase is due to polymerization and crystallization phenomena. Note that the ϵ-CL curve makes it possible to subtract the heating step of the mixture.

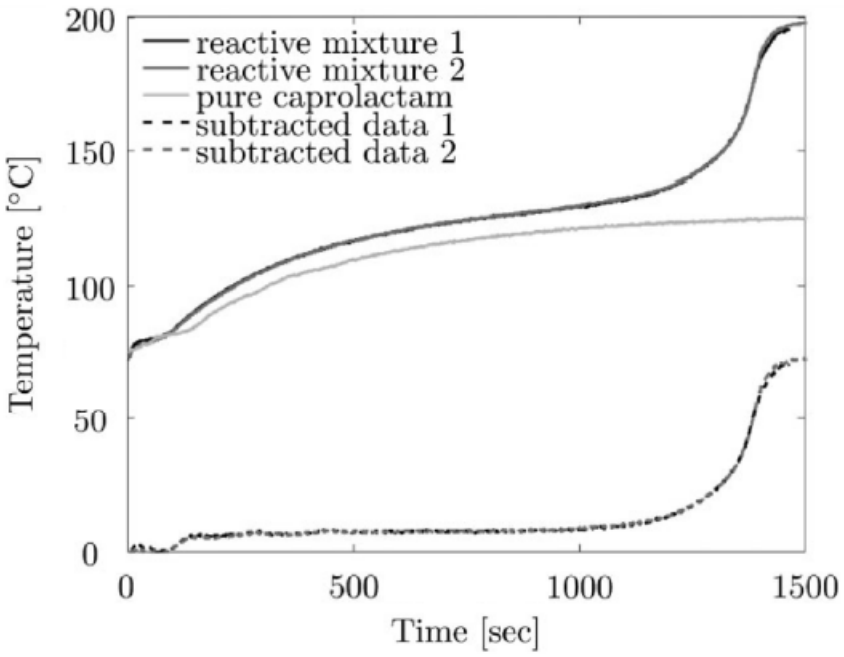

Figure 1.9: Temperature evolution during the anionic polymerization of PA6 in an adiabatic reactor [38]

This method has the advantage of using a high quantity of the reactive mixture (a few hundred grams), which ensures good homogeneity and reproducibility. However, the temperature dependence of the polymerization/crystallization phenomena cannot be investigated because isothermal synthesis is not possible within the adiabatic reactor.

1.1.3.3 *In situ* monitoring of heat flow

Differential scanning calorimetry (DSC) is a technique to monitor the *in situ* synthesis of PA6. Indeed, the heat released by the polymerization/crystallization is measured continuously as a function of time and temperature and then compensated by the apparatus to remain at the set temperature (Appendix). This allows measuring the reaction exothermicity. Isothermal synthesis can be performed using this technique to investigate the temperature dependence of the polymerization/crystallization.

The first studies using DSC mainly focused on the influence of the nature and concentration of catalysts on the kinetics [39–43]. Khodabakhshi et al. [44] studied the synthesis of PA6 under several isothermal and anisothermal conditions in DSC. In the meantime, they observed the initial crystallization temperature with different heating ramps using an optical microscope coupled to a heating stage. From this, they could define the onset of the crystallization peak on the DSC thermograms. However, their study focused on a reactive mixture compatible with 3D printing, which requires very fast kinetics, achieved through high concentrations of catalysts.

Recently, Vicard et al. [17] investigated the polymerization/crystallization coupling for composite applications. The characterization of the synthesis reaction by DSC leads to specific heat flow curves with two convoluted exothermic peaks (Figure 1.10(a)). The first peak does not necessarily correspond to polymerization. Due to the inverse temperature dependence of polymerization and crystallization in the range of the PA6 synthesis, crystallization can be initiated before reaching the maximum polymerization kinetics and leads to an exothermic crystallization peak [17]. Nevertheless, for synthesis temperature higher than 170°C, the two phenomena are decoupled and the DSC curve shows two deconvoluted exothermic peaks (Figure 1.10(b)).

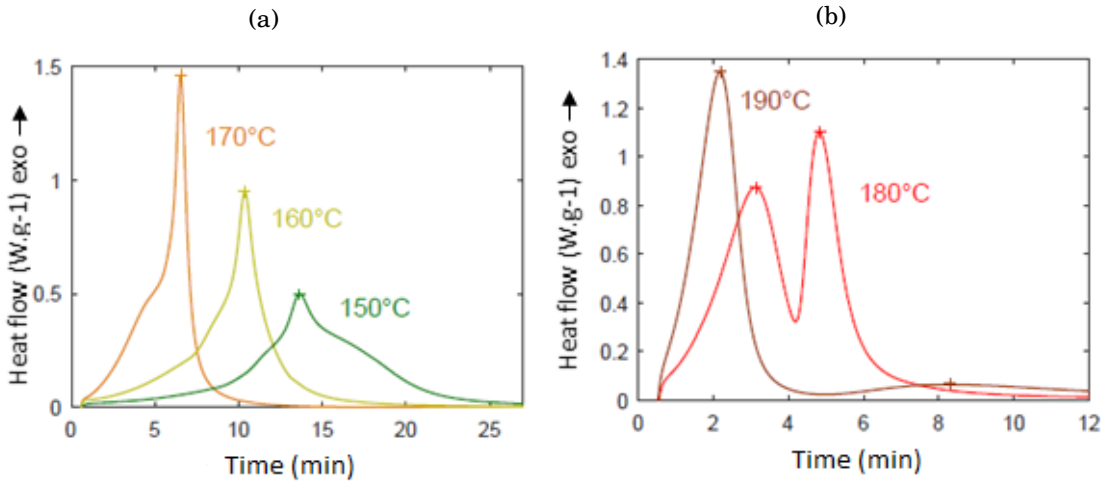

Figure 1.10: DSC thermograms of isothermal syntheses of PA6 with the MgBrCl /HDCL system at (a) 150-160-170°C and (b) 180°C-190°C [17]

1.1.4 Characteristics of the synthesized PA6

During the synthesis, the physical and chemical properties of the material change. First, the creation of polymer chains and their growth can be characterized by the conversion rate and the molar mass. In addition, the crystallization of growing chains during the synthesis can be estimated by the degree of crystallinity and the crystal morphology. The mechanical properties of the synthesized PA6 finally depends on the chain formation and organization.

1.1.4.1 Conversion degree

The conversion rate X_p characterizes the amount of monomer consumed during the polymerization at instant t. It is defined by the Equation (1.1) where [M] and $[M]_0$ (mol. L^{-1}) are the monomer concentrations at instant t and at the initial state respectively:

$$X_p = 1 - \frac{[M]}{[M]_0} \tag{1.1}$$

The conversion rate of PA6 obtained by AROP of ϵ-CL has been studied by Zhang et al. [45]. Their approach is based on the determination of the mass ratio of the polymerized product, from which the residual monomer is removed. The residual monomer can be removed by different techniques such as dissolution or thermal degradation, the most used technique being the thermogravimetric analysis (TGA) [45, 46]. It involves measuring the evolution of the mass of a sample as a function of temperature. Since the evaporation of ϵ-CL occurs from 100°C [45, 47, 48] and the degradation of PA6 from 300°C [45, 49–51], two mass losses are visible during a heating ramp in TGA (Figure 1.11). Therefore, the first mass loss corresponds to the mass of the residual monomer.

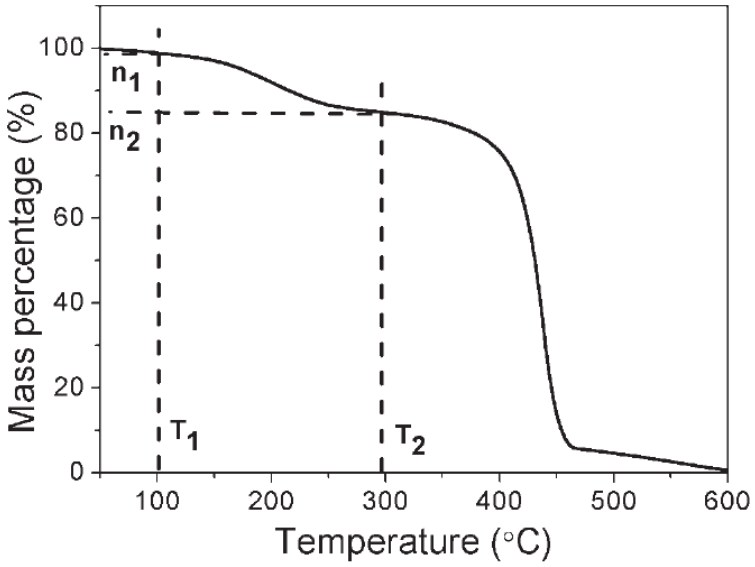

Figure 1.11: Typical TGA curve of a PA6 synthesized by anionic polymerization (ramp from 25 to 600°C at 10°C/min) [45]

In the case of PA6 AROP, the conversion rate X_p^∞ can thus be calculated using Equation (1.2), in which $m_{\epsilon-CL}$ refers to the residual mass of $\epsilon - CL$ and m_0 is the total mass of the sample. In a composite, the mass of the reinforcements must be subtracted from the total mass of the sample.

$$X_p^\infty = 1 - \frac{m_{\epsilon-CL}}{m_0} \tag{1.2}$$

Increasing the concentration of residual monomer results in a significant decrease in viscosity. In addition, the residual monomer ratio may include water and oligomers. These molecules as well as the monomer plasticize the amorphous phase and increase the mobility of the chains in the melting temperature range. Consequently, increasing their concentrations leads to a reduction on the glass transition temperature T_g and melting temperature T_m [52, 53]

The conversion rate depends mainly on the catalyst-activator couple used, the concentration of the reagents, the presence of moisture and the synthesis temperature [13, 15, 16]. In addition, the crystallization process has a significant effect on the conversion rate because polymerization and crystallization occur simultaneously and reactive centers can be trapped in the crystals [52, 53].

1.1.4.2 Molar mass

In addition to the conversion rate, the polymerization is also characterized by the growth of molecular chain length. This is characterized by the degree of polymerization DP giving the average mass by number M_n, the average mass by weight M_w and the average viscosimeric mass M_v (in general $M_n < M_w < M_v$). The polymolecularity index I_p also describes the heterogeneity of the polymer [23].

Like all polymers, the properties of PA6 obtained by AROP (e.g. melting temperature and toughness) not only depend on the M_w but also on the chain length distribution. The ability of the material to absorb energy is for instance strongly related to the M_w [53, 54]. Also, in the low M_w range, the T_g directly depends on the M_w until it stabilizes for high M_w because of chain entanglement [52, 53, 55]. Moreover, M_w has a slight influence on the elongation without impacting the modulus and ultimate stress [53].

The PA6 obtained by AROP has a Mw between 50 000 and 210 000 g.mol^{-1} and a M_v between 25 000 and 120 000 g.mol^{-1}, which corresponds to very high molar masses compared to PA6 obtained by hydrolytic polymerization for which M_w is between 20 000 and 70 000 g.mol^{-1} [16, 23, 24, 53]. The chain length distribution I_p is between 1 and 2.5 [23, 52, 56]. Several parameters influence the molar mass in particular the concentration of the reagents and the temperature of synthesis [23, 24, 53, 56].

1.1.4.3 Crystallinity

The crystalline phase of a polymer is characterized by the degree of crystallinity which represents the ratio of the crystalline phase to the amorphous phase. This crystallinity degree is commonly evaluated using DSC by carrying out a heating ramp until total melting. The crystallinity degree X_c^{∞} is calculated from the enthalpy of the endothermic melting peak ΔH_m and from the melting enthalpy Delta $\Delta H_c^{100\%}$ of the polymer 100% crystalline according to the Equation (1.3):

$$X_c^{\infty} = 1 - \frac{\Delta H_m}{\Delta H_c^{100\%}} \tag{1.3}$$

It should be noted that the value of Delta $\Delta H_c^{100\%}$ is theoretical since a polymer cannot be 100% crystalline. Since several values of such enthalpy were reported in the literature (190 J/g [10, 53, 57], 230 J/g [48, 58] or 240 J/g [43, 59, 60]), the comparison of the crystallinity degree with the literature must therefore be made with care.

The anionic synthesis of PA6 leads to high degrees of crystallinity compared to commercial PA6 [24, 48, 53, 58, 61–63]. Van Rijswijk et al. [26] show that it is possible to reach crystallinity degrees up to 50%. As mentioned in Section 1.1.2.3, the crystallinity degree strongly depends on the synthesis temperature [26] and on the molar mass of the synthesized polymer [53].

Concerning the crystal morphology, the PA6 crystallizes in two main crystal lattice forms: α and γ. These phases are differentiated by the arrangement of the amide groups between the PA chains. The α crystal lattice is more thermodynamically stable. Its structure is monoclinic (Figure 1.12). The PA6 chains are oriented antiparallel and their hydrogen bonds are in the same plane and parallel to the lamella plane. The melting temperature associated to the α phase is about 222°C and its density is about 1.23. The second γ crystal lattice is pseudo-hexagonal (Figure 1.12). In contrast to the α lattice, the hydrogen bonds are formed between the parallel chains and consequently their orientation is no longer parallel to the plane of the lamellas. This phase is characterized by a melting temperature of 214°C and a density of 1.16 [23, 64–66].

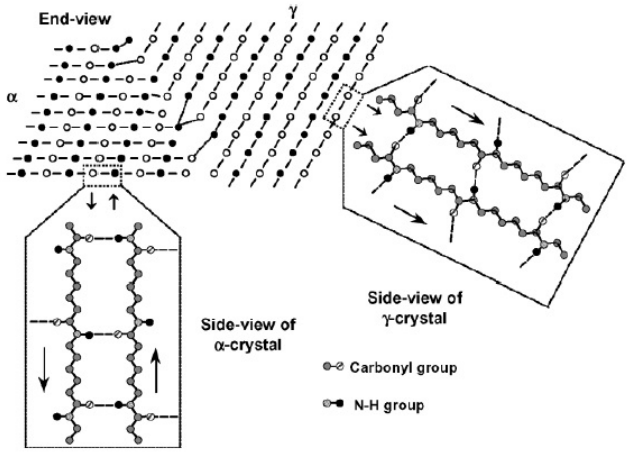

Figure 1.12: Schematic representation of the α and γ crystal lattice structure of PA6 [65]

By WAXD observation, the α lattice shows two main diffraction peaks for $2\theta \approx 20$ ° and 24 °. On the other hand, the γ crystal lattice is characterized by a diffraction peak around $2\theta \approx 21.3$°. In the case of PA6 synthesis by AROP, there is mainly formation of more stable α crystals [23, 66–68], as shown in Figure 1.13. This phase ensures high mechanical properties to the material. Hornsby et al. [66] found that the cooling rate

and the presence of residual monomer explain the formation of the less stable γ crystals. Accordingly, it is possible to promote the formation of α structure crystals by removing the residual monomer and with slower cooling rates. In addition, the γ phases can be transformed into α phases by melting the polymer, then slow cooling, or by heating the polymer to temperatures above 160°C.

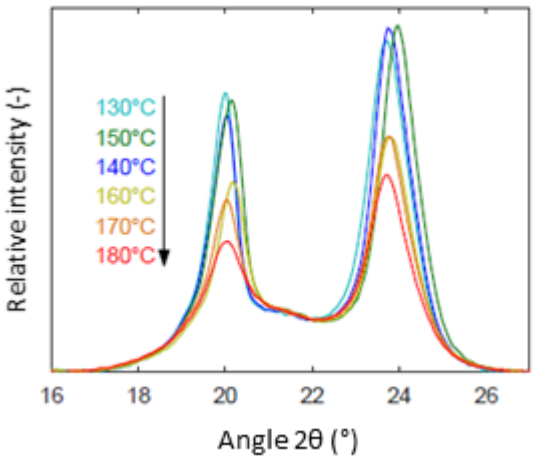

Figure 1.13: WAXS scans of anionic PA6 samples synthesized under isothermal conditions between 130 and 180°C [17]

1.1.5 Mechanical properties

The mechanical properties in tensile, flexural, impact and shear strength are described in several works [13, 26]. Table 1.1 summarizes some mechanical properties of the PA6 synthesized by AROP in dry and wet conditions compared to the PA6 synthesized by polycondensation. It is important to note that moisture acts as a plasticizer on polyamides resulting in a decrease of both T_g and tensile properties. Hence, increasing the crystallinity allows to limit the moisture absorption [53].

Table 1.1: Mechanical properties of PA6 synthesized by AROP [15]

	Anionic PA-6		Hydrolytic PA-6		Star-branched PA-6
	DAM	Conditioned[a]	DAM	Conditioned[a]	Conditioned[a]
Tensile strength [MPa]	75	55	85	65	52
Flexural Modulus [GPa]	3.0	2.2	2.3	0.7	1.2
Elongation at break [%]	10	25	10	350	59
Density [g/cm^3]	1.14	1.14	1.15	1.14	–
Shore D	82	78	80	65	–
Equilibrium water absorption [%]					
23 °C, 50% RH	–	3.5	–	2.0	–
23 °C, 100% RH	–	9.0	–	6.5	–
Melting point by DSC [°C]	220	220	215	215	208

[a] 23 °C, 25% RH. DAM, dry as moulded; RH, relative humidity.

In general, the mechanical properties of PA6 depend on several factors that can be divided into three groups: (i) material factors (e.g.,M_w and crystallinity), (ii) environmental factors (e.g., relative humidity), and (iii) stress factors (e.g., nature of stress and duration etc.) [24, 53]. For example, a high degree of crystallinity increases the elastic modulus and the tensile strength. Besides, Chaichanawong et al. [69] showed that the yield strength, tensile strength, flexural strength and elastic modulus can decrease with water absorption.

1.1.6 Conclusion

The ring-opening polymerization reaction mechanism has attracted interest in recent years. First, it does not generate sub-products that require purification steps. Then, the molecular weights obtained by AROP are generally higher than those obtained by polycondensation. The specific feature of the anionic synthesis of PA6 is the strong coupling of polymerization and crystallization. Indeed, both phenomena occur simultaneously during the synthesis and exhibit an inverse temperature dependence requiring an accurate control. Moreover, several factors influence the polymerization kinetics and, consequently, the characteristics of the synthesized polymer (moisture environment, nature and concentration of the reagents, synthesis temperature for instance). Above-cited advantages explain the interest of developing composites materials manufactured by AROP reactive process. Several types of materials may be used as reinforcements such as carbon fibers, glass fibers, graphene and carbon nanotubes or fillers such as silica or glass particles [4–6]. In this study, attention is paid to glass reinforcements which are the most widely used materials for PA6 composites as they offer a good compromise between properties and manufacturing cost.

1.2 Glass reinforced anionic PA6 composites

The manufacture of PA6/glass reinforcements composites using a reactive process imposes several challenges. The complex chemistry of the reactive system requires some adaptations and precautions compared to conventional methods. Some adapted processes will be described in what follows. Furthermore, several types of reinforcements can be used (short or long glass fibers or glass particles) in PA6/glass composites, which influence the final properties of the resulting material. Other parameters, such as humidity, can also affect the composites mechanical properties. This section will also propose a recall of some typical features of glass reinforced composites.

1.2.1 Manufacturing glass reinforced composites with an AROP PA6 matrix

Reactive processes are based on the impregnation of the fibers by the reactive mixture which then polymerizes around them. The use of the reactive system in a liquid process

requires some adaptations compared to thermoset composites. Indeed, thermoset resins generally require only one tank before impregnation because the reaction is essentially initiated by the temperature. However, the anionic PA6 reactive system requires two heated tanks and a mixing head in the reactive mixture preparation unit before impregnation (Figure 1.14). The first tank contains the ϵ-CL monomer and the catalyst and the second one contains the monomer and the activator. This allows to separately melt the reagents and prevent a premature polymerization. An inert environment is required in both tanks to avoid reaction deactivation by moisture (Section 1.3.1.2). The dosage of the two solutions (usually 1:1) is carried out using high pressure pumps. The mixing head is then used to mix and homogenize the reactive system and to inject it into the mold. Moreover, tools must also be compatible with the reactive mixture chemistry in order to avoid parasitic reactions and disruption of the polymerization process.

It is important to note that the viscosity of the reactive system is a crucial parameter for reactive process manufacturing. The viscosity must not exceed 1 Pa.s [70]. Beyond this value, the impregnation quality decreases, which affects the final properties of the resulting composite [2]. Indeed, the initial reactive system is mainly composed of ϵ-CL monomer whose viscosity is lower than 10 mPa.s in the molten state (at a temperature higher than about 70°C). During synthesis, the increase of molar mass of PA6 chains, the increase of PA6 concentration and the formation of crystalline zones lead to a continuous increase of the viscosity until reaching a value higher than 10^6 Pa.s [13, 71–73]. Consequently, after passing through the mixing head, the injection time is conditioned by the evolution of the viscosity which depends on the synthesis kinetics and its influencing factors (Section 1.1.2).

Several reactive processes have been used to manufacture reactive thermoplastic matrix-based composites. In this section, four processes will be presented: (i) Reaction injection molding (RIM) (ii) Vacuum infusion (VI) (iii) Reactive pultrusion (RP) and (iv) Reinforced reaction injection molding (RRIM). Note that other processes used for neat resin are described in the literature such as casting [74, 75] and rotational molding [13, 76–79].

1.2.1.1 Reaction injection molding (RIM)

The RIM process is similar to the RTM process for thermosets. A dry fiber preform is inserted between two solid molds, then the resin is injected with a high pressure (8-10 bar) to impregnate this preform [80–83]. The viscosity of the resin should not exceed 1 Pa.s in order to obtain a homogenous impregnation [2]. The reagents of the resin are separated in two tanks. This prevents premature polymerization. Then, the components of the two tanks are mixed just before entering the mold as shown in Figure 1.14. The composite is then demolded after the complete polymerization of the resin. The clamping force required to keep the mold closed increases with the size of the part. Therefore, the size of composites parts manufactured by this process is limited. The advantage of the

RIM process is the fast cycle time and the ability to manufacture complex shaped parts. However, it induces high tooling cost.

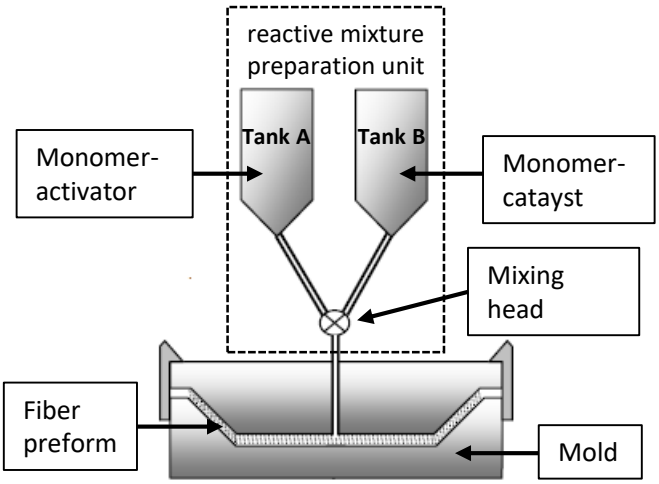

Figure 1.14: Schematic representation of RIM process (from [2])

1.2.1.2 Vacuum infusion (VI)

In this process, a dry fiber preform is inserted inside a mold with a solid half and a flexible half. The vacuum is used to compact the preform and then impregnate it with resin as illustrated in Figure 1.15 [10, 48, 84]. The maximum resin viscosity required is 1 Pa.s. As in the RIM process, two tanks of resin are needed to avoid premature resin polymerization. The contents of the two tanks are mixed and then dispensed into a buffer vessel which allows to separate the pressure required for the resin dispensing and the vacuum required to promote the infusion. The atmospheric pressure is sufficient to clamp the mold in this case, which allows to manufacture parts with unlimited size. Another advantage of this technique is the low tooling cost due to the low pressures employed. The disadvantage of the VI process is the flexibility and the life span of the half mold, which is usually used only once and may also lead to a poor surface quality on the top side of the part. It should be noted that despite the possibility of using low pressures, part sizes are often limited by the pot life of the reactive system.

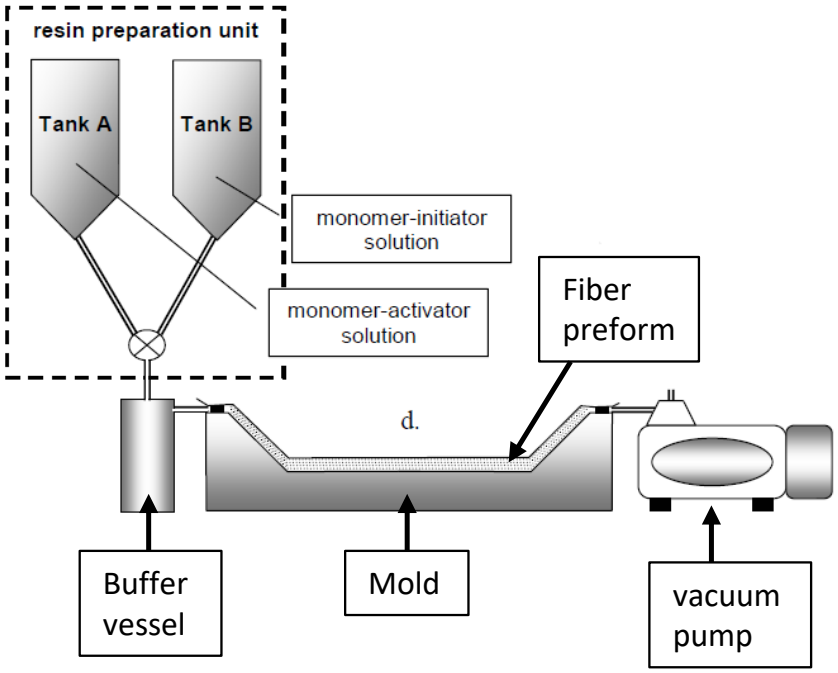

Figure 1.15: Schematic representation of VI process (from [2])

1.2.1.3 Reactive pultrusion

This process consists of impregnating the fibers with the reactive mixture and then pulling them through a die (Figure 1.16). The fibers first pass through a preheating module to reach the manufacturing temperature. They are then inserted into a pultrusion die, into which the reactive mixture is injected. The fibers are thus impregnated into the pultrusion die. In the case of reactive synthesis, its cross-section is longer, allowing polymerization to occur. The part is then solidified in the cooling module and demolded. The viscosity of the resin should not exceed 1 Pa.s because the pressures used are generally low (0.1 to 0.9 bar) [85]. This process makes it possible to manufacture unidirectional composites and profiles with continuous section and high fiber content [86, 87].

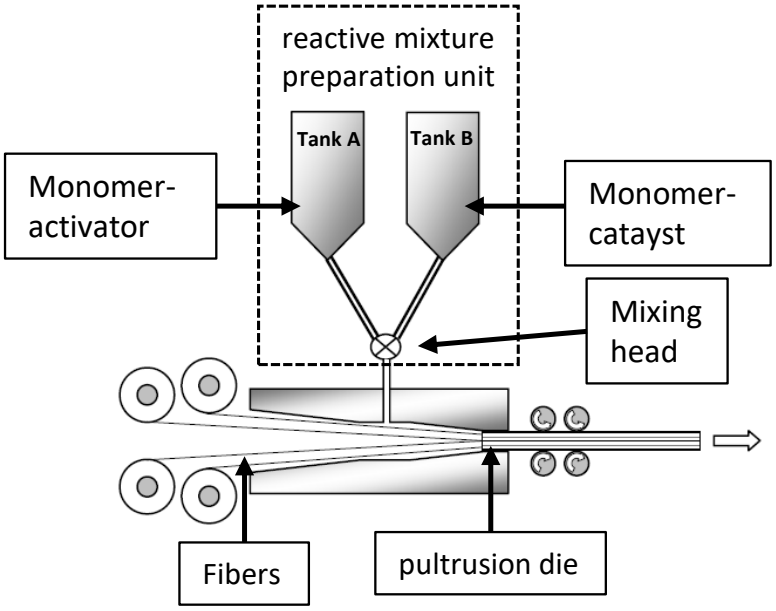

Figure 1.16: Schematic representation of RIM process (from [24])

1.2.1.4 Reinforced reaction injection molding (RRIM)

This process is based on the same principle as RIM. In this case, short fibers or particles are added to the mixture in the two tanks before being injected into the mold as shown in Figure 1.17. The process has the same advantages and disadvantages of the RIM process mentioned above. Moreover, the composites obtained with this technique have a low reinforcement content because the addition of fibers or particles to the mixture is limited by viscosity issues. In the case of short fiber-based composites, reinforcements are also randomly distributed within the composite, leading to isotropic mechanical properties [88, 89].

1.2.2 Mechanical properties of glass reinforced PA6 composites

Several authors have studied the mechanical properties of commercial PA6/GF composites [90–96]. Han et al. [97] compared the mechanical properties using short and long glass fibers. Very few studies have investigated the mechanical properties of anionic PA6 based composites reinforced with glass fibers [26, 98]. Yan et al. [99] described the mechanical properties of anionic GF/PA6 composites made by vacuum assisted resin infusion (VARI). The anionic PA6 was synthesized using NaCL as a catalyst and HDCL as an activator while the glass reinforcement was a plain-woven fabric. Table 1.2 summarizes the mechanical properties of the resulting composites as well as the effect of different post-heat treatments on the properties. Chen et al. [100] demonstrated that anionic PA6/GF composites with a high continuous glass fiber content can be successfully manufactured using a pultrusion

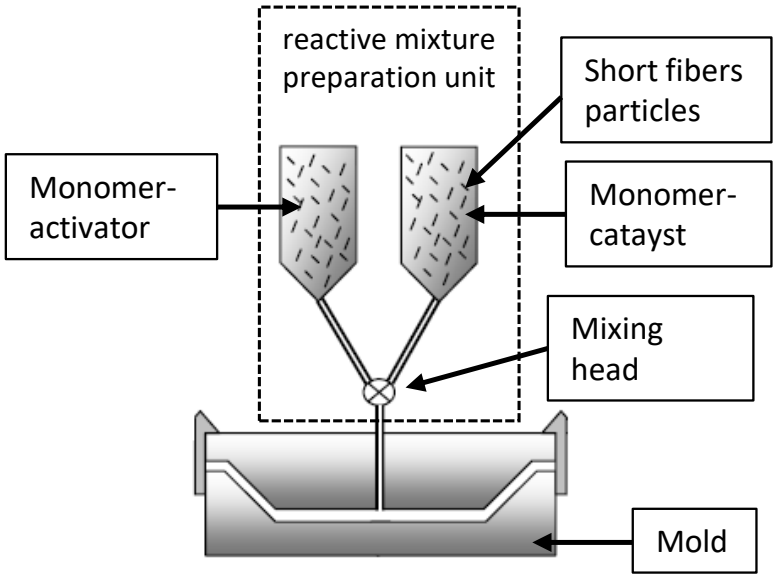

Figure 1.17: Schematic representation of RRIM process (from [24])

process. They showed that with a heating zone temperature of 150°C, the crystallinity of the PA-6 matrix increases, which significantly increases the flexural strength and flexural modulus of the composites. These properties also increase with increasing fiber content.

Table 1.2: Mechanical properties of the anionic PA6/GF composites and effect of different post-heat treatments on the properties [99]

	Tensile strength (MPa)	Tensile modulus (GPa)	Flexural strength (MPa)	Flexural modulus (GPa)	ILSS (MPa)
Untreated	433.5 ± 10.0	22.0 ± 1.2	396.4 ± 29.4	23.5 ± 1.2	43.3 ± 1.9
Quenched	330.3 ± 13.5	17.0 ± 1.3	330.7 ± 31.8	20.0 ± 0.5	38.3 ± 2.2
Annealed	442.8 ± 24.0	22.1 ± 1.6	402.9 ± 28.5	21.5 ± 0.8	51.5 ± 2.0

Recently, Van Rijswijk [101] studied the effect of the mold temperature on the mechanical properties of anionic PA6/GF composites made by vacuum infusion process. Figure 1.18 shows that the Inter-Laminar Shear Stress (ILSS) of the anionic PA6 based composites is higher than those of the commercial PA6 based composites (same thickness, same fiber textiles, same fiber content) and exhibits a maximum at a synthesis temperature of 180°C. However, they demonstrated that PA6 based composites are sensitive to moisture absorption, which can reduce their mechanical properties.

1.2.3 Conclusion

The synthesis of PA6 by AROP is the most suitable for the manufacture of composites by reactive process because of its various advantages. As detailed previously, the chemistry of this synthesis is rather complex. The optimization of anionic PA6 based composites

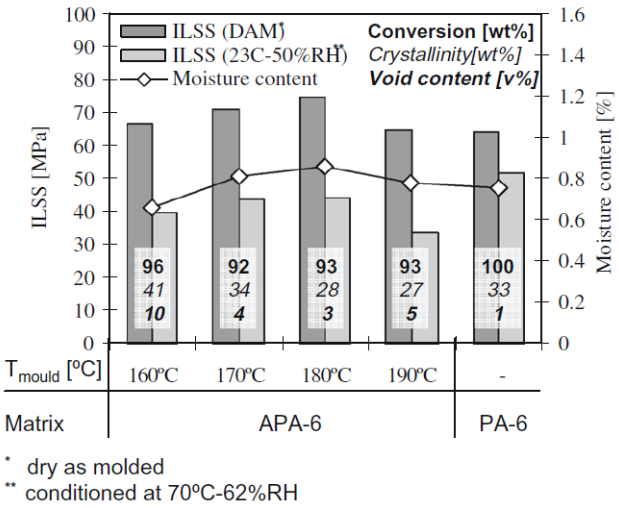

Figure 1.18: Comparison of the Inter-Laminar Shear Stress (ILSS) of reactively processed anionic PA-6 composites and melt processed PA-6 composites and effect of moisture absorption [101]

by reactive process thus relies on the control of the *in situ* polymerization kinetics of the reactive systems and of the simultaneous crystallization process. Focusing on anionic PA6 /glass composites, another important issue for overall properties stands in the interfacial interactions between matrix and reinforcements. Under mechanical stress, this is a key point for an efficient load transfer between the two phases. In this way, we propose now to review research studies dedicated to the control of interfacial interactions between glass reinforcements and anionic PA6 matrix.

1.3 Interaction between glass reinforcements and the reactive system during the synthesis of glass/anionic PA6 composites

During the manufacture of glass reinforced anionic PA6 composites, the resin synthesis reaction occurs around the reinforcements. Due to the extreme sensitivity of PA6 to labile protons, the anionic ring opening polymerization can be affected by the chemical functions in contact with the reactive mixture. Since a reinforcement represents a huge surface, it can interfere with the synthesis reaction. Hence, controlling the reinforcement surface chemistry is crucial because it not only influences the polymerization and crystallization processes, but it also controls the fiber-matrix adhesion and the resulting mechanical properties. In a first step, this section aims at underlining the need of a surface treatment compatible with AROP reaction through the analysis of the interaction of raw glass surface with the reactive mixture of ϵ-CL. The surface treatment with silanes, which is the most used technique for surface preparation, is then presented. The influence of silane type is finally analyzed

1.3.1 Interfacial interaction of AROP with raw glass surface

1.3.1.1 Reaction deactivation

In the case of anionic ring-opening polymerization, the glass reinforcements must be treated before the composite synthesis. Indeed, the hydroxyl groups present on the glass surface can disturb or even inhibit the reaction due to the reaction of labile protons with the catalyst. Van Rijswijk et al. [10] showed that untreated glass fibers significantly reduce the conversion rate due to the deactivation of the catalyst by hydroxyl groups of the glass fiber surface. The deactivation mechanism is shown in Figure 1.19: anions are transformed into monomer by leaving their positively charged cations in the proximity of the glass surface (negatively charged). Therefore, it is necessary to control the amount of hydroxyl groups in order to reduce their negative effect on the polymerization reaction during synthesis and to avoid the related decrease of the mechanical properties of the composite.

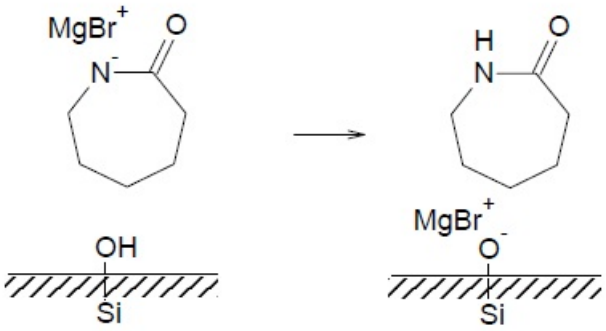

Figure 1.19: Deactivation of the catalyst by hydroxyl groups on the glass surface [10]

1.3.1.2 Effect of moisture and surface impurities

Raw glass reinforcements are very hygroscopic, which may deactivate the reaction by the water present on the surface of the untreated reinforcements. Moreover, when handling untreated glass reinforcements, all kinds of organic dust can be deposited on the surface. Depending on their nature, they can deactivate or locally disturb the anionic polymerization. Figure 1.20 shows an example of a disturbed polymerization, in which an unreacted monomer is trapped between the fibers [10]. Therefore, it is necessary to treat the surface of the glass reinforcement before introducing it into the composite for the anionic polymerization.

1.3.2 Silane treatment (Silanization)

There are many treatments to modify the surface of glass, depending on the application (e.g. plasma, Piranha etc.). Jal et al. [102] describe several techniques for the chemical

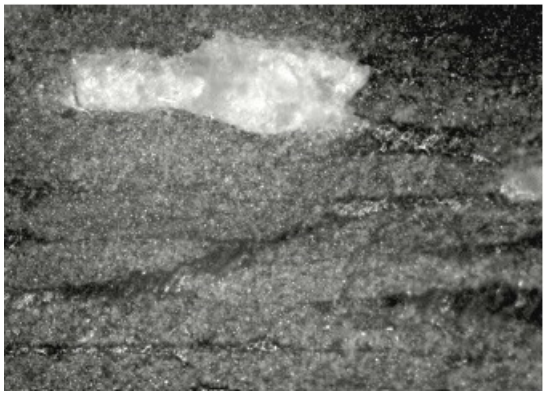

Figure 1.20: Unreacted monomer trapped between untreated glass fibers [10]

functionalization of the silica surface which is similar to the glass surface. Grafting silanes on glass surface is, however, the most conventional surface preparation technique.

1.3.2.1 Grafting mechanism of a silane on the glass surface

Coupling agents used for glass surface treatment are organosilanes, composed of a carbon chain with an " R " function at one end and a " silane " function at the other end as illustrated in Figure 1.21.

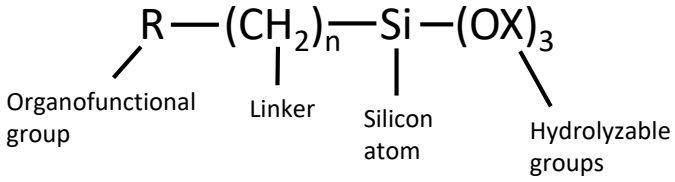

Figure 1.21: Chemical structure of an organosilane coupling agent

The "R" function interacts with the matrix at the composite interface. Thus, it must be compatible and composed of reactive functions able to create bonds with the matrix used. The "silane" function allows the grafting of the organosilane on the glass surface by hydrolysis and condensation.

The grafting mechanism of a silane on the glass surface is similar to that of the interaction between silane and silica because in both cases, the reactive functions of the surface are the hydroxyl groups. This mechanism, illustrated in Figure 1.22, is well described in the literature [102, 103]. An aqueous solution allows the hydrolysis of the silane and the formation of silanol groups. Initially, the formed silanol groups interact with the hydroxyl groups on the glass surface via hydrogen bonds. Then, the condensation of these moieties generates siloxane bonds.

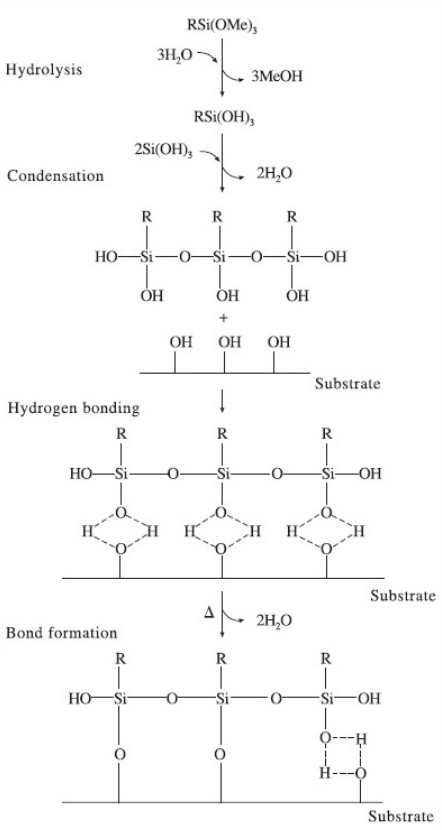

Figure 1.22: Grafting mechanism of an organosilane on the glass surface

1.3.2.2 Silane treatments compatible with conventional PA6 matrix

In the case of PA6/glass composites, the most used agents are aminoalkoxysilanes, in particular 3-aminopropyltriethoxysilane (APTES) and γ-glycidoxypropyltrimethoxysilane (GPS). Indeed, the amine functions of APTES can create covalent bonds with the carboxyl of PA6 or weak hydrogen bonds with the carbonyl. For GPS, the reaction with the amine groups of PA6 is similar to that of a typical difunctional epoxy prepolymer cured with a diamine curing agent, except that the molecular lengths of the epoxy prepolymer and curing agent are higher [104]. Under adequate conditions, each amine end group of PA6 is able to react with an epoxy group to form a branched or even cross-linked network. Generally, the silane concentrations are low, which reduces the possibility to form cross-linkings and favors the branching formation. In this case, the formation of a branched polymer is not desirable because it influences the molar masses and decreases the matrix properties [53]. For commercial PA6 with a carboxyl end group, the carboxylic acid end group can react with the epoxide to form covalent bonds. These reactions are described by Huang and Chang [105], who showed that the reactivity of the epoxide with the amine is significantly higher than that with the carboxyl. This favors the formation of branching and decreases the matrix and composite properties. As aminosilanes appear as the more suitable for the improvement of glass/PA6 composites interface, they are the most widely used coupling agents for these systems.

1.3.2.3 Interaction of silane treated surface with the *in situ* synthesis of PA6

For PA6 synthesis by AROP, the reinforcement treatments must be compatible with the reactive mixture in order to avoid disturbing the polymerization. These treatments can be divided into two types: non-reactive treatments that promote interaction at the reinforcement-matrix interface without modifying the synthesis reaction and reactive treatments that contribute to the reaction while creating bonds at the interface.

Non-reactive interactions

Non-reactive treatments aim to create an interfacial bond between the reinforcement and the matrix without affecting the polymerization and/or crystallization processes. As in the case of commercial PA6 matrix (Section 1.3.2.2), amine-terminated silanes represent good candidates to improve interfacial adhesion.

Li et al. [104] described the various potential reactions between PA6 obtained by *in situ* polymerization and the silica surface treated with two different silanes: APES (amine-terminated) and GPS (epoxy-terminated). From these results, it was shown that the epoxy groups of GPS can react with the amines of PA6, generating branching. On the other hand, the primary amines of APES are able to interact with the carbonyl of the PA6 chains through hydrogen bonds.

Van Rijswijk et al. [101] show that at high temperature (>160°C) and after a given time (>30 min), a transamidification reaction is observed between the aminosilane and the PA6 matrix during anionic polymerization. This transamidifaction makes possible the formation of covalent bonds between the aminosilane and the matrix. However, it leads to the breakage of PA6 chains as shown in Figure 1.23. Although transamidification improves the interface by creating a covalent bond between the reinforcement and the matrix, it leads to a decrease of the molar mass of the PA6 chains and thus to a degradation of the mechanical properties of the matrix.

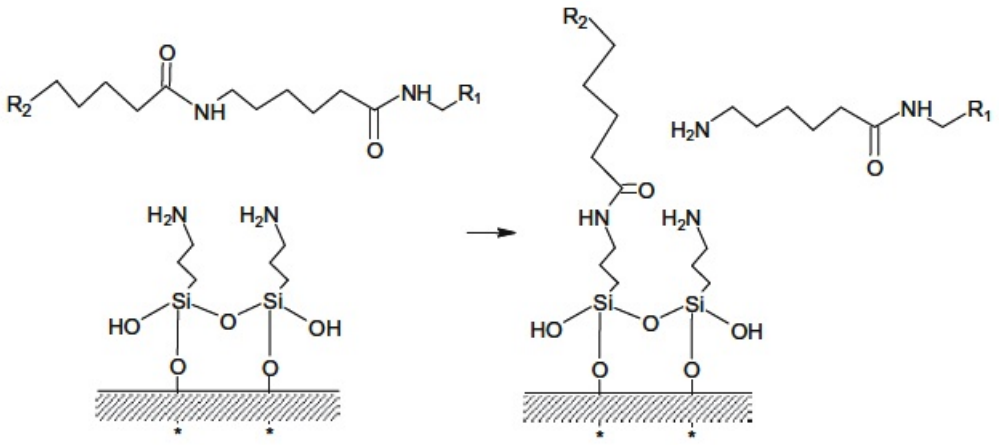

Figure 1.23: Interaction between the grafted aminosilane on the surface of glass reinforcement and the PA6 matrix by transamidification reaction [101]

Furthermore, although the primary amine protons of APES are more basic (PKa ≈30)

and less labile than those of water (PKa ≈14), they can disrupt the polymerization because caprolactam magnesium bromide catalyst (PKa ≈ 45) can take up the amine protons instead of interacting the activator [14]. Accordingly, it seems relevant to consider reactive treatments that participate to the reaction and can prevent the phenomena of either disruption or deactivation of the synthesis reaction.

Parasitic reactive interactions

Reactive treatments participate to the AROP by grafting a reagent to the surface of the reinforcement. The commonly used technique is to graft the reaction activator on the surface of the reinforcement, which initiates the reaction from its surface and thus creates an interfacial covalent bond between the reinforcement and the matrix (see also Section 1.4.4).

With N-acetylcaprolactam activators, a deblocking reaction occurs at high temperature (about 160°C) that creates an isocyanate group (step 1 of Figure 1.24). The latter can thus react with the amide group of PA6 and lead to the formation of branching (step 2a of Figure 1.24) [101]. In addition to the formation of branching, the released isocyanate groups generated by the deblocking of the hexamethylene-1,6-dicarbamoylcaprolactam activator can form urea bonds with the aminosilanes present on the glass surface (Van Rijswijk et al. [101], step 2b of Figure 1.24). The reaction of isocyanates with amines is very fast and starts at low temperatures (60-80°C). This leads thus to the activator grafting on the fiber surface.

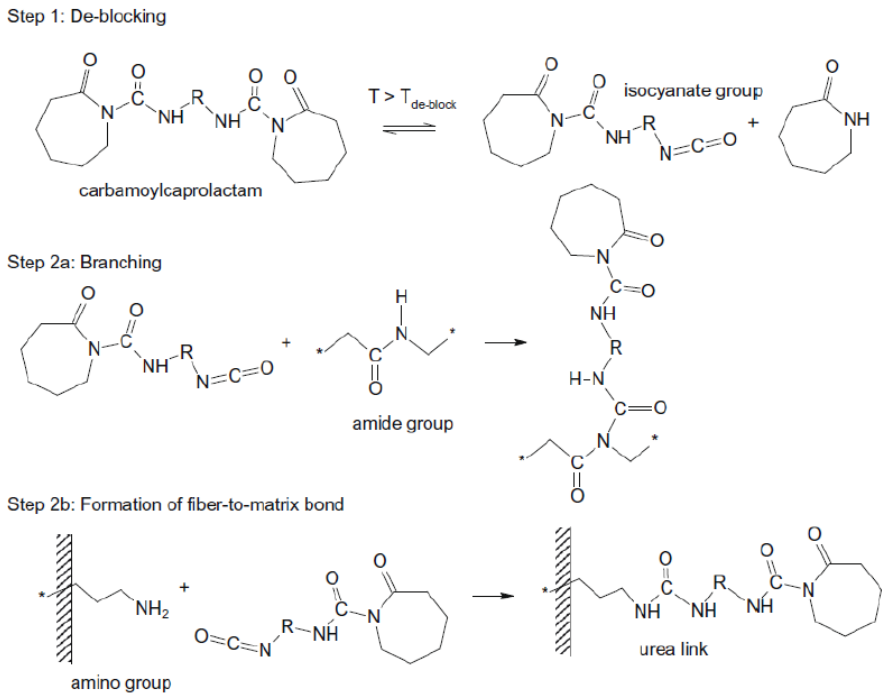

Figure 1.24: Activator deblocking. Step 1: Deblocking, Step 2a: Branching formation, Step 2b: Formation of the covalent bond between fiber and matrix through the urea bond [101]

As a result, the activator can be present in the reactive mixture in two configura-

tions, according to the deblocking equilibrium: the blocked configuration that allows the polymerization of the monomers and the deblocked configuration that results in the interfacial bonding and branching. When the synthesis temperature is above the deblocking temperature, the activator exists more in its deblocked configuration, which increases the possibility to form an interfacial bond rather than initiating polymerization [101]. This leads to a reduction in the molar masses of the PA6 chains and to the decrease of the matrix properties. In addition, the reaction of the activator with the silane amine decreases the concentration of the activator, which affects the formulation of the reaction mixture. Note that this reaction depends on time and can be limited by the reaction of the activator with a monomer through fast synthesis kinetics.

1.3.3 Effect of interfacial interaction on composite properties

1.3.3.1 Effect on crystallization

The crystallization mechanism is composed of two steps: germination (or nucleation) and crystal growth. The primary germination corresponds to crystal seeds formation. Once the primary germination is initiated, the crystalline growth starts from the formed seeds by successive addition of the chain segments on the growth front.

The study of Bessell et al. [106] shows the effect of the sized fibers on the crystallization mechanism of PA6 obtained by AROP. It was shown that the crystallization changes randomly. The non-uniform distribution of the sizing on the surface of the fibers explains the irregularities of the crystal growth. Indeed, the coupling agent locally dissolved in the PA6 during polymerization can participate to the nucleation. This coupling agent contribution to nucleation and crystal growth was confirmed by its reduction when the sizing was removed. However, a slight nucleation was always observed after removing the sizing, which may be due to the glass surface. Even if the type of coupling agent was not described in this study (used of commercial glass fibers with a PA6 compatible coupling agent), coupling agents are generally silanes, especially aminosilanes. From that, it can be stated that the silane contributes to the nucleation during the synthesis and promote crystallization.

On the other hand, Van Rijswijk et al. [101] estimate that the creation of a covalent bond between the reinforcement and the matrix could decrease the degree of crystallinity. Indeed, these interfacial bonds seem to limit the mobility of the polymer chains, which disturbs the crystallization process. Reducing the crystallinity degree tends to decrease the strength and stiffness of composites. This is specially true in humid conditions due to the important water absorption of the amorphous phase and related plasticizing effect of water.

1.3.3.2 Effect on mechanical properties

Several studies have described the consequences of the surface treatment of glass reinforcements on the mechanical properties of the PA6-based composite. Some examples will be presented in this section.

Rusu et al. [107] studied the impact of the treatment of silica nanoparticles with APTES and of the silica content on the mechanical properties of PA6/Silica composites. The composites were synthesized by *in situ* anionic polymerization. Figure 1.25 shows the flexural strength and modulus curves of treated and untreated particles according to the particle content. Particle silanization allows a significant improvement of both flexural strength and modulus. The flexural strength improvement with particle treatment can be explained by the improvement of the interface adhesion between the reinforcements and the matrix. The higher composite flexural modulus obtained with treated particles indicates that modified particles can restrict the mobility and deformability of PA6 macromolecules. Furthermore, the decrease observed above 4.0% by mass of both treated and untreated particles is due to the agglomeration of the nanoparticles that decreases the filler surface area and thus the polymer-filler interface. This leads to a decrease of the interfacial interactions and consequently of the flexural strength. It was also shown that the particle silanization increases significantly the impact resistance, which is again explained by the improved adhesion between the particles and the matrix [107].

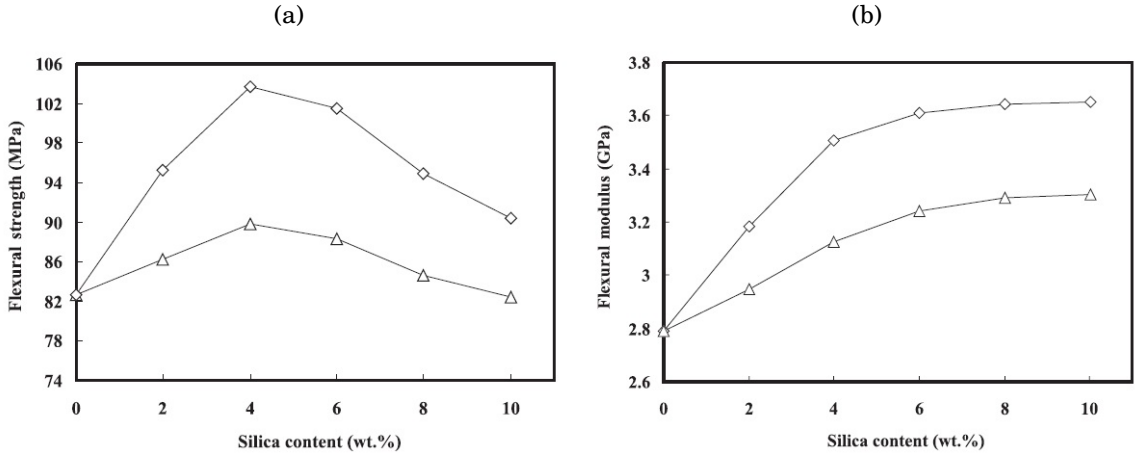

Figure 1.25: (a) Flexural modulus and (b) flexural strength versus silica particle content for Nylon 6/SiO2 nanocomposites: (Δ) untreated and (◇) silanized particles [107]

In the same context, Li et al. [108] showed that the treatment of silica particles with aminosilane APTES leads to a better the dispersion of the reinforcement in the matrix and avoids the aggregation. Also, the interfacial interaction between the treated silica and the matrix significantly improves the flexural (modulus and strength) and impact properties of the PA6/silica composite. Such improvement of properties is due to the interaction between the primary amines of APTES and the carbonyls of PA6 via hydrogen bonds. A critical value of silane concentration is observed for which interactions and mechanical properties are maximal. Beyond that point, the significant entanglement of the molecular

chains at the interface due to the excess of NH_2 groups prevents their movements in the proximity of the reinforcement which thus decreases the interfacial interactions. Besides, a low concentration of aminosilane reduces the interfacial bonds, which in turn decreases the mechanical properties

1.3.4 Effect of processing conditions on the interfacial interactions and final properties

Van Rijswijk et al. [101] investigated the effect of mold temperature on the formation of interfacial bonds between the activator and the aminosilane on the fiber surface and its influence on the mechanical properties of anionic PA6/glass fiber composites. The fibers were silanized by APTES. It was shown that the interface performance is enhanced at high mold temperature for two reasons :

- the activator is mostly in the deblocked form in this case, which favors the formation of interfacial bonds (Section 1.3.2.3),
- the chains initiated in the proximity of the fiber also reach higher lengths and can create more entanglements with the other chains.

When an interfacial bond is created between the activator and the aminosilane, it thus improves the inter-laminar shear strength of the composite. However, the properties of the matrix decrease at high temperatures. As a result, there is some compromise to find between two issues. In the case considered by the authors, it was shown that a temperature of 180°C allows to achieve optimal properties for the composite [101].

1.3.5 Conclusion

Existing studies of the literature have shown that using raw surface for glass reinforcement is not relevant for the anionic PA6 synthesis. Therefore, the grafting of a silane coupling agent is necessary to remove hydroxyl groups, increase the interfacial interactions and, consequently, improve the composite interface performance.

Although grafting of silanes brings many benefits, it must ensure good compatibility with the matrix. Indeed, a not suitable silane may have a negative influence on the polymerization of the reactive mixture. Therefore, several silane-based strategies are used to improve the glass reinforcements/PA6 interactions. However, there are very few works dedicated to the specific case of PA6 matrix synthesized by AROP.

The surface modification by a silane is performed in many steps. Moreover, several factors can influence the grafting mechanism, which in turn influences the properties of the resulting composite. Therefore, it is necessary to review the different steps of the glass reinforcement surface preparation in order to control and optimize such grafting mechanism

1.4 Glass surface modification with silanes

The surface modification of the glass reinforcements starts with a calcination treatment that cleans the surface from organic contaminants and leads to the condensation of hydroxyls groups (dehydroxylation). Although the -OH groups negatively influence the synthesis of anionic PA6, they represent the further silane grafting sites on the glass surface. So after that, a surface activation is necessary to regenerate the hydroxyls (rehydroxylation) essential for the reaction with the silane. Finally, the silane is condensed on the surface after its hydrolysis

In order to optimize such protocol, it is important to study separately each step of the glass surface modification. Moreover, the condensation of the silane in the presence of water leads to a loss of its reactivity. Therefore, understanding the hydrolysis and condensation phenomena is necessary to control the silane grafting on the glass surface.

1.4.1 Calcination (dehydroxylation)

In most cases, the surface cleaning of glass fibers is carried out by calcination to remove impurities and previously applied treatments from the surface. After calcination, the condensation of silanol groups at high temperature leads to the creation of siloxane groups, which reduces the number of hydroxyl groups (dehydroxylation). It is thus of main importance to monitor the density of OH groups after calcination treatment and to understand the influence of calcination parameters (specially temperature and time) on the resulting number of hydroxyl groups. Indeed, an adequate calcination treatment will limit the negative effect of hydroxyls on the synthesis reaction without preventing the silane grafting.

Young [109] has studied the influence of the calcination temperature on the number of condensed hydroxyl groups (during dehydroxylation) that could be regenerated (rehydroxylation). He observed that rehydroxylation was only possible up to some calcination temperature threshold, above which the condensation of some hydroxyl groups became irreversible and the number of hydroxyl groups that could be regenerated decreased. Such irreversibility can be explained by two mechanisms:

- Mechanism 1: The condensation of two neighboring silanol groups could result in a Si-O-Si bond under considerable strain if the two silicon atoms were not separated by an appropriate distance. Thus, it can be assumed that such a bond could be rehydroxylated due to the stress itself or the proximity of the neighboring silanol sites. However, with heating to higher temperatures, the surface mobility could be sufficient to relieve the stress, perhaps by forming a different type of surface bond, and thus the siloxane group formed would no more be susceptible to rehydroxylation [109] (Figure 1.26(a)).

- Mechanism 2: one assumes the possibility of the presence of more than one hydroxyl group attached to the surface silicon atoms. In this case, the elimination of a single water molecule at lower temperatures would leave a site that could physically adsorb water and thus initiate rehydroxylation. When the second hydroxyl group is removed at higher temperatures, the site would no more physically adsorb water and that part of the surface could not be rehydroxylated [109] (Figure 1.26(b)).

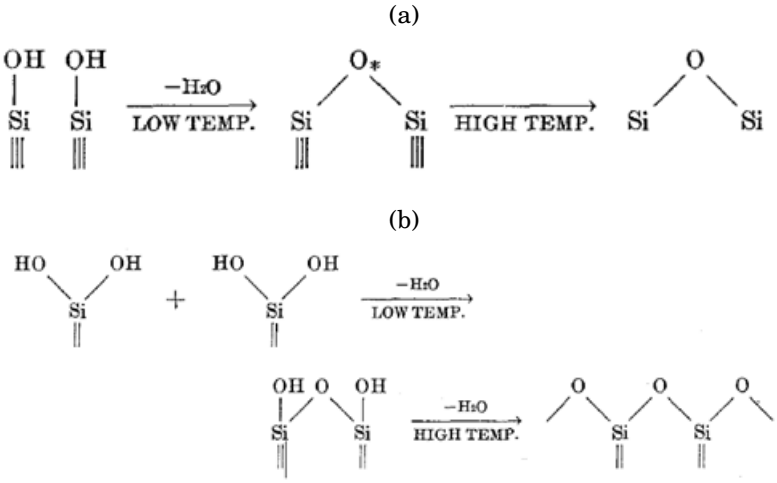

Figure 1.26: Effect of calcination temperature on neighboring silanol groups condensation according to (a) mechanism 1 and (b) mechanism 2 [109]

More specifically, the maximum number of dehydroxylated sites that could be reversibly rehydroxylated was reached for a calcination temperature of 450°C as shown in Figure 1.27. This tendency was confirmed by Hair [110], who studied the evolution of the hydroxyl groups surface density as a function of the calcination temperature by IR spectroscopy. Zhuravlev [111, 112] has also identified the temperatures of dehydration, dehydroxylation and rehydroxylation, and demonstrated that dehydroxylation and siloxane formation could occur over a temperature range comprised between 200°C and 400-500°C, while full regeneration of hydroxyl groups in this range could be completed. In agreement with previous works, the concentration of hydroxyl groups decreased above this temperature range and only partial regeneration was possible.

From these studies, calcination at 450°C appears to be the best configuration for maximum reversible dehydroxylation. Such a temperature thus preserves all of the hydroxyls that can be rehydroxylated, which is an important consideration for the silanization process (Section 1.3.2.1). Yet, it should be underlined that the influence of the calcination time remains much less studied and understood by the literature.

1.4.2 Surface activation (rehydroxylation)

The activation of the glass reinforcements surface aims at hydrolyzing the siloxane groups and regenerating the hydroxyl groups that further represent interaction functional groups

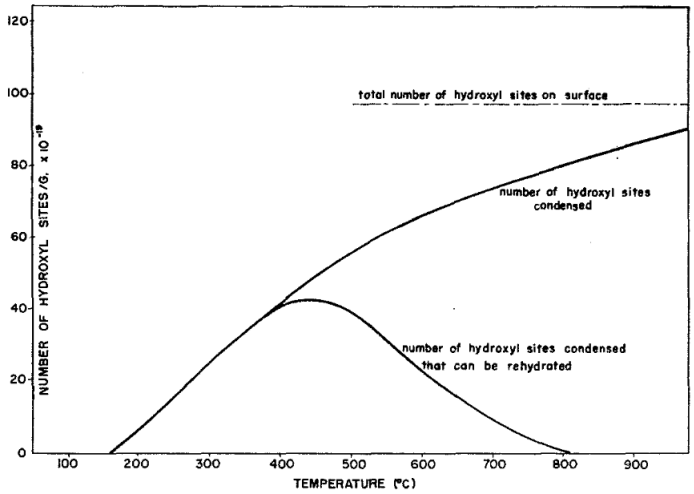

Figure 1.27: Evolution of the number of condensed hydroxyl groups that could be regenerated [109]

for coupling agents. Surface activation is sometimes used as a treatment as it induces the formation of hydrogen bonds between the amide functions of PA6 with hydroxyls. In the case of AROP, this is not suitable because of the inhibition of the AROP by the hydroxyls. However, it is a required step for grafting well adapted sizing functions by condensation.

Different protocols exist for activating a glass surface. Immersion in a Piranha solution (a mixture of sulfuric acid and hydrogen peroxide) is an efficient technique for the generation of Si-OH functional groups [113–115]. However, this technique is difficult to be considered industrially and the mixture is extremely aggressive and highly reactive. Mutua et al. [116] compared three glass microspheres treatments (a Piranha solution, an aqueous hydrochloric acid (HCl) solution and an aqueous sodium hydroxide (NaOH) solution) before beads silanization with an aminosilane (APTES). It was concluded that the treatment in hydrochloric acid allows the better interaction of the microspheres with the aminosilane thanks to the significant generation of hydroxyl groups. The sodium hydroxide treatment also leads to a good fixation of the silane (but less important than hydrochloric acid), while Piranha treatment shows the lowest content of silane on the surface due to a weak rehydroxylation. Finally, Gonzalez-Benito et al. [117] compared the rehydroxylation process of glass fibers in water with neutral pH and in 10% aqueous HCl acid solution. The results show that rehydroxylation in HCl acid induces the regeneration of more hydroxyl groups. Sever et al. [118] confirmed the efficiency of rehydroxylation in acid solution and also observed that the increase of the treatment time increases the quantity of silanol groups.

1.4.3 Factors influencing the silane grafting on the surface

After rehydroxylation, hydroxyl groups become available again on the glass surface. Hydrolysis of silane leads to silanol Si-OH groups able to form covalent bonds with surface hydroxyls by condensation reactions (see Figure 1.22). This section focuses, in particular,

on the factors influencing the grafting mechanism

1.4.3.1 Hydrolysis time

Ideally, the silane hydrolysis generates a significant amount of silanol groups. However, the hydrolysis of the silane is coupled with its condensation, reducing its reactivity. The study of Brochier et al. [119] aims to follow the evolution of the reactive functions of 14 various silanes in an aqueous solution under acidic conditions by NMR of silicon (^{29}Si). The results showed that the maximum reactivity of trimethoxysilane (APTMS, DAMS and TAMS) is reached very fast (before 1h of reaction). On the other hand, triethoxysilane (APTES and IZPES) and other silanes reach their maximum reactivity after 2h and 3-6h of reaction respectively. For example, the hydrolysis of APTES was about 61% after 2h of reaction, while the hydrolysis of APTMS was about 74% after only 33 min. This shows that methoxy groups are hydrolyzed more rapidly than ethoxy groups. Furthermore, a very important and fast decrease of reactivity was observed for the amino silanes that lost between half and three quarters of their reactivity after 6h of reaction. For the majority of the other silanes not containing amine, the reactivity decreases slowly and regularly.

Consequently, it seems that the optimal time for hydrolysis is 40 min to 50 min before the addition of the glass reinforcement. Indeed, this time promotes the hydrolysis and thus, allows to reach a maximum of reactive functions of the silane during the treatment. Moreover, it has been concluded that trimethoxysilanes are better than triethoxysilanes since they allow a faster and more efficient hydrolysis, and therefore they provide a better reactivity.

1.4.3.2 Influence of silanization time and silane concentration

Sever et al. [118] studied the effect of silanization time on the surface modification of glass fibers by FTIR spectroscopy. By comparing the spectra of silanized fibers with those of untreated fibers, it was shown that silanization time has an influence on the interaction between the silane and the glass fiber. Unfortunately, no overall trend could really be deduced from these results. However, authors observe that increasing the silanization time beyond 30 min and up to 60 min increases the contact angle between the silanized glass fibers and water drop. This is due to the formation of very thick layers of silane on the surface of the glass fiber that provide them a hydrophobic character (see also the following section). Note that the study of Sever et al. [118] is restricted to silanization times up to 60 min, and the study of treatment for longer times would be very relevant.

On the other hand, the concentration of the silane has also a very important effect on the treatment. Sever et al. [120] also studied the influence of the concentration of γ-glycidoxypropyltrimethoxysilane (GPS) on the properties of GF/epoxy composites, that can be extrapolated to the case of GF/PA6. Three silane concentrations were used (0.1, 0.3, and 0.5%). The results show that silanization at 0.5% gives the best composites mechanical properties with for instance an increase of around 37% in tensile strength compared

to untreated case. However, some authors have also noted an increase in mechanical properties at concentrations above 0.5% [108, 121]. Therefore, such a concentration is insufficient and it is necessary to increase it to more than 0.5% to determine optimal silane concentration.

1.4.3.3 Interaction between aminosilanes and glass

Aminosilanes, especially 3-aminopropylalkoxysilanes, are widely described in the literature and represent the silanes commonly used for the treatment of glass or silica reinforcements [101, 104, 108, 121–125] . They are also widely used in PA6-based composites for their compatibility with these matrices through the amine functions (Section 1.3.2).

The presence of amine functions provides unique properties to aminosilanes. Indeed, the amine groups can catalyze, in an inter- or intramolecular way, the reaction between silane molecules and silanol groups on the surface to form siloxane bonds. As a result, aminoalkoxysilanes are more reactive than alkylalkoxysilanes in the presence of water, which can lead to uncontrolled polymerization of the aminosilanes and thus form multilayers, as illustrated in Figure 1.28 [126, 127]. In addition, the amine groups can create hydrogen bonds with surface silanol groups, resulting in weakly attached silanes on the surface. Furthermore, covalently bonded aminosilane layers generally have an inhomogeneous grafting distribution due to the presence of vertically positioned silane molecules and horizontally positioned silane molecules [127].

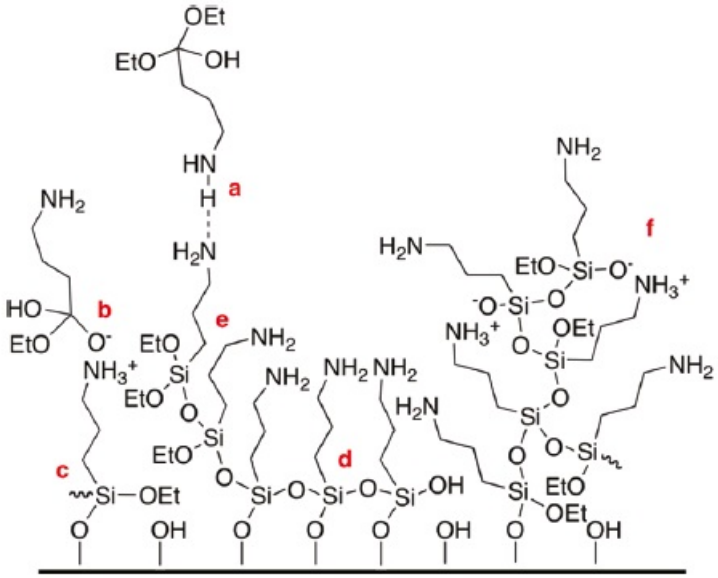

Figure 1.28: : APTES-derived layers with structural irregularities: individual silane molecules can be included in the layer via (a) hydrogen bonds, (b) electrostatic attraction, (c) covalent bonds with the substrate and (d) horizontal and (e) vertical polymerization with neighboring silanes; (f) the silane oligomers/polymers created can react and/or interact with functionalities present at the fiber/matrix interface [127]

Aminosilanes can also lead to a hydrolysis of the siloxane functions due to the catalyzing effect of the amine functions, which results in a loss of the silane layers in aqueous solution. Consequently, this negatively influences the functionalization of the glass surface. For this reason, Asenath Smith and Chen [126] aimed to minimize the loss of functionality of silanes by optimizing the silanization conditions. It was shown that hydrolysis, catalyzed by the amine functions, can be minimized by controlling the length of the alkyl chain. Thus, aminosilanes with longer alkyl chains than propyl may also be good candidates for treatment in aqueous solutions. This is due to steric hindrance created by a longer alkyl chain that prevents catalyzing silane detachment by hydrolysis.

1.4.4 Reactive silanes

It was shown in Section 1.3.2.3 that aminosilane, especially APTES, can lead to parasitic reactions that reduce the activator concentration, affect the matrix properties and, consequently, decrease the resulting composite properties. To overcome these problems, it is possible to graft the activator on the reinforcement surface, allowing to initiate the polymerization from the surface and avoid parasitic reactions. The first technique is based on the reaction, described by Van Rijswijk et al. [101], between the deblocked isocyanate and the silane primary amine. The technique starts by grafting an aminosilane (APTES) to the surface of the reinforcement. Then a diisocyanate is deblocked by heating the activator to a temperature of around 160°C. The resulting isocyanates react with the silane amines to form urea bonds. Thus, this grafted activator initiates the polymerization reaction from the surface of the reinforcement and allows the creation of covalent bonds at the interface. However, this technique is very long because it involves several steps. Moreover, it is difficult to control the activator deblocking. In addition, APTES silane can form uncontrolled multilayers as explained in the previous section, and steric hindrance may limit the number of NH_2 functions accessible by the deblocked molecule.

Another functionalization technique to graft the activator to the surface of the reinforcement was described by Yang et al. [128]. Their work focused on the modification of the surface of carbon nanotubes using hydroxyl groups as reactive sites for grafting the activator. Their technique can therefore be applied to glass reinforcement which surface is also covered with hydroxyl functions. According to this study, the supposed mechanism of activator grafting for the functionalization of glass reinforcements is described in Figure 1.29. It consists, firstly, to graft a Toluene DiIsocyanate (TDI) on the surface through the reaction of the para isocyanate with the hydroxyls present on the reinforcement surface. Then, the other free isocyanate reacts with the ϵ-caprolactam monomer to form the N-acetylcaprolactam function of the activator, which allows to initiate the polymerization reaction

However, this technique has several drawbacks. First, the free isocyanate could react with another hydroxyl group of the neighboring reinforcement because the reaction with the hydroxyl of the same reinforcement is limited by steric hindrance. Therefore, this

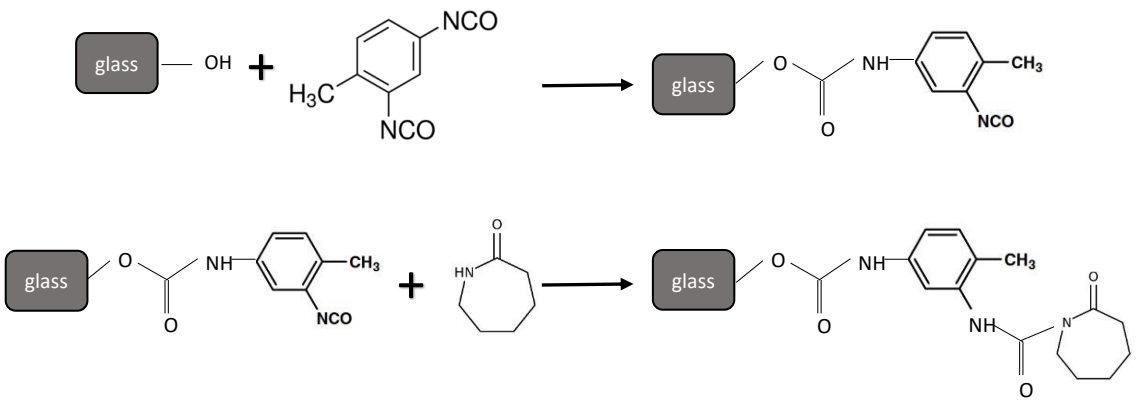

Figure 1.29: Mechanism for grafting the activator to the surface of glass reinforcements using Toluene DiIsocyanate (TDI)

consumes all the isocyanate groups of the TDI, avoids the reaction between the isocyanate group and the monomer and therefore prevents the formation of the N-acetylcaprolactam function. In addition, TDI is extremely reactive, carcinogenic and toxic. Thus, its handling is difficult and requires rigorous precautions.

1.4.5 Conclusion

In this section, it was underlined that an adequate calcination treatment limits the negative effect of hydroxyls on the synthesis reaction. More specifically, calcination at 450°C seems to be optimal choice since it offers a good compromise for a maximum reversible dehydroxylation. However, as far as we know, the study of the influence of calcination time has not yet been studied in the literature. In addition, rehydroxylation in an aqueous solution of HCL acid allows to regenerate a maximum of hydroxyl groups that could react with the silane during the grafting process. Regarding silanization, it appears as the best treatment to improve fiber-matrix adhesion during the manufacture of PA6/glass composites by *in situ* synthesis. Silanes require a hydrolysis time in order to achieve maximum reactivity, which can be defined between 40 and 50 min. Moreover, the concentration of the silane and the silanization time are crucial for the grafting. Typically, a silanization at more than 0.5% for a minimum treatment time of 60 min seems to give an efficient grafting. At last, the aminosilanes, that are the most used agents for PA6/glass composites, have several characteristics, especially the formation of multilayers. These features change according to the structure of the aminosilane. Accordingly, strong attention should be given to the compatibility of the considered silane with the matrix and to the types of interactions between glass reinforcements and PA6 matrix obtained by AROP.

1.5 Conclusion

This literature review highlights the interest of the PA6 reactive system for the thermoplastic composites manufacturing by liquid process. However, the strong coupling between polymerization and crystallization and the reaction sensitivity to the environment induce a complexity to control the synthesis. One of the key parameters of this synthesis during the composite manufacturing is the interaction with the reinforcement. Indeed, the difficulty to properly tune the surface chemistry of glass reinforcements is probably one of the reasons why only a few works relate the role of interfacial interaction on the anionic polymerization and anionic PA6/glass composite properties. To date, the few works that investigate the role of glass surface chemistry on the PA6 AROP, focuses on a single type of silane, namely aminosilane. It is widely used with conventional polyamides: hydrogen bonds are created between the PA6 carbonyl and the primary amine of the silane. Yet, the nature of the silane coupling agents is a crucial parameter for optimizing the composite properties. It controls the interfacial bonds between the matrix and reinforcement, and so, the reinforcement-matrix adhesion and the resulting composite properties. Moreover, the control of the hydroxyl groups present on the glass surface is also an important parameter for the synthesis optimization since they disturb the reaction. Despite its undeniable interest, the influence of the surface chemistry on the properties of glass reinforcements/PA6 composites obtained by AROP still needs to be investigated.

Controlling interfacial interactions at the reinforcement-matrix interface by monitoring hydroxyl groups and silane coupling agent grafting can improve the synthesis kinetics and the composite properties. Therefore, it is, first, necessary to investigate the effect of the hydroxyl groups density on the anionic PA6 synthesis kinetics. Secondly, the large variety of silanes requires a thorough study of their interactions during and after the anionic PA6 synthesis reaction, in order to propose a treatment adapted to the chemistry of the reactive system. For example, it was shown that the use of a silane other than APTMS with a different alkyl chain length is interesting for the creation of more homogeneous and stable silane layers. Moreover, the techniques described in the literature for the grafting of a reactive treatment are difficult to apply because of their complexity. For this reason, it is necessary to develop a new technique for the grafting of one of the reagents on the reinforcement surface. This allows to create covalent bonds at the interface to improve its performance. Finally, the role of surface treatments and interfacial interactions on the mechanical properties of anionic PA6/glass reinforcement composites should be further investigated. This allows thus to optimize the reactive thermoplastic composites manufacturing process through suitable synthesis kinetics and to improve the resulting composite properties.

CHAPTER 2

TAILORING THE HYDROXYL GROUPS DENSITY OF GLASS SURFACE FOR AROP OF PA6

Contents

2.1 Materials **47**

2.1.1 Reinforcement 47

2.1.2 Reagents for PA6 synthesis and silane 49

2.1.3 Reactive mixture preparation 50

2.2 Characterization of PA6 synthesis by Differential scanning calorimetry (DSC) **51**

2.2.1 Sample preparation 51

2.2.2 DSC analysis 51

2.3 Preliminary tests: Influence of the hydroxyl groups density **51**

2.3.1 Preliminary Silanization 52

2.4 Control of the hydroxyl groups surface density and adaptation of the silanization process to the anionic PA6 synthesis **55**

2.4.1 Analysis techniques 55

2.4.2 Characterization of the surface density of hydroxyl groups on glass particles 57

2.4.3 Comparison of the rehydroxylation protocols 63

2.4.4 Controlling the –OH quantity regenerated during the silanization treatment 64

2.4.5 Polymerization and crystallization kinetics after silane grafting . 66

2.5 Conclusion **70**

Introduction

In the case of polyamide 6 (PA6) matrices obtained by anionic ring opening polymerization of ϵ-caprolactam monomers, the reactive mixture, also comprising a catalyst and an activator reacts in contact with the surface of the glass reinforcement during the composite manufacturing. The literature review shows that the surface of glass fibers is not suitable for anionic ring-opening polymerization. Indeed, the hydroxyl groups on the glass surface disturb the polymerization reaction due to the labile protons that deactivate the catalyst. This can also lead to a significant reduction in the degree of monomer conversion [10]. Consequently, the use of an organosilane coupling agent is a good option to remove the hydroxyl groups from the surface of glass fiber while enhancing adhesion at the fiber-matrix interface when the end of the organosilane is well chosen. Indeed, silanes form covalent bonds by reacting with the hydroxyl groups at the glass surface, via condensation reactions. For this reason, carefully controlling the grafting protocol of a silane at the glass surface, before composite manufacturing, is essential. Alkoxysilane coupling agents are usually grafted at the surface of glass fibers from an aqueous solution. Accordingly, treatment in an aqueous solution can also lead to rehydroxylation of the glass surface, and regeneration of the hydroxyls from the siloxane groups [111, 117]. As a result, rehydroxylation increases the surface density of hydroxyl groups, impacts the grafting degree of organosilanes, and ultimately increases the residual hydroxyl groups surface density. Therefore, grafting silanes on glass fibers is clearly a delicate and complex dynamic process resulting from a competition between the condensation of the silanes on the surface, which decreases the number of -OH groups, and rehydroxylation, which leads to a regeneration and an increase in the surface concentration of these groups. This competition depends on several factors especially silanization time. In order to improve the properties of anionic PA6 based composites, optimizing the surface treatment of particulate or fiber reinforcements must therefore be realized in association with an adequate control over the polymerization process of the matrix. While the effect of calcination temperature on the hydroxyl groups surface density has been extensively investigated (section 1.4.1), a special attention is dedicated in this chapter to the effect of calcination time. In addition, the effect of the silanization treatment time, and the competition between the condensation and rehydroxylation reactions during the silanization process in an aqueous solution, will be investigated.

This chapter is divided into several sections. Firstly, the choice of the materials used throughout the study will be presented and justified. Then, the procedure of the *in situ* synthesis of PA6 and PA6/glass composite in DSC will be detailed. Secondly, preliminary tests showing the influence of hydroxyls on the synthesis reaction will be presented. Based on these tests, a study will be carried out to bring a better understanding regarding the surface treatment protocols for the preparation of glass composite reinforcements, by means of a systematic and rigorous monitoring of the –OH surface density during the silanization steps. This methodology is implemented using techniques such as TGA

coupled with IR spectroscopy. Finally, the impact of the silane grafting protocol is evaluated on the polymerization and crystallization kinetics of the model system composed of a PA6 matrix synthesized by anionic ring opening polymerization, reinforced by silanized glass microparticles, by means of DSC measurements.

2.1 Materials

2.1.1 Reinforcement

2.1.1.1 Choice of reinforcement

Mortazavian et al. [129] showed that fiber orientation influences mechanical properties of PA6/short glass fiber composites, especially tensile strength and elastic modulus. Güllü et al. [130] also studied the influence of fiber length on mechanical properties of this composite system and showed that increasing the fiber length improves the tensile strength. These effects of fiber length and orientation on mechanical properties were also observed for other types of composites [131]. The fiber length and orientation also influence the mechanical properties of long fiber reinforced PA6 based composite [132]. Han et al. [97] showed that the mechanical properties of PA6 / long glass fiber composites (with an average diameter of 10 μm) are influenced by the fiber length and mainly by the fiber-matrix interface.

This work aims to analyze the interfacial interactions between the glass reinforcement and the anionic PA6 resin during the *in situ* composites synthesis. It was shown previously that the properties of short or long fiber reinforced composites depend on the fiber length and orientation and the fiber-matrix interface. Accordingly, we chose glass micro-particles of a size representative of glass fibers diameter as reinforcement, which are model particles for the anionic PA6/glass reinforcement system in order to focus on interface effects and avoid combined influence of fibers length and orientation.

Glass microparticles were purchased from SOVITEC company (France) with an average diameter of 4 μm. A SEM image of the raw glass beads is presented in Figure 2.1. This particle size was chosen according to two criteria: (1) the diameter was chosen in order to have a surface area equivalent to the fibers with a diameter of 5 μm in a composite with a fiber volume content of 60% which is the most commun fiber volume fraction in the composite industry; (2) the volume fraction of microparticles should not exceed 30% in order to facilitate the mixing process during the mixture preparation.

2.1.1.2 Size distribution

The measurement of the particle size distribution allows to confirm the average diameter given by the supplier's data sheet, which is 4 μm. Moreover, the hydroxyl density and the grafting degree depend mainly on the specific surface area, which also depends on the diameter distribution. Therefore, it is necessary to thoroughly determine this diameter

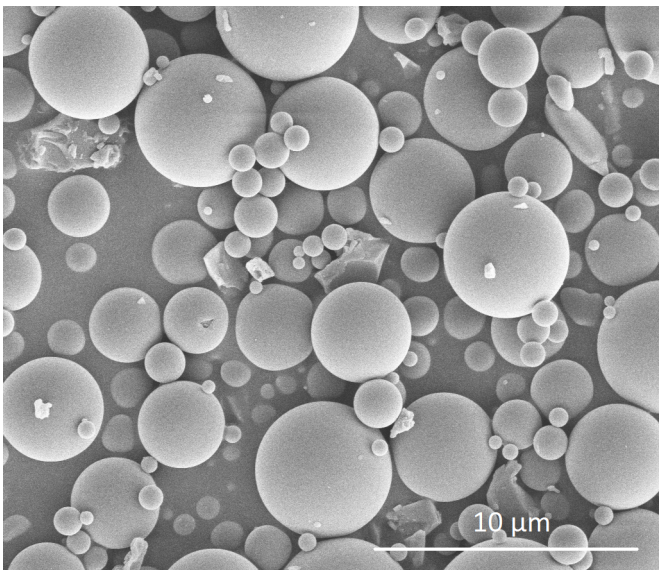

Figure 2.1: SEM observation of as-received glass micro-particles

distribution in order to estimate the accuracy in the surface calculation in the subsequent analyses.

The measurement of the particle size distribution was performed with a MasterSizer 3000, Malvern Panalytical. This granulometer allows to characterize particles from 0.01 to 3500 μm according to laser diffraction principle. The measurement was carried out with a dry process, in which the powder is dispersed in an air flow of variable pressure. This pressure was set at 3.5 bars in order to obtain an optimal dispersion.

The granulometer results give several characteristics to define the size distribution, they are presented in Table 2.1. The results show that the average diameter by volume of 4.01 μm is consistent with the average diameter given by the supplier. The D10 shows that 10% of the particles have a diameter lower than 1.46 μm. By combining it with the D50 which suggests that 50% of the particles have a diameter less than 3.68 μm, it can be concluded that most of the particles have a size between 1.46 and 3.68 μm. This is confirmed by the D90 which indicates that 90% of the particles are less than 7.14 μm in diameter. These results also show that some particles can have a diameter greater than 7.14 μm or less than 1.46, which indicates a fairly broad particles size distribution. To confirm these results, the size distribution was characterized.

Figure 2.2 shows the volume percentage of particles as a function of diameter. The particles have a broad distribution, the largest sizes being up to about 12 μm while few particles measure less than 500 nm. Such distribution can affect the specific surface area measurement, because small particles tend to form aggregates, which can influence the estimation of the hydroxyl and/or silane grafting group densities.

Table 2.1: Description and values of the diameters obtained by laser granulometry

Diameter	Description	Values (μm)
D10	10% of the particles volume are below this size	1.46
D50	50% of the particles volume are below this size (median diameter)	3.68
D90	90% of the particles volume are below this size	7.14
D[4,3]	Average diameter by volume	4.01

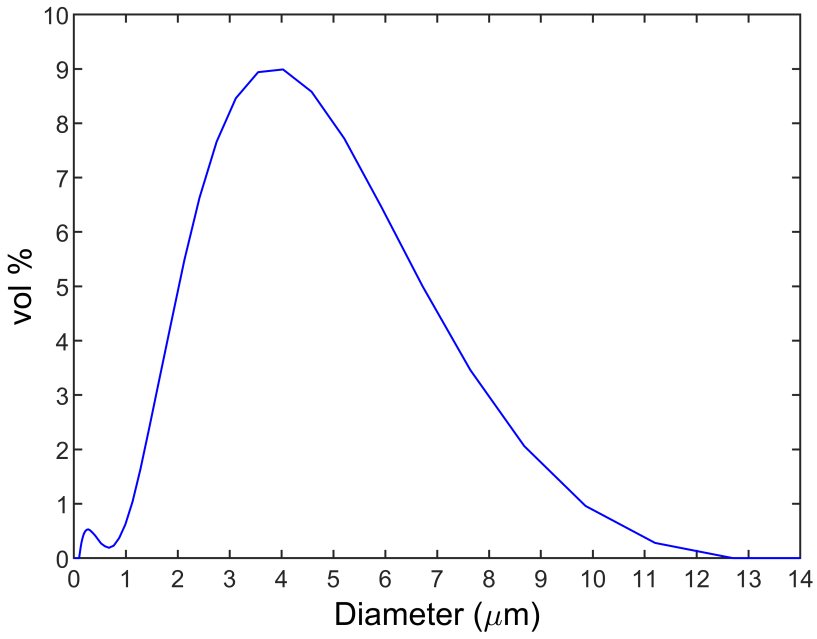

Figure 2.2: Percentage by volume of particles as a function of diameter

2.1.2 Reagents for PA6 synthesis and silane

The reagents for the anionic ring opening polymerization of PA6 are chosen according to Vicard's work [23], they are the following:

- Monomer ϵ-CL under the tradename "AP-NYLON® Caprolactam"
- Catalyst-caprolactam magnesium bromide (MgBrCL) - "Nyrim® C1" (1.4 mol.kg $^{-1}$ in caprolactam)
- Activator-bifunctional hexamethylene-1,6-dicarbamoylcaprolactam (HDCL) - "Brüggolen® C20P" (2.0 mol.kg $^{-1}$ in caprolactam)

Indeed, the type of reagents has a significant influence on the synthesis kinetics. Among the reactive systems mentioned in Section 1.1.1.2, MgBrCL catalyst coupled to HDCL activator seems to be suitable for reactive composite manufacturing. Indeed, this reactive system, whose reaction mechanism is described in Figure 1.2, requires an initiation time

to ensure higher mold filling times and a good impregnation before the initiation of the polymerization [15]. In addition, the total synthesis time is relatively short after the polymerization starts [13, 23].

The reagent were all kindly supplied by the Brüggemann Chemical company, Germany (5 kg of AP-NYLON® Caprolactam, 1 kg of Nyrim® C1 and 1 kg Brüggolen® C20P). Thus, the whole study was performed with the same reagent batch.

Furthermore, it was shown in Section 1.1.2.2, that the ratio between the catalyst and the activator has a significant influence on the polymerization kinetics [15]. The formulation of MgBrCL/HDCL used for all the study was 0.79/1.10 mol% of CL. This ratio provides a reasonable compromise between the initiation time at low temperature and the total polymerization time [23]. We target a time as fast as possible to be suitable for the composite industry.

The silane 3-(2-aminoethylamino)propyltrimethoxysilane (AEAPTMS, 96%) was supplied by Fisher Scientific.

2.1.3 Reactive mixture preparation

For studying the polymerization and cristallization kinetics by DSC, 150 g of reactive mixture was made with a ratio of 0.79/1.10 mol% of CL for the MgBrCL/HDCL couple. Thus, 11.59 g of catalyst and 11.59 g of activator were added to 126.82 g of monomer. All samples used for the DSC experiments were taken from this mixture (4-10 mg for each sample), which allowed to compare the results by eliminating the uncertainties due to the reactive mixture making.

Since storage and processing have to be conducted in a moisture free environment due to the sensitivity of the reaction to water, the products were dried overnight at 30°C under vacuum before each synthesis. Then, all handling was realized in an inert atmosphere in a glove box (nitrogen stream; relative humidity below 2%).

The mixture was prepared first by adding the monomers in a beaker at 70°C with stirring on a magnetic hot plate. After total melting of the monomers, the catalyst was added, followed by the activator after total melting of the catalyst, under moderate stirring. Then, the mixture was quenched in liquid nitrogen to prevent initiation of the reaction, before storing in a hermetic container at -18°C. It was considered that the reaction does not begin during the preparation of the mixture and, thus, the conversion rate of each extracted sample is considered to be zero.

The reactive mixture was brought to room temperature, in a dry atmosphere, before sample extraction to avoid condensation. The DSC pans were prepared under inert atmosphere in the glove box for the following analyses. The pans preparation and the *in situ* synthesis procedure in DSC will be detailed in the following section.

2.2 Characterization of PA6 synthesis by Differential scanning calorimetry (DSC)

2.2.1 Sample preparation

Neat resin samples were prepared by adding 4-10 mg of the reactive mixture in hermetically sealed aluminum DSC pans under an inert atmosphere, to prevent monomer evaporation and moisture absorption. In the case of glass particles/PA6 composites, a small quantity of particles was poured into the pan first. Then, it was transferred to the glove box and the reactive mixture was added under inert atmosphere to reach a content of 30±3 vol% in glass particles, for a total mass of 10-12 mg. An example of the calculation is presented below:

For m_{gp} = 5.70 mg of glass particle and m_{rm} = 5.17 mg of reactive mixture, the particle mass content χ_m (wt%), calculated using the Equation (2.1), is 52.44%:

$$\chi_m = \frac{m_{gp}}{m_{gp} + m_{rm}} * 100 \tag{2.1}$$

Thus, the particles volume content χ_v (vol %) can be calculated using Equation (2.2), which gives a percentage of 31.03% with the masses considered above:

$$\chi_v = \frac{\chi_m}{\frac{\chi_m}{100} + \frac{\rho_p}{\rho_m} * (1 - \frac{\chi_m}{100})} \tag{2.2}$$

in which ρ_p = 2.5 g.cm^{-3} is the glass particle density, ρ_m = 1.02 g.cm^{-3} is the reactive mixture density and χ_m is the particle mass content.

2.2.2 DSC analysis

Reactions kinetics were investigated under isothermal conditions. All the samples were first heated at 300°C/min from 25°C to a fixed temperature T_{iso} = 180°C. Then, they were maintained at T_{iso} for 50 min. This temperature was chosen in order to decouple the polymerization and crystallization processes [17] and, therefore, to identify their respective kinetics. Finally, the samples were cooled to 0°C at -10°C/min. After synthesis and cooling, each sample was heated from 0°C to 270°C at 10°C/min to obtain the melting temperature and enthalpy of the PA crystalline phase.

Each test was repeated at least twice for ensuring the reproducibility of the results.

2.3 Preliminary tests: Influence of the hydroxyl groups density

First, a batch of composites was prepared with pristine particles. The reaction takes place at the particle surface (as received and without further treatment). The aim is to check

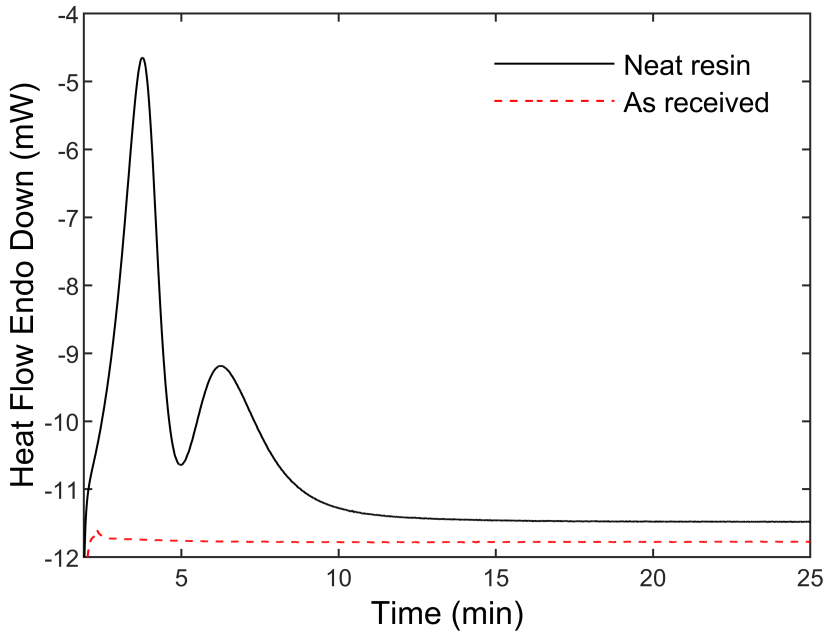

Figure 2.3: DSC curves of isothermal syntheses at 180°C of PA6 and PA6-glass particles composites synthesized with pristine particles

the compatibility of the surface of the particles used with the polymerization. The results were compared to the neat resin without particles, the both are displayed in Figure 2.3.

The DSC thermogram of the neat resin, black solid line in Figure 2.3, displays two peaks: the first one is related to monomer polymerization and the second one is related to the crystallization of PA6 [17]. The DSC thermogram of the synthesis with as-received particles shows no peak at all, which indicates that the polymerization did not occur. The reason is that the particles surface completely inhibits the reaction due to catalyst deactivation by the -OH groups according to the mechanism described in Section 1.3.1.1. Therefore, it is necessary to treat the particles in order to remove the surface hydroxyl groups.

2.3.1 Preliminary Silanization

The most commonly used technique for tailoring of glass surface is to graft a silane coupling agent. This results in modifying the surface tension of the glass, improving the interfacial glass/matrix adhesion in composites, but also removing the -OH groups. The silane reacts with the glass surface hydroxyls, reducing the remaining hydroxyl groups. Indeed, the formed silanol groups, after silane hydrolysis, interact with the hydroxyl groups via hydrogen bonds. Then, the condensation of these moieties generates siloxane bonds (see the grafting mechanism in Figure 1.22, Section 1.3.2.1).

2.3.1.1 Literature grafting protocol

The grafting protocol described in the literature (Chapter 1, Section 1.4) was used. First, the particles were calcinated at 450°C for 2 h. The calcination process allows to clean the surface from organic contaminants and to remove any previously applied treatment. Next, the glass beads were reactivated in a 10 %(v/v) aqueous hydrochloric acid solution for 3 h. The activation allows the hydrolysis of the siloxane groups and the regeneration of hydroxyls since these functions react with the silane

After acidic activation, an aqueous solution of AEAPTMS (5% (v/v)) was prepared. The pH was adjusted to 4-5 with acetic acid. The mixture was stirred for about 45 min. After hydrolysis of the silane, 50 g of calcinated glass particles was added to 100 ml of solution with stirring overnight. The mixture was then heated for an additional 2 h at 100°C to condense the silanol groups on the surface and to remove the traces of methanol from the hydrolysis of the methoxysilane. The particles were finally rinsed twice with ethanol and twice with water to remove the unreacted silanes, then dried for 2 h at 115°C. The particles treated with this protocol are named AEAPTMS-1. The steps of the grafting protocol and the effect of each step on the particle surface chemistry are schematically shown in Figure 2.4.

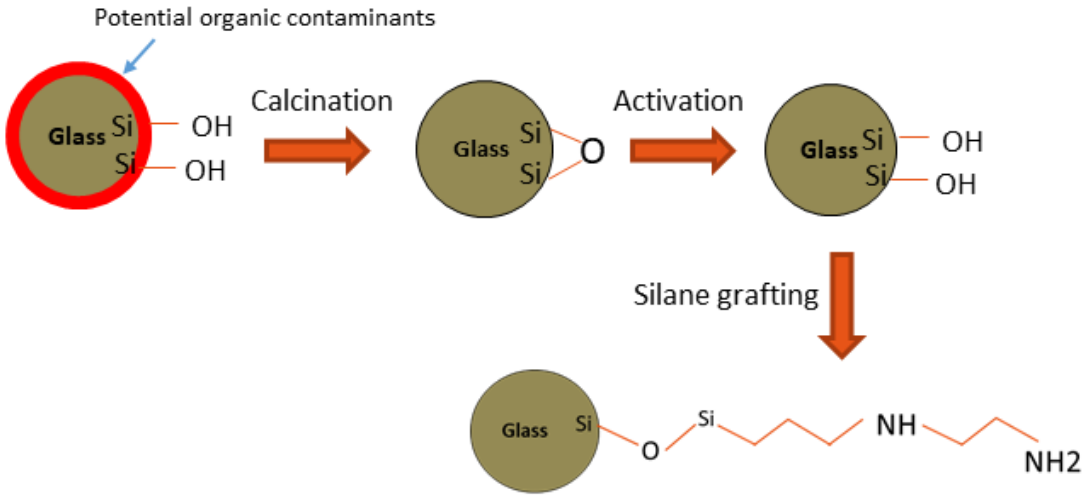

Figure 2.4: Schematic of the surface modification steps of glass particles with AEAPTMS silane with the effect of each step on the surface chemistry

2.3.1.2 Surface characterization

The surface of the AEAPTMS-1 particles was characterized by TGA to verify the efficiency of the treatment and to ensure the successful grafting of the AEAPTMS to the surface. The tests were carried out with a TGA1 STARe System-METTLER TOLEDO. The pristine and the treated particles were heated from 25°C to 450°C at 10°C/min in an air atmosphere for 2 h. Air was chosen to favor a full combustion of organic compounds with O_2.

Table 2.2 shows the mass loss of the two types of particles. Compared to the untreated beads, the results show that the mass loss increases significantly after treatment which confirms the presence of silane on the surface of the treated particles.

Table 2.2: TGA mass loss of AEAPTMS-1 particles compared to the mass loss of pristine particles

Particle type	Total mass loss (%)
As received	0.2
AEAPTMS-1	0.72

2.3.1.3 Polymerization and crystallization kinetics after silane grafting

After demonstrating that the grafting of the silane onto the surface of the glass beads was successful, a composites batch was synthesized with the AEAPTMS-1 particles to investigate the influence of the surface treatment on the polymerization. In principle, the silane grafting on the surface should reduce the number of hydroxyls that inhibit the reaction, we expect the polymerization of the matrix despite the presence of the particles within the reactive mixture.

Figure 2.5 presents the results of the composite synthesized with AEAPTMS-1 particles compared to the neat resin. The thermogram in former case shows a complete inhibition of the reaction despite the particles treatment. This inhibition could be due to the high number of hydroxyls remaining on the surface after silane grafting. Indeed, the acidic activation allows to regenerate almost all the hydroxyls of the particles surface. During the grafting step, the silane reacts with a proportion of -OH groups but a high number of inaccessible hydroxyls remain on the surface due to steric hindrance created by the silane chains [127, 133]. These unreacted hydroxyls remain on the surface after the treatment and they cause reaction inhibition.

These results show that the grafting protocol described in the literature is not suitable for the synthesis of anionic PA6. Therefore, it is necessary to develop a new grafting protocol compatible with the synthesis reaction in order to preserve the reaction from the negative effect of hydroxyl groups of the glass particles surface.

Accordingly, a comprehensive study is carried out to control the hydroxyl density during all steps of the glass particle surface modification by a silane coupling agent. This study will allow to follow the evolution of the hydroxyl groups and to propose a grafting protocol allowing a proper synthesis of the anionic PA6 matrix reinforced by silanized glass particles.

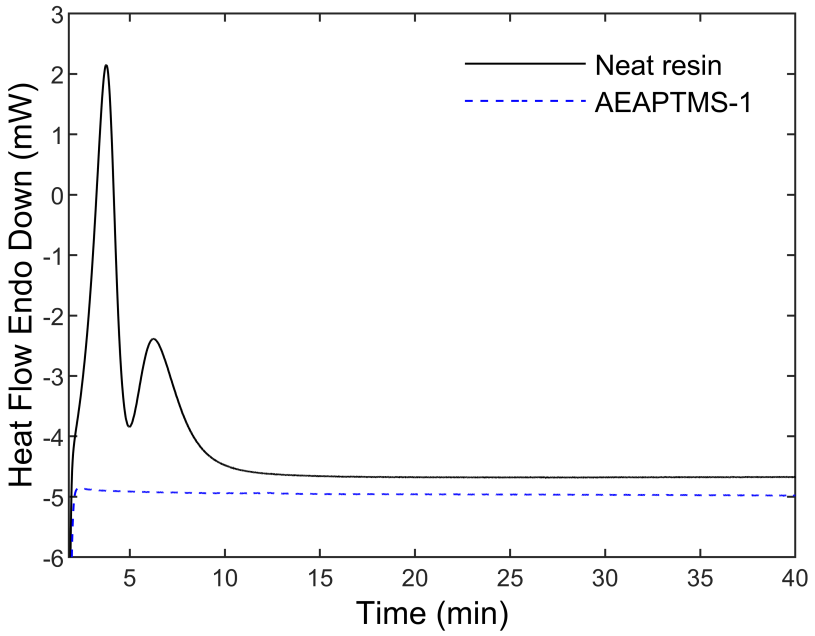

Figure 2.5: SC curves of isothermal syntheses at 180°C of PA6 and PA6-glass particles composites synthesized with AEAPTMS-1 particles

2.4 Control of the hydroxyl groups surface density and adaptation of the silanization process to the anionic PA6 synthesis

2.4.1 Analysis techniques

Different techniques have been used to quantify the hydroxyls surface density, such as deuterium exchange, titration or nuclear magnetic resonance spectroscopy (NMR) [111, 112, 134–144]. These techniques typically provide comparable density values. Thermogravimetric analysis (TGA) is another relevant technique to monitor the dehydration and dehydroxylation processes, and thus to determine the surface density of hydroxyl groups [142, 143, 145, 146]. Once dehydration is completed, the loss of physically adsorbed water can be subtracted from the total loss to estimate the number of surface-bound hydroxyl groups. TGA can also be coupled with mass or IR spectroscopy for better precision on the evolution of the hydroxyl groups surface density, and to distinguish the dehydration from the dehydroxylation processes [147]. Kellum et al. [145] compared the amounts of physically adsorbed water, and surface-bound -OH, using different techniques. The -OH densities calculated from the TGA results were quite comparable to values obtained from other conventional methods, confirming that TGA can provide accurate values. Mueller et al. [146] also highlighted the TGA reliability and reproducibility to determine the surface density of hydroxyl groups. Moreover, as physically adsorbed water can be separated from silanol condensation with TGA, it allows an accurate estimation of the -OH density value.

Finally, it was demonstrated that the mass loss induced by physically adsorbed water is not impacted by the drying conditions during dehydration, so that the hydroxyl density was not affected neither. These results confirm that it is possible to distinguish both the dehydration and dehydroxylation processes by TGA [146]. Accordingly, this technique was chosen in this study to evaluate the hydroxyl groups density on the glass particles surface.

The TGA procedure and and other techniques used in this section are described hereby.

2.4.1.1 Specific surface area measurement

The specific surface area was measured with a 3Flex BET instrument from Micromeritics. This apparatus measures the volume of adsorbed gas (nitrogen) on the surface of the samples at the temperature of liquid nitrogen (77K) up to a relative pressure of 1 bar in order to plot a complete adsorption isotherm. A preliminary degassing at 50°C for 11 h was performed to clean the surface of the samples from any molecules that could obstruct the access to the pores. The specific surface area was then calculated by using the BET model in a suitable pressure range.

2.4.1.2 Thermogravimetric analysis (TGA)

The TGA experiments were carried out with a TGA1 STARe System-METTLER TOLEDO. First, the mass loss due to physically adsorbed water was determined by heating the glass particles from 25°C to 150°C at 10°C/min under air atmosphere. The temperature was then held at 150°C for 2 h. This temperature was chosen as a mean value based on the literature [111, 145, 146]. The resulting mass loss was subtracted from the total mass loss obtained after each test [145, 146] .

Next, the glass particles were heated from 25°C to 450°C at 10°C/min in an air atmosphere. The temperature was maintained at this value until the sample mass stabilized. This maximum temperature was chosen in order to obtain a maximum number of dehydroxylated sites that could be reversibly rehydroxylated following the work of Young and Zhuravlev [109, 112] (Section 1.4.1). Above this temperature, the number of hydroxyl sites that can be regenerated decreases, which lowers the total number of available hydroxyl sites after rehydroxylation, which afterwards affects the control over the silane grafting process. More specifically, this temperature prevents the removal of all silanols from the surface and thus allows silane grafting. Indeed, above this temperature, the condensation of silanols becomes more important and irreversible, leading to the irreversible loss of most (or all) hydroxyl groups, subsequently inhibiting silane grafting [109–112].

After silanization, the treated particles were characterized by TGA, in order to quantify the amount of grafted silane, and to calculate the grafting density, following the same calcination protocol as described above. Air was used as an analysis purge gas in order to accelerate and ensure complete silane degradation before reaching the calcination temperature employed in this work (450°C), allowing to subsequently quantify the total amount of grafted silane [148].

2.4.1.3 FTIR spectroscopic measurements

Transmission FTIR spectra were acquired with a Bruker Vertex 70 spectrometer. The particles were blended with high purity infrared grade KBr powder at 1.5-2 wt% and pressed into pellets for measurements. The spectra were recorded between 400 cm^{-1} and 4000 cm^{-1} with a resolution of 2 cm^{-1}. Before measurement, a background was obtained with a pure KBr pellet.

2.4.2 Characterization of the surface density of hydroxyl groups on glass particles

The particles were first calcinated at 450°C for 2 h to remove impurities from the surface. Then, they were rehydroxylated for 8 h in a 10%(v/v) aqueous hydrochloric acid solution, under stirring at room temperature, to saturate the surface with hydroxyl groups. These particles are designated as *fully rehydroxylated particles*. After complete rehydroxylation, the particles were washed several times with distilled water until the pH stabilized at a value of 7.0, before drying at 115°C for 2 h. Samples of these fully rehydroxylated particles were then calcinated at 450°C for up to 24 h in a TGA instrument, in order to follow the evolution of the hydroxyl groups surface density as a function of calcination time.

2.4.2.1 Effect of the initial calcination time on the –OH surface density

In order to calculate the hydroxyl surface density on glass particles by TGA, it is necessary to determine the mass loss specifically related to the dehydroxylation process, by excluding the mass loss related to the physically adsorbed water. The amount of adsorbed water is obtained by heating the particles for 2 h at 150°C. For the fully rehydroxylated particles, the associated mass loss during this heating step is shown in Figure 2.6. The TGA results show that the percentage of physically adsorbed water is 0.34%. During this step, dehydroxylation does not occur because the associated onset temperature (200°C) is not yet reached [111, 112]. Thus, this percentage was subtracted from the total mass loss after the dehydroxylation heating cycle, which then allows the calculation of the hydroxyls surface density.

Furthermore, the stabilization of the mass loss after about 1.5 h of dehydration shows that all physically adsorbed water has been removed. This stabilization also confirms that dehydroxylation has not yet started at 150°C. Therefore, this drying condition is adequate as it leads to complete dehydration, while avoiding the onset of dehydroxylation [112]. This dehydration temperature thus ensures a clear separation between the processes of evaporation of physically adsorbed water, and silanol condensation, which provides accuracy and reliability for the calculation of the hydroxyl groups surface density value.

TGA total mass loss for the fully rehydroxylated particles as a function of time, at 450°C is shown in Figure 2.7(a). The mass loss stabilizes after approximately 24 h, which corresponds to maximum dehydroxylation. Subtracting the mass loss due to the physically

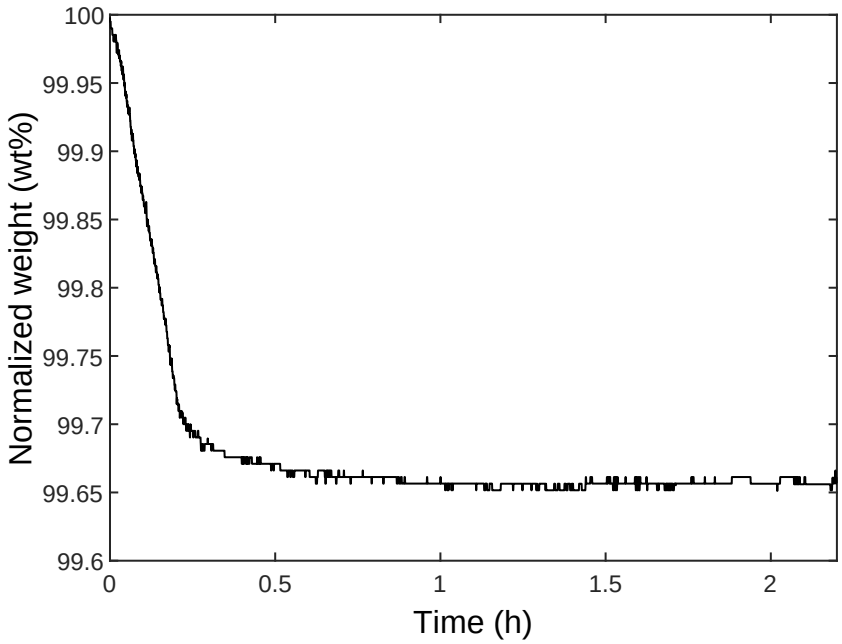

Figure 2.6: Thermogram of the normalized mass of the fully rehydroxylated particles in acid, heated at 150°C for 2 h. The mass loss corresponds only to the physically adsorbed water at the surface of the particles, since the onset of dehydroxylation has not been reached yet

adsorbed water from the total mass loss gives the amount related only to dehydroxylation, and thus leads to the hydroxyl groups surface density d_{OH} (in OH.nm^{-2}) given by Equation (2.3):

$$d_{OH} = \frac{2 * \Delta m * Na}{100 * M * S} \tag{2.3}$$

in which Δm (wt %100) is the TGA mass loss percentage, Na is Avogadro's constant, M is the molecular mass of water (g.mol^{-1}) and S ($m^2.g^{-1}$) is the specific surface area of glass particles obtained by BET. The factor 2 is added because one water molecule is lost by condensation of two hydroxyls.

Equation (2.3) yields to a hydroxyl surface density value of 460 OH.nm^{-2} for the fully rehydroxylated particles. Yet, it has been reported in the literature that the hydroxyl density on a glass surface cannot exceed 6 OH.nm^{-2} [111]. However, several authors have shown that it is quite possible to find much higher values, mostly because of the specific surface measurement technique [149–151]. Indeed, the specific surface considered in the calculation was obtained by the BET technique. This method is based on the adsorption of nitrogen gas and is often criticized since a large amount of microporosities are not accessible to the nitrogen molecules at 77 K, and as a result are not considered in the measurement [149, 150, 152–155].

The particles used in this study have an average diameter of 4 μm as demonstrated above by laser granulometry (Section 2.1.1.2). However, this technique showed that the particles distribution is rather broad and 10% of the particles have a diameter less than 1.46 μm. In addition, some particles have a diameter below 500 μm as displayed in

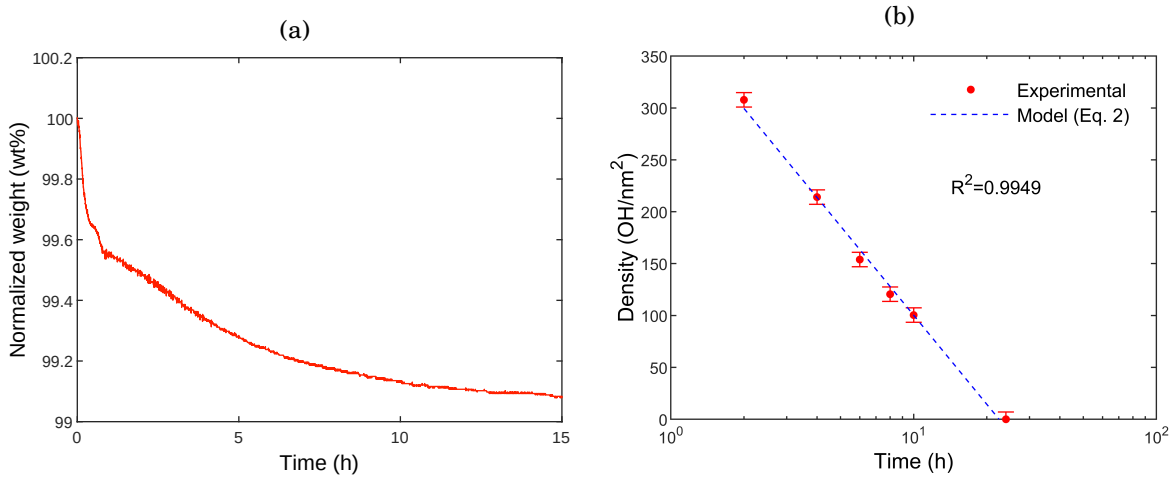

Figure 2.7: (a) TGA thermogram of the normalized mass of fully rehydroxylated particles heated and maintained at 450°C for 24 h, (b) Evolution of the hydroxyl groups surface density as a function of calcination time, for the fully rehydroxylated particles (logarithmic scale). The dotted blue line is a linear regression

Figure 2.2. The SEM micrographs in Figure 2.8 show that these small particles can form aggregates. This generates very fine micro/nanoporosities not detectable by BET analysis. Consequently, the specific surface area of glass particles is underestimated, leading to very high values of hydroxyl densities. Moreover, the total hydroxyl surface concentration for the fully rehydroxylated particles is 0.77 mmol OH.g^{-1}, which is consistent with the literature [112, 149]. However, after dividing this value by the specific surface area (1 $m^2.g^{-1}$) to calculate the hydroxyl density, the value increases significantly. This confirms that the high values of the hydroxyl density are due to the specific surface area measurement.

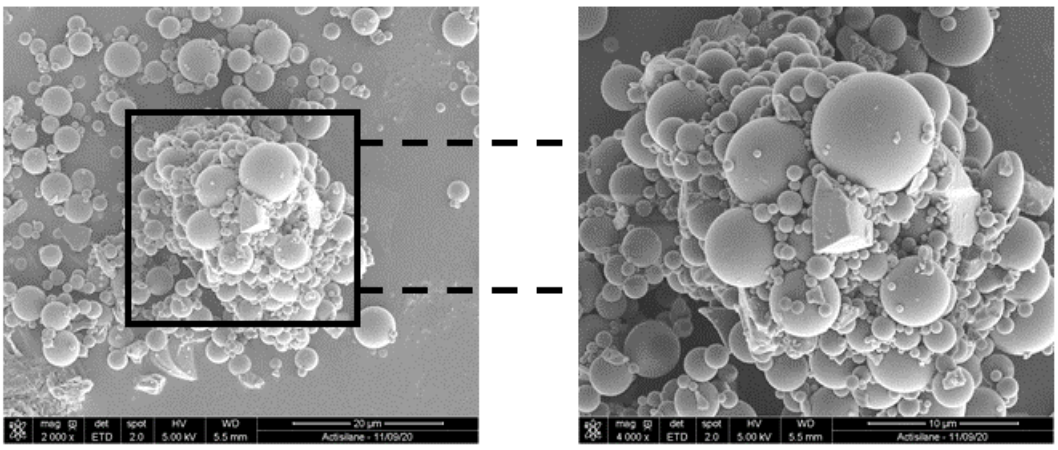

Figure 2.8: Thermogram of the normalized mass of the fully rehydroxylated particles in acid, heated at 150°C for 2 h. The mass loss corresponds only to the physically adsorbed water at the surface of the particles, since the onset of dehydroxylation has not been reached yet

Although the calculated hydroxyl density value for the fully rehydroxylated particles is quite high at 460 OH.nm^{-2}, it will be considered, in this work, as a reference value that

will be used for comparison purposes. From this reference value, it will be indeed possible to follow the evolution of hydroxyl groups density on the surface after each treatment.

Figure 2.7(b) illustrates the evolution of the mass loss and, consequently, the surface density of hydroxyl groups remaining at the surface, as a function of calcination time at 450°C. The results confirm the gradual decrease of hydroxyl groups at the surface, with a clear trend modeled by Equation (2.4):

$$d_{OH} = -285.06 log(t) + 385.36 \tag{2.4}$$

in which d_{OH} (OH.nm^{-2}) is the hydroxyl groups surface density, and t (h) is the calcination time. Considering the good fit between the experimental results and the linear regression model, as seen in Figure 2.7(b), it is thus possible to estimate the required calcination time for a targeted hydroxyl surface density.

The FTIR spectra of the fully rehydroxylated particles, and for the particles subsequently calcinated for 2 h to 24 h, are illustrated in Figure 2.9(a). The results show a main peak in-between 3430 cm^{-1} and 3500 cm^{-1} attributed to the hydroxyl groups. The intensity of the peak decreases progressively by increasing the calcination time, until it almost disappears after 24 h of calcination. Such a decrease confirms the progressive surface dehydroxylation, and is consistent with the gradual mass loss observed by TGA. The transmittance peak T (%) as a function of calcination time t (h) can be fitted quite well with a linear regression (Equation (2.5)):

$$T = 12.55 log(t) + 80.26 \tag{2.5}$$

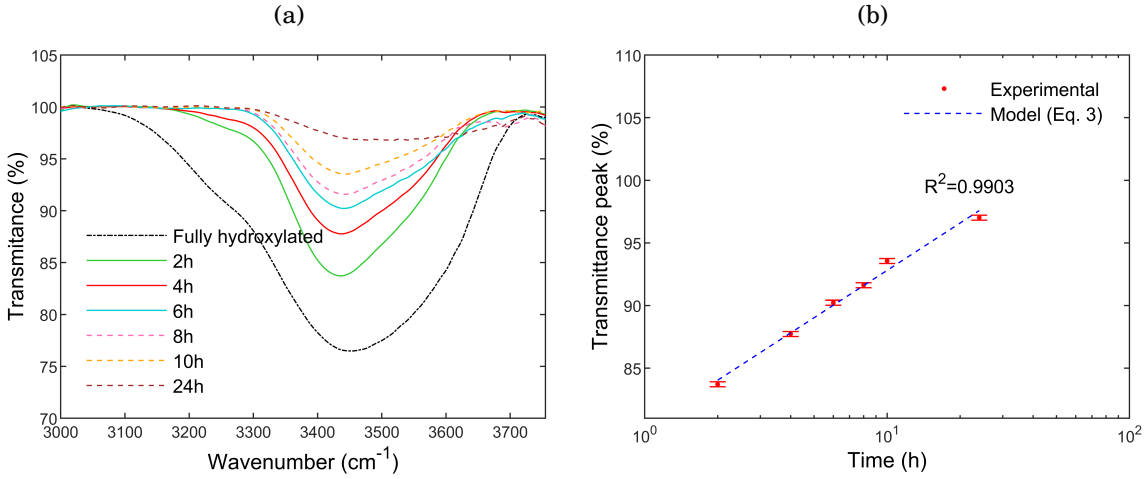

Figure 2.9: (a) Infrared spectra of initially rehydroxylated glass particles, as a function of the subsequent calcination time at 450°C, (b) Evolution of the transmittance peak T as a function of calcination time at 450°C. The dotted blue line corresponds to the linear regression of the Transmittance as a function of log(t) for the peak located in-between 3430 and 3500 cm^{-1}

By combining Equations (2.4) and (2.5), it is then possible to establish an interrelationship between the hydroxyl surface density and the transmittance (Equation (2.6)):

$$d_{OH} = -22.71T + 2208.38 \tag{2.6}$$

The fully rehydroxylated particles show a peak with a broad band around 3432 cm^{-1}. This peak gradually shifts to a higher wavenumber and its width decreases with increasing calcination time, up to 3500 cm^{-1} for the particles calcinated for 24 h. Indeed, the wavenumber strongly depends on the interactions between the hydroxyl groups and their environment. When hydroxyl groups form hydrogen bonds, the associated wavenumber decreases [150]. For the fully rehydroxylated particles, the hydroxyls are sufficiently close to each other to form hydrogen bonds. When the hydroxyls are removed by increasing the calcination time, the -OH groups remaining at the surface become progressively isolated, which increases the wavenumber.

The creation of hydrogen bonds between adjacent hydroxyls can proceed via different paths, leading to two categories of hydroxyls: (1) Hydroxyls linked via one hydrogen bond or more. These hydroxyls show a very large absorption peak, with a maximum below 3600 cm^{-1}. In this case, the wavenumbers of the hydroxyls both giving and accepting protons are lower compared to hydroxyls only giving a proton, due to a cooperative effect; (2) Hydroxyls able to create an additional hydrogen bond, with a wavenumber at 3720 cm^{-1}, for terminal hydroxyls, and at 3742 cm^{-1} for free geminal hydroxyls without any hydrogen bonding interaction. From the IR spectroscopy results, all particles, regardless the calcination time or rehydroxylation conditions, seem to have hydrogen bonded hydroxyls as supported in Figure 2.9(a). This is consistent with the results found in the literature, since it has been shown that dehydroxylation continues up to 1000°C [109, 111, 112]. Therefore, -OH groups may remain on the surface after calcination at 450°C and may bond to each other if they are close enough. Our results show that the -OH groups remaining on the surface interact via hydrogen bonding since the wavenumber, regardless of the treatment, is below 3600 cm^{-1}. Thus, the dehydroxylation process decreases the number of -OH groups, resulting in a gradual decrease in peak intensity and number of hydrogen bonds, before the wavenumber finally shifts to higher values.

2.4.2.2 Impact of dehydroxylation on PA6 polymerization

In this section, composites were synthesized and analyzed by DSC with two types pf particles: the fully rehydroxylated ones and the particles calcinated from 2 h to 24 h. The aim is to determine the effect of calcination time on the polymerization and crystallization kinetics of PA6. The results are compared with the neat resin.

The DSC thermograms of the composites are presented in Figure 2.10. The signal corresponding to fully rehydroxylated is flat. Compared to the neat resin, the fully rehydroxylated particles completely inhibit the reaction similarly to raw particles, which confirms the significant presence of -OH groups.

In contrast, we see that the curves corresponding to 2, 4 and 6 h exhibit the two peaks attributed to polymerization and crystallization. The peaks are shifted towards

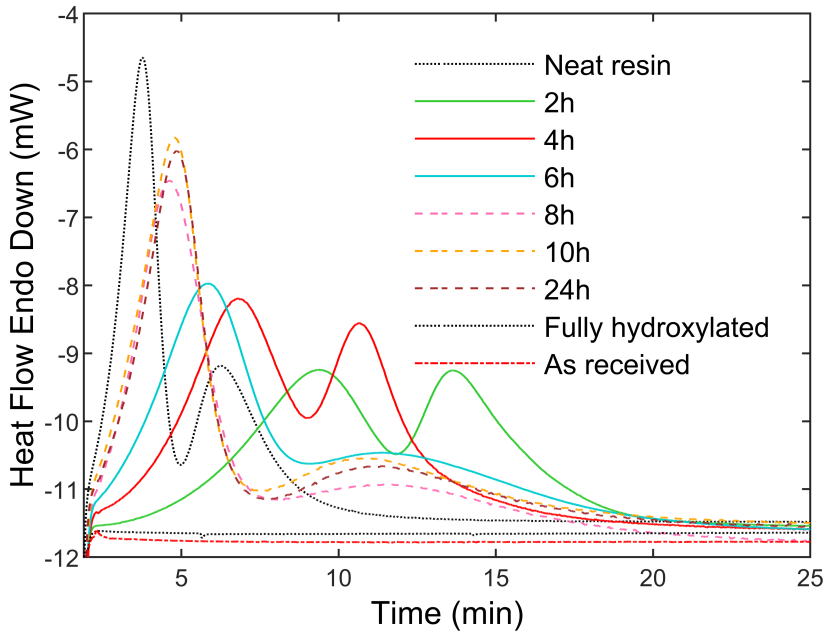

Figure 2.10: DSC thermograms of PA6/glass particles composites in isothermal syntheses at 180°C, for the particle calcination time ranging from 0 h (fully rehydroxylated) to 24 h, compared to the neat resin

shorter times when the calcination time increases. In means that the polymerization and crystallization levels significantly increase by increasing the calcination time up to 8 h. Then, the peaks are superimposed for 8, 10 and 24 h, which signify that the polymerization and crystallization stabilize for calcination times longer than 8 h. This improvement is due to surface dehydroxylation and to the partial removal of hydroxyl groups during calcination, which limits the catalyst deactivation.

The stabilization of the polymerization/crystallization kinetics after 8 h of calcination time indicates that the remaining -OH surface density has no significant influence on the polymerization/crystallization phenomena. The polymerization/crystallization kinetics do not change significantly when the calcination time last longer than 8 h. The difference in kinetics compared to the pure resin is due to the hydroxyls that remain on the surface.

Calcinating for at least 8 h yields an hydroxyl surface density of about 120 OH.nm^{-2} (from the results in Figure 2.7(b)), with a minimum impact on the polymerization and crystallization phenomena. From this point, this threshold surface density will be identified as N_{limit}.

After calcinating for 10 h, the residual hydroxyl surface density is about 100 OH.nm^{-2}, according to Equation (2.3). This last condition is an adequate compromise that provides some level of adjustment, considering the following silane grafting process in an aqueous solution that leads to surface rehydroxylation. Ultimately, the aim is to optimize the treatment time without exceeding the number of surface –OH groups N_{limit}, in order to avoid a negative impact on the polymerization/crystallization kinetics.

2.4.3 Comparison of the rehydroxylation protocols

We aim to compare in this section the effect of a 10% HCl solution and a pH 4-5 acetic acid aqueous solution on the hydroxyl density. After calcination, controlling the rehydroxylation process during the silanization step is crucial in order to avoid an excessive regeneration of –OH at the particles surface, which can slow down or inhibit the polymerization/crystallization processes. The methodology often used in the literature for the rehydroxylation of glass particles is by immersion in an hydrochloric acid (HCl) solution [117, 118] (see Section 1.4.2). However, this technique may regenerate an excessive number of surface -OH. Therefore, another approach consists in simultaneously regenerating (moderately) the hydroxyls at the particles surface, and grafting the silane agent. This protocol aims at generating a sufficient number of OH for the silane grafting process, without regenerating residual OH. Therefore, comparing the rehydroxylation process in HCl 10%, and in the silane treatment bath (aqueous solution adjusted at pH 4-5 with acetic acid, but without the silane agent at this step) is relevant in order to select the most appropriate approach for the silane grafting step, without negatively influencing the polymerization/crystallization processes. The glass particles were thus calcinated for 24 h at 450°C to eliminate a maximum amount of hydroxyl groups. Half of the calcinated particles were then immersed in the 10% HCl solution, and the second half was added to the aqueous solution adjusted at pH 4-5 with acetic acid (silane treatment bath, without the silane), for 3 h in both cases.

The TGA results in Table 2.3 show that the density of regenerated hydroxyls after 3 h is significantly higher in 10% HCl. In contrast, the silanization treatment bath yields moderate rehydroxylation after 3 h, and the density of regenerated hydroxyls remains low and sufficient for adequate silane grafting. These results were confirmed by FTIR spectroscopy as presented in Figure 2.11. The spectra show that the particles rehydroxylated for 3 h in 10% HCl present a peak with a large band similar to the case of the fully rehydroxylated particles. This indicates that after 3 h, the maximum -OH density at the surface has already been reached. However, the particles rehydroxylated in the silanization bath show a peak with features similar to the particles calcinated for 24 h, with a slightly higher intensity due to the regeneration of the hydroxyls.

Table 2.3: TGA mass loss and hydroxyl surface density for glass particles calcinated for 24 h, and calcinated particles subsequently rehydroxylated in the silanization solution (aqueous solution adjusted at pH 4-5 with acetic acid, without the silane), or in 10% HCl, for 3 h

Sample name	TGA mass loss (%)	Hydroxyls density ($OH.nm^{-2}$)
Calcinated 24 h	0	0
Silanization treatment bath 3 h	0.17	113
10% HCl solution 3 h	0.69	461.7

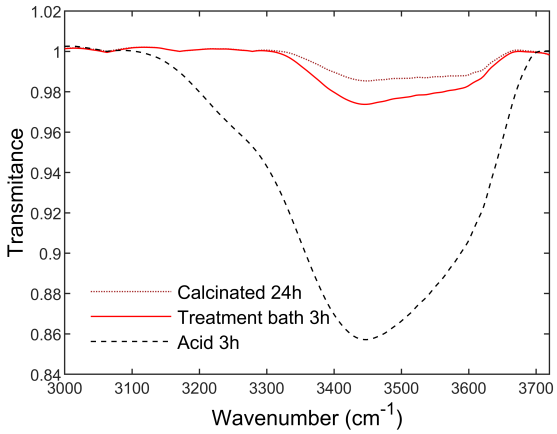

Figure 2.11: Comparison of FTIR spectra for the glass particles calcinated for 24 h, and particles rehydroxylated respectively in the silanization solution (aqueous solution adjusted at pH 4-5 with acetic acid, without the silane), and in 10% HCl, for 3 h

The hydroxyl density measured by TGA, and the -OH peak intensity obtained by FTIR spectroscopy, for the particles rehydroxylated in 10% HCl, are very high compared to the particles rehydroxylated in the silanization treatment bath, for the same treatment time. This shows that the regeneration rate of hydroxyls in 10% HCl is very high and might not be suitable for the synthesis of anionic PA6. Therefore, the use of an aqueous solution at pH 4-5 for both rehydroxylation and silanization processes simultaneously appears to be more appropriate since it offers much more control over rehydroxylation by avoiding excessive –OH regeneration. In addition, simultaneous rehydroxylation and silanization also eliminates an additional step in the surface treatment process: no acidic rehydroxylation step is needed.

2.4.4 Controlling the –OH quantity regenerated during the silanization treatment

When silanization is performed in an aqueous solution, the rehydroxylation and silanization processes occur simultaneously. Although this solution offers a moderate rehydroxylation as shown in the previous section, it could again lead to excessive hydroxyl regeneration – especially if the silane concentration has significantly decreased due to its reaction at the particles surface. These regenerated and unreacted -OH could then remain at the surface and slow down or inhibit the polymerization of the PA6 matrix. Therefore, controlling the evolution of the hydroxyl groups surface density during the silanization process, as a function of time, is also required.

The rehydroxylation process was evaluated by monitoring the regeneration of hydroxyl groups at the surface of the calcinated particles when treated in the silanization aqueous solution (composed of distilled water adjusted at a pH of 4-5 with acetic acid, but without the silane agent). Glass particles were treated in this solution for 2, 3 or 6 h respectively, at room temperature. Silanization in mild acidic conditions allows to promote the formation

of silanol groups and to slow down the self-condensation reaction between the resulting hydrolyzed silanol groups [119]. Then, the particles were rinsed twice with ethanol, twice with water, and dried for 2 h at 115°C.

Table 2.4 shows the evolution of the hydroxyl groups regeneration at the particles surface, in the silanization solution (aqueous solution at pH 4-5 adjusted with acetic acid, without the silane at this point), as a function of time. The adsorbed water has been subtracted from the results, see the procedure in Section 2.4.2.1. As expected, prolonging the treatment gradually increases the surface density of hydroxyl groups.

Table 2.4: Evolution of TGA mass loss and hydroxyl surface density, for particles calcinated for 10 h, and then partially rehydroxylated in the silanization solution (without the silane) for 2 h, 3 h and 6 h.

Treatment time in silanization solution (without silane)	TGA mass loss [a] (± 0.01%)	Density of hydroxyls d_{OH} (± 7 OH.nm^{-2})
0 h (calcinated)	0.14	93
2 h	0.19	127
3 h	0.24	160
6 h	0.31	207

[a] Physically adsorbed water has been removed from the mass loss, leaving only the dehydroxylation process.

The FTIR spectroscopy results in Figure 2.12(a) show an increase in the intensity of the peak relative to -OH groups with increasing treatment time, which confirms the regeneration of hydroxyl groups in the silanization solution. The peak intensity after 2 h of treatment is lower compared to 3 h and 6 h, but slightly higher compared to the calcinated particles, indicating moderate hydroxyl regeneration.

In order to assess the effect of the treatment time in the silanization solution on the polymerization/crystallization kinetics, composites were synthesized with particles first calcinated for 10 h, and subsequently rehydroxylated in the solution for 2 h, 3 h and 6 h. Figure 2.12(b) shows the DSC thermograms of the composites during the synthesis. The polymerization/crystallization kinetics for the composite synthesized with calcinated particles is slightly shifted compared to the neat resin, as explained in Section 2.4.2.2. The polymerization/crystallization kinetics are significantly slowed down with increasing treatment time. The 2 h treatment yields the fastest kinetics among all of the treated particles conditions.

The differences observed between the composite prepared with strictly calcinated particles, and calcinated particles subsequently rehydroxylated for 2 h, is due to the regenerated hydroxyl surface density, which exceeds the N_{limit} threshold (see Section 2.4.2.2). However, the resulting density does not completely inhibit the polymerization reaction. It is expected that this slight excess could be compensated by the grafting of the silane coupling agent, which is examined in the next section.

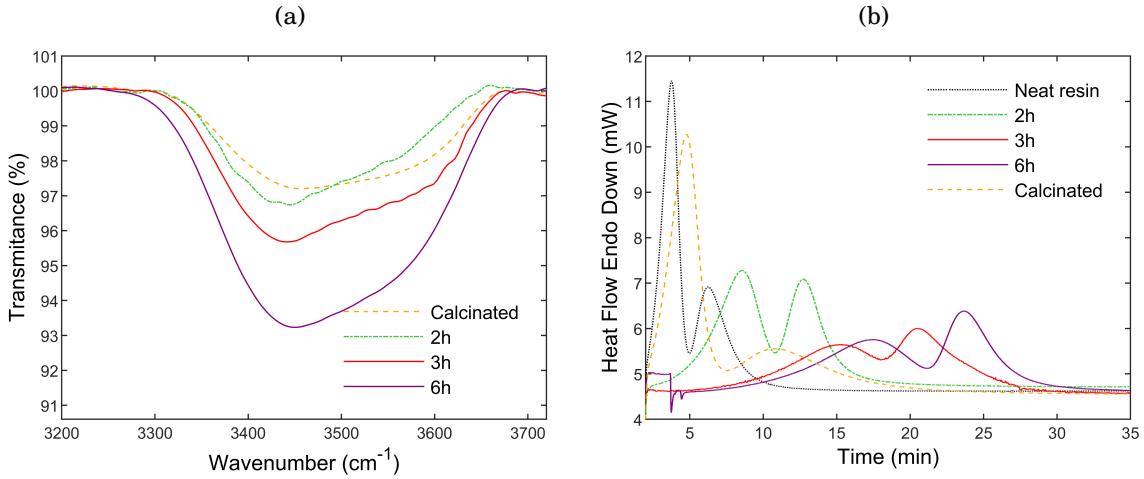

Figure 2.12: (a) FTIR spectra of glass particles calcinated for 10 h and subsequently partially rehydroxylated in the silanization solution (without the silane) for different durations, (b) DSC curves of isothermal syntheses at 180°C of PA6-glass particles composites, synthesized with partially rehydroxylated particles for 2 h, 3 h and 6 h in the silanization solution (without the silane agent), compared to the DSC curves of the pure resin and PA6-glass particles composites synthesized with the calcinated particles

In addition, since silane grafting at a surface is limited by steric hindrance [156], the grafting density typically exhibits a maximum value [156, 157]. As a result, overprolonging the grafting time after the maximum silane surface density is reached only results in increasing the number of inaccessible –OH. These inaccessible hydroxyls remain on the surface and can slow down, and ultimately inhibit, the polymerization reaction. In the present case, treating the particles in the silanization bath (without the silane) for 2 h results in moderate rehydroxylation (d_{OH}=127 OH.nm^{-2} $\approx N_{limit}$, see Section 2.4.2.2). Such a duration was thus chosen for the following silane grafting experiments.

2.4.5 Polymerization and crystallization kinetics after silane grafting

Firstly, an aqueous solution of AEAPTMS (5%(v/v)) was prepared. The pH was adjusted to 4-5 with acetic acid. The mixture was stirred for about 45 min. After hydrolysis of the silane, 50 g of calcinated glass particles were added to 100 ml of solution with stirring for 1 h (or 3 h). The mixture was then heated for an additional 1 h (or 3 h) at 100°C to condense the silanol groups on the surface and to remove the traces of methanol from the hydrolysis of the methoxysilane. The particles were finally rinsed twice with ethanol and twice with water to remove the unreacted silanes, then dried for 2 h at 115°C.

2.4.5.1 Silane surface modification and its influence on polymerization and crystallization

Figure 2.13 shows the FTIR spectra of freshly calcinated particles (450°C, during 10 h), compared to calcinated particles subsequently silanized for 2 h. The peak related to the hydroxyls almost disappears after silanization, which demonstrates that almost all hydroxyls have reacted during the grafting process. As a result, silane grafting allows for an almost complete elimination of both the residual hydroxyls remaining after 10 h of calcination, and the regenerated hydroxyls during the silanization treatment.

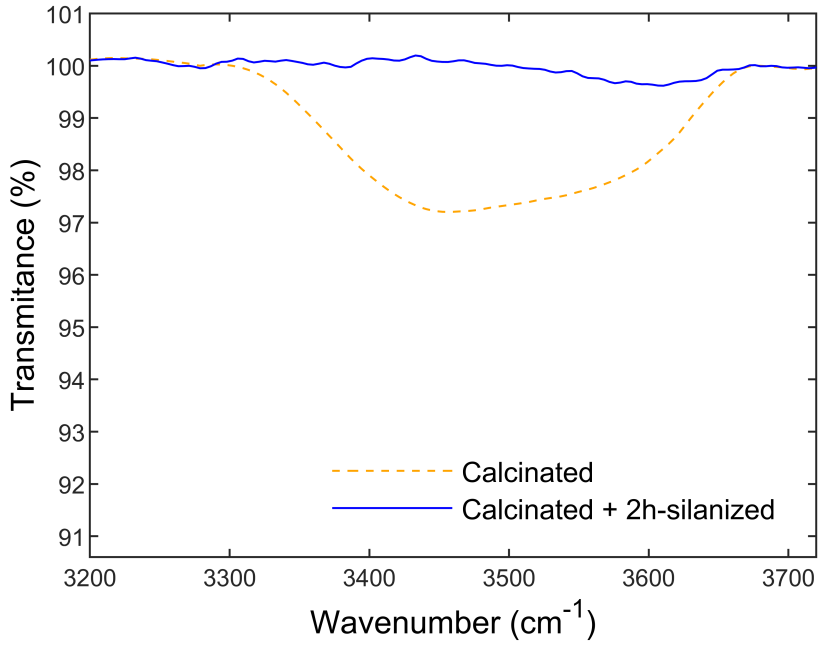

Figure 2.13: (a) FTIR spectra of calcinated particles and calcinated + 2 h-silanized particles

For the silanized particles, the mass loss measured by TGA includes both the loss of –OH groups, and the loss of the grafted silane. It is thus possible to deduce the mass loss related only to the –OH groups from Equation (2.6), that provides the hydroxyl groups surface density from the transmittance peak. Accordingly, Table 2.5 shows the total mass loss, hydroxyl mass loss, and silane mass loss, for particles silanized for 2 h, compared to the calcinated particles. The mass loss related to the -OH groups decreases considerably after silanization. These results confirm the successful grafting of the silane agent on the surface of the particles.

In thermal measurements, especially TGA tests on silanized glass reinforcements, the total mass loss is not only due to the decomposition of surface grafted silanes, but also to dehydroxylation. Therefore, it is possible to deduce the number of hydroxyls from the IR spectra using the same methodology described in Section 2.4.2.1, which allows to calculate the mass fraction associated to the loss of hydroxyls and to separate it from the mass loss related to the decomposition of the surface bonded silanes. This allows to determine the real grafting degree and to tune the surface modification process.

Table 2.5: TGA mass loss relative to the hydroxyls and silanes, for particles initially calcinated then silanized for 2 h, compared to strictly calcinated particles

Particle type	Total mass loss (%) ± 0.01	Weight loss related to hydroxyls (%)	Weight loss related to silane (%)
Calcinated	0.14	0.14	None
Calcinated+ silanized for 2 h	0.71	0.05	0.66

Next, the effect of silane grafting on the polymerization/crystallization processes was evaluated by DSC in Figure 2.14. The composites were synthesized with particles silanized for 2 h. The results are compared to the neat resin, the freshly calcinated particles (10 h), and particles rehydroxylated for 2 h in the silanization solution (but without the silane agent, see also Section 2.4.4). The thermograms confirm that the addition of the silane coupling agent accelerates the reaction, compared to the rehydroxylated particles without the silane agent. As expected, the excess hydroxyl surface density (compared to N_{limit}) was fully compensated by the addition of the silane agent. In fact, the residual hydroxyl surface density after silanization is even lower than N_{limit}, which accelerates the reaction - the achieved polymerization kinetics is similar to freshly 10 h calcinated particles. Therefore, the simultaneous rehydroxylation and silane grafting reactions offer an adequate silanization process that prevents excessive rehydroxylation.

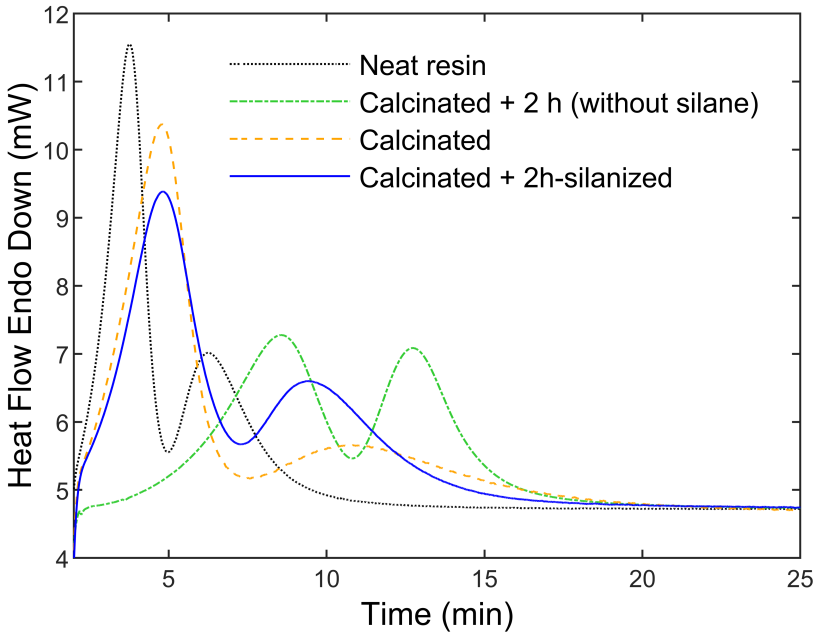

Figure 2.14: (b) DSC curves of isothermal syntheses at 180°C of PA6 and PA6-glass particles composites synthesized with calcinated particles, rehydroxylated particles for 2 h in the silanization solution (without silane) and calcinated + 2 h-silanized particles

The crystallization of the composite containing silanized particles is faster compared to the composite with calcinated particles, as reported in Table 2.6. In addition, both the melting temperature and enthalpy increase with silane grafting. This could be due to the particles/matrix interactions at the interface in the case of silanized particles, which could promote crystallization.

Table 2.6: Crystallization peak, melting temperature (T_m) and melting enthalpy (ΔH_m) of PA6-glass particles composites synthesized with calcinated particles and calcinated + 2h-silanized particles

Particle type	Cristallization peak (± 0.4 min)	T_m (± 0.3°C)	ΔH_m (± 0.6 J.g^{-1})
Calcinated	9.16	213.1	67.4
Calcinated + silanized for 2 h	7.83	215.6	71.2

The DSC thermograms show that the polymerization and crystallization onsets for the different composites are always delayed compared to the neat resin. This could be due to the presence of the glass particles in the reactive mixture limiting the mobility of the reactive species. The improvement of both polymerization and crystallization kinetics with the silanized particles, however, supports the compatibility of the silane modified particles with the resin. Indeed, the presence of primary amine groups in the AEAPTMS silane could lead to the formation of hydrogen bonds at the particle-matrix interface, between the carbonyl of PA6 and the primary amines of the silane (Section 1.3.2.3).

Accordingly, the grafted amino-silane on the glass particles not only eliminates surface bonded hydroxyls that slow down the polymerization process, but also can improve particulate-matrix adhesion (Section 1.3.3.2). It is thus interesting to note that the silanized calcinated particles, and the strictly calcinated particles, display similar polymerization rates in Figure 2.14, since the grafted aminosilane does not participate to the polymerization reaction itself. However, the crystallization is slightly faster with silanized particles, which could be due to the enhanced interactions with the matrix (Figure 2.14, Table 2.6). In addition, it was reported that grafted silanes can contribute to crystal nucleation [106]. Therefore, this contribution of the silane, in promoting crystallization, increases the melting temperature and enthalpy of PA6.

2.4.5.2 Relevance of the developed protocol

In order to confirm the relevance of the established protocol, the silanization time was increased to 6 h. Then, the 6 h silanized particles were characterized by FTIR spectroscopy and compared to the 2 h silanized particles in Figure 2.15(a).

The result shows a significant increase in the intensity of the hydroxyl peak with increasing the treatment time. This means that the grafting of the silane on the particles surface reaches a maximum and then stabilizes. Increasing the treatment time leads

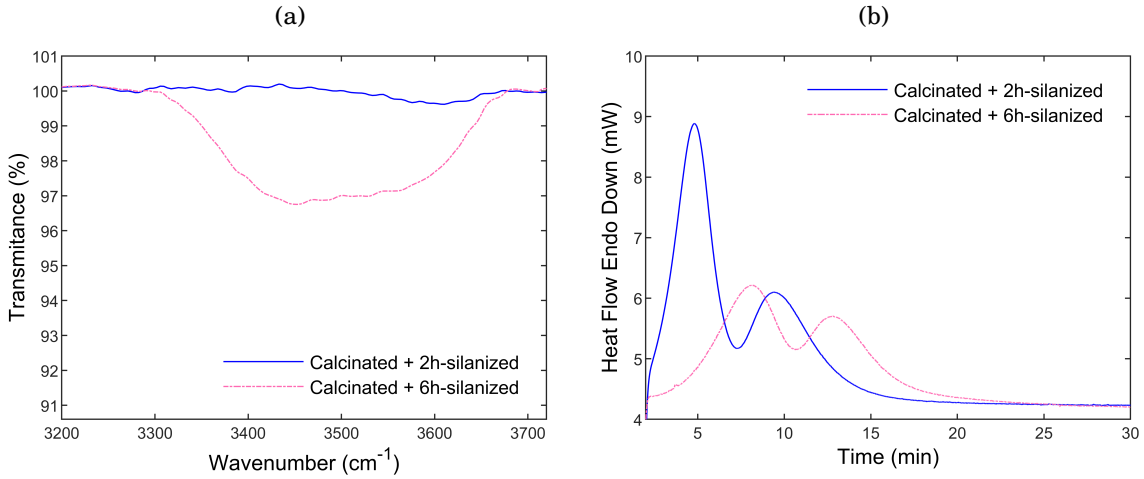

Figure 2.15: (a) FTIR spectra of 2 h and 6 h silanized particles. (b) DSC curves of isothermal syntheses at 180°C for composites synthesized with 2 h and 6 h silanized particles

to regeneration of hydroxyl groups inaccessible to the silane chains, which remain on the surface and can negatively impact the polymerization. This is confirmed by the DSC thermograms illustrated in Figure 2.15(b). The composites were synthesized with calcinated + 6 h silanized particles, and the polymerization/crystallization kinetics were compared to composites containing calcinated + 2 h silanized particles. The trapped and unreacted OH groups indeed slowed down the polymerization and crystallization processes.

2.5 Conclusion

This chapter demonstrates that carefully tailoring and monitoring the surface chemistry of reinforcing particulates is necessary in order to optimize the processing of anionic PA6 based composites. In this system, it is critical to determine the initial surface concentration in hydroxyl groups, and to precisely monitor both rehydroxylation and silane grafting reactions during the silanization process, in order to maximize the PA6 polymerization reaction rate and crystallization – failing to do so can ultimately result in the complete inhibition of the polymerization reaction due to catalyst deactivation.

The hydroxyl groups surface concentration is systematically characterized and quantified by TGA and FTIR spectroscopy, for the complete particle surface modification sequence, from the dehydration, dehydroxylation and rehydroxylation processes, to the silanization step, as a function of treatment time and conditions – allowing to establish a direct relationship between FTIR transmittance and hydroxyls surface density. Then, the impact of the particles surface chemistry on the polymerization and crystallization of the PA6 based composites is quantified by DSC.

The exact determination of the number of hydroxyl groups is tricky because of the

uncertainty on the specific surface measured by BET. Indeed, the microporosities created by the particle aggregates are not detectable by this technique, which considerably underestimates the value of the specific surface area.

It has been shown that dehydration can be separated from dehydroxylation by TGA, allowing the determination of the number of hydroxyl groups by dehydroxylation without considering the water physically adsorbed on the surface.

The effect of the calcination time at 450°C on the dehydroxylation was highlighted through the monitoring of the quantity of hydroxyls as a function of time. Then, the *in situ* synthesis of anionic PA6 composites with the glass particles calcinated at different times was assessed. An excessive hydroxyl quantity on the glass surface inhibits the polymerization of PA6. Thus, we identify a suitable calcination time which limits hydroxyl quantity allowing to promote the polymerization reaction. A calcination time of 10h at 450°C appears as a relevant condition for this synthesis.

Compared to rehydroxylation under severe acid conditions, both the rehydroxylation and silanization processes can be realized simultaneously in the silanization bath in mild acidic conditions without any negative impact on the polymerization reaction, the silane agent gradually replacing the regenerated hydroxyls, if the process is quantified and carefully monitored – removing one processing step. The effect of treatment time on the competition between condensation and rehydroxylation during silane grafting from aqueous solution was identified. A treatment time of 2 hours presents a good compromise between the number of regenerated hydroxyls reacting during the treatment, which improves the polymerization/ crystallization kinetics.

To our knowledge, the control of the amount of hydroxyl groups during calcination or grafting of a silane coupling agent on the surface of glass particles has not been reported until now. In our application, this control allows to preserve the polymerization and crystallization kinetics during the *in situ* synthesis of anionic PA6 based composite. Many other applications can benefit from improved -OH groups control using the same protocol, such as composites manufacturing, glass coatings for hydrophobic surfaces, antibacterial and antifungal surfaces, waterproof windows, antifouling coatings for eyeglasses and any other application requiring silane treatment. This protocol will be used in the rest of the study.

CHAPTER 3

IMPACT OF SILANE INTERFACIAL CHEMISTRY ON THE SYNTHESIS OF ANIONIC PA6 GLASS REINFORCED COMPOSITES

Contents

3.1 Surface treatments **76**
3.1.1 Low chemical interactions 77
3.1.2 Weak bonds 77
3.1.3 Strong bonds 78
3.1.4 Silane grafting 81
3.2 Particle surface characterization **82**
3.2.1 FTIR spectroscopy 82
3.2.2 X-ray Photo-electron Spectroscopy 84
3.2.3 Confocal laser scanning microscopy (CLSM) 89
3.2.4 Thermogravimetric Analysis (TGA) 92
3.2.5 Contact angles 94
3.3 Influence of the surface treatment on PA6 polymerization and crystallization **97**
3.3.1 Influence on PA6 synthesis kinetics 97
3.3.2 Impact on the conversion degree and crystallization 98
3.3.3 Relationship between surface chemistry of glass particles and polymerization/crystallization kinetics 100
3.4 New reactive treatment synthesis **102**
3.4.1 MONOMSILANE synthesis mechanism 103

3.4.2 Procedure for the MONOMSILANE synthesis and grafting 104
3.4.3 Particle surface characterization 104
3.4.4 Contact angle 106
3.4.5 Overview of the monomer grafting on the particle surface 107
3.4.6 Influence of the MONOMSILANE treated particles on PA6 polymerization and crystallization 108
3.5 Conclusion **111**

Introduction

The interaction between the reinforcement and the matrix at the interface of the composite is crucial to improve the mechanical properties. Indeed, the load transfer during a mechanical stress is conditioned by the quality of the interface and, consequently, by the type of the reinforcement-matrix interfacial interaction. Thus, the grafting of a silane coupling agent on the glass particles surface improves the interface performance and composites properties. However, in the case of anionic PA6/glass composite, the grafted silane interacts directly with the matrix during the *in situ* synthesis and an unsuitable coupling agent can negatively influence the polymerization. Therefore, in addition to hydroxyls, the nature of silane coupling agent also has a significant influence on PA6 polymerization. It is, thus, necessary to select, synthesize and graft adequate coupling agents on the reinforcement for the reactive synthesis of anionic PA6 according to the targeted interfacial interaction.

It is possible to create different types of interfacial bonds between the glass particles and the matrix depending on the nature of the silane "R" function (Section 1.3.2, Figure 1.21). Although the importance of the interface on the properties of the composite was highlighted in the literature, the existing works on anionic PA6 focused on one type of aminosilane, which is commonly used with conventional polyamides [10, 107, 108]. Hydrogen bonds are created between the PA6 carbonyls and the primary amines of the silane, as explained in Section 1.3. In addition, only one publication has emphasized the role of the silane coupling agent on the AROP of PA6 [101]. It focuses on a single aminosilane which is 3-aminopropyltriethoxysilane (APTES). Hence, the influence of the surface treatment, in particular the silane type and its effect on the filler-matrix interaction and the synthesis of anionic PA6 were not investigated. Indeed, the control of the type of reinforcement-matrix interaction at the interface according to the surface treatment and the silane grafted on the glass particles surface is a critical point on the polymerization and crystallization kinetics of the anionic PA6 and especially, as it drives the properties of the resulting composite material.

Therefore, before investigating the role of the grafted silane on the mechanical properties of GF/PA6 composites, the impact of the silane chemistry at the fiber-matrix interface during the polymerization and crystallization of the PA6 matrix must be analyzed and understood.

This chapter then focuses on understanding the impact of the silane agent chemistry, on the polymerization and crystallization of PA6/glass particles composites. Our approach is based on an optimized grafting protocol that ensures efficient anionic ring-opening polymerization of ϵ-caprolactam, with high degrees of monomer conversion and silane grafting, as described in the previous chapter. Three types of complementary silane chemistries, leading to distinct interfacial interactions with the PA6 matrix, are considered: (i) First, an hydrophobic silane minimizing the interfacial interactions; (ii) Second, two aminosilanes forming hydrogen bonds with the PA6 matrix; (iii) Third, a grafted silane

containing the activator and monomer reactants, in order to involve the glass surface in the polymerization reaction and therefore generate covalent bonds at the interface. A systematic and rigorous characterization of the silanized glass surface was performed by Fourier Transform Infrared (FTIR) spectroscopy, X-ray photoelectron spectroscopy (XPS), confocal laser scanning microscopy (CLSM), thermogravimetric analysis (TGA), and contact angles measurements. Finally, the impact of the chemical nature of the silane on the polymerization and crystallization kinetics was evaluated via DSC measurements.

3.1 Surface treatments

The chemical structures of four types of silanes, and the expected interactions with the anionic PA6 matrix, are presented in Table 3.1. The first three silanes were purchased from Fisher Scientific and used as received. The last one was specially synthesized. All of them are described in this section.

Table 3.1: Name and structure of the considered silanes and related interfacial interactions expected with the anionic PA6 matrix

Name	Chemical structure	Interaction with anionic PA6
Trimethoxy(propyl)-silane (TMPS, 98%)	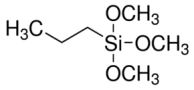	Low interactions
(3-Aminopropyl)trimethoxysilane (APTMS, 97%)	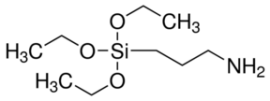	Weak hydrogen bonds
3-(2-Aminoethylamino)-propyltrimethoxysilane (AEAPTMS, 96%)	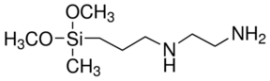	Weak hydrogen bonds
ACTISILANE	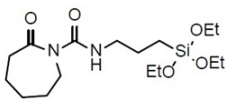	Strong covalent bonds

3.1.1 Low chemical interactions

Trimethoxy(propyl)silane (TMPS, 98%) was selected to generate a hydrophobic surface with minimum interactions with the PA6 matrix. Indeed, the CH3 groups present at the silane end are non-polar and prevent interactions with the hydrophilic matrix. The grafting mechanism is shown in Figure 3.1.

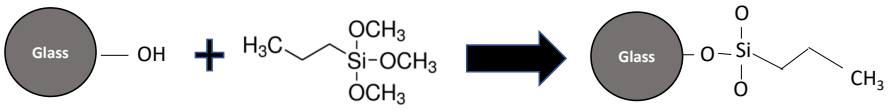

Figure 3.1: Grafting of TMPS on the glass particle surface

3.1.2 Weak bonds

Two aminosilanes terminated with primary amines were used to create hydrogen bonds between the glass particles and the PA6 matrix. Indeed, the amine groups are able to create hydrogen bonds with the PA6 carbonyl [104]. 3-Aminopropyl)trimethoxysilane (APTMS, 97%) was chosen because it is currently used with anionic PA6 reinforced with glass particles [10, 101, 107, 108] and is therefore an adequate system for comparison purposes. However, although APTMS can catalyze the formation of siloxane bonds, the primary amines of this silane also catalyze their hydrolysis, which leads to the formation of unstable silane layers [127, 158]. As explained in Section 1.4.3.3, it is possible to minimize hydrolysis catalyzed by amine functions by controlling the length of the alkyl chain [126]. Accordingly, Zhu et al. [127] showed that 3-(2-Aminoethylamino)propyltrimethoxysilane (AEAPTMS, 96%) allows to create stable silanol bonds due to secondary amine groups. Indeed, the secondary amines of these silanes can catalyze the siloxane bond formation and the steric hindrance created by the chain length prevents catalyzing the hydrolysis. In addition, this silane allows to obtain reproducible silane layers. Therefore, AEAPTMS represents a better candidate for surface modification by aminosilanes. The grafting mechanism for both silanes is shown in the Figure 3.2.

(a)

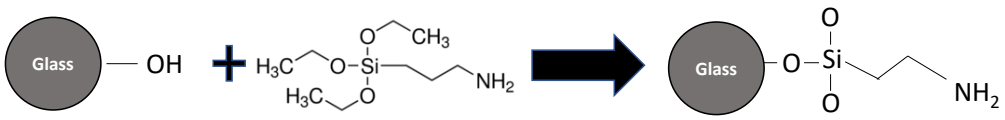

(b)



Figure 3.2: Grafting mechanism of aminosilanes on the surface of glass particles. (a) APTMS (b) AEAPTMS

3.1.3 Strong bonds

Currently, the coupling agents frequently used are aminosilanes. The interaction at the reinforcement/matrix interface with this type of silane is based on weak bonds, especially hydrogen bonds. However, it was shown that these coupling agents can negatively impact the anionic polymerization. Indeed, the primary amines of the aminosilanes decrease the reactivity of the matrix as explained in Section 1.3.2.3. In addition, the transamidation reaction described by Van Rijwisk et al. [101] between the aminosilane and the matrix induces PA6 chain breakage close to the interface, which decreases the molar weight in this region and reduces the final mechanical resistance of the composites (Section 1.3.2.3). As a reminder, the technique based on the work of Van Rijswijk et al. [101] is very long and involves several steps. On the other hand, the technique described by Yang et al. [128] based on the use of TDI could be limited by the loss of the isocyanate functions, which prevents the activator formation. Moreover, the handling of TDI requires rigorous precautions due to its toxicity. For this reason, a new technique was developed to graft the polymerization activator onto the surface of the particles. A new coupling agent named ACTISILANE containing the N-acetylcaprolactam function of the activator at its end was synthesized from 3-isocyanatopropyltriethoxysilane (95%). ACTISILANE was grafted onto the surface of the particles according to the mechanism shown in Figure 3.3. The synthesis of ACTISILANE and its optimized procedure is detailed in the following section.

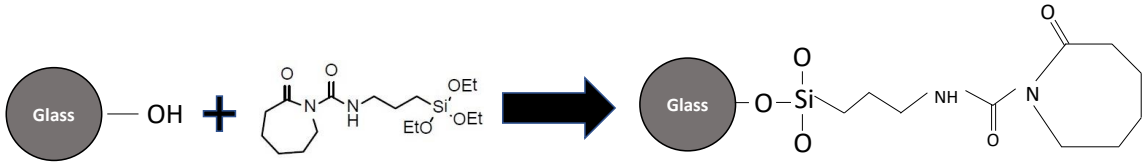

Figure 3.3: Grafting mechanism of ACTISILANE on the surface of glass particles

3.1.3.1 Procedure for ACTISILANE synthesis

ACTISILANE was synthetized by adding 21.95 ml of 3-isocyanatopropyltriethoxysilane (IPTS, 95%) and 10 g of monomer ϵ-caprolactam in a hydrophobic beaker under inert atmosphere in a glove box. The mixture was then heated to 70°C under stirring and left in the glove box for 4 h. In order to optimize the nitrogen consumption by the glove box, the beaker was hermetically closed and taken out of the glove box. It was then left to react for 72 h at 70°C under stirring to ensure a complete reaction. The resulting product is liquid and translucent.

3.1.3.2 Synthesis mechanism of ACTISILANE

The isocyanate function in IPTS has a high reactivity due to its strong polarization. Indeed, the carbon with a partially positive charge is located between the more electronegative nitrogen and oxygen atoms, which results in a high electrophilicity. This electrophilicity makes the isocyanate very reactive towards nucleophiles, especially amines. Initially, the electrophilic carbon of the isocyanate function is attacked by the free electron pair of the nitrogen present in the amide function of the caprolactam. This results in the formation of a urea function and the formation of the carboxamide function. In a second step, a proton exchange leads to the formation of the N-acetylcaprolactam function. The mechanism of the reaction is shown in Figure 3.4.

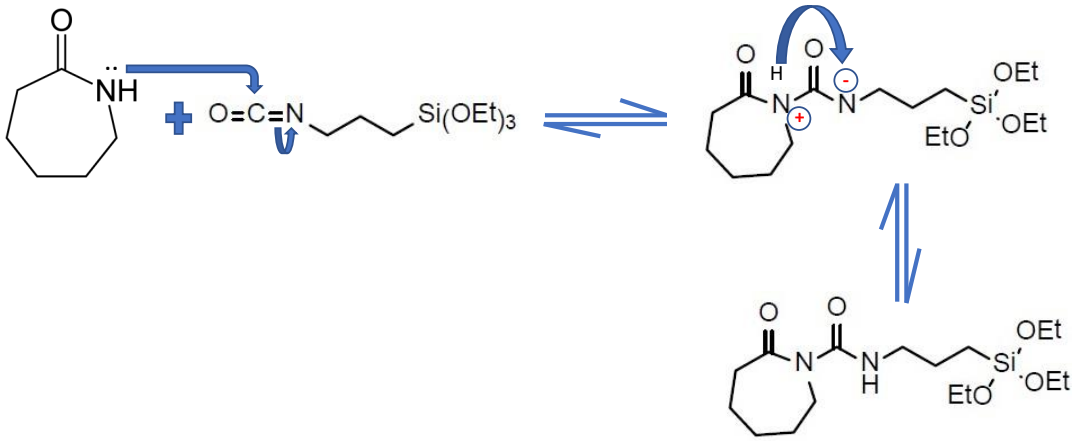

Figure 3.4: Reaction mechanism for the synthesis of the ACTISILANE coupling agent

3.1.3.3 Characterization of the synthesized ACTISILANE

The synthesized ACTISILANE was characterized by Fourier transform infrared spectrometry with a Perkin Elmer Spectrum One apparatus in Attenuated Total Reflectance (ATR) mode to verify the efficiency of the reaction and to ensure the formation of the N-acetylcaprolactam function. A Diamant/ZnSe crystal was used and the spectra were measured in a wavelength range between 650 and 4000 cm^{-1} with a resolution of 1 cm^{-1}.

The change in the chemical functions due to the reaction was followed by comparing the spectra of the ACTISILANE to those of the monomer (ϵ-caprolactam) and to the spectra of 3-isocyanatopropyltriethoxysilane. The spectra of ACTISILANE and the monomer were obtained by analyzing both products. Due to its high toxicity (acute inhalation toxicity, severe skin burns and eye damage), 3-isocyanatopropyltriethoxysilane was not analyzed with our FTIR spectrometer. Instead, its spectrum was obtained from the product supplier. Moreover, 3-isocyanatopropyltriethoxysilane is very sensitive to humidity. It must be handled under an inert gas, which also makes its analysis unmanageable with our spectrometer.

The comparison of the monomer and ACTISILANE spectra is shown in Figure 3.5(a), the 3-isocyanatopropyltriethoxysilane spectra is presented in Figure 3.5(b). The peak at 2272 cm^{-1} characteristic of the isocyanate function is present in the spectra of 3-isocyanatopropyltriethoxysilane. Then, it disappears on the spectra of ACTISILANE, which shows that the isocyanate function has completely reacted. Moreover, the peak at 1667 cm^{-1} on the monomer spectra characteristic of the carbonyl function of lactam has been transformed into two peaks on the ACTISILANE spectrum. The first one at 1657 cm^{-1} characterizes the carbonyl of the ring and the second peak at 1702 cm^{-1} characterizes the carbonyl of the urea bond. This confirms the reaction of the isocyanate function with the monomer containing a single carbonyl and the formation of the N-acetylcaprolactam function containing two carbonyls. The other transformations observed in the spectra confirm the efficiency of the reaction. Indeed, the two peaks at 3080 and 3200 cm^{-1} characterizing the N-H bond in the "cis" form were transformed into a single peak on the ACTISILANE spectra at 3280 cm^{-1} characterizing the N-H bond of the urea function. In addition, the appearance of the peaks at 1536, 1397 and 1166 cm^{-1} confirm the presence of N-H bonds, and the asymmetric and symmetric stretch of the N-C-N bond, respectively, of the urea function formed in the ACTISILANE. The other peaks between 1400 and 1500 cm^{-1} and between 2800 and 3000 cm^{-1} characterize the CH_2 bonds. The large peaks between 500 and 1100cm^{-1} in ACTISILANE correspond to siloxane and silanol bonds confirming the conservation of its functions after synthesis. These results confirm that the synthesis reaction of ACTISILANE was successful.

It would be possible to characterize the synthesized product by NMR for deeper structural analysis and to conclude on the reaction yield. Nevertheless, the reaction was considered complete by the disappearance of the isocyanate function and the appearance of the large peak at 1702 cm^{-1} characteristic of the carbonyl of the urea function. Moreover,

(a)

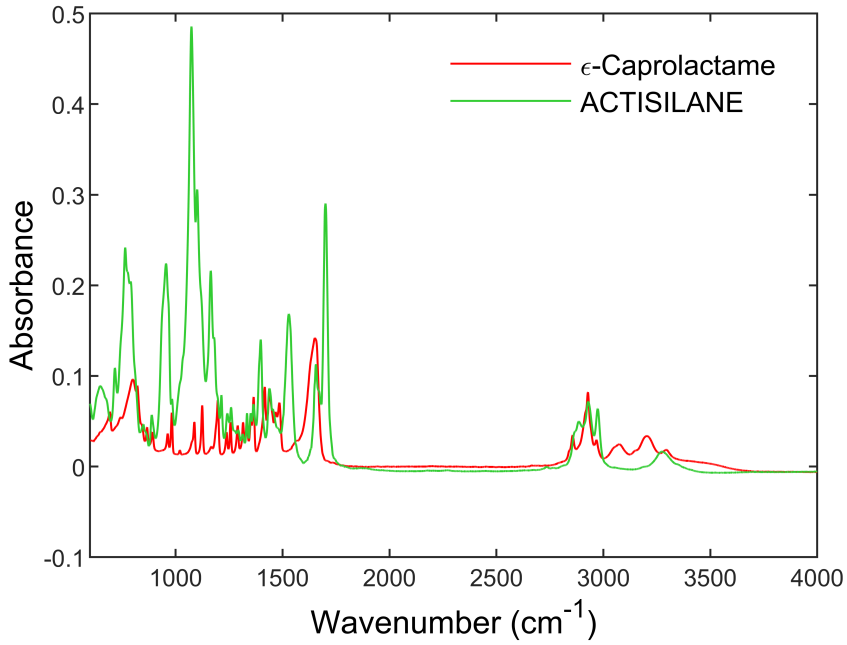

(b)

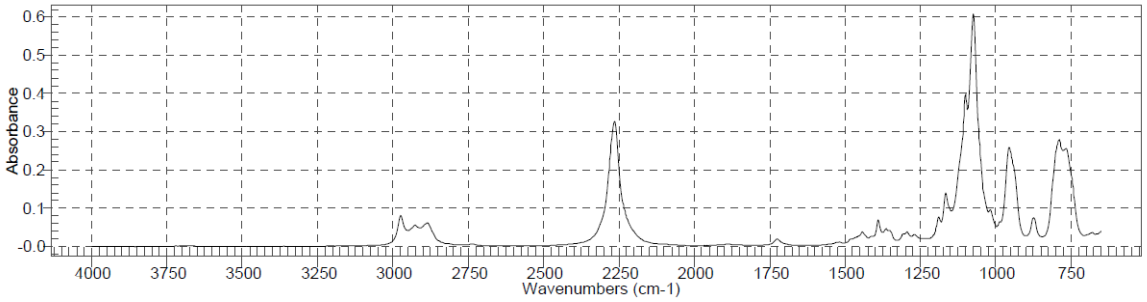

Figure 3.5: FTIR spectra of (a) ϵ-caprolactam (monomer) and synthesized ACTISILANE (b) 3-isocyanatopropyltriethoxysilane

the product obtained was considered as pure because no solvent was used during the synthesis.

3.1.4 Silane grafting

The conventional silane grafting protocol for glass reinforcements started with a calcination step in order to clean the surface from organic contaminants. Then, an activation of the glass surface in an aqueous solution of hydrochloric acid was carried out, which allowed the hydrolysis of the siloxane groups and the regeneration of hydroxyls that are then used to condense the silanes. However, the duration of each step strongly affects the density of the remaining -OH surface groups on the glass particles, and consequently the AROP of PA6, which in some cases may result in the total inhibition of the reaction as demonstrated in the previous chapter. By thoroughly controlling the quantity of -OH groups at the glass particles surface during the whole surface modification sequence, from

the dehydration, dehydroxylation and rehydroxylation processes, to the silanization step, as a function of treatment time and conditions, an optimal grafting protocol was defined in the previous chapter.

Based on Chapter 2 results, the main steps of the surface treatment consist in calcinating the particles for 10 h at 450°C, followed by simultaneous rehydroxylation and silanization for 2 h. This protocol allows for significant silane grafting onto the glass surface, while limiting the presence of residual hydroxyl groups. The silanes were added to an aqueous solution at a 5%(v/v). The pH was then adjusted to 4-5 with acetic acid. As a reminder, silanization was carried out in acidic conditions to promote the formation of silanols and to slow down self-condensation between the resulting hydrolyzed silanol groups [119]. The mixture was stirred for about 45 min. After silane hydrolysis, the glass particles were added to the solution and stirred for 1 h. The mixture was then kept at 100°C for 1 h to condense the silanol groups on the surface and to remove traces of methanol from the hydrolysis of the methoxysilanes. Finally, the particles were rinsed twice with ethanol and twice with water to remove the unreacted silanes, before drying for 2 h at 115°C. The same grafting protocol was used for all of the silanes, except in the case of the ACTISILANE, for which water was replaced by ethanol since the synthesized silane is not soluble in water.

3.2 Particle surface characterization

The silanized particles were characterized by FTIR spectroscopy, XPS, CLSM, TGA and contact angle measurements. The results were compared to the results on calcinated particles (untreated particles), used as a reference, to evaluate the extent of surface modification.

3.2.1 FTIR spectroscopy

3.2.1.1 Procedure

FTIR spectroscopy analyses in transmission mode were performed on a Bruker Vertex 70 spectrometer. Untreated and surface modified glass particles were mixed with high purity infrared grade KBr powder at 1.5-2 wt%, and pressed into pellets. The spectra were measured between 400 and 4000 cm^{-1} with a 2 cm^{-1} resolution. A background was obtained with a pure KBr pellet before measuring the spectra of each glass particle sample.

3.2.1.2 Results

The spectra of untreated and TMPS treated particles are compared in Figure 3.6(a). The appearance of a number of peaks between 2850 and 2970 cm^{-1} is characteristic of CH_2 and CH_3 bonds, and confirms the presence of grafted silanes on the surface of the treated

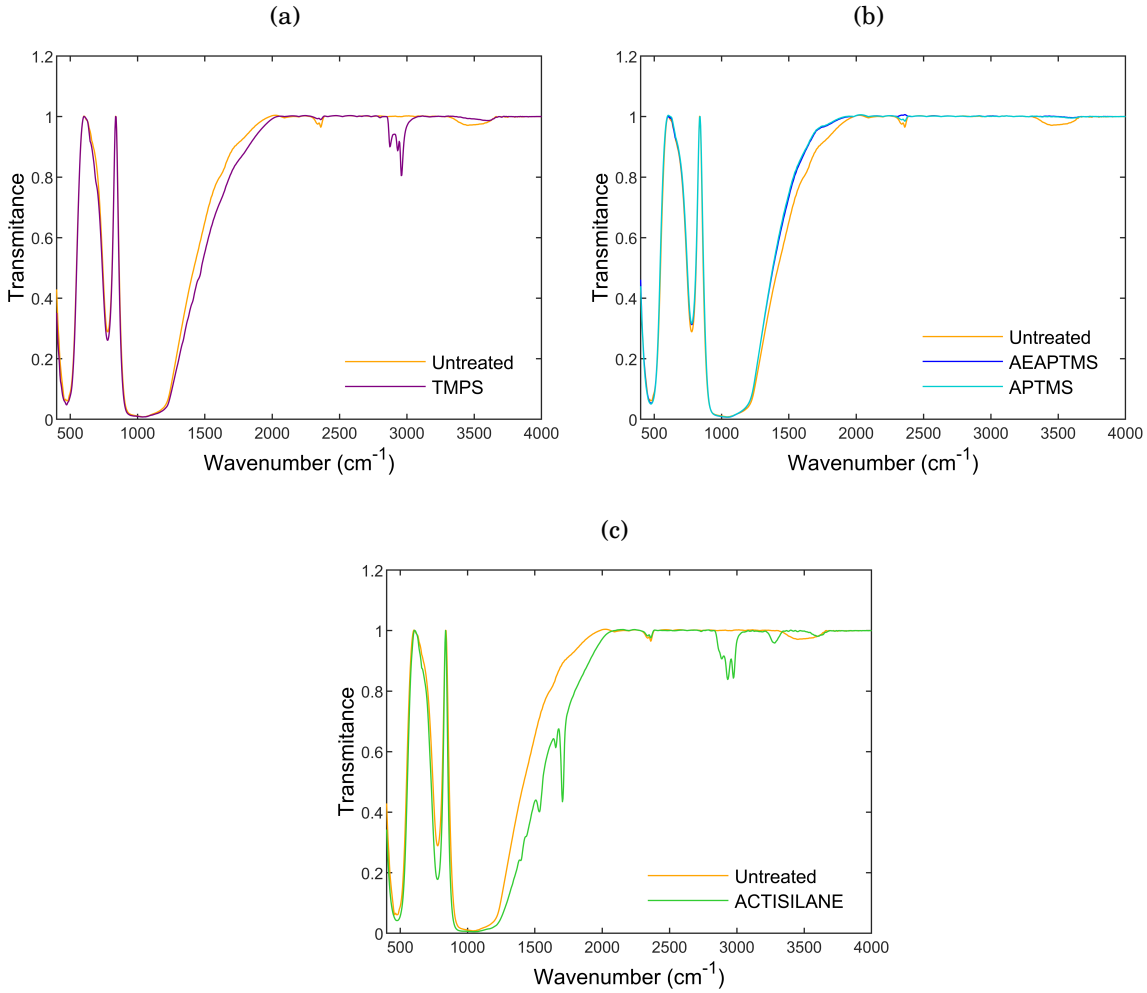

Figure 3.6: FTIR spectra of untreated particles compared to the spectra of particles treated with (a) TMPS, (b) APTMS and AEAPTMS, and (c) ACTISILANE

particles. Moreover, the peak at 3500 cm^{-1} related to hydroxyl groups that can be observed in the spectra of the untreated particles almost disappears in the spectra of the treated ones. This supports the condensation reaction of -OH groups with silanes, as well as the relevance of the grafting protocol used to limit the hydroxyls surface density

Figure 3.6(b) shows the spectra of the particles treated with APTMS and AEAPTMS, compared to the spectra of the untreated particles. As in the previous case, the reduction of the peak at 3500 cm^{-1} related to the -OH groups indicates the reaction of these groups with the silanes. However, the spectra do not show the presence of the amine group peaks on the surface of the particles. Theoritically, the N-H function is characterized by a peak, between 3250 and 3450 cm^{-1} related to the stretching vibration, and another one between 1530 and 1650 cm^{-1} related to the bending vibration - these peaks are not obvious in our signals. Thus, other techniques of surface characterization are necessary in order to further analyze the surface chemistry and confirm the presence and the retention of the amine groups on the surface after grafting.

Figure 3.6(c) shows the spectra of particles treated with the ACTISILANE, compared to the spectra of untreated particles. The ACTISILANE functions on the surface of the

treated particles are obvious. First, the peaks between 2850 and 2970 cm^{-1} are associated to the presence of CH_2 groups. Then, the peaks at 3280 and 1536 cm^{-1} correspond of the N-H bond of the urea function initially visible in the spectra of the synthesized ACTISILANE (Figure 3.5(a)), which reappear in the spectra of the treated particles, confirming its successful grafting and the retention of the chemical functions. The same conclusion stems from the peaks at 1657 and 1702 cm^{-1}, related to carbonyl groups. On the other hand, the intensity of the peak at 3500 cm^{-1} for the untreated particles, relative to hydroxyls, decreases in the spectrum of the treated particles, and it shifts to 3600 cm^{-1}. As demonstrated in Section 2.4.2, the wavenumber of hydroxyl groups decreases when they are involved in hydrogen bonds [150]. In the case of untreated particles, the hydroxyls groups create hydrogen bonds since they are close to each others. Then, the reaction with silane leads to decrease the number of -OH groups which becomes progressively isolated, which shifts the signal to higher wavenumbers.

3.2.2 X-ray Photo-electron Spectroscopy

3.2.2.1 Procedure

The XPS experiments were performed by Jérôme Evan at CIRIMAT, ENSIACET-INP Toulouse. The photoelectron emission spectra were recorded using a monochromatic Al K-alpha (hυ = 1486.6 eV) source on a ThermoScientific K-Alpha system. The X-ray spot size was about 400 µm. The pass energy was fixed at 30 eV with a step of 0.1 eV for core levels and 160 eV for surveys (step1 eV). The spectrometer energy calibration was done using the Au $4f_{7/2}$ (83.9 ± 0.1 eV) and Cu $2p_{3/2}$ (932.8 ± 0.1 eV) photoelectron lines. XPS spectra were recorded in direct mode N (Ec) and the background signal was removed using the Shirley method. A flood gun was used to neutralize charge effects on the top surface. The glass particles were glued onto a carbon adhesive tape prior to entering in the chamber.

3.2.2.2 Results

XPS allows a finer analysis of the chemical composition of a surface. The elements are probed within 10 nm depth. This analysis is complementary to the FTIR spectroscopy investigation to check the presence and the conservation of the grafted chemical functions, in particular the amine functions of the particles treated with the aminosilanes - not detected on FTIR spectra - and N-acetylcaprolactam function. Three samples were selected for the XPS analysis. The untreated particles that are used as a reference. Second, the APTMS treated particles were analyzed since the alkyl chain of this silane is simpler to interpret than AEAPTMS. In addition, APTMS is the most commonly used, which allows a comparison with the literature. Finally, the particles treated with the ACTISILANE were considered since this silane exhibits a rather complex termination and requires an extensive analysis due to its novelty.

Survey scans

The survey scan allows to determine the chemical elements present on the surface and gives the atomic ratio of each element. An example of survey scan for particle treated with ACTISILANE is given in Figure 3.7.

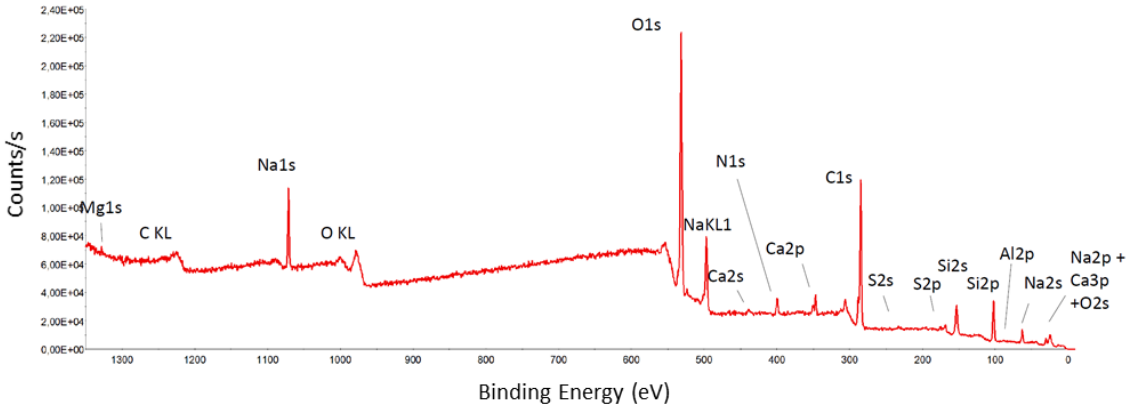

Figure 3.7: Survey scan of particles treated with ACTISILANE

The ratios of elements on the surface of the particles are compared in Table 3.2. Silicon, calcium, oxygen, sodium and magnesium are specific to glass particles, while carbon, oxygen and nitrogen come from the silanes. A significant amount of carbon is also detected on the surface of the untreated particles, which comes from atmospheric pollution and the carbon tape used to support the particles. Since all the samples were prepared in such a way, comparing the evolution of the ratios after grafting is relevant.

Table 3.2: Identification and quantification of elements from XPS analysis for the untreated particles, and particles treated with APTMS and ACTISILANE

Atoms	Binding Energy (BE)	Atomic (%)		
		Untreated	APTMS	ACTISLANE
Si 2p	103.1	16.0	16.7	12.3
C 1s	285.0	35.4	41.0	43.2
O 1s	532.0	38.6	34.0	32.5
N 1s	400.0	-	2.4	2.7
Na 1s	1701.4	6.1	3.7	6.5
Ca 2p3/2	346.2	1.9	1.4	1.5
Mg 1s	1303.1	Traces	Traces	Traces

The evolution of the C/Si and O/Si ratios are preferred in the literature to characterize coupling agents [123, 124]. The results in Table 3.3 show an increase of the C/Si ratio after the grafting of both silanes, in agreement with the higher number of carbons in the grafted chains. The O/Si ratio varies as a function of the type of silane: it decreases in the case of APTMS because grafting reduces the amount of oxygen (only the oxygen of silanols after hydrolysis is still present). Thus, the amount of grafted oxygen is lower than the

amount of grafted silicon. However, this ratio increases in the case of the ACTISILANE because oxygen atoms remain in its structure. The quantity of grafted oxygen is thus higher compared to the quantity of grafted silicon. Accordingly, the C/Si ratio increases more than the C/O ratio in the case of the ACTISILANE, which is the opposite trend to what is observed for APTMS.

Nitrogen is not present on the surface of untreated particles, but it appears on the surface of silanized particles. This supports not only the presence of the silanes on the surface of the treated particles, but also the preservation of the amine functions after grafting, supporting also the FTIR spectroscopy results. For both types of grafted surfaces, the N/Si ratio is lower than 1, which is consistent with the literature [124]. It is explained by the significant presence of Si on the glass particle surface.

However, since silicon, carbon and oxygen are present both in the silanes and at the surface of the untreated particles, the calculated ratio relative to silicon can be affected by the change in the silicon percentage according to the silane type. In order to overcome this limitation, it is interesting to focus on an element specific to the surface of glass particles and that is not present in the silane, i.e. Calcium. Indeed, the use of various modifying oxides during the glass manufacturing is reflected as traces in its final composition. In particular, the use of calcium oxide to increase the chemical resistance, luster and decrease the solubility of glass leads to the appearance of calcium on its surface during XPS analysis. The C/Ca, O/Ca and Si/Ca ratios are given in Table 3.3. Previous comparisons based on silicon are confirmed by respective ratios based on calcium, which supports the successful grafting of silanes on the surface of glass particles. The increase of the O/Ca ratio in the case of APTMS is noteworthy, contrary to the O/Si ratio. Indeed, the grafted silane contains silicon and oxygen atoms specific to the silanol function, but it does not contain calcium. Thus, silane grafting increases the O/Ca ratio whereas the O/Si ratio decreases since the added silicon after grafting is higher than oxygen.

Table 3.3: Atomic concentrations relative to silicon and calcium, for untreated particles and particles treated with APTMS and ACTISILANE

Atoms	/Si			/Ca		
	Untreated	APTMS	ACTISLANE	Untreated	APTMS	ACTISLANE
C	2.2	2.4	3.5	18.4	29.3	30.4
O	2.4	2.0	2.6	20.1	24.3	22.9
N	-	0.1	0.2	-	1.7	1.9
Si	-	-	-	8.3	11.9	8.7
C/O	0.9	1.2	1.3	0.9	1.2	1.3

High resolution scans

Also, XPS analysis allows to identify the atomic chemical environment and to estimate the chemical bonds created by each atom. This is achieved by deconvolving the high-resolution scans of the selected atoms for each treatment. In our case, the high-resolution scans were

performed on C 1s, O 1s and Si 2p for the untreated particles, then the same atoms adding the high-resolution spectrum of N 1s for the treated particles. The deconvolution peaks and atomic percentages of silicon Si 2p and oxygen O 1s do not present relevant results, so the focus was put on the C 1s and N 1s atoms.

(a)

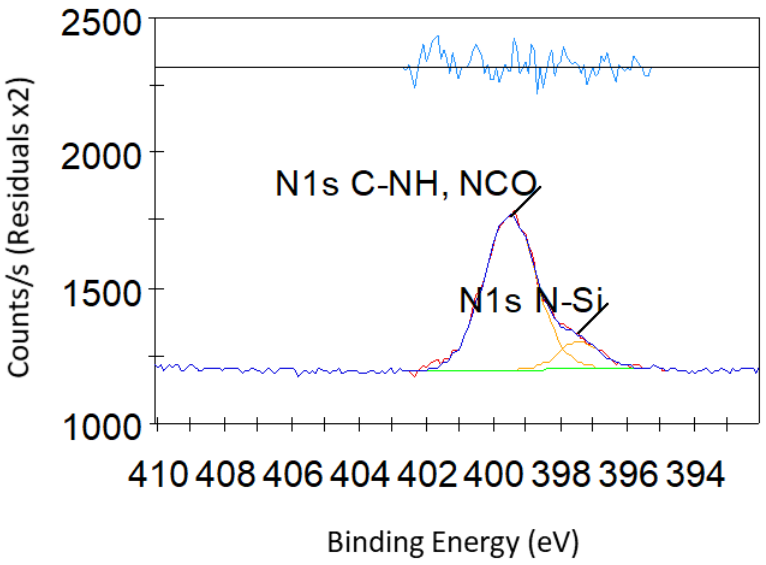

(b)

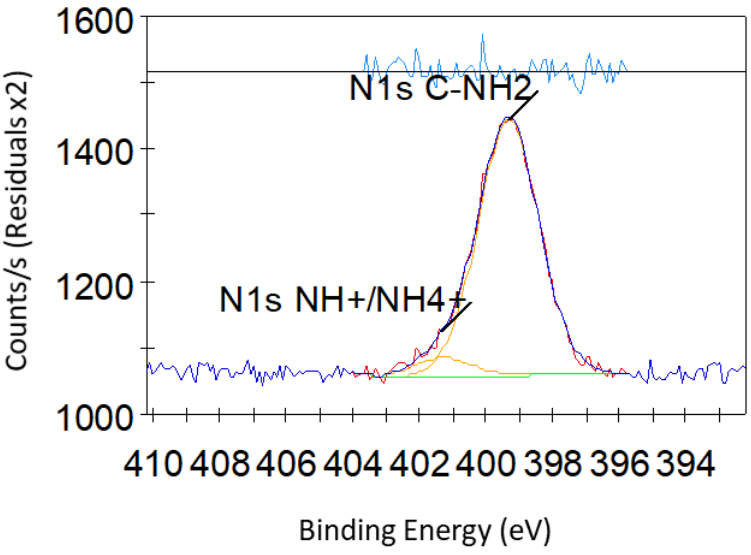

Figure 3.8: High resolution scans of N 1s for particles treated with (a) ACTISILANE (b) APTMS

Figure 3.8 shows an example of a high-resolution scan of the N 1s atom for ACTISILANE particles compared to that of APTMS particles with the corresponding peak deconvolution. The comparison of both scans shows that the nitrogen present in the APTMS particles is mainly engaged in $C-NH_2$ bonds. This is due to the primary amines of the silane chain. A slight peak related to NH^+/NH_4^+ bonds also appears which may be due to the protonation of the primary amines during hydrolysis. Concerning ACTISILANE,

the spectrum shows that the nitrogen present on the surface forms mainly N=C=O/C-NH bonds which are due to the carbonyls of the N-acetylcaprolactam function of the activator as well as to the presence of a secondary amine in the ACTISILANE molecule. The slight peak of the N-Si bond may be due to a parasitic reaction between the silanol and the amine.

In order to quantify the evolution of chemical bonds after grafting, the atomic percentages of the bonds formed by each atom can be determined. Table 3.4 presents the bond atomic percentages obtained from the high resolution spectra of carbon C 1s and nitrogen N 1s for the three types of particles analyzed.

Table 3.4: Identification and quantification of chemical bonds from high-resolution scans of C 1s and N 1s for the untreated particles and particles treated with APTMS and ACTISILANE

Atoms	Identification	Binding Energy (BE)	Atomic (%)		
			Untreated	APTMS	ACTISLANE
C 1s	CC, CH, C-Si-O (C1)	284.6	30.3	32.0	31.8
	CN, C-O (C2)	286.1	1.9	4.7	5.1
	O-C=O (C3)	288.3	3.2	4.3	6.3
N 1s	$C-NH_2$	399.3	-	2.2	-
	NH^+/NH_4^+	401.3	-	0.2	-
	N-Si	397.5	-	-	0.3
	C-NH, N=C=O	399.5	-	-	2.3

The percentage of carbon C1 increases after treatment due to the addition of CH bonds of the alkyl chain of the silane. In addition, a significant increase is observed for the C2 bonds after grafting. This indicates the presence of nitrogen bonded to carbon (CN), thus confirming the conservation of the silanes amines. The increase of the C3 bond in the case of APTMS is very slight and not significant. However, in the case of ACTISILANE, the increase of this bond is more significant due to the presence of carbonyl groups in the grafted silane, which demonstrates the conservation of these functions after grafting. This agrees with the FTIR spectroscopy results.

The calculated percentage of NH^+/NH_4^+ and N-Si functions for APTMS and ACTISILANE particles respectively are very low and could be neglected. Therefore, the nitrogen present on the surface of APTMS particles forms mainly primary amines $C-NH_2$, which confirms the previous result of the C 1s high-resolution scan. Consequently, this supplements the FTIR spectroscopy results obtained for aminosilane in which the peaks related to the amine functions were not observed. Furthermore, the atomic percentage of the bonds formed by the nitrogen of ACTISILANE particles show that it is mainly involved in C-NH and NCO bonds. This is consistent with the C 1s high resolution scan. It confirms the successful grafting of the activator onto the particle surface.

Despite the consistency of the high resolution scan results with those of the survey scans and the FTIR spectroscopy, , some bonds have the same binding energy (BE), which may affect the interpretations. Therefore, this analysis must be supplemented with a deeper chemical environment investigation of each atom for example by the NMR technique.

3.2.3 Confocal laser scanning microscopy (CLSM)

3.2.3.1 Procedure

To visualize the efficiency of the surface treatments, the glass particles were treated with fluorescein 5-isothiocyanate (FITC) and observed by confocal microscopy. 1 mg of FITC (Fisher Scientific) was dissolved in 10 ml of absolute ethanol. Then, 10 mg of silanized glass particles were added to the solution. The mixture was stirred for 16 h in the dark at room temperature. The particles were next rinsed twice with ethanol and twice with water to remove the unreacted FITC. The FITC-labeled glass particles were finally dispersed in DMSO in order to reduce the refractive-index mismatch between the suspending media, the particles and the microscope cover slip. All images were taken laser scanning Leica SP8 confocal microscope and with the same lighting conditions to get a semi-quantitative comparison value. A PMT (PhotoMultiplier Tube) detector collected light emitted in the range 501-681 nm. Excitation of the fluorophore was ensured with a laser at λ_{ex} = 488 nm, and the laser was set to 0.2% of its full-power. An oil-immersion 40X objective with a numerical aperture of 1.3 was used. The images were acquired with the microscope set to the resonant mode and by doing 8-lines averages to improve the signal-to-noise ratio. The pinhole was set at 1 Airy Unit (≈ 61 μm), which results in an optical section thickness of 0.985 μm. The zoom factor was set to 6.81. Given the setting and the resolution (1024 x 1024 pixels), the images represented an area of 42.7 x 42.7 μm^2. The microscopic analyses were performed in the Pôle d'Etudes et Recherche de Lacq R & D center (TotalEnergies SE) by Dr. Enric Santanach Carrreras

3.2.3.2 Results

Confocal fluorescence microscopy was used to confirm the XPS results showing the presence of nitrogen and the retention of the primary and secondary amine functions on the surface of the particles treated with the aminosilanes and the ACTISILANE. For that purpose, fluorescein 5-isothiocyanate (FITC) was grafted and used as a probe to identify the presence of amines. The isocyanate group reacts with primary and secondary amines to form stable urea functions.

The images obtained by confocal microscopy are shown in Figure 3.9. Figure 3.9(a) displays a reference sample: untreated particles that have been in contact with FITC. Figure 3.9(b) shows the TMPS grafted particles. In both cases, the low level of fluorescence that is detected can be attributed to the non-specific adsorption (physisorption) of FITC.

Indeed, the -N=C=S groups of FITC selectively react with $-NH_2$ and -NH groups, and no reaction occurred with the surface functions for these particles. In addition, the raw glass particles not treated with FITC, under the same observation conditions, do not exhibit any fluorescence (Figure 3.9(c)). This confirms the slight non-specific adsorption of FITC on the surface of untreated and TMPS treated particles. On the contrary, as expected, the glass particles treated with the aminosilanes display significant fluorescence intensity compared to the untreated particles (Figure 3.9(d), 3.9(e)), confirming the presence of amine functions.

In order to have a semi-quantitative analysis of the grafting efficiency, ImageJ software was used. For at least 36 particles having undergone one type of treatment, the radial intensity profile was measured and averaged over 360°. The grafting density was then considered proportional to the peak grey value for comparison of the different types of particles. The results are reported in Figure 3.10 for all surface treatments. Error bars represent the standard deviation. Microscopy observations on TMPS treated particles not having seen FITC were also performed. An intensity level comparable to that one measured with non-treated particles was found.

The particles treated with AEAPTMS show a significant higher fluorescence level compared to the particles treated with APTMS. This is due to the presence of both primary and secondary amines on the AEAPTMS chains, while APTMS only contains primary amines. In addition, the silane multilayers formed by APTMS by vertical polymerization [126, 158] generate a higher steric hindrance than AEAPTMS which, in contrast, forms more homogeneous silane layers [127]. This increases the number of accessible amine functions in the particles treated with AEAPTMS. Thus, their reactivity with the FITC agent is greater, which explains their higher fluorescence intensity.

Finally, the fluorescence level observed for the ACTISILANE treated particles (Figure 3.9(f)) is lower compared to the TMPS treated particles, and is close to that one of the untreated particles. This indicates that, although the particles treated with ACTISILANE contain a secondary amine function as demonstrated by FTIR spectroscopy and XPS, the reaction of this function with the FITC agent is limited. Consequently, the fluorescence intensity may thus be partly due to physisorbtion. The grafted ACTISILANE and FITC are both relatively bulky molecules. Hence, the steric hindrance is likely to be the cause for the limited reaction between FITC and the ACTISILANE secondary amines and, consequently, the low fluorescence intensity.

Confocal fluorescence microscopy therefore confirms the grafting efficiency and the presence of amine groups on the surface of the particles treated with the aminosilanes, in agreement with previous results given by FTIR spectroscopy and XPS.

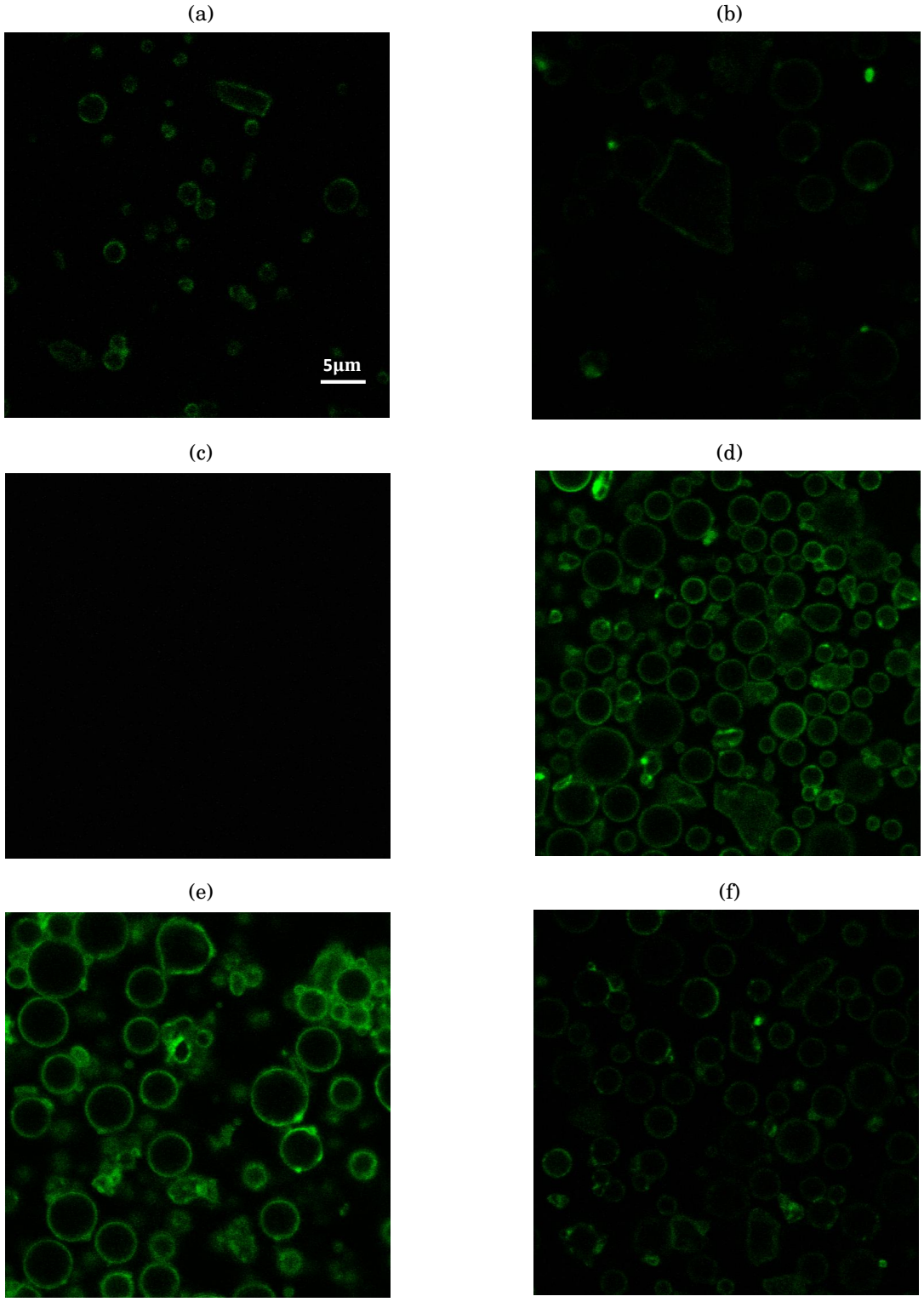

Figure 3.9: Confocal fluorescence microscopy images of (a) untreated particles, compared to particles treated with (b) TMPS, (c) Raw glass particles not treated with FITC, (d) APTMS, (e) AEAPTM and (f) ACTISILANE

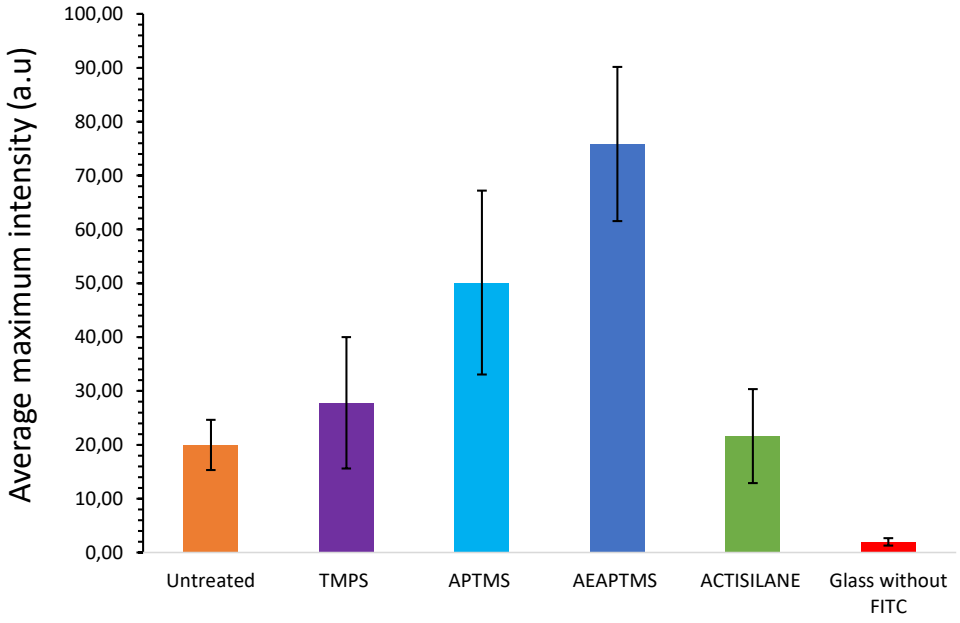

Figure 3.10: Average maximum fluorescence intensity of untreated particles, compared to particles treated with APTMS, AEAPTMS, and the ACTISILANE

3.2.4 Thermogravimetric Analysis (TGA)

3.2.4.1 Procedure

The mass loss of the treated glass particles as a function of temperature was monitored with a Mettler Toledo TGA1 STARe System. The glass particles were heated from 25°C to 450°C at 10°C/min under air flow, then held at this temperature for 15 h until the mass is stabilized. This temperature was chosen in agreement with the temperature of the first calcination step.

3.2.4.2 Results

TGA analysis was used to quantify the surface density of the grafted silanes. To do so, the mass loss related to the residual hydroxyl groups was subtracted from the total mass loss of the silanized particles after calcination, following a procedure described in the previous chapter (Section 2.4.5.1). The results are displayed in Table 3.5.

The total mass loss for the untreated particles is 0.14%, corresponding to the loss of -OH groups. For the treated particles, the mass loss related only to -OH groups can be calculated from the transmittance peak at 3500 cm^{-1} obtained by FTIR spectroscopy using Equation (2.6) in Section 2.4.2.1. Therefore, the mass loss of the residual hydroxyl groups was subtracted from the total mass loss for the silanized particles according to the corresponding transmittance.

After subtracting the mass loss related to -OH groups, the results still show a considerable mass loss related to the silane groups, confirming again significant silane grafting on

Table 3.5: TGA mass loss of silanized particles compared to the mass loss of untreated particles. The mass loss related to silane and the silane surface density are noted Δm_{silane} and the d_{silane} respectively

Particle type	Total mass loss (± 0.05%)	FTIR Transmittance at 3500 cm^{-1} (%)	Δm_{silane} (%)	d_{silane} (molecule.nm^{-2})
Untreated	0.14	93.12	-	-
TMPS	2.26	94.69	2.17	184
APTMS	1.33	95.51	1.27	89
AEAPTMS	0.71	95.51	0.65	30
ACTISILANE	2.02	94.11	1.91	51

the surface. Equation (3.1) gives the grafted silane surface density:

$$d_{silane} = \frac{\Delta m_{silane} * Na}{100 * M * S} \tag{3.1}$$

in which d_{silane} is the silane surface density (molecule.nm^{-2}), Δm_{silane} is the silane mass loss measured by TGA (%), Na is Avogadro's constant, M is the silane molecular weight (g.mol^{-1}), and S is the specific surface area of glass the particles obtained by BET ($nm^2.g^{-1}$).

The results are displayed in Table 3.5. They are relatively high compared to literature values reported for alkoxysilane monolayers - between 2.1 and 4.2 molecule·nm^{-2} [158–161]. This overestimation can originate from the specific surface measurement as explained in Section 2.4.2.1. Indeed, the specific surface area obtained by the BET technique and used in the calculation is underestimated, which results in an overestimation of the surface density values. On the other hand, some authors have also reported that it is also possible to reach high grafting densities. However, in this case, this was due to the formation of silane multilayers [162, 163]. For example, De Palme et al. [162] found a density of 29 molecules.nm^{-2} for a grafted aminosilane on ferrite nanoparticles by a TGA measurement.

The silane density on the surface of treated particles also depends on the silane nature, and especially its reactive functions. Indeed, the nature of the organofunctional groups on each silane has a role in the hydrolysis and condensation kinetics and, consequently, it influences the grafting kinetics [119, 164, 165]. For example, Asenath et al. [126] showed that amine groups can catalyze, either inter- or intramolecularly, the reaction between silane molecules and surface silanol groups to form siloxane bonds. For this reason, aminoalkoxysilanes are more reactive in water than alkylalkoxysilanes. Therefore, grafted aminoalkoxysilanes can block neighboring surface hydroxyls via two-dimensional self-assemblies (horizontal polymerization) and local multilayers (vertical polymerization) for APTMS (as explained in Section 1.4.3.3), and by the steric hindrance caused by the longer chain length for AEAPTMS. This explains the lower grafting density obtained for the aminosilanes compared to TMPS. The ACTISILANE is the largest molecule and also leads to important steric hindrances. Its grafting density stands in the same range as

AEAPTMS, again quite far from TMPS.

It is quite difficult to obtain similar grafting densities with different silanes because each of them as its own grafting kinetics. Nevertheless, adjusting the factors influencing this kinetics to have comparable grafting densities is possible (Section 1.4.3). Such factors are in particular the concentration of the silane, the pH, and/or the silanization time. As an example, the silanization time was already optimized in chapter 2. However, these factors will also influence the quantity of residual hydroxyl groups, which could further negatively impact the polymerization kinetics. All this makes the control of the grafting density rather complex, considering the number of residual hydroxyls and the impact on the polymerization.

3.2.5 Contact angles

3.2.5.1 Procedure

The contact angles of pristine and surface-modified particles were measured at 25°C with a DIGIDROP goniometer from GBX equipped with a white light source and a camera KRUSS. Contact angle is an indirect measurement of surface wetting. When a droplet spreads out over a surface, its contact angle becomes smaller than 90°. Complete wetting occurs when the droplet is flat corresponding to a contact angle of 0°. The surface tension is often calculated using Young's equation from contact angles. However, the experiment requires flat and smooth surfaces. In our case, the contact angle values are used only for comparison purpose. Other techniques such as Washburn experiment would have been more appropriate to reach the surface tension, but this method is more complicated to perform, in particular with micrometric particules.

Flat surfaces were prepared by compressing particles into pellets. 10.5 μl drops of deionized water were carefully deposited on the sample surface. This volume was chosen to ensure that the drop would detach and fall on the surface by gravity. Images were acquired automatically at 24 frames per second. The first image after the water drop fell on the glass particles surface was selected as a reference for measuring the contact angle values. The dynamic contact angle was also analyzed by measuring the contact angle value over time on successive images. The contact angle was recorded every 0.1 s.

3.2.5.2 Results

The surface polarity of the treated particles was analyzed in terms of wettability, via the measurement of contact angles. This allows to monitor the hydrophilic/hydrophobic change of the surface after the silanization treatment.

Figure 3.11 shows an example of the contact angle images obtained for untreated particles compared to particles treated with TMPS, APTMS and ACTISILANE.

Table 3.6 displays the contact angle values of both untreated and silanized particles. The contact angle of the untreated particles is zero, the water drop is absorbed immediately

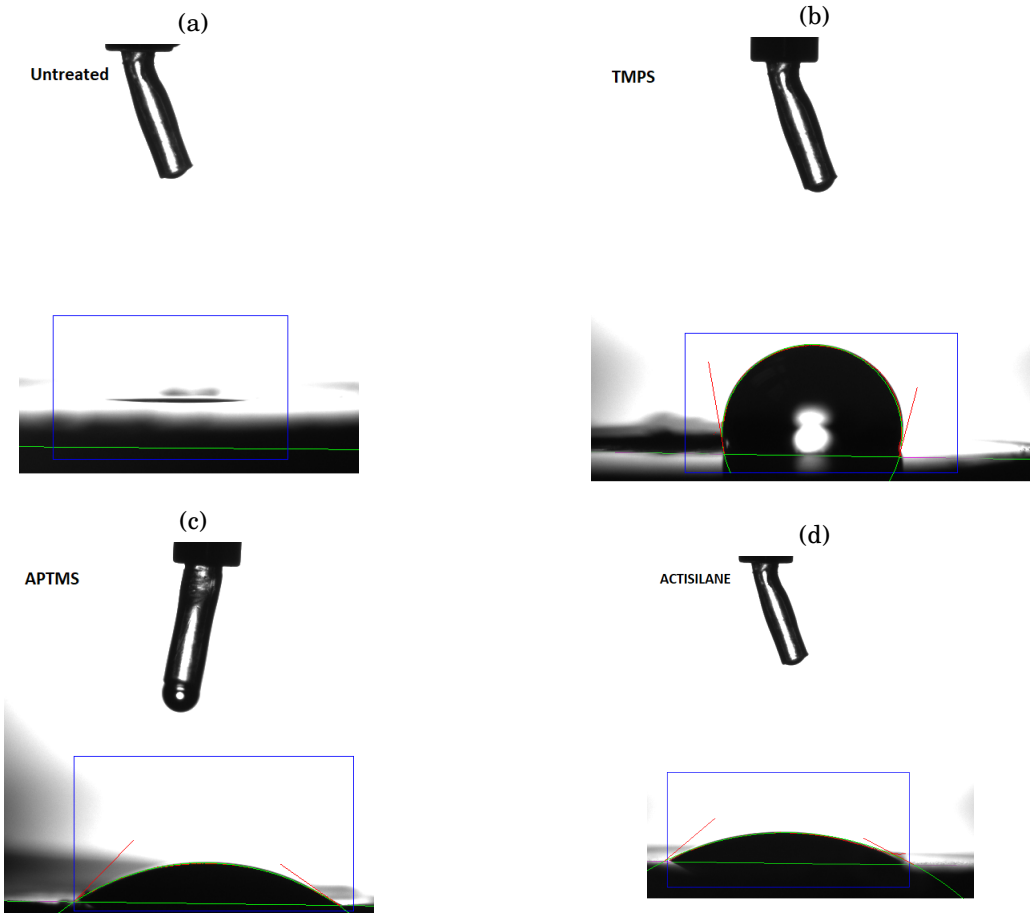

Figure 3.11: Contact angle images of (a) untreated particles, compared to particles treated with (b) TMPS, (c) APTMS and (d) ACTISILANE

after touching the surface. The surface of the untreated particles is, as expected, quite hydrophilic due to the large number of -OH groups present on their surface.

Table 3.6: Contact angle values of untreated and treated particles according to the type of treatment and expected type of interaction with the PA6 matrix ± 1

Expected interaction with PA6	Treatment type	Contact angle (°)
-	Untreated (calcinated)	0
Low chemical interaction	TMPS	103
Weak bonds	APTMS	35
Weak bonds	AEAPTMS	19
Strong bonds	ACTISILANE	28

The contact angle is higher for the silanized particles, and it reaches 103° for the TMPS case. Such increase again confirms the presence of the grafted silane layer at the surface of the treated particles [117, 118], and values obtained stand in agreement with the literature [117, 118, 124, 133].

The difference in contact angle values between the treatments is due to the nature and surface density of the grafted silanes. Indeed, the treatments for which weak and

strong bonds with PA6 are expected contain hydrophilic functions - especially primary and secondary amines. These functions increase the hydrophilicity of the surface and decreases the contact angle to a value below 90°. On the other hand, TMPS possesses non-polar $-CH_3$ end groups and yields an hydrophobic surface, which significantly increases the contact angle value.

The different wettability behavior may also be explained by the silane surface density. Indeed, the confocal microscopy results suggest that AEAPTMS bears more accessible amine functions compared to APTMS, which increase the hydrophilicity of AEAPTMS. Moreover, APTMS gives a higher grafting density compared to AEAPTMS, which could be due to the formation of multilayers by vertical polymerization. Therefore, the contact angle results follow a trend similar to the grafting density values, as described in Table 3.5 (TMPS > APTMS > ACTISILANE > AEAPTMS > untreated).

In order to confirm these trends, the dynamic contact angles are plotted as a function of time, until the drop was totally adsorbed (except in the case of the TMPS treatment for which the drop remained on the surface). Theoretically, the adsorption rate decreases with a decrease in surface hydrophilicity which corresponds to an increase in static contact angle [117, 124]. As shown by Figure 3.12, the dynamic measurements are thus consistent with the static ones.

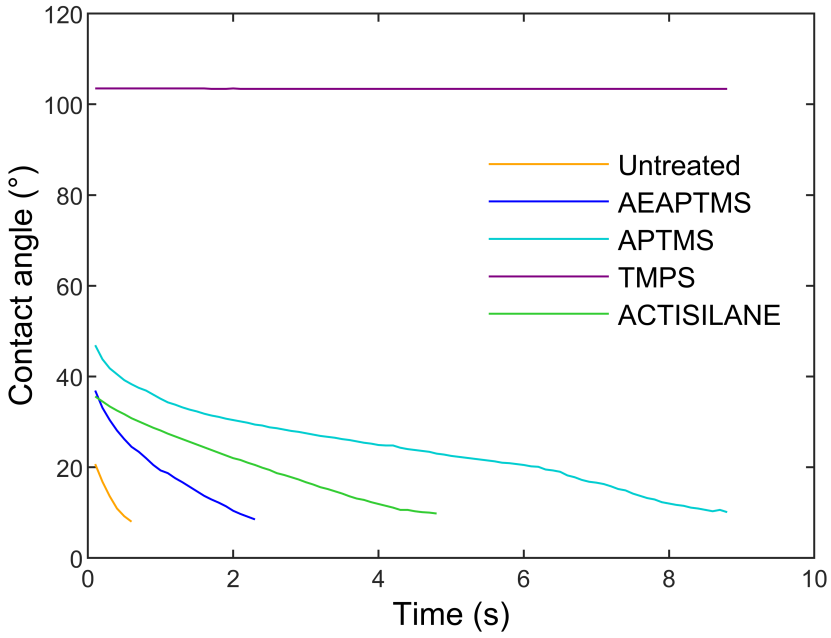

Figure 3.12: Water drop contact angle as a function of time for the different silane treatments

The evolution of the water drop contact angle is a way to predict the level and types of interactions between the particles and the PA6 matrix, since PA6 has a hydrophilic character. Indeed, the TMPS treatment is highly hydrophobic, which should minimize the PA6/particles interactions. In contrast, the particles treated with AEAPTMS, APTMS and the ACTISILANE should promote stronger interfacial interactions.

3.3 Influence of the surface treatment on PA6 polymerization and crystallization

The influence of each silane treatment on the polymerization and crystallization of polyamide 6 was investigated by DSC using the same procedure described in Section 2.2. The composites were synthesized with untreated particles, as well as with particles treated with the different silanes. The results are compared to the neat resin.

3.3.1 Influence on PA6 synthesis kinetics

DSC experiments on all samples were performed in isothermal conditions at 180°C. The DSC thermograms associated to the synthesis of PA6 in glass particles-filled composites are displayed in Figure 3.13, for all five types of particles. As a reference, the DSC thermogram of the neat resin is shown in each figure. In this case, the polymerization and crystallization peaks occur around 3 min and 7 min, respectively.

As a reminder, in presence of untreated particles (Figure 3.13(a)), the signal is flat, showing that the polymerization reaction dit not occur. This is due to the incompatibility of the raw glass surface with anionic PA6 synthesis due to the significant amount of -OH groups, as demonstrated in Chapter 2.

The DSC thermograms obtained for the silane-grafted particles are presented in Figure 3.13(b) to 3.13(d). In all cases, polymerization and crystallization take place. As for the pure resin, all DSC thermograms exhibit a double peak related to the polymerization reaction and crystallization of PA6, ensuring that the treatments and developed protocols are compatible with the synthesis of anionic PA6.

A more in-depth analysis also shows that the particles treated with TMPS, having a hydrophobic surface, significantly slow down the reaction (Figure 3.13(b)): the full cycle lasts 30 min in the presence of glass particles treated with TMPS, instead of 10 min for the neat resin. For the particles treated with the aminosilanes (Figure 3.13(c)), the reaction is faster than for TMPS, suggesting an increased compatibility between the selected aminosilanes with the AROP reaction. However, the polymerization and crystallization processes remain slower compared to the neat resin, with a 50% increase in synthesis duration.

Finally, with the ACTISILANE, grafting the activator on the glass particles surface results in synthesis and crystallization kinetics nearly identical to those of the neat resin, as displayed in Figure 3.13(d). This is due to the higher amount of available activator in the system that allows to initiate the polymerization directly from the surface of the particles, in addition to the bulk initiation of the AROP. This last results suggests that it would be possible to manufacture PA6-based glass particles composites, with synthesis features identical to the neat resin, to obtain reinforced materials.

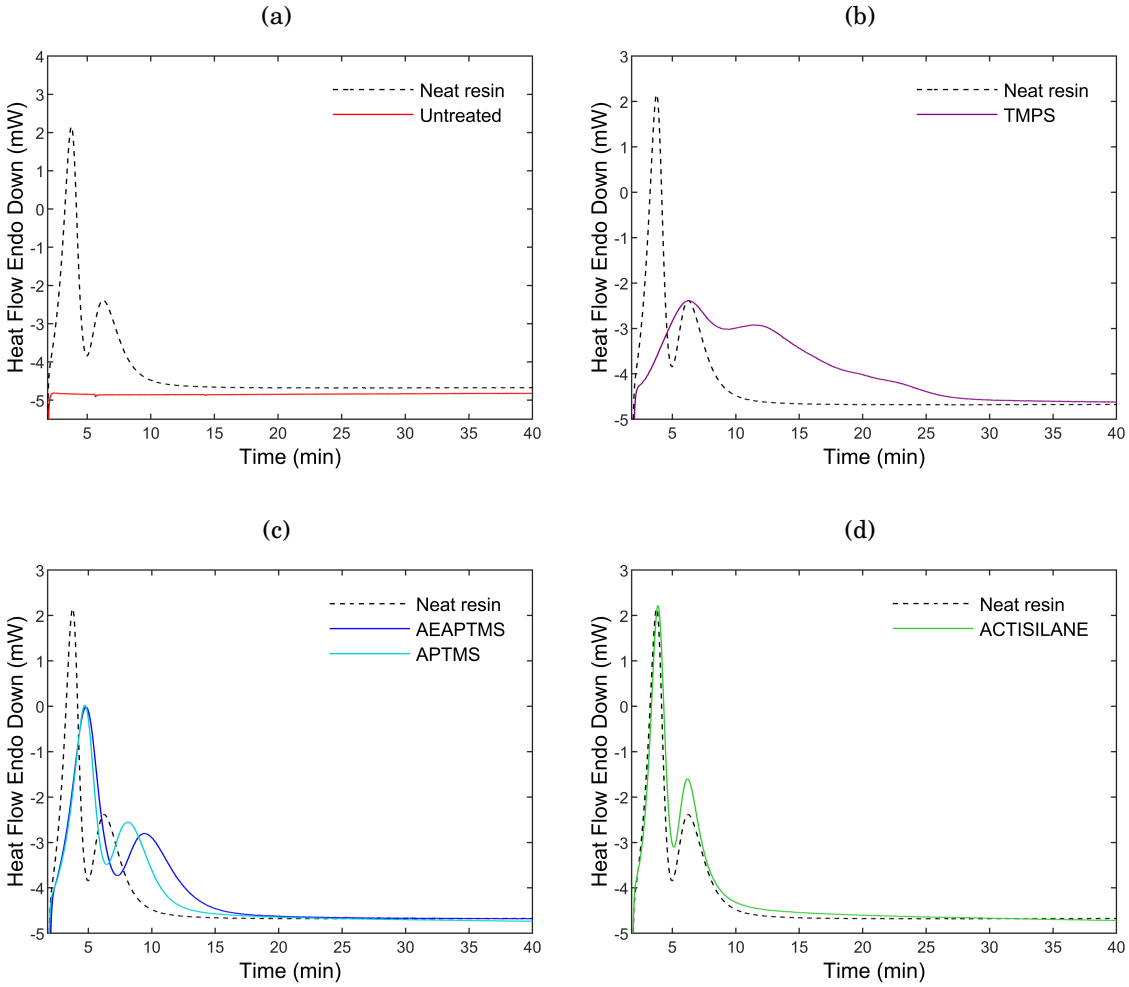

Figure 3.13: DSC thermograms of isothermal syntheses at 180°C of PA6 and PA6-glass particles composites synthesized with (a) untreated particles, and particles treated with (b) TMPS, (c) APTMS/AEAPTMS, and (d) ACTISILANE. The neat resin polymerization thermogram is illustrated for a comparison purpose

3.3.2 Impact on the conversion degree and crystallization

Next, the degree of conversion and crystallinity of the PA6 matrix were measured. After the isothermal step, the samples were cooled from 180°C to 0°C at -10°C.min^{-1}, and then heated to 270°C at 10 °C.min^{-1}. Both DSC thermograms for the cooling and heating cycles are shown in Figure 3.14 for the neat resin, and the composites synthesized either with the untreated particles, or the particles silanized with the ACTISILANE. Only the curves of neat resin and composites synthesized with ACTISILANE treated particles are presented, which are representative of the other treatments. The latter were studied following the same procedure and display similar thermograms.

During the cooling cycle, an exothermic peak on the curve of the untreated particles indicates the presence of unreacted ϵ-caprolactam, the latter crystallize at 25°C (Figure 3.14(a)). This peak is not visible on neat resin and ACTISILANE based composite, for which the reaction was almost complete.

In complement, during the heating step, no exothermic peak corresponding to residual

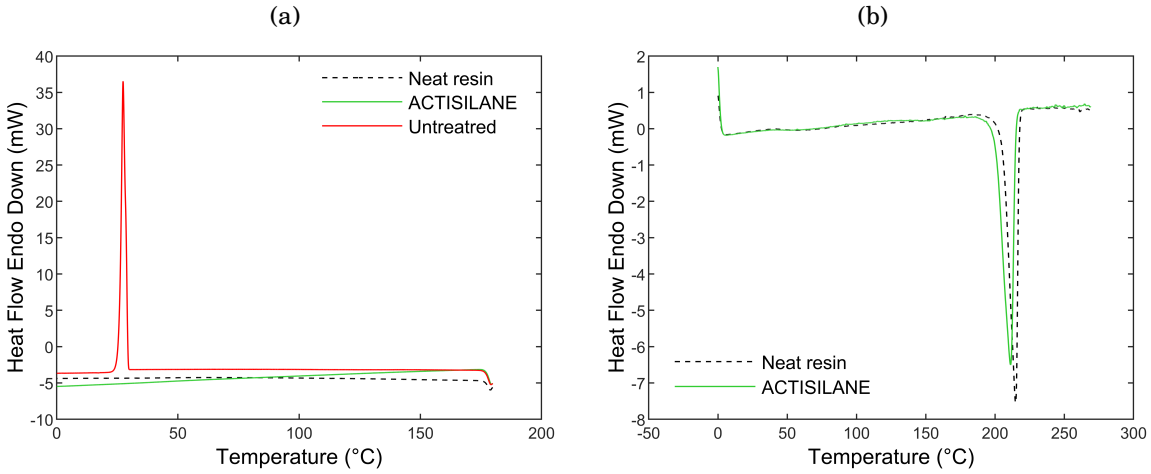

Figure 3.14: DSC curves of PA6 and PA6-glass particle composite synthesized with untreated and ACTISILANE treated particles: (a) cooling cycle from 180°C to 0°C at -10 °C/min (b) heating cycle from 0°C to 270°C at 10°C/min

unreacted monomer polymerization was observed for both the neat resin and ACTISILANE treated particles (Figure 3.14(a)). This indicates an almost complete consumption of the monomer and, consequently, a very high degree of conversion. However, this information is not sufficient to confirm a nearly complete conversion since uncrystallized monomers could remain trapped into the PA6 crystalline lamellas [17].

Also, the melting temperatures determined by DSC are an indicator of the conversion degree. The results are displayed in Table 3.7. Khodabakhshi et al. [44] showed that the melting temperature of PA6 depends on the conversion degree. For example, for a melting temperature of 210°C, they measured a conversion degree of 90%, whereas for a temperature of 215°C the conversion reached 96% (a conversion rate of 100% is not achievable) [17, 166–169]. In our case, the melting temperatures range between 211°C and 215°C, which suggests a high conversion degree, and a very low remaining quantity of unreacted monomers after synthesis.

The degree of conversion of ϵ-caprolactam into PA6 can be calculated from the total heat of reaction Q_{tot} obtained from the isotherm step, which is the sum of the polymerization enthalpy ΔH_p^∞ and the crystallization enthalpy ΔH_m. The latter represents the melting enthalpy measured upon heating during a subsequent step to the isothermal synthesis at 180°C. Hence, the degree of conversion X_p^∞ is defined according to Equation (3.2), in which $\Delta H_p^{100\%}$ refers to the total enthalpy of polymerization obtained from Vicard et al. [17] ($\Delta H_p^{100\%}$ = 123.5 J.g^{-1}) :

$$X_p^\infty = \frac{Q_{tot} - \Delta H_m}{\Delta H_p^{100\%}} \tag{3.2}$$

As shown in Table 3.7, all of the composites prepared with silanized particles lead to a degree of conversion higher than 95%. It is worth noticing that all composites melting enthalpies indicate a very high degree of crystallinity, compared to the bulk crystallization

of the neat PA6, as already highlighted in previous studies [16, 17, 45, 170]. This high degree of crystallinity could be attributed to surface induced nucleation. However, a high degree of crystallinity is also observed for TMPS-treated particles, whose surface is hydrophobic. Another mechanism is thus probably responsible for the high degree of crystallinity.

Table 3.7: Melting temperature (T_m), melting enthalpy (ΔH_m), total enthalpy (Q_{tot}), polymerization enthalpy (ΔH_p^∞) and degree of conversion (X_p^∞) of PA6 after the synthesis of PA6/glass particles composites with different types of grafted silanes

Sample	T_m (± 0.3°C)	ΔH_m (± 0.6 J.g^{-1})	Q_{tot} (± 1.4 J.g^{-1})	ΔH_p^∞ (± 0.9 J.g^{-1})	X_p^∞ (± 0.7%)
Neat resin	213.1	70.4	190.9	120.5	97.6
TMPS	215.9	72	189.9	117.9	95.5
APTMS	214.5	74.2	194	119.8	97
AEAPTMS	215.6	71	189.2	118.2	95.7
ACTISILANE	211.2	73.5	190.6	117.1	98.5

3.3.3 Relationship between surface chemistry of glass particles and polymerization/crystallization kinetics

The grafting protocol that was used to prepare the glass particles surfaces not only ensured an efficient grafting of the selected silanes, but also led to a high degree of conversion of the ϵ-caprolactam monomer ($\approx$ 95%). This demonstrates that a thorough control over the surface hydroxyl density for the entire silanization process prevents activator deactivation and makes it possible to achieve a proper polymerization of the reactive mixture.

The nature of the silane strongly affects the surface density of the grafted silane. In fact, the TMPS allows to reach the highest grafting density (Table 3.5). Conversely, the use of AEAPTMS, which contains primary and secondary amine functions, results in the lowest grafting density. In addition to the influence of the silane molecular size, these results are driven by the different hydrolysis-condensation kinetics and by the secondary reactions that may occur during silanisation. In particular, horizontal and vertical polymerization catalyzed by the presence of amine groups, and the resulting steric hindrance, may explain this result. This steric effect, and the formation of silane multilayers, are also responsible for the grafting difference observed between APTMS and AEAPTMS. Indeed, APTMS is more susceptible to form local multilayers of amines by vertical polymerization [126, 158].However, AEAPMS has a longer alkyl chain, which favors a more homogeneous aminated surface [127].Despite a higher grafting density of APTMS (as attested by the TGA results, Table 3.5), the higher steric hindrance for surface modified by this silane yields to lower fluorescence intensity than AEAPTMS (Figures 3.9(d) and 3.9(e)).

Although the significant differences in surface grafting densities could impact the hydrophilic/hydrophobic character of the glass particles, the contact angles are consistent with the nature of the silanes. TMPS turns the surface hydrophobic, whereas the amine functions in the aminosilanes and ACTISILANE yield more hydrophilic surfaces (Figure 3.12), thus improving the interfacial affinity with the hydrophilic monomer.

This specific effect of the silane functions on the change in polymerization reaction and crystallization is also highlighted in Figure 3.13. The hydrophobic character of the TMPS-treated particles substantially slows down the polymerization, whereas the reaction time is only increased by about 50% with hydrophilic aminosilanes. Since these silanes are not directly involved in the polymerization reaction, this delay appears to be correlated to the wettability of the glass surface.

As demonstrated in Section 1.3, the presence of NH_2 groups in aminosilanes leads to the formation of hydrogen bonds at the particle-matrix interface between the PA6 carbonyls and the amines of the silane [104]. In addition, the reaction kinetics can be influenced by crystal nucleation at the particle surface during the polymerization process, but also by the species diffusing in the reaction mixture around the glass particles – all features that must be sensitive on the particle surface chemistry [171]. As illustrated in Figure 3.13(c), the polymerization/crystallization thermograms obtained in the presence of glass particles treated with the aminosilanes show identical polymerization peaks, but subtly yet clear differences in crystallization kinetics. This indicates that the type of silane and grafting levels influence the crystallization process, including nucleation effect differences at the glass surface [172]. However, the type of aminosilane seems to have no effect on the PA6 polymerization. The slower polymerization kinetics in the presence of aminosilane-treated particles, compared to the neat resin, is therefore most likely a diffusion limited effect of the reactive species into the material, due to their affinity with the glass surface, and to the spatial hindrance caused by the glass particles themselves. This explanation is also consistent with the slower kinetics observed in the presence of TMPS-grafted particles. By limiting the chemical affinity of the glass surface with the monomers, the spatial hindrance of the particles is increased, which in turn limits to a higher extent the diffusion process of the reagents, without affecting the final degree of conversion.

In the case of the ACTISILANE grafted particles, the synthesis kinetics is similar to the neat resin. In contrast with the other tested silanes, the grafted activator allows the glass surface to participate to the reaction, and polyamide chains are directly initiated from the surface. The presence of the activator on the glass surface globally increases the concentration of activator in the reactive mixture, consequently increasing the mixture reactivity. This higher reactivity must counterbalance the spatial hindrance of the glass particles, leading to a synthesis time nearly identical to that of the neat resin.

The original approach consisting in initiating the polymerization reaction directly from the surface of the reinforcing particles brings a significant acceleration of the synthesis

reaction of anionic PA6 based composites in the presence of glass reinforcements. As a reminder, the study has been carried out on glass surface to avoid orientation effect, but we target to transfer the results to glass fibers. ACTISILANE grafted fibers would simplify the manufacturing process by eliminating the addition of the activator in the mixture (e.g. eliminating an additional tank containing the activator in the liquid processes described in Section 1.2.1). Moreover, since the activator is directly grafted at the surface of the glass fibers, the ACTISILANE treatment could improve the mechanical strength at the interface by creating strong covalent bonds between the glass particles and the matrix. In the end, this which would probably result in shifting the ultimate tensile strength of the composites towards higher values – an aspect that will be analyzed in the next chapter.

3.4 New reactive treatment synthesis

From the previous results, it was concluded that the ACTISILANE reactive treatment accelerates the polymerization and crystallization kinetics until reaching a similar kinetic as the neat resin. Therefore, reactive treatments seem very suitable for the anionic PA6 composites synthesis since they involve the glass reinforcement surface in the reaction. This surface treatment prevents the combined negative effect of spatial hindrance and hydroxyl groups caused by the glass reinforcement on the synthesis kinetics. Moreover, the reactive treatments create covalent bonds between the reinforcement and the matrix at the interface. A better load transfer and improved mechanical performance of the composite are thus expected by using such silane treatment.

The reaction activator and catalyst are often used in very small quantities compared to the monomer, the range is typically 0.5 to 4 mol%. Hence, the activator grafting on the reinforcement surface can unbalance the reagent ratios. Indeed, for a high filler content, the reinforcement surface gives rise to a significant amount of grafted activator. This is actually the most probable explanation for the identical reaction kinetics of the ACTISILANE treated composite with the neat resin.

Controlling the amount of grafted activator at the surface of the reinforcement is possible, as demonstrated in Section X. However, it remains difficult to achieve a targeted density due to the complex grafting kinetics. Therefore, grafting the reaction monomer onto the particle surface is the best strategy for avoiding these issues. Indeed, the monomer represents the main component in the reactive mixture. Thus, the amount of grafted monomer on the mixture ratios is negligible, while involving the particles surface in the reaction. This allows to create covalent bonds between the reinforcement and the matrix and to improve the interfacial adhesion. This strategy was never explored in the literature so far, most probably because of the difficulty to achieve monomer grafting.

Currently, there is only one strategy for grafting a reactive treatment onto the surface of the particles: grafting the reaction activator. Instead of the technique reported in the literature (Section 1.4.4), a new approach was developed in this study to graft the reaction

activator. A similar strategy was here used to graft the monomer onto the surface of the glass reinforcement. The strategy developed in this study to graft the monomer on the particles surface consists in modifying the "R" function of a commercial silane agent in order to substitute it by a monomer prior to graft the synthesized silane on the glass particle surface. The new silane containing the ϵ-caprolactam monomer at its end is named MONOMSILANE.

To do so, several steps were required. The first step consisted in chemically modifying a coupling agent, the second one was to graft it onto the particle surface. The modification and grafting mechanisms are detailed in a first section. Then, the results of particle surface characterization are presented and the grafting efficiency is discussed. Finally, the impact of the monomer grafting on the polymerization and crystallization of the synthesized composites is analyzed through reaction kinetics and thermal transitions in DSC.

3.4.1 MONOMSILANE synthesis mechanism

The first step of the MONOMSILANE synthesis consisted in modifying a silane agent to create an ϵ-caprolactam molecule at the end of the alkyl chain. The chosen silane is the 3-glycidoxypropyltrimethoxysilane GLYMO (Figure 3.15(a)) having an epoxide function at its end. Indeed, the epoxide function is known to be highly reactive towards primary amines [173, 174]. Therefore, 3-amino-2-azepanone (Figure 3.15(b)) was used to functionalize the GLYMO silane with a monomer molecule via the reaction between the 3-amino-2-azepanone primary amine and the silane epoxide.

(a) (b)

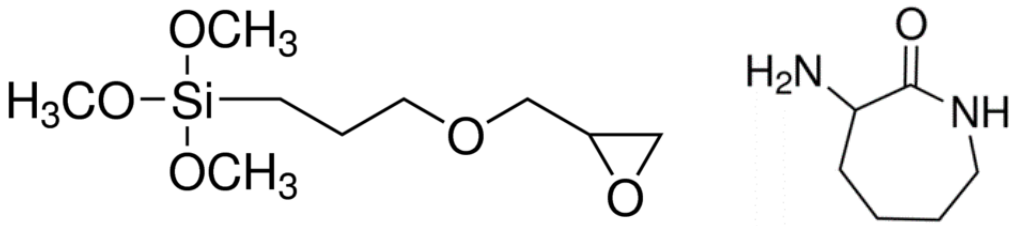

Figure 3.15: chemical structure of (a) 3-glycidoxypropyltrimethoxysilane GLYMO (b) 3-amino-2-azepanone

The reaction mechanism of the silane modification is shown in Figure 3.16. In the case of 3-amino-2-azepanone, the primary amine groups reactivity towards epoxides is very high due to the formation of active hydrogen bonds, making this reaction very fast and favoring the formation of the ϵ-caprolactam at the end of the new synthesized silane.

Primary amines are bifunctional towards epoxides. Therefore, the GLYMO silane proportion is twice higher than the 3-amino-2-azepanone molecule (molecular ratio 2 : 1). The use of a monoepoxide and a low silane amount for the preparation of the monomsilane avoids the potential cross-linking as in the case of epoxy-amine thermosets. Furthermore, by using a low silane concentration, the hydroxyl groups number generated after the

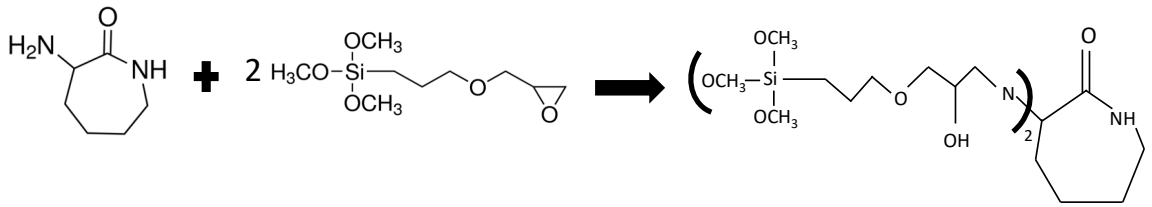

Figure 3.16: Reaction mechanism for the synthesis of the MONOMSILANE coupling agent

reaction of epoxides with amines is very low compared to the hydroxyl quantity present on the glass particles surface. Therefore, the influence of these hydroxyls formed during the MONOMSILANE synthesis on the polymerization can be neglected.

The synthesized product was not characterized to avoid handling of toluene for toxicity reason. However, Fischer and Ritter [175] described the reaction of 3-amino-2-azepanone with a diepoxide glycerol diglycidyl ether. Based on their results showing an efficient and fast reaction between the two products, it was assumed that the new silane synthesis was successful.

3.4.2 Procedure for the MONOMSILANE synthesis and grafting

In a hydrophobic beaker, 0.58 g of 3-amino-2-azepanone was dissolved in 100 ml of toluene (anhydrous, 99.8%) at 80°C. The beaker was sealed to prevent toluene evaporation. After total dissolution, 2 ml of GLYMO was added and left for 3 h at 80°C. After reaction, the mixture was cooled to 25°C. Then, 35 ml of ethanol was added to ensure silane hydrolysis. The ethanol quantity added was chosen to have a ratio of 5% of silane in ethanol, the same ratio used in the previous treatments. After silane hydrolysis, 50 g of glass particles were poured into the beaker. The next steps were similar to those described in Section 3.1.4. The MONOMSILANE grafting mechanism on the particle surface is illustrated in Figure 3.17.

3.4.3 Particle surface characterization

The particles silanized with MONOMSILANE were characterized by FTIR spectroscopy, TGA and contact angle to evaluate the grafting efficiency.

3.4.3.1 FTIR spectroscopy

Figure 3.18 shows the FTIR spectrum of particles treated with MONOMSILANE compared to those of calcined particles. As in the previous cases of treated particles (Figure 3.6), the disappearance of the peak at 3500 cm^{-1} confirms the reaction of -OH groups with the

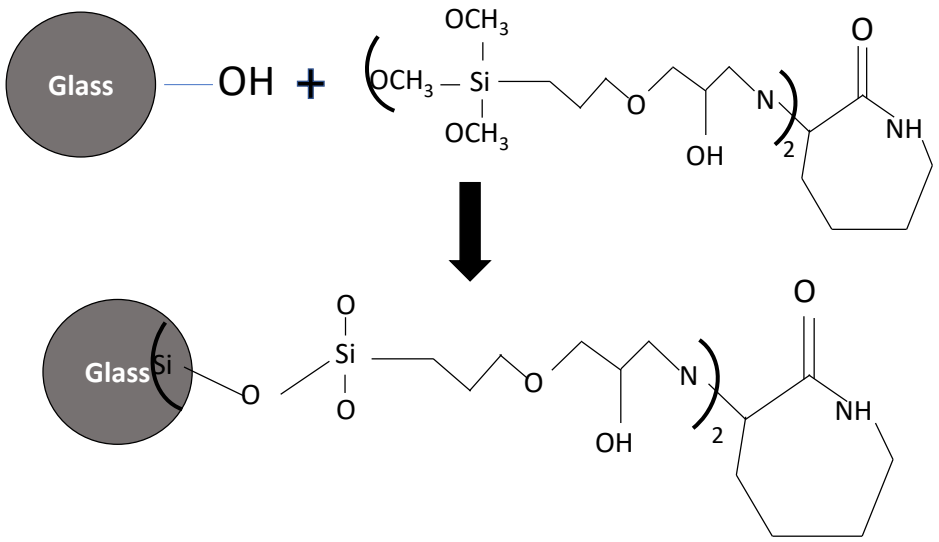

Figure 3.17: Grafting mechanism of MONOMSILANE on the surface of glass particles

silane. Moreover, the disappearance of the peak related to the hydroxyl groups shows that the -OH groups formed after the epoxide ring opening represent a very low quantity, as expected.

However, the spectra do not show any peak related to the monomer's bonds, especially the CH_2 and NH groups. Therefore, further analysis of the chemical composition of the particle surface, using for instance XPS or NMR, is needed to confirm the presence of the monomer on the surface after grafting.

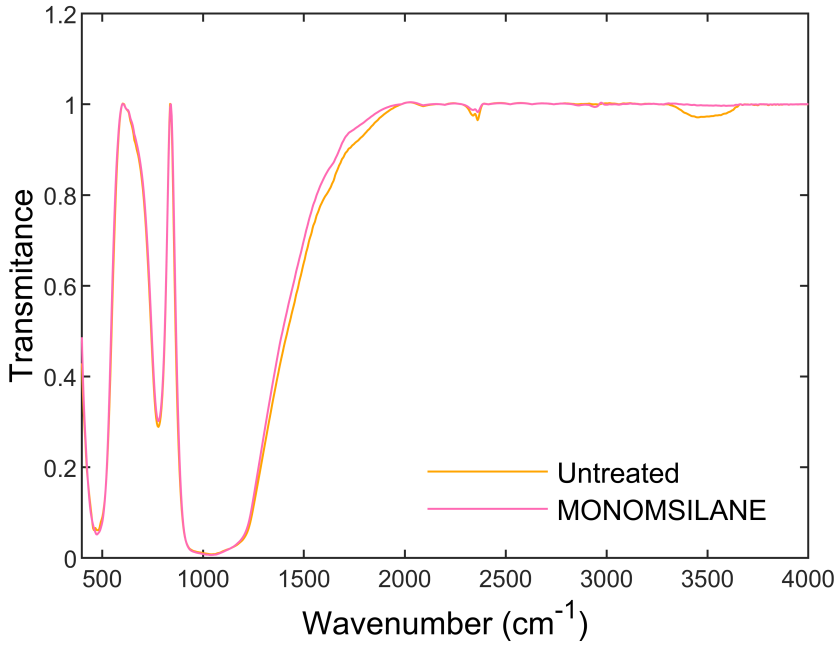

Figure 3.18: FTIR spectra of untreated particles and particles treated with MONOMSILANE

3.4.3.2 TGA

TGA mass loss was used to quantify the grafted silane quantity on the particle surface. As in the previous cases, the residual hydroxyl mass loss was subtracted from the total mass loss using the same procedure described in Section 3.2.4. Then, the grafting density was calculated using Equation (2.6). The results of the particles treated with MONOMSILANE, compared to the results of the untreated particles are presented in Table 3.8.

Table 3.8: TGA mass loss of silanized particles with the MONOMSILANE compared to the mass loss of untreated particles. The mass loss related to silane and the silane surface density are noted Δm_{silane} and the d_{silane} respectively

Particle type	Total mass loss (± 0.05%)	FTIR Transmittance at 3500 cm^{-1} (%)	Δm_{silane} (%)	d_{silane} (molecule.nm^{-2})
Untreated	0.14	93.12	-	-
MONOMSILANE	0.91	95.51	0.86	12

First, the TGA results show that the mass loss increases significantly with MONOMSILANE particles compared to untreated particle even after subtracting the residual -OH groups. This confirms the silane deposition on the surface of the treated particles. Moreover, the grafting density seems to be high considering the grafted molecule size. This is mainly due to the specific area effect described in Section 2.4.2.1. Moreover, MONOMSILANE is a bulky molecule with a high molar mass, which explains the rather low density value compared to previous treatments. However, the mass loss value related to the silane agrees with the expectations, attesting a successful grafting.

3.4.4 Contact angle

Measuring the contact angle allow to evaluate the surface wettability of MONOMSILANE-treated particle resulting from the silane deposition on the surface. Also, the results give some information about the particle/matrix interaction. A hydrophilic surface promotes the reactive species diffusion and thus favors the interfacial interactions. The contact angle of MONOMSILANE treated particles was measured using the same procedure described in Section 3.2.5. The contact angle image is shown in Figure 3.19 and its value is given in Table 3.9 compared to the untreated particles.

Table 3.9: Contact angle images of particles treated with MONOMSILANE

Expected interaction with PA6	Treatment type	Contact angle (°)
-	Untreated (calcinated)	0
Strong bonds	MONOMSILANE	62

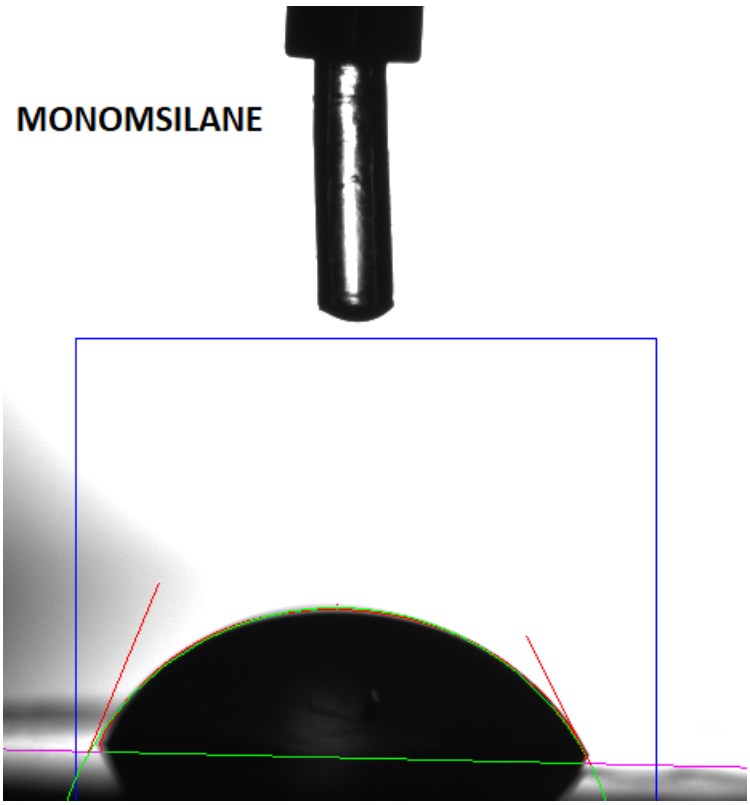

Figure 3.19: FTIR spectra of untreated particles and particles treated with MONOMSILANE

The contact angle increases significantly after silane grafting compared to untreated particles. This increase in the static contact angle value is mainly due to the high number of CH_2 groups contained in the MONOMSILANE chain. Their presence also explains the higher contact angle value compared to other treatments (Table 3.6). Despite the significant increase in the contact angle indicating the silane deposition, the surface remains hydrophilic because of the amine functions involved in the monomer as stated by the contact angle lower than 90°.

Regarding the dynamic contact angle, the change is slightly slower than that of APTMS in Figure 3.12, which is consistent with the higher static contact angle value obtained compared to other treatments. This indicates a successful silane grafting, although the surface remains mainly hydrophilic.

3.4.5 Overview of the monomer grafting on the particle surface

Although the surface characterization of the MONOMSILANE-treated particles shows a successful surface modification, the chemical functions related to the ϵ-caprolactam were not detected by FTIR spectroscopy analysis of the treated particle surface. Therefore, further analysis, in particular NMR, FTIR spectroscopy or XPS analysis on the synthesized product before its grafting on the particles surface is necessary to confirm the formation of the monomer molecule after MONOMSILANE synthesis.

In this context, it is important to note that an XPS analysis was carried out on another

batch of glass particles treated with MONOMSILANE prepared with the same protocol. The results are presented in Table 3.10 and compared to the same batch of untreated particles.

Table 3.10: Identification and quantification of elements from XPS analysis for the untreated particles and particles treated with MONOMSILANE (analysis carried out on another batch of glass particles)

Atoms	Binding Energy (BE)	Atomic (%)	
		Untreated	MONOMSILANE
Si 2p	103.1	20.8	15.9
C 1s	285.0	25.3	34.9
O 1s	532.0	46.4	42.2
N 1s	400.0	-	1.5
Na 1s	1701.4	1.4	5.5
Ca 2p3/2	346.2	Traces	Traces
Mg 1s	1303.1	Traces	Traces

First, the presence of nitrogen on the treated particle surface is due to the -NH function of the monomer molecule. In addition, the results show a significant increase in the carbon percentage on the treated particle surface. This is attributed to the high CH_2 group content in the ϵ-caprolactam ring as well as to the carbon contained in the MONOMSILANE alkyl chain. This proves the presence of the monomer on the glass particle surface. Nevertheless, NMR would be required to confirm the presence and conservation of ϵ-caprolactam after silanization.

3.4.6 Influence of the MONOMSILANE treated particles on PA6 polymerization and crystallization

The influence of the particle surface modification with MONOMSILANE on the polymerization and crystallization kinetics was studied in DSC according to the protocol described in Section 2.2. The results are compared to the neat resin.

3.4.6.1 Influence of the MONOMSILANE treated particles on PA6 synthesis kinetics

Figure 3.20 shows the DSC thermogram of the composite synthesis with the MONOMSILANE treated particle compared to the thermogram of the neat resin. The particle treatment with MONOMSILANE allows to reach a synthesis kinetics similar to that of the neat resin. This suggests that the particles do not have a negative influence on the polymerization and that the MONOMSILANE treatment is compatible with the synthesis reaction. Moreover, the synthesis kinetics is quite similar to that obtained with the particles treated with ACTISILANE. AS in this last case, the surface of MONOMSILANE

treated particles is involved in the reaction and the monomer grafting on the surface favors the reactive species diffusion into the material. Therefore, the effect of the spatial hindrance caused by the particles is counterbalanced again, which improves the synthesis kinetics. To conclude, these results support the successful monomer grafting on the surface of the particles.

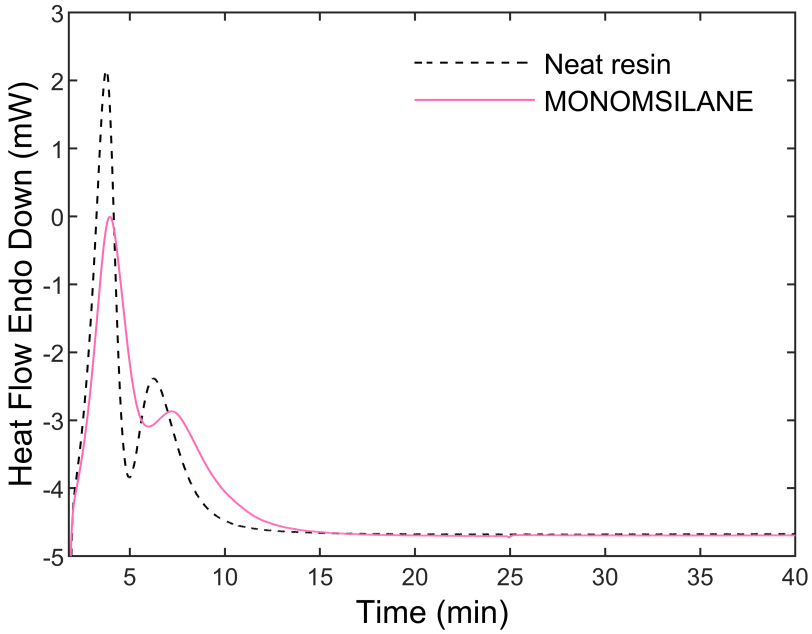

Figure 3.20: DSC thermograms of isothermal syntheses at 180°C of PA6 and PA6-glass particles composites synthesized with MONOMSILANE particles

3.4.6.2 Impact of MONOMSILANE treated particles on the conversion degree and crystallization

As for the other treatments, the melting enthalpy and temperature as well as the conversion degree were measured by carrying out a cooling step at -10°C.min^{-1} from 180°C to 0 °C, followed by a heating ramp at 10 °C.min^{-1} to 270°C. The DSC thermograms of the composites containing the MONOMSILANE particles, compared to those of the neat resin, are presented in Figure 3.21. No exothermic peak appears during both cooling and heating cycles, which demontrates the almost total monomer consumption during the synthesis. The melting temperature and enthalpy obtained during the heating cycle are presented in Table 3.11.

The melting enthalpy obtained with the MONOMSILANE treated particle is significantly higher compared to the pure resin and other treatments. This supports the presence of the monomer on the surface of the particles through two hypotheses. First, the high polymerization kinetics, shown in the previous section, resulted in an enhanced reactive species diffusion. This favors the nucleation that can occur from the particles surface [106] and increases the crystallinity degree. The second hypothesis is based on the work

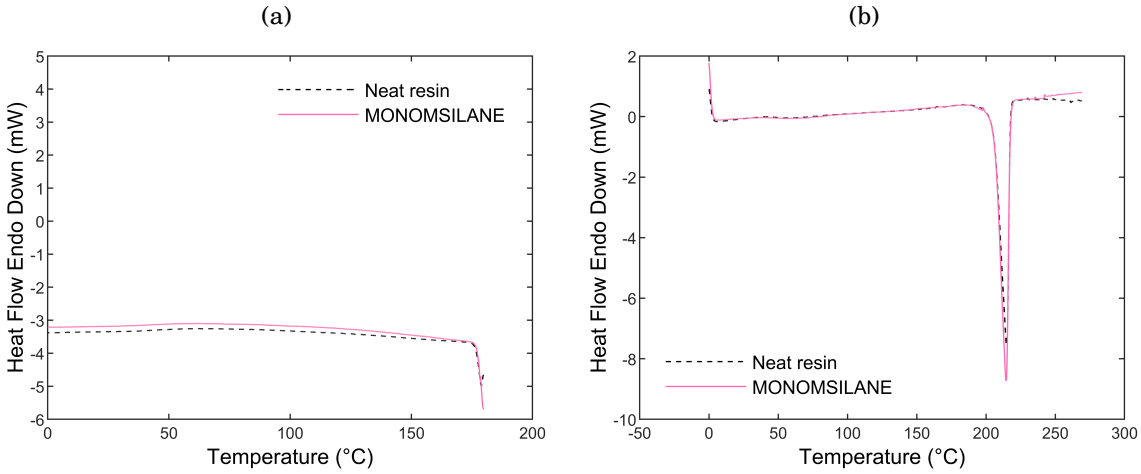

Figure 3.21: DSC curves of PA6 and PA6-glass particle composite synthesized with MONOMSILANE treated particles (a) cooling cycle at -10 °C.min^{-1} from 180°C to 0°C (b) heating cycle from 0°C to 270°C at 10°C.min^{-1}

Table 3.11: Melting temperature (T_m), melting enthalpy (ΔH_m), total enthalpy (Q_{tot}), polymerization enthalpy (ΔH_p^∞) and degree of conversion (X_p^∞) of PA6 after the synthesis of PA6/glass particles composites with MONOMSILANE treated particles

Sample Sample	T_m (± 0.3°C)	ΔH_m (± 0.6 J.g^{-1})	Q_{tot} (± 1.4 J.g^{-1})	ΔH_p^∞ (± 0.9 J.g^{-1})	X_p^∞ (± 0.7%)
Neat resin	213.1	70.4	190.9	120.5	97.6
MONOMSILANE	214.7	81.8	203	121.2	98.1

of Lee et al. [176] who suggested that the presence of ϵ-caprolactam promotes the PA6 crystallization process during the anionic synthesis by AROP. Indeed, at the initial stage of crystallization, the crystals may exhibit structures swollen by residual monomer. This residual monomer amount in the crystalline region gradually decreases as the reaction proceeds, and thus the crystalline structure is enhanced due to the morphological modification at the supermolecular level. Subsequently, the crystallization of the uncrystallized portion entrapped in the crystals occurs as the reaction progresses, which improve the crystallinity. Therefore, the degree of crystallinity increases when crystallization occurs in the presence of residual monomer compared to crystallization occurring at the end of the polymerization. In our case, it is possible that the monomer grafted to the particle surface does not react at the initial stage of crystallization due to the reduced mobility of monomers bonded to the particle surface. This may increase the residual monomer amount at the early stage of polymerization and leads to plasticization of the intercrystalline zone. This plasticization can favor the polymer chains mobility up to late during synthesis, which thus improve the overall crystallinity. Hence, this increases significantly the melting enthalpy.

Furthermore, as explained previously in Section 3.3.2, the melting temperature signifies that the conversion degree is high and the monomer is almost completely consumed

[44]. This is confirmed by the calculated conversion degree using equation (3.2), which provides a conversion of 98.1%.

The previous results show that MONOMSILANE treated particles have a notable compatibility with the anionic PA6 synthesis by improving its synthesis kinetics and conversion. This treatment also dramatically improves the degree of crystallinity when comparing the melting enthalpy of the neat resin and other treatments. This strongly supports the presence of the grafted monomer on the particle surface.

3.5 Conclusion

This chapter highlights the significant impact of the surface chemistry of the glass particles on the polymerization and crystallization of the anionic PA6 matrix. Indeed, the interaction of the reactive mixture with the glass surface affects the synthesis process according to the surface chemistry. For this reason, a suitable surface treatment is targeted to ensure reactants/glass surface compatibility.

The approach consists in tuning the glass surface chemistry to create three types of interactions at the particle-matrix interface. Such surface properties were reached by silane grafting. First, the particles were treated with a silane that prevented interactions between the particles and the PA matrix. Secondly, the selected aminosilanes allowed to create weak bonds at the interface. Finally, a reactive coupling agent was developed to induce the formation of covalent bonds between the glass surface and the PA6 matrix during the polymerization.

The different types of silanes were chosen according to the type of interaction desired with the matrix: some are commercial ones, others were specifically synthesized in this study by suggesting a new approach for the creation of covalent bonds at the interface. The synthesis and grafting protocols of the silanes were optimized in order to have a good grafting combined to controlled residual hydroxyl groups density.

After silane grafting, the surface of the treated glass particles was characterized by combining several techniques. The results were compared to those of the untreated particles and showed the successful grafting of the coupling agents to the surface as well as the preservation of the chemical functions of each grafted agent.

Then, the effect of such chemical interactions on the polymerization and crystallization of anionic polyamide 6 was investigated. The results demonstrate that the synthesis kinetics of anionic PA6-glass bead composites is affected by the chemical nature of the glass surface. The DSC results showed that the treatments applied to the particle surface are compatible with the reaction and favor the polymerization of the matrix. Regardless the type of silane, the degree of conversion was higher than 95%. Moreover, the formation of the crystalline structure during the synthesis is affected by the surface treatments most likely because of a nucleation effect of the modified glass surface.

Finally, polymerization and crystallization kinetics similar to that of the neat resin

were reached with a specifically synthesized reactive coupling agents. In such silane agents, the activator and the monomer of the reaction were grafted directly on the glass particle surface. In the case of grafted activator, the polymerization is initiated from the glass surface, resulting in the creation of covalent bonds between the particles and the matrix. In order to further investigate the effect of reactive silanes on the synthesis kinetics and the physical and chemical properties of the resulting composite, we have developed a new approach which consists in grafting the monomer on the particles surface. This allows the particles to participate in the reaction while avoiding the disadvantages of the activator grafting. In this case, the monomer grafting improved the synthesis kinetics and exhibits a dramatic enhancement of the crystallinity compared to the other treatments. Moreover, with the monomer grafted on the particles surface, covalent bonds can be created at the particle/matrix interface for a better interfacial adhesion. Accordingly, these developed reactive treatments of the glass reinforcement show a total compatibility with the anionic PA6 synthesis, improving not only the synthesis kinetics but also the physical and chemical of the resulting composite.

This chapter brings new fundamental insight on the importance of controlling the surface chemistry of glass reinforcements to promote the polymerization and crystallization kinetics of anionic polyamide 6. Through control of the interactions at the particles-matrix interface, higher mechanical properties of the composites are expected. The influence of the glass particles surface chemistry on the mechanical properties of the resulting composite is analyzed in the next chapter.

CHAPTER 4

INVESTIGATION OF THE PROPERTIES OF ANIONIC PA6 BASED COMPOSITES ACCORDING TO GLASS PARTICLES SURFACE TREATMENTS

Contents

4.1 Manufacturing of anionic PA6/glass particles composites **114**

4.1.1 Manufacturing specifications 114

4.1.2 Tested process for composites manufacturing 116

4.2 Physical and chemical characteristics **124**

4.2.1 TGA 125

4.2.2 DSC 129

4.3 Composite mechanical properties and interface analysis **134**

4.3.1 Analysis techniques and experimental conditions 134

4.3.2 Kinematic field measurements 135

4.3.3 Mechanical properties 141

4.3.4 Fracture surfaces analysis 149

4.4 Conclusion **152**

Introduction

In Chapter 2, a surface treatment protocol was developed and optimized in order to control the hydroxyl density during the surface modification of glass reinforcements. Then, several types of surface treatments were applied and the effect of each treatment on the polymerization/crystallization was studied (Chapter 3). This allowed to control the interactions at the composite interface during resin synthesis and to obtain a synthesis kinetic similar to that of neat resin. However, in addition to the effect on synthesis kinetics, the surface chemistry also influences the mechanical properties of the anionic PA6/glass composite. Indeed, since it controls the load transfer, the quality of the reinforcement-matrix interface is a crucial factor for the composite mechanical properties. This interface depends mainly on the sizing applied to the reinforcement surface and more specifically on the coupling agent. It is therefore necessary to evaluate the mechanical performance of composites made by treated particles in order to identify the effect of each treatment on the properties.

This Chapter aims at describing the manufacturing process for composite materials involving treated particles. Different manufacturing strategies are used to prepare composite specimens that are analyzed in order to evaluate the polymerization and crystallization quality during this large-scale synthesis. These results are specially compared to experimental data recorded by DSC. Then, the manufactured materials are characterized by tensile tests coupled with digital image correlation in order to evaluate both the mechanical properties and the homogeneity of the specimens according to the type of interfacial interaction generated by the grafted silane. The relevance of the developed treatments is finally discussed in the case of large-scale processing of anionic PA6/glass composites.

4.1 Manufacturing of anionic PA6/glass particles composites

4.1.1 Manufacturing specifications

Glass fiber/PA6 composite materials involving the anionic ring opening polymerization of ϵ-caprolactam are generally manufactured using a Reactive Resin Infusion Molding (RRIM) process equipped with two inert tanks containing the activator with monomer and the initiator with monomer respectively (Section 1.2.1.4). A mixture head ensures the preparation and homogenization of the reactive mixture right before fiber infusion. In the present study, the use of glass beads did not allow to use this processing route, and the glass particles had to be introduced in the reactive mixture before mold filling.

In our case, the mixture composed of resin (monomer + catalyst + activator) and glass particles, noted RP, was first prepared. After total melting of the reagents, the glass particles were added progressively with a targeted particle content of 50 wt% (30 vol%),

similar to that used in the DSC synthesis. Such manufacturing process requires the following specific conditions:

- The preparation of the reactive mixture must be achieved inside a glove box to avoid the negative effect of humidity on the synthesis reaction (Section 1.3.1.2); it is recommended to use as few tooling as possible because of the limited space available inside the glove box,
- Addition of glass particles should be done under moderate stirring using a turbine stirrer with vertical blades (Figure 4.1), in order to ensure a homogeneous dispersion of particles in the mixture, and a magnetic stirrer to avoid their sedimentation at the bottom of the beaker,
- It is necessary to ensure a good mold seal to avoid the contact with air during the curing process in the case it is performed out of the glove box,
- The reactive mixture comprising the monomer, catalyst and activator melts at 70°C with a very low viscosity allowing to facilitate the manufacturing ; below this temperature, the solidification and crystallization of the reactive mixture prevents the resin casting and stops the composite manufacturing - it is therefore necessary to heat at a temperature higher than 70°C all the material in contact with the reactive mixture in order to maintain it in a liquid state and ensure good homogeneity,
- The interval between processing and curing should be sufficiently short to avoid glass particle sedimentation due to the density difference between the particles and the resin (around 2.5 $g.cm^{-3}$ for the particles and around 1.02 $g.cm^{-3}$ for the matrix).

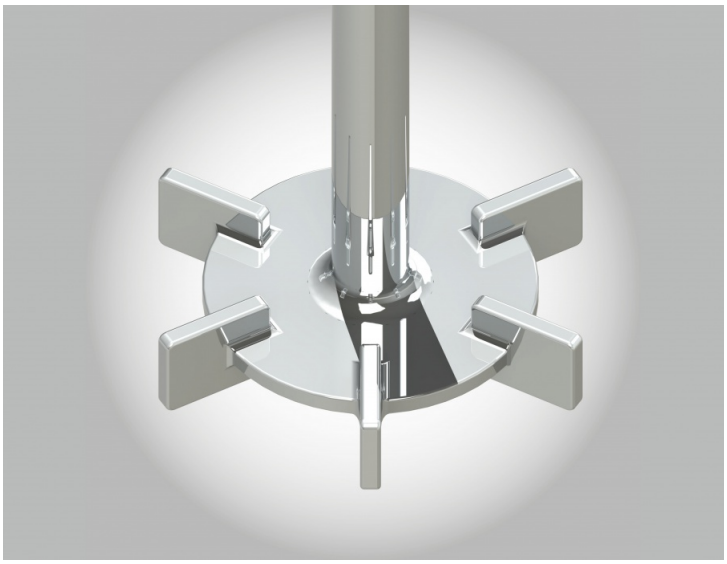

Figure 4.1: Turbine stirrer with vertical blades

4.1.2 Tested process for composites manufacturing

As described previously, the composite manufacturing has many constraints. Hence, several processes were tested and optimized in order to obtain a homogeneous, reproducible and usable composite on which mechanical tests could be performed. Some tested processes are described in the following section, the optimized manufacturing process used to prepare the tensile tests specimens is then detailed.

4.1.2.1 Casting in a sealed mold (CSM)

Procedure

The first process consisted in casting the RP mixture in a closed tooling composed of two aluminum plates. The edges of the mold were prepared with a silicone seal, which gave shape and thickness to the composite, and a mastic applied around the seal to ensure a good sealing and to avoid the moisture absorption outside the glove box (Figure 4.2(a)). The whole system was fixed with double clip clamps as shown in Figure 4.2(b). Thus, the effective volume was inside the silicone seal. An aperture was made on the top side of the mold which allowed pouring the RP mixture in the mold cavity (Figure 4.2(a)).

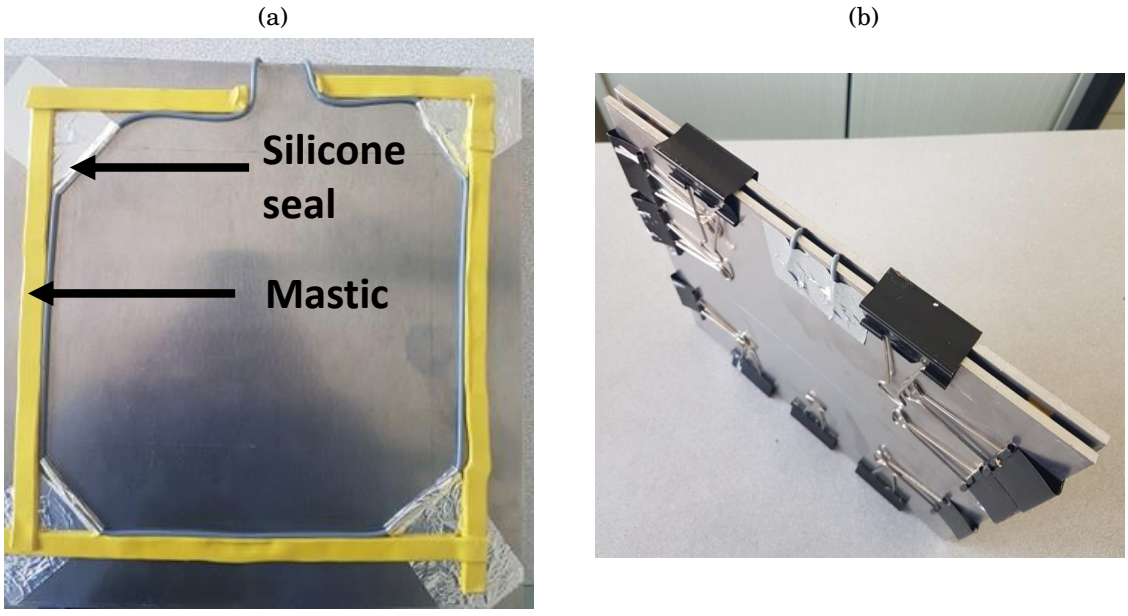

Figure 4.2: Mold preparation for the CSM process

During the RP mixture preparation inside the glove box, the mold was heated to 90°C in order to avoid the solidification of the RP mixture when it is in contact with cold mold sides. Once the mixture was ready, the mold was transferred to the glove box and the mixture was poured into the mold vertically through the top aperture. After the mold filling, the top aperture was closed with mastic and the whole system was deposited vertically in the oven heated at 180°C and left to react for 50 min.

Results

Figure 4.3 shows the composite sample obtained with the CSM process. The white traces appearing on the sample correspond to the glass particles. This indicates that a significant sedimentation of the particles occurred during the reaction in the oven leading to an agglomeration of the particles at the bottom of the mold cavity. Therefore, particles distribution in the resulting composite was clearly not homogeneous.

To overcome this problem, a rotational system was developed to ensure mold rotation during the curing step (Figure 4.4(a)). However, the samples manufactured by this system still contained a high void content and, sometimes, large holes as shown in Figure 4.4(b). The significant void content is due to a mixture leakage during the curing step that was systematically observed when using this protocol.



Figure 4.3: Composite manufactured by the CSM process

(a) (b)



Figure 4.4: CSM process with rotational system: (a) rotational system during curing, (b) manufactured composite

4.1.2.2 Vacuum infusion casting (VIC)

Procedure

In order to strengthen the mold sealing, the second tested procedure consisted in infusing the RP mixture in a sealed mold. The tooling was again made of two aluminum plates separated by two silicon seals that gave thickness to the specimen, but contrary to the previous set-up, the whole system was assembled with screws and nuts to avoid leakages and to ensure a good sealing (Figure 4.5).

In this configuration, instead of pouring the RP between the two plates, vacuum was used to cast the RP into the mold through an inlet port. The infusion was carried out vertically in order to optimize the mold filling and to avoid residual void formation. The RP mixture was infused by a vacuum pump at 0.5-0.6 bar, entering through the inlet casting port located on the bottom of the mold and filling it vertically from bottom to top until reaching the outlet casting port. Thanks to transparent silicon hoses connected to the inlet and outlet hoses, the infusion could be stopped manually when the RP was exiting from the mold through the outlet. Valves were installed at the mold inlet and outlet allowing to stop the mixture infusion as soon as it appears at the silicone hose of the outlet port. This avoided any void infiltration inside the specimen (Figure 4.6). Note finally that all the equipment in contact with the RP mixture (hoses, mold) were heated to 90°C to avoid the mixture solidification in the channels and ensure a homogeneous infusion.

Results

Figure 4.7 shows a composite obtained with the VIC process. As for CSM, the manufactured composites contained a high void content with large vertical voids. Moreover, they exhibited

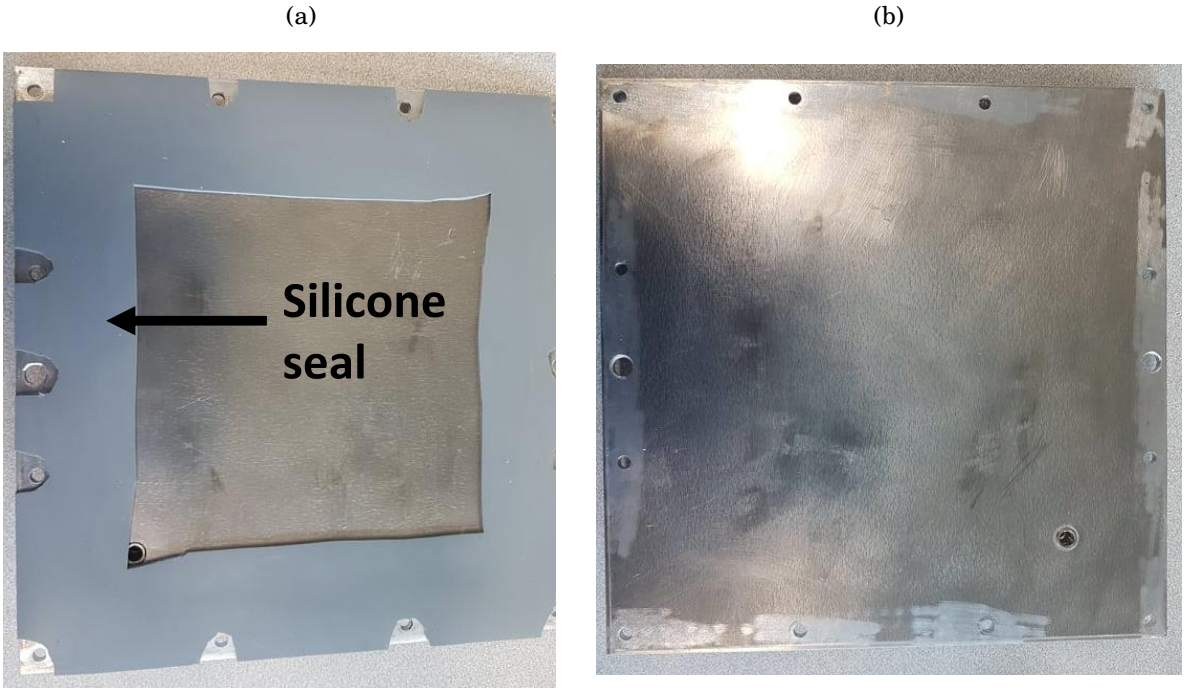

Figure 4.5: Mold preparation for VIC process

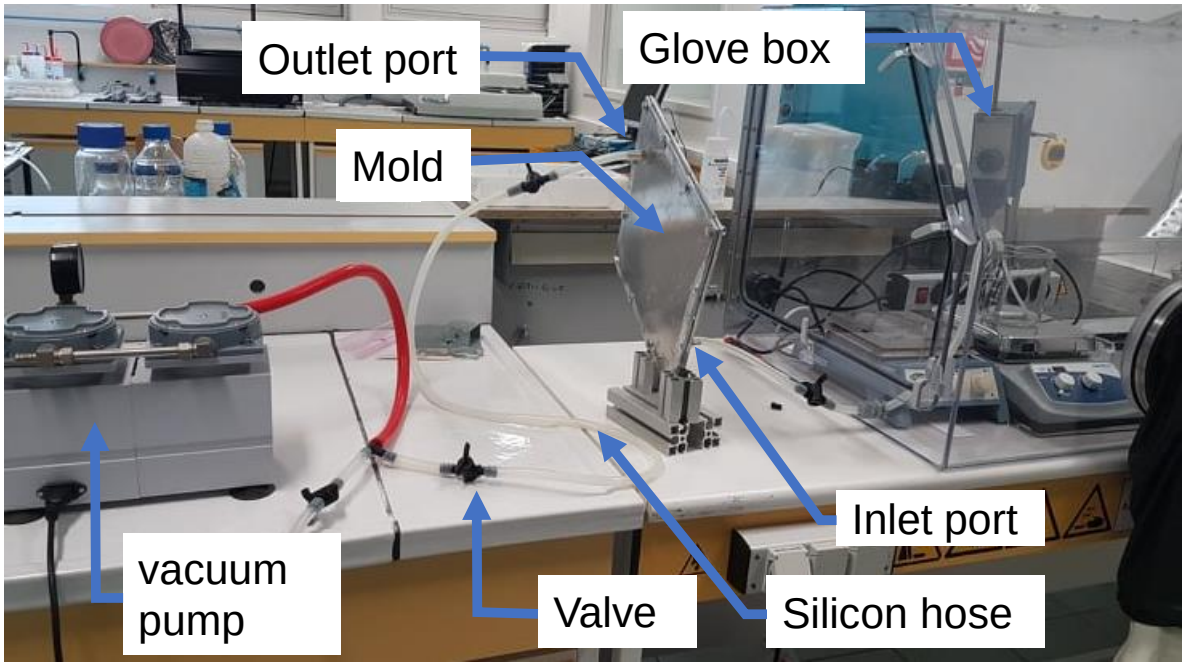

Figure 4.6: Installation of the VIC process

a poor quality of surface aspect with a white layer causing an important roughness. Here again, this can be attributed to monomer evaporation during the curing step, but also to the chemical shrinkage of the mixture related to polymerization. Indeed, although the mold cavity was entirely filled with the RP and that a strong mold sealing was used, large

voids are obtained indicating a significant variation of the mixture volume.

(a) (b)



Figure 4.7: Manufactured composites with VIC process

4.1.2.3 CSM and VIC processes analysis

After several trials with the CSM and VIC processes described above, it was concluded that the white layer formed on the composites surface is due to the monomer evaporated during the synthesis and then condensed on the cooling step. Indeed, the monomer starts evaporating from 100°C and the evaporation thus rapidly occurs at ambient pressure if the molar mass of reactants is not rapidly increased. When polymerization is carried out within a rotating air oven in a closed and rotational mold, the mixture is heated by the hot air. The thermal inertia of the mold walls then does not allow obtaining a high heating rate that is required for obtaining a high polymerization kinetics. Therefore, this favors the monomer evaporation before the polymerization starts. Furthermore, the evaporated monomer was also the origin of the high void content obtained in the previous trials. In fact, after evaporation, the formed gas inside the mold is diffused in the composite sample due to the rotation of the mold in the oven, which leads to its dispersion and the creation of a high void content. This was also the reason for the mixture leakage observed in the CSM process due to the overpressure.

Consequently, to limit the formation of defects during the sample preparation, two main strategies could be explored: either increasing the pressure in the mold cavity for shifting evaporation towards higher temperatures or increasing the heating rate of the mixture for accelerating the polymerization process. This is this second strategy that was preferred for the preparation of tensile test samples.

4.1.2.4 Casting in an open mold (COM)

Procedure

The new process developed to overcome previous manufacturing issues was based first on the mixture heating during the curing process in order to reach the polymerization temperature rapidly and limit the monomer evaporation. Higher heating rates also limited particles sedimentation thanks to the rapid increase of the mixture viscosity induced by the fast polymerization and crystallization. In addition, the polymerization was carried out in an open mold in order to release the generated gas and avoid the formation of voids in the composite. Also, since the mold rotation generated a dispersion of the formed gas in the sample, synthesis was carried out without rotation.

In order to achieve the previous requirements, a new mold was developed based on the shape of the tensile specimens. This way, tensile samples were directly obtained and the composite cutting step that could influence the composite properties was eliminated. The mold was composed of two parts: a support (lower part, Figure 4.8(a)) and five cavities in the form of tensile specimens (upper part, Figure 4.8). The two parts were fixed with screws and nuts and can be detached to facilitate the demolding step without damaging the specimens.

First, the silicone was applied to the cavities edges to ensure a good sealing between the base plate and the plate with cavities. Both mold parts were then assembled and left overnight for the silicone to dry (Figure 4.8(c)). The next day, the mold was heated to 200°C to complete the silicone cross-linking and to evacuate any potential void that may be introduced into the specimens during the silicone curing process. The whole system was then introduced into the glove box and heated with a hot plate until the temperature inside the mold cavities reached 180°C (polymerization temperature). Once reacted, the mold was air cooled and then the tensile specimens were carefully demolded.

This process made it possible to overcome all the limitations of the previous procedures. Indeed, the mold and the reactive mixture heating were optimized because they were carried out in contact with the heating plate, on the contrary of the heating in the oven with the rotating air. Moreover, this technique allowed to better control the polymerization temperature than for processes in oven where temperature could only be recorded by the controller. With COM, the direct access to the open mold was possible without impacting the specimens and the cavities temperature was checked by a thermocouple to ensure that it reached 180°C before adding the mixture.

Results

Figure 4.9 shows the tensile specimens obtained by the optimized COM process. As it can be observed, the samples were homogeneous although white traces could be observed on the surface of specimens. This was due to the condensation of some of the evaporated monomer and these traces could be easily cleaned since they represented a very thin layer at the surface of the tensile test samples.

(a) (b)

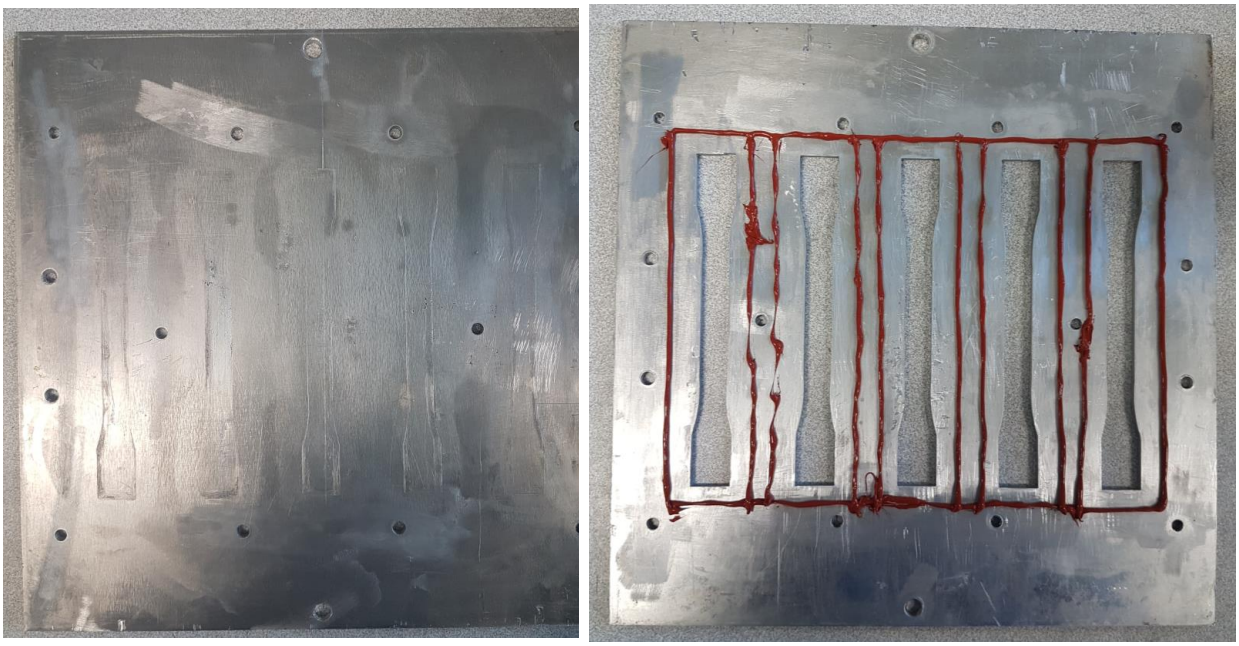

(c)

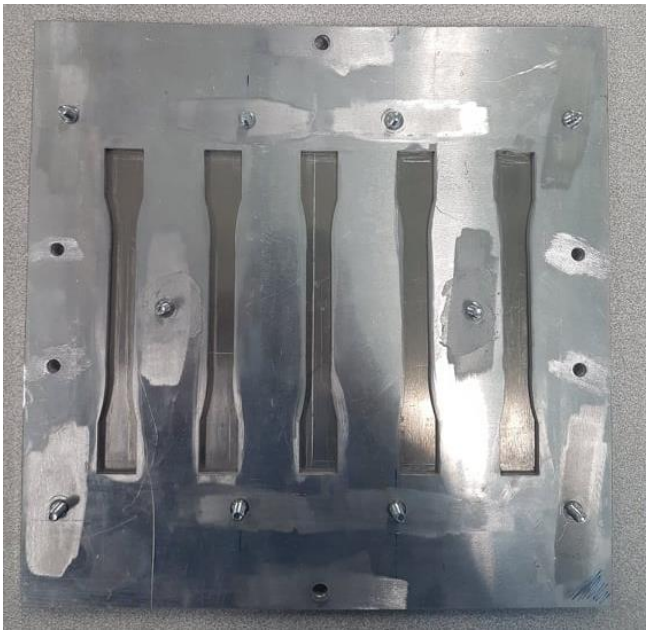

Figure 4.8: Mold preparation for COM process

During synthesis, the evaporated monomer was released and condensed mainly on the glove box walls. Therefore, no void was observed inside the composite specimens. The amount of evaporated monomer during synthesis $m_{\epsilon-CL}^{evaporated}$ was quantified using the following equation:

$$m_{\epsilon-CL}^{evaporated} = 1 - \frac{m_{specimens} + m_{residual}}{m_0} \tag{4.1}$$

in which $m_{specimens}$ is the total mass of the manufactured specimens, $m_{residual}$ is the mass of the residual mixture that remains in the beaker after casting and m_0 is the initial



Figure 4.9: Installation of the VIC process

mass of the mixture (resin + particles) introduced in the beaker.

In the case of TMPS composites, the evaporated monomer ratio is 6.15%. Indeed, the polymerization and crystallization kinetics are rather slow with TMPS particles as shown in Figure 3.13(b). Consequently, a very important monomer quantity evaporated during the manufacturing, which led to the formation of a high void content in the composite specimens before the end of the reaction. In addition, the high evaporated monomer amount during the TMPS composites manufacturing induced a significant pollution of the glove box (Figure 4.10). Therefore, it confirmed that the hydrophobic TMPS treatment significantly slows down the polymerization and crystallization kinetics, as shown by DSC. This treatment makes the manufacture of anionic PA6/glass composites very difficult to control and leads to a poor quality of composite specimens. Consequently, mechanical tests could not be performed on this composite configuration

On the contrary, the ratio of evaporated monomer was 2.56% (respectively 1.54%) for composites containing calcinated particles and particles treated with aminosilanes (resp. for neat resin specimens and composites containing ACTISILANE and MONOMSILANE treated particles). The difference between the evaporated monomer ratio according to the particles type is due to the difference of the synthesis kinetics. Indeed, the ACTISILANE and MONOMSILANE treated particles allow a fast polymerization/crystallization kinetics, as demonstrated in Section 3.3. This limits the monomer evaporation before the polymerization starts. On the other hand, the polymerization in the presence of the

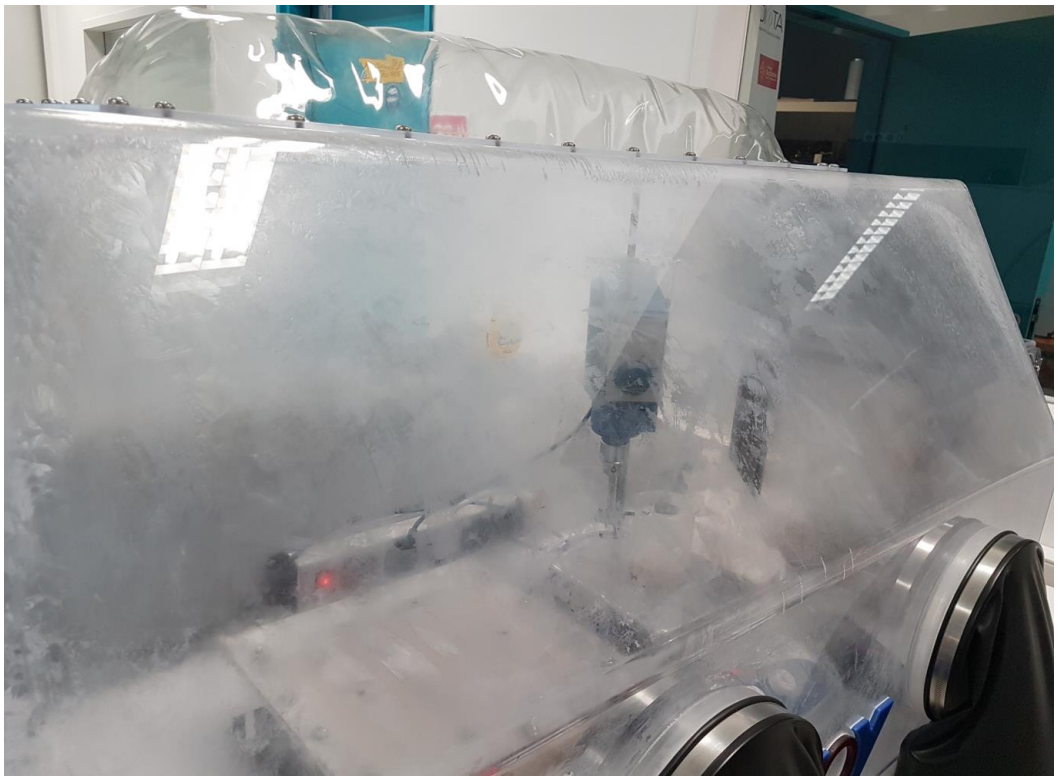

Figure 4.10: Glove box pollution by the evaporated monomer during TMPS composites manufacturing

calcinated particles and those treated with aminosilanes is slower and, therefore, a higher amount of monomer evaporates during the composites manufacturing. Yet, for all these treatments, the evaporated monomer during the manufacturing represented a small quantity. All specimens exhibited a very good quality and could be exploited for the subsequent mechanical analyses.

After manufacturing, the composite specimens were stored under vacuum, then dried at 70°C for at least 4 h before any further analysis.

4.2 Physical and chemical characteristics

After the process optimization and the composite specimens manufacturing, the physico-chemical characteristics of the manufactured composites were evaluated by TGA and DSC in order to evaluate the particle content and the conversion and crystallinity degrees.

In the rest of the chapter, the name of the composites containing each kind of particles will be simplified according to the particles treatment. For example, "APTMS composites" denotes composites containing particle treated with APTMS.

4.2.1 TGA

4.2.1.1 Procedure

The particle content and the conversion degrees were determined using the TGA. The samples of neat resin and composites containing the different treated particles were added to the TGA crucible with careful attention to moisture absorption. Then, each sample was heated from 25°C to 500°C at 5°C/min under a nitrogen atmosphere to avoid oxidation phenomena. Moreover, it was considered that the residual ϵ-CL does not react during this heating step since the polymerization kinetics is very slow once the temperature of monomer evaporation is reached, especially when the polymer is already synthesized.

4.2.1.2 Results

Figure 4.11 shows the TGA curves and their derivatives for the neat resin and calcinated composites specimens. The calcinated composites curve is representative of the other treatments (APTMS, AEAPTMS, TMPS and MONOMSILANE) which have the same shape. The case of ACTISILANE composites is discussed later.

At 500°C, the resin is almost completely degraded since the total mass loss of the neat resin is higher than 96% and stabilizes. The offset obtained with a total loss of 100% could be due to the calibration of the device. Three ranges of mass loss can be identified in each curve as shown in Figure 4.11. The first mass loss between 100°C and 260°C is due to the unreacted monomer evaporation [17, 45]. The water evaporation occurs in the same range but this amount is considered negligible thanks to the precautions taken during the sample preparation to avoid moisture absorption. The second mass loss that starts from about 300°C and the third mass loss from about 320°C are related to PA6 degradation. The transition between the last two mass losses is characterized by an inflection that distinguishes oligomers degradation from the polymer chains degradation.

In considering that the temperature ranges of monomer evaporation and oligomer degradation do not overlap, a transition temperature between the two intervals could be identified on the derivative curve between 250°C and 280°C (dotted line in Figure 4.11). The mass loss below this temperature could thus be associated to the residual monomer amount $m_{\epsilon-CL}$ and this value was therefore used to calculate the conversion degree.

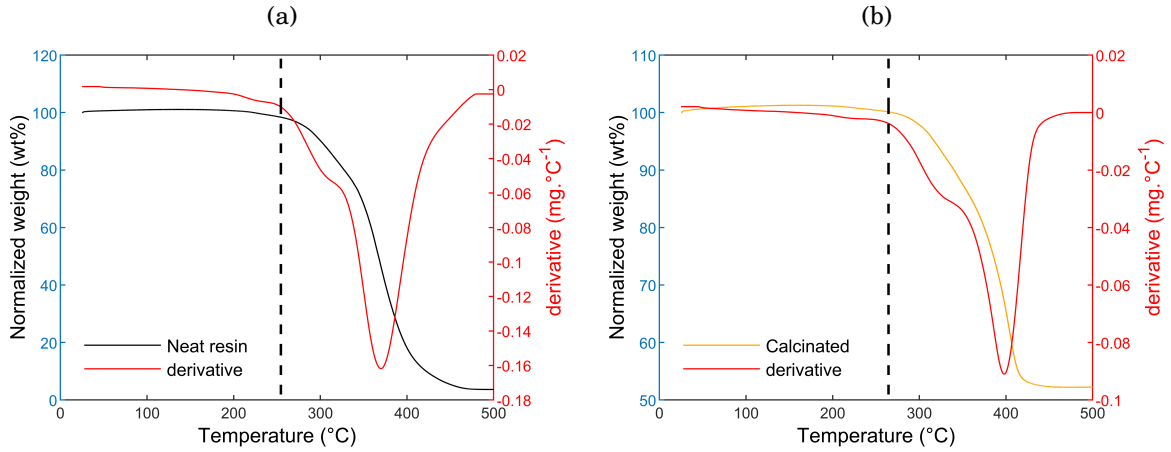

Figure 4.11: TGA curve and its derivative for specimens of (a) neat resin and (b) composites containing calcinated particles

The ACTISILANE composites mass loss, shown in Figure 4.12, is different from the other curves. The derivative curve shows two distinct intervals of mass loss. The first one, between 210°C and 320°C, is due to the oligomers and short chains degradation. The second interval starts from 320°C and corresponds to the PA6 degradation. Moreover, the derivative curve does not show a mass loss related to residual monomer. Instead, the mass loss due to short chain degradation around 250°C is higher compared to the neat resin and other composites. These two major differences with neat resin and other treatments can be attributed to the presence of activator molecule grafted on the surface of glass particles. Indeed, the activator grafting on the particles surface indirectly increases the activator concentration in the reactive mixture, which leads to an acceleration of the polymerization kinetics by increasing the number of chain initiation points in the RP (Figure 3.13(d)). In the end, this promotes shorter chain formation and the consumption of monomer during polymerization. This effect is schematically described in Figure 4.13.

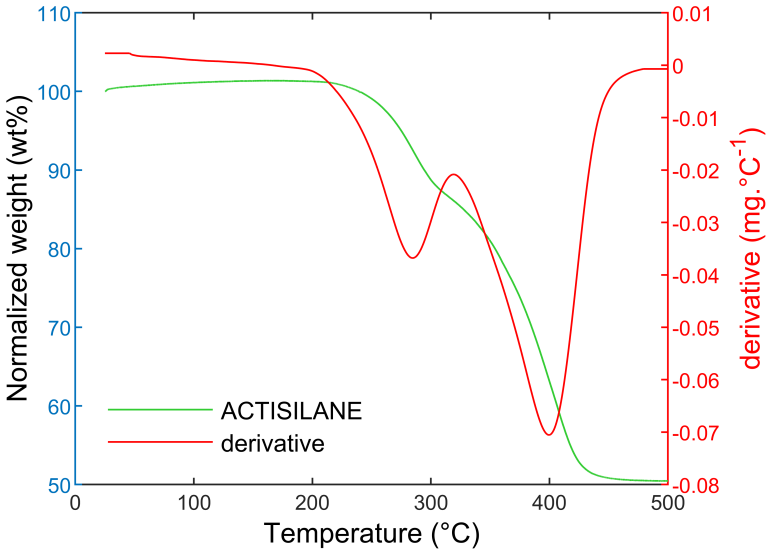

Figure 4.12: TGA curves and their derivatives of composites containing ACTISILANE treated particles

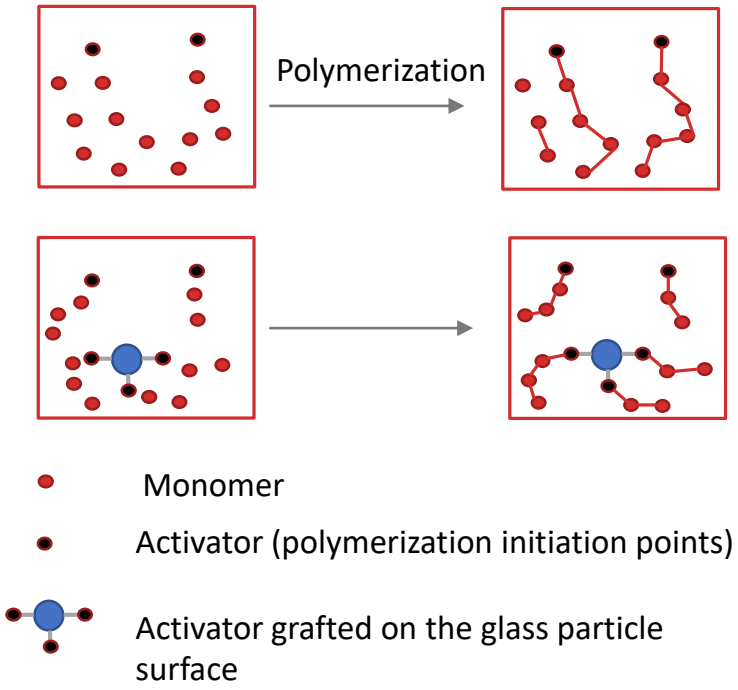

Figure 4.13: Effect of increasing initiation points on the length of the formed polymer chains after polymerization

The particle content (χ_m, %) in the manufactured composite specimens was determined according to following equation :

$$\chi_m = (1 - \frac{m_r}{m_t}) * 100 \tag{4.2}$$

in which m_r is the mass loss obtained from TGA which corresponds to the resin mass and m_t is the total mass of the sample.

Next, the conversion degrees of the neat resin and composite specimens were characterized using the procedure described in Section 1.1.4.1. For the composite samples, the particles mass was calculated using the previously calculated χ_m, then it was subtracted from the total sample mass. In addition, for the composites containing the silanized particles, the mass loss related to the silane (Table 3.5) according to the particle content in the sample was subtracted from the total mass. Therefore, the conversion degree of the neat resin specimens (X^{∞}_{p-nr}), of the composites containing the untreated particles (X^{∞}_{p-ca}) and the composites containing the silanized particles (X^{∞}_{p-si}) were calculated according to Equations (4.3), (4.4), (4.5) respectively.

$$X^{\infty}_{p-nr} = (1 - \frac{m_{\epsilon-CL}}{m_t}) * 100 \tag{4.3}$$

$$X^{\infty}_{p-nr} = (1 - \frac{m_{\epsilon-CL}}{m_t(1 - \frac{\chi_m}{100})}) * 100 \tag{4.4}$$

$$X^{\infty}_{p-si} = (1 - \frac{m_{\epsilon-CL}}{m_t - \frac{\chi_m}{100} m_t(1 + \frac{\Delta m_{silane}}{1-\Delta m_{silane}})}) * 100 \tag{4.5}$$

Table 4.1 shows the particles contents and the conversion degrees obtained for each specimen. All specimens particles contents almost corresponded to the targeted content of 50 wt%. This indicates a good homogeneity and particle distribution in the composite specimens since the TGA samples were taken in different zones. In addition, this confirms that the particles do not sediment during the mixture preparation or during the polymerization. Furthermore, the results in Table 4.1 show that the specimens of neat resin and all composites, regardless of the particle type, had conversion degrees higher than 95%. These results are consistent with the conversion degrees obtained by DSC (Section 3.3.2, Tableau 3.7) and demonstrate a good polymerization of the resin during the manufacturing process.

Table 4.1: Conversion degree of the neat resin specimens and the composite specimens containing the different types of particles

Sample	Particle content χ_m (± 1%)	Degree of conversion (± 0.7%)
Neat resin	0	97.1
Calcinated	53	98.5
TMPS	52	96.3
APTMS	53	98.6
AEAPTMS	51	97.4
ACTISILANE	51	98.5
MONOMSILANE	52	98.2

It is important to note that the monomer evaporated during the specimens manufacturing was not considered in the calculation of the conversion degrees. In the case of TMPS composites, the conversion degree decreases to 90.1% after considering the evaporated monomer according to Equation (4.6):

$$X_{p-si}^{\infty} = (1 - \frac{m_{\epsilon-CL+m_{\epsilon-CL}^{evaporated}}}{m_t - \frac{\chi_m}{100} m_t (1 + \frac{\Delta m_{silane}}{1-\Delta m_{silane}})}) * 100 \tag{4.6}$$

In this case, it is possible that this significant reduction of the conversion has an important influence on the matrix properties, especially the molar mass. On the other hand, the amount of evaporated monomer is low and the conversion degree decreases by almost 2% for the aminosilane composites and 1% for the neat resin and the ACTISILANE and MONOMSILANE composites, after considering this amount in the calculation, which makes its influence negligible.

4.2.2 DSC

4.2.2.1 Procedure

The crystalline phase content formed during the specimens manufacturing can be evaluated through the melting enthalpy ΔH_m. The latter is obtained by integrating the endothermic peak of a heating ramp from 25°C to 270°C at 10 °C/min. The melting enthalpy was adjusted according to the matrix mass:

$$\Delta H_m = \frac{100 * \Delta H_{mt}}{100 - \chi_m} \tag{4.7}$$

in which ΔH_m (J.g^{-1}) is the melting enthalpy related to the polymer, ΔH_{mt} (J.g^{-1}) is the melting enthalpy obtained from DSC and χ_m (%) is the particle content determined by TGA. From that, the crystallinity degree X_c^{∞} was calculated using Equation (1.3) by assuming the melting enthalpy $\Delta H_c^{100\%}$ of a 100% crystalline PA6 to be 190 J.g^{-1}.

Then, each sample was cooled in DSC from 270°C to 0°C at 10°C/min to achieve a controlled crystallization from the molten state. Hence, the crystallization enthalpy and temperature during the cooling step was determined. Finally, a second heating ramp from 0°C to 270°C at 10 °C/min was carried out in order to compare the melting enthalpies of the crystalline phase formed during manufacturing and those formed upon cooling in DSC configuration. This allows to further analyze the crystallization obtained during the composites manufacturing.

4.2.2.2 Results

Crystallization during synthesis

Figure 4.14 shows the DSC thermograms of the 1st heating cycle of the neat resin and the calcinated and ACTISILANE composites, that are representative of all other composites. As in the case of the DSC synthesis, all specimens did not show any exothermic peak

indicating the polymerization of residual monomers. This confirms the almost complete consumption of monomers and stands in agreement with high conversion degrees obtained.

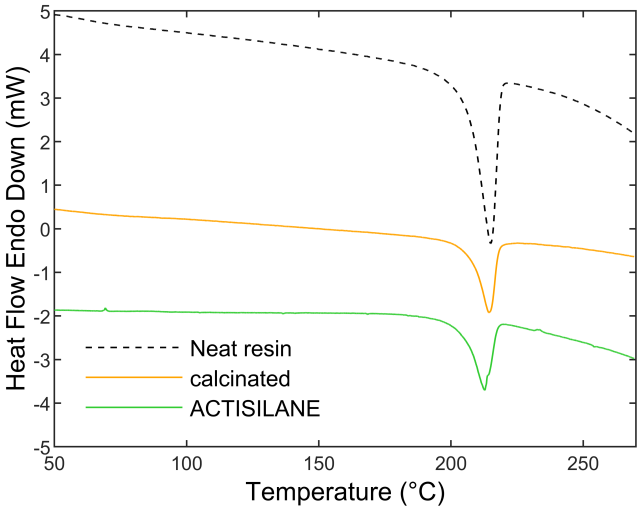

Figure 4.14: DSC thermograms of the heating cycle from 0°C to 270°C at 10°C/min of the neat resin specimens and the composites synthesized with calcinated and ACTISILANE treated particles

Table 4.2 presents the melting enthalpie ΔH_m and temperature T_m as well as the crystallinity degree obtained for various composites samples. First, these results were consistent with the previous results of the isothermal synthesis in DSC (Table 3.7), which indicates a good crystallization during the manufacturing process. This also proves the reliability and the reproducibility of the synthesis reaction despite the scale difference. The crystallinity degrees obtained were particularly high compared to the crystallinity degrees of commercial PA6 as demonstrated in the literature (Section 1.1.4.3).

Table 4.2: Melting temperatures and enthalpies and crystallinity degree of PA6 specimens and PA6/glass particles composites with different types of particles surface treatment. The results are obtained after a 1st heating cycle from 0°C to 270°C at 10°C/min

Sample	Melting temperature T_m (°C) ± 0.6	Melting enthalpy ΔH_m (J.g^{-1}) ± 1	Crystallinity degree X_c^{∞} (%) ± 1
Neat resin	215	69.5	36.6
Calcinated	214.3	54.4	28.6
TMPS	220.8	78.2	41.2
APTMS	215.7	70.5	37.1
AEAPTMS	214	65.6	34.5
ACTISILANE	212.8	67	35.3
MONOMSILANE	215.5	85.2	44.8

The crystallinity degrees obtained for all the composites containing treated particles were almost the same than that of the neat resin except for the calcinated particles where

the enthalpy and the crystallinity degree were lower. Indeed, the particles addition in the reactive mixture can limit the polymer chains mobility because of the spatial hindrance induced by the presence of glass particles. Moreover, the polymer chains adsorption on the particles surface may form loops and tails that reduce the free volume and the chains degree of freedom [177, 178] and can disturb the crystallisation process in the particles vicinity [179, 180]. In the case of treated particles, it is possible that the silane contribution to nucleation [106, 171, 172, 180] counterbalances the negative effect of particle hindrance. In addition, the silane chains grafted on the particle surface increase the free volume at the interface region, which gives more freedom to the polymer chains compared to the calcined particles, and promotes their mobility. Hence, these factors induced to a crystallinity level equivalent to that of the neat resin.

Furthermore, the MONOMSILANE treatment led to a high crystallinity degree compared to the other treatments. The monomer grafted on the surface could favor the crystallization according to the two mechanisms presented in Section 3.4.6 : (i) First, the monomer grafted on the surface could favor the reactive species diffusion, which favors the nucleation; (ii) Second, the plasticization effect of the intercrystalline zones by the presence of residual monomer- potentially the monomer grafted on the particle surface-in the crystals at the initial stage of crystallization favors the chains mobility. This improves thus the overall composite crystallinity [176].

The melting temperature of ACTISILANE composites was lower than other composites and neat resin. The same results were obtained during the DSC synthesis as shown in Table 3.7. As explained earlier, the activator grafting creates several reaction initiation points from the particles surface (Figure 4.13). This can lead to an increase in nucleation points. Therefore, for the same crystallinity degree, the PA6 crystallized in the presence of the ACTISILANE-treated particles led to smaller crystal sizes and hence a lower T_m. In addition, the ACTISILANE treated particles containing the activator accelerate the polymerization. This can increase the polymer chains mobility and allows the chains to crystallize with shorter lengths compared to the neat resin.

The TMPS specimens had high melting temperature and enthalpy, and a high crystallinity degree compared to the other composites and the neat resin. As previously demonstrated, the polymerization kinetics with TMPS particles is relatively slow (Figure 3.13(b)), which favors crystallization due to the opposite thermal dependence of the two phenomena (Section 1.1.2.3). This thus increases the melting temperature and the crystallinity degree and decreases the conversion degree [11, 16, 25, 26]. Furthermore, a second mechanism can explain the rise in the crystallinity degree of TMPS composites. When the polymerization kinetics decreases, the reactive chain ends can also be trapped inside the crystals as shown in Figure 4.15 [26]. Subsequently, the resulting morphology promotes the plasticization effect process described above.

Crystallization from the molten state

Representative thermograms of the cooling cycle and the 2nd heating cycle are shown in

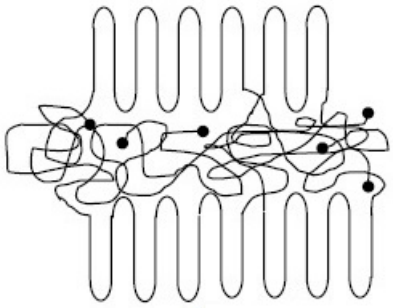

Figure 4.15: Trapping of the reactive chain ends inside the crystals [26]

Figure 4.16. The melting peaks for all the samples were wider with a slight inflection compared to the melting peaks obtained during the first heating cycle. This indicates the formation of a broad distribution of crystalline lamellae thickness during the crystallization from the molten state. These lamellae have different sizes leading to the appearance of an inflection due to the melting of small ones [23]. Overall, the melting enthalpy after crystallization from the molten state was lower than the melting enthalpy obtained after crystallization during synthesis. This attested the good crystallization of the specimens during manufacturing

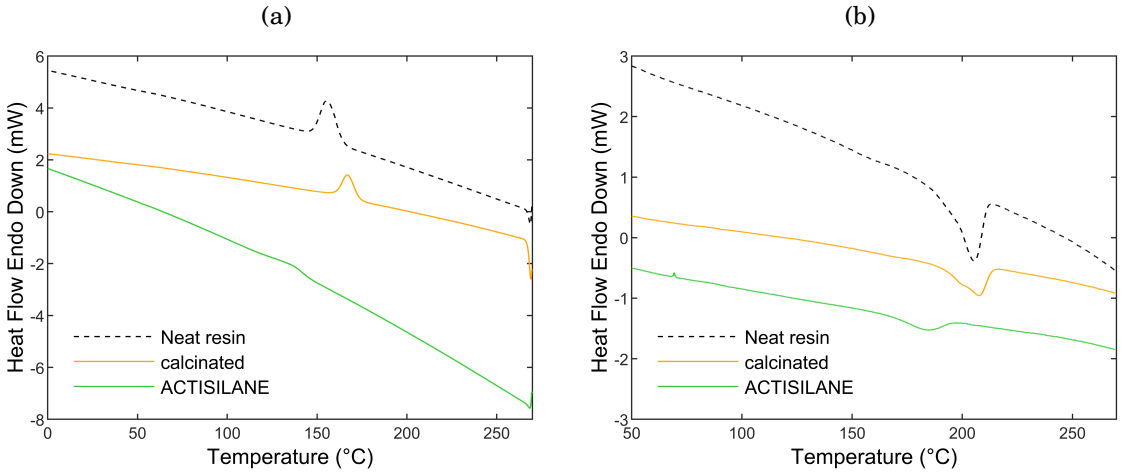

Figure 4.16: DSC thermograms of neat resin specimens and the composites synthesized with calcinated and ACTISILANE treated particles: (a) cooling cycle from 270°C to 0°C at -10°C/min, (b) 2nd heating cycle from 0°C to 270°C at 10 °C/min. Other samples displayed thermograms very similar to those of the composites with calcinated particles

The thermogram of ACTISILANE composites was different from other thermograms by the shape and the position of the crystallization and melting peaks. Both peaks were smaller and shifted at lower temperatures compared to the other specimens. This reflected a lower crystallization during cooling.

To confirm this tendency, Table 4.3 shows the crystallization temperature T_c and enthalpy ΔH_c obtained during cooling and the melting temperature and enthalpy of the second heating cycle for all composite specimens. First, a difference between the

crystallization enthalpy and the melting enthalpy was observed. This is also reported in the literature and may be due to cold crystallization during the heating ramp or to a melting/recrystallization phenomenon [23, 181, 182]. Comparing the various samples, the temperatures and enthalpy of crystallization and melting showed the same trends.

As expected, only the ACTISILANE composites had a lower crystallization temperature than the neat resin. These composites and those containing calcinated particles also had lower enthalpy compared to the neat resin. The PA6 chains architecture, distribution, and interactions with the particles can explain, at least partially, the differences in temperature and enthalpy observed during crystallization from the molten state. First, the polymer chains in ACTISILANE composites form covalent bonds with particles. This reduces their mobility once the first crystallization has been performed during synthesis, in addition to the architectural heterogeneity created by the increase of the initiation points [53, 101]. Consequently, the crystallization enthalpy from the molten state decreased significantly. The low crystallization temperature could be due to the formation of short chains resulting in thinner lamellae compared to the other cases [23]. Regarding calcinated particles, the lower crystallization enthalpy than neat resin is due to the reduction of the chains mobility induced by the presence of particles having limited interactions with the matrix and that disrupt the crystallization process [183–185].

Concerning other treatments, the crystallization and melting enthalpies observed are higher than that of the neat resin. This could be due to the enhanced nucleation by the presence of silane, which promotes the formation of a higher percentage of crystalline phase.

Table 4.3: Crystallization temperature (T_c) and enthalpy (ΔH_c) measured on DSC curves obtained upon cooling from 270°C to 0°C at -10°C/min, melting temperature (T_m) and enthalpy (ΔH_m) on the curve of 2nd heating cycle from 0°C to 270°C at 10°C/min and Crystallinity degree (X_c^{∞}) for PA6 specimens and PA6/glass particles composites with different types of particles surface treatment

	Cooling step		2nd heating cycle		
Sample	T_c (± 0.6°C)	ΔH_c (± 1 J.g^{-1})	T_m (± 0.6°C)	ΔH_m (± 1 J.g^{-1})	X_c^{∞} (± 1%)
Neat resin	156.4	33.8	205.4	30	15.8
Calcinated	167.8	31.2	207.5	27.6	14.5
TMPS	170.7	34.6	211.9	32.4	17.1
APTMS	163.3	43.5	207	37	19.5
AEAPTMS	165.6	50.2	209	45	23.7
ACTISILANE	136.9	23.2	35.3	185	10.2
MONOMSILANE	162.2	48.8	207.6	43.8	23.1

4.3 Composite mechanical properties and interface analysis

4.3.1 Analysis techniques and experimental conditions

The influence of interfacial phenomena on the mechanical properties of the manufactured composites was evaluated by tensile tests. These tests were performed using an Instron tensile machine equipped with a 50 kN load cell. According to ASTM D638 [186], a cross-head speed of 5 mm/min was chosen and specimens were designed according to Type I tensile geometry. The samples dimensions are given in Figure 4.17. The standard method recommends a thickness below 7 mm. In our case, an average thickness of 3.2 ± 0.5 mm was measured for all specimens

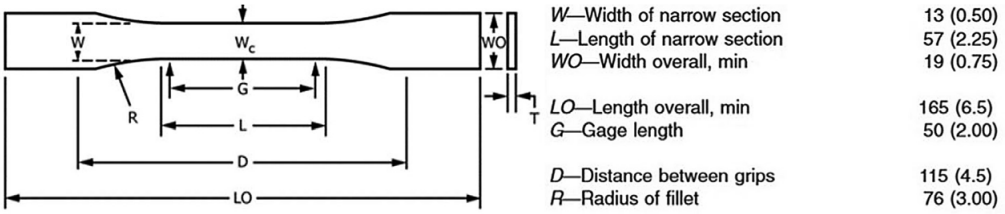

Figure 4.17: Sample measurements of tensile specimens in mm (in.), ASTM D638 Type I [186]

As explained before, water absorbed by PA6 can affect the mechanical properties of the composite. Therefore, all specimens were dried for at least 4 h at 70°C before trials. A set of four composite samples of each surface chemistry was tested at ambient conditions, but the experimental results were discarded when the samples broke in clamps, thus reducing the number of data.

It is also noted that the TMPS composite specimens were not considered due to their high void content. MONOMSILANE composites are not presented either due to the manufacturing defects of these specimens. Figure 4.18 shows SEM images of MONOMSILANE composite fracture surface, which demonstrate major defects at the fracture zone. These defects are mainly due to a high voids content and strong heterogeneity in the composite. Indeed, only a small quantity of treated particle was available for manufacturing. So, the use of the turbine stirrer was not possible due to the small volume. Instead, only the magnetic stirrer was used, which resulted in poor particle distribution during the mixing and casting steps.

For the monitoring of displacement and strain during the mechanical tests, Digital image correlation (DIC) was chosen in order to obtain full field strain data and avoid the influence of contact gauge sensors. Also, this technique allows a continuous monitoring during the experiment to assess the deformation homogeneity of the specimens and their behavior during the tensile test.

(a)

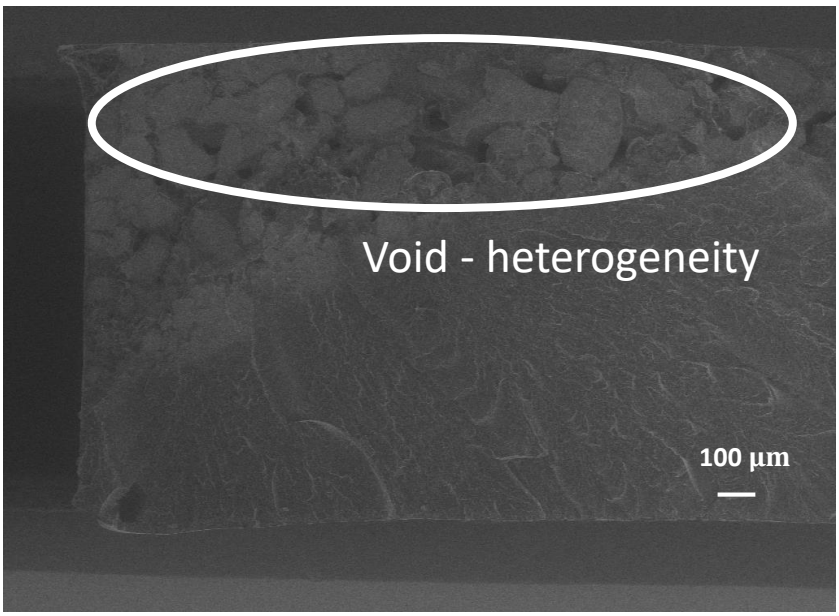

(b)

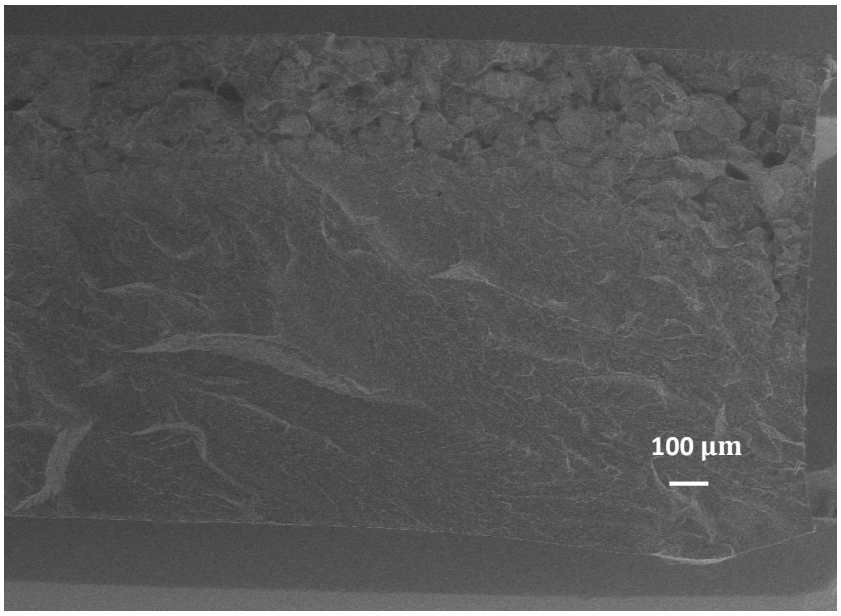

Figure 4.18: SEM images of the fracture surface of MONOMSILANE composites

In what follows, the measurement technique and the obtention of kinematic fields are first explained. In a second part, the composites mechanical properties are presented and analyzed according to the particle-matrix interaction type at the interface.

4.3.2 Kinematic field measurements

Among the different measurement techniques, the digital image correlation (DIC) method is now commonly used and reported as a very efficient technique for the surface strain measurements. DIC is an optical technique based on digital image processing and numerical computation. It directly provides full-field displacements and strains by comparing digital images of the sample surface in the undeformed (or reference) and deformed states

respectively. Several configurations of DIC measurements can be distinguished regarding the number of images of the scene taken simultaneously and the equipment used for capturing digital images. Basically, one optical camera allows the determination of 2D surface measurements and multiple cameras configurations allows obtaining 3D displacement fields of sample surfaces. The most conventional configuration consists in using a single digital camera fixed in front of a planar object surface in order to achieve 2D image correlation. This method does not require a complex surface preparation and the displacement field post-processing for calculating the strain fields is relatively easy [187].

Since the manufactured specimens have a planar surface and assuming no out-of-plane displacements, the displacement and strain fields during the tensile test were evaluated using the 2D DIC method. In this section, the basic principles and concepts of 2D DIC are described. Then, the experimental preparation and the results of the displacement and strain fields are presented and analyzed

4.3.2.1 Fundamentals of 2D DIC

In general, 2D DIC field measurements involve three steps: (i) sample and experiment preparation; (ii) recording of images of the sample planar surface during the test; (iii) post-processing of the acquired images using computer software to obtain the displacement and calculate strain fields.

The images of the sample surface are spatially discretized by a CCD (Charge Coupled Device) sensor assigning for each pixel a gray level which pattern will be exploited for identifying the location of each point of the sample surface in the image. The sample surface then must have a random distribution of gray intensity (i.e. the random speckle pattern). This pattern deforms together with the sample surface, which provides information about the deformation. The speckle pattern can be the sample natural texture, but in most cases, it is artificially created using black and white paint or other techniques.

The camera is placed so that its optical axis is normal to the sample surface (Figure 4.19). This allows to obtain an image of the sample surface in different states during the test. After recording the digital images before and after deformation, a DIC software calculates the displacement of numerous image points by comparing the digital images taken at different times. The basic principle of the DIC technique is to identify the location of the same points over a sequence of images corresponding to the different states of deformation as illustrated in Figure 4.20. A square subset is selected for comparison, rather than an individual pixel, as it ensures the uniqueness of the gray levels pattern in the image, which allows to distinguish it from the other subsets. Therefore, the point P displacements are calculated by choosing a square reference subset of pixels centered at point P(x_0, y_0) of the reference image and then tracking its corresponding position in the deformed image.

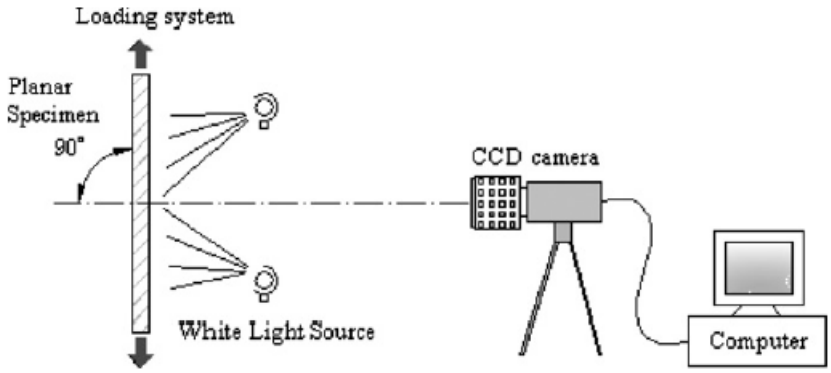

Figure 4.19: Typical experimental setup of the 2D DIC method [187]

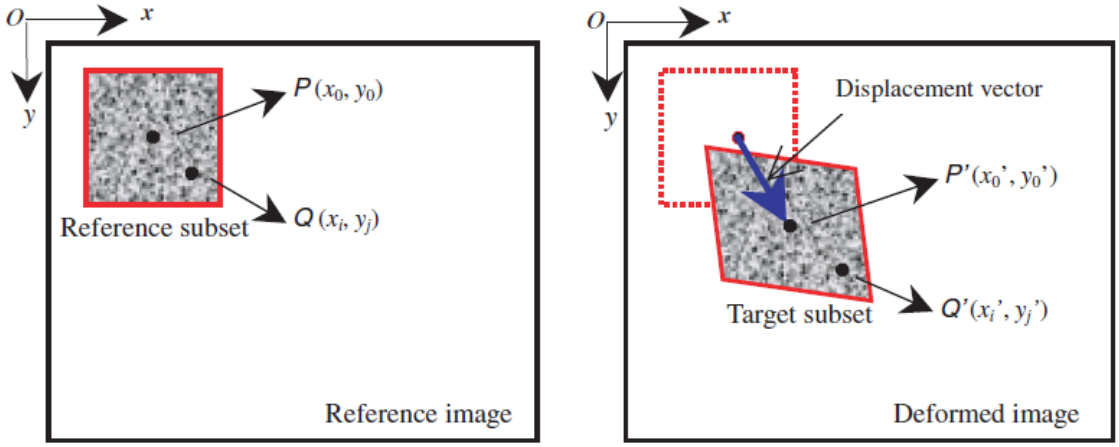

Figure 4.20: Reference square subset before and after deformation [187]

4.3.2.2 Sample preparation and experimental conditions

A speckle pattern was applied to the surface of all specimens with black and white paints (Figure 4.21). The deposition of this artificial speckle must be create a level of contrast high enough to ensure recognition by the camera CCD sensor of the different levels of grey. It should be noted that the quality of this speckle (in particular its homogeneity) has been validated with regard to the grey levels distribution (Figure 4.22).



Figure 4.21: Example of a speckle pattern

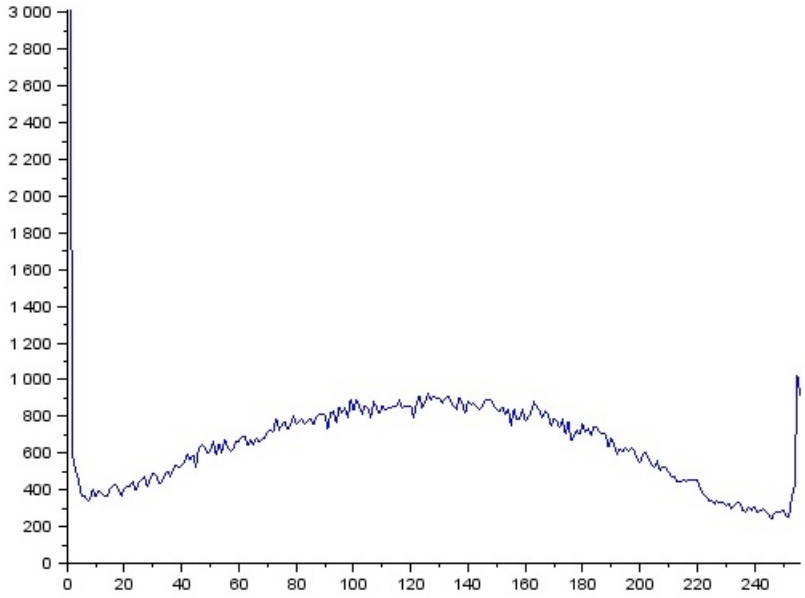

Figure 4.22: Speckle characterization : distribution of the grey levels

The sensor used is composed of a CCD camera 1392 x 1040 pixels. A 35mm lens was used with a distance of about 500mm from the specimen (Figure 4.23). A calibration is then necessary which consists in defining a number of parameters (exposure time, depth of field) in order to obtain a clear image. In addition, a lighting by halogen projector was used to improve the pattern contrast in the images.

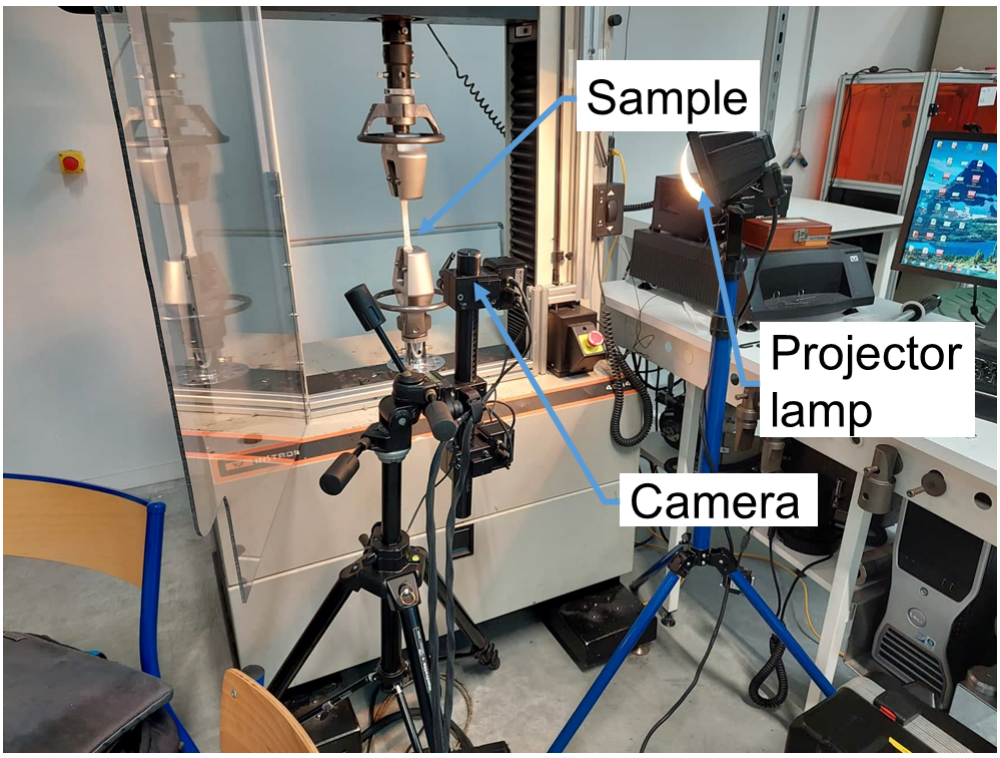

Figure 4.23: Setup of 2D DIC measurements

The image acquisition and post-processing software used is ARAMIS 2D, which perfor-

mance is described in Bornert et al. [188]. A first image is taken at the beginning of the test as a reference image (Figure 4.20). Then, a series of images of the deformed specimen are taken during the tensile test with a frequency of one image per second until the end of the test.

The post-processing allows to obtain the displacement and strain fields in the measurement plane (x,y). It requires to define the calculation method (total for classical measurements or by step for large deformation), the correlation window (or square subset size) at the center of which the displacements are measured and the subset step which represents the distance between two measurement points (Figure 4.24). In our case, we have used a total calculation method with a subset size of 19mmx19mm and a step of 15mm.

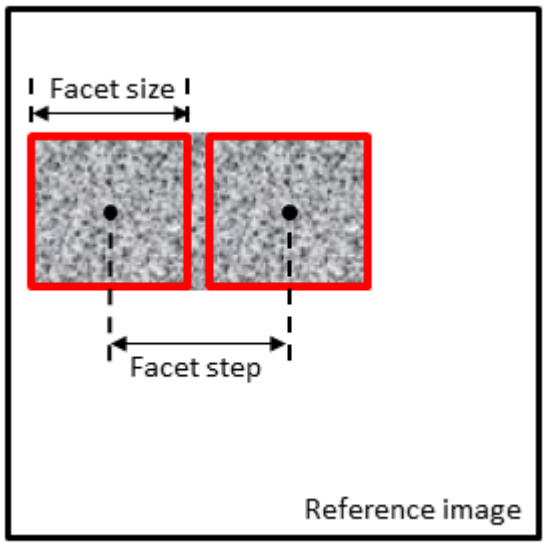

Figure 4.24: DIC calculation parameters

4.3.2.3 Results

The evolution of the displacement and strain fields is illustrated on the case of APTMS composites. The other specimens had exactly the same kinematic behaviour. The images acquisition gave more than 60 images along the whole tensile test, and three representative instants were selected to show the evolution of the displacement and strain fields during the test, that is 20, 50 and 80% of the maximum load.

Figures 4.25, 4.26, and 4.27 show the displacement and strain fields in the (x,y) plane for the three selected instants - axis x corresponding to the tensile direction. We observed a gradual and important displacement along x quite typical of the applied load. The displacements along y were much weaker and corresponded to the specimen alignment in the tensile machine.

The results show uniform longitudinal (ϵ_{xx}) and transversal (ϵ_{yy}) strains all along the test until failure. Such feature is in line with the overall homogeneity of composite materials related to the homogeneous distribution of the particles within the matrix. This supported also the representativeness and reliability of the results. Moreover, with the acquisition frequency used (one image per second), the specimen failure could be easily identified.

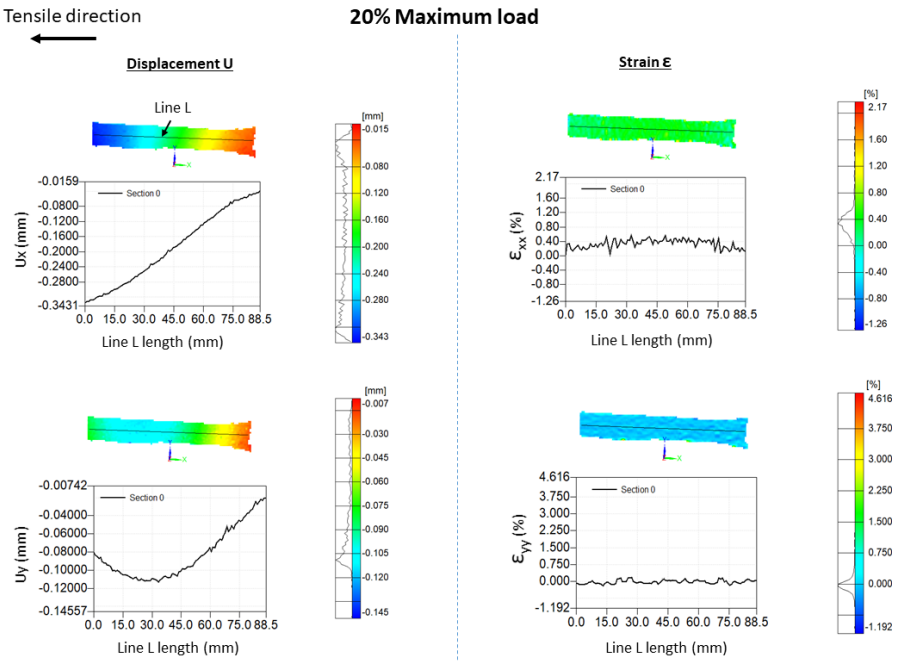

Figure 4.25: Kinematic fields of APTMS composites during a tensile test at 20% maximum loading

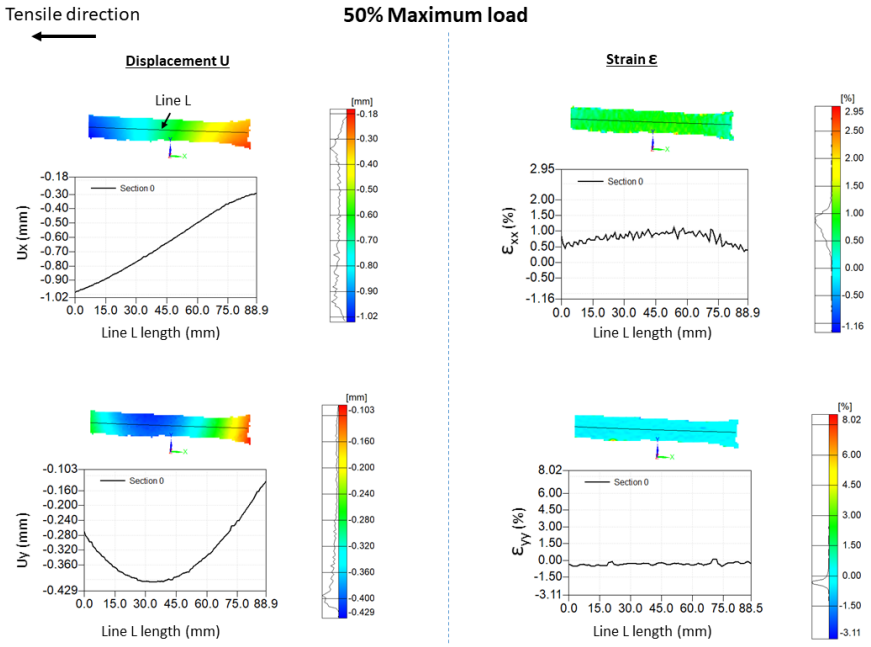

Figure 4.26: Kinematic fields of APTMS composites during a tensile test at 50% maximum loading

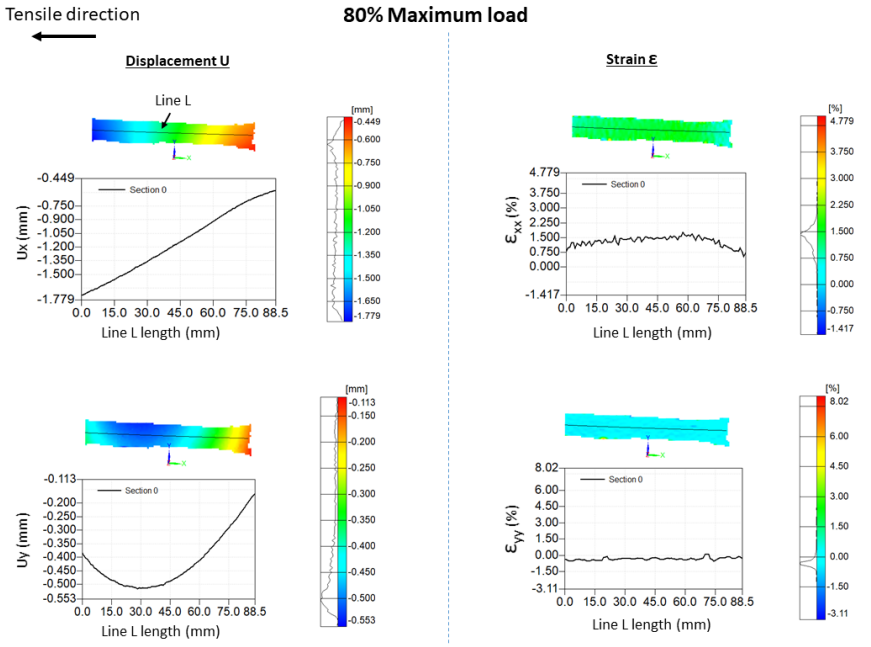

Figure 4.27: Kinematic fields of APTMS composites during a tensile test at 80% maximum loading

4.3.3 Mechanical properties

4.3.3.1 Tensile strength and modulus

The tensile properties of the composites are presented in this section. In this way, Figure 4.28 shows an example of the axial stress-strain curves obtained for each of the studied materials. The axial stress value is derived from the force applied by the machine and

related to the section of the specimen, while the axial strain corresponds to the moving crossbeam of the machine and related to the specimen length.

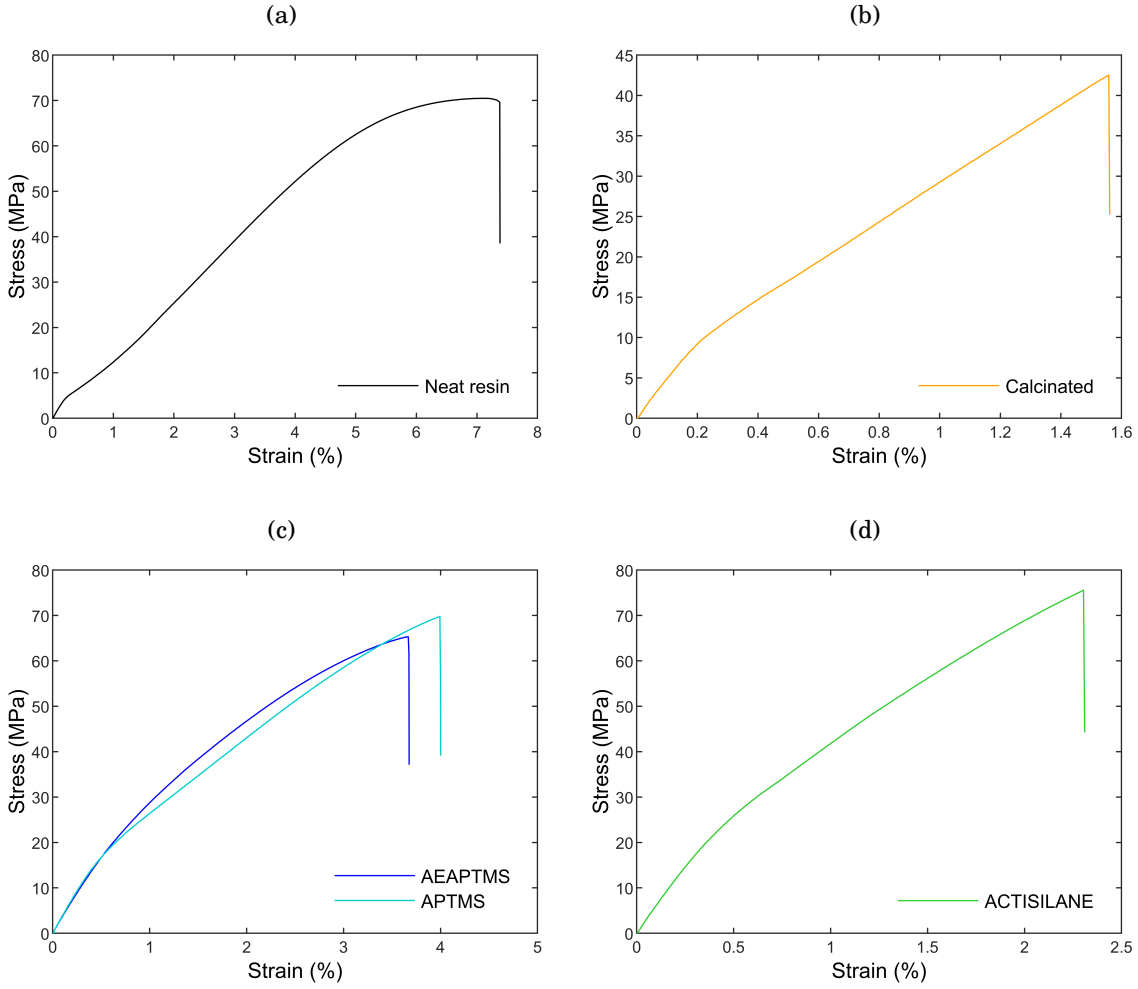

Figure 4.28: Typical stress-strain curve of (a) anionic PA6 and PA6-glass particle composites manufactured with (b) calcinated particles, (c) aminosilane treated particles and (d) ACTISILANE treated particles

The neat resin curve in Figure 4.28(a) shows an almost transitional character of a rubbery and a plastic behavior. Such a behavior is explained considering the T_g zone (around 50°C) which is close to the test temperature (around 24°C). This is reflected by a decrease, followed by an increase of the slope, before the plastic domain is reached at high deformation. Indeed, after a short linear part at low strain, the stress and strain relation became not proportional. It can result from an alignment of the polymer chains in the stress direction, which gives an elastic deformation at low stresses due to changes in the distances between neighboring chains. Then, the chains are extended, always in the elastic domain, resulting in a slight delayed elasticity due to changes in the macromolecular configuration. Finally, a plastic deformation appears due to the sliding of macromolecular chains one on another and a significant mobility at high strain

In the case of composites, an elastoplastic behavior is also observed and the same trend is observed whatever the surface chemistry. However, a sharper change in slope

of curves strain-stress for calcinated and APTMS based composites is measured every time. First, before the slope change, a rigidity enhancement is observed in all cases due to the addition of hard particles measured by the increase of the tensile modulus - initial slope calculated in the first linear part at low strains (Figure 4.29). The value obtained with the neat resin is consistent with the literature for anionic PA6 [26, 189–192]. As expected, the modulus is increased with the addition of hard microparticles showing a higher stiffness. By comparing the tensile modulus of composites, by decreasing order, ACTISILANE treated particles, followed by calcinated particles exhibit higher moduli compared to the aminosilanes particles-based composites.

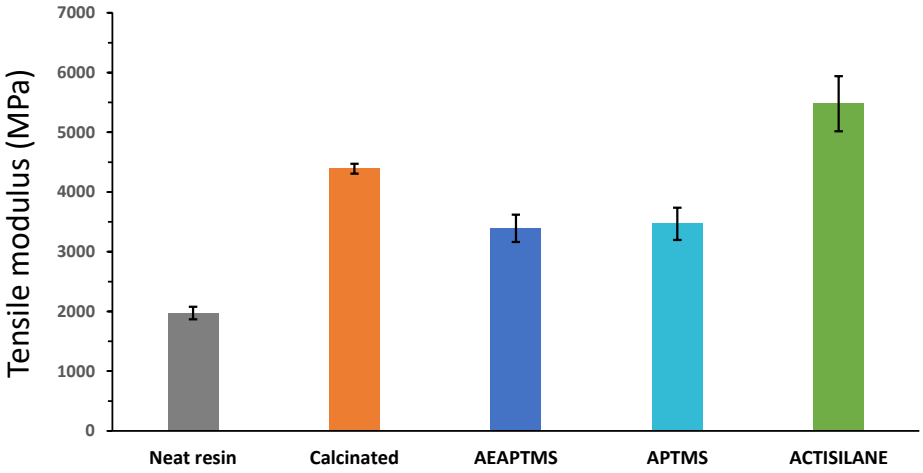

Figure 4.29: Average modulus of PA6 specimens and PA6/glass particles composites with different types of particles surface treatment

Then, the slope change is related to the beginning of plastic zone corresponding to intermolecular slippage. It is observed at different strain levels according to the particles type. In the case of calcined composites, the loss of linearity is more intense and occurs at very low deformations. This could reflect the short range physical interactions between the particle surface and the molecules leading to a fast polymer chain slippage on the particle surface. On the other hand, the composites containing particles treated with aminosilanes and ACTISILANE exhibit a delayed loss compared to the previous case. This could come from a slower chain slippage. Moreover, the comparison of curves obtained for the composites in Figure 4.30 shows a higher rigidity in the whole strain range in the case of ACTISILANE due to an overall increase of the material cohesion.

The tensile properties are also characterized by the maximum stress and the elongation at break by opposition with the tensile modulus measured at weak strains. As shown in Figure 4.31, the tensile strength value obtained with the neat resin (about 68 MPa) was again consistent with the literature [26, 189–192], demonstrating a suitable manufacturing process and supports the trustworthiness of our results.

The addition of the calcined particles leds to the lowest maximum stress and elongation at break compared to aminosilane and ACTISILANE composite. The composites containing

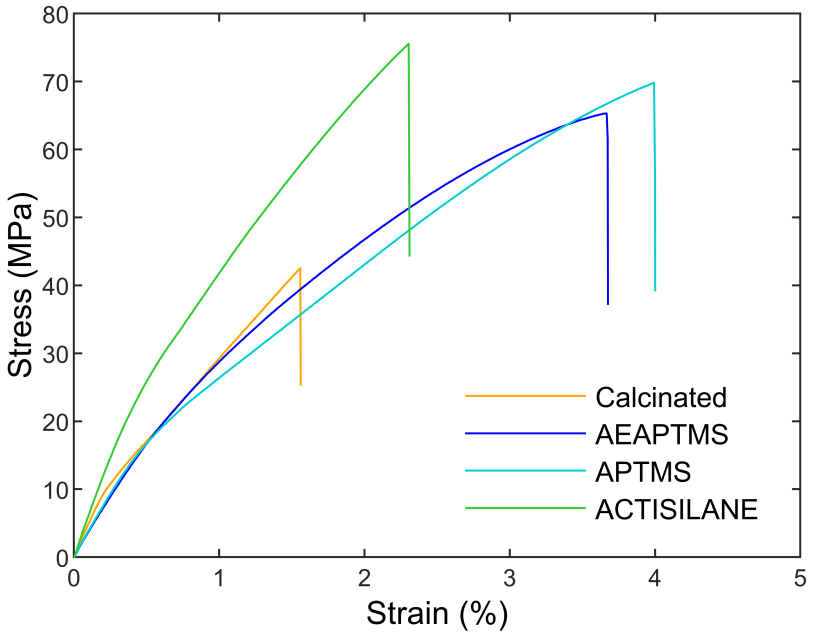

Figure 4.30: Comparaison of the stress-strain curves of PA6-glass particle composites manufactured with calcinated particles, aminosilane treated particles and ACTISILANE treated particles

the aminosilane particles showed a peak stress almost similar to that of the neat resin but a lower maximum elongation. Values obtained for either APTMS or AEAPTMS were in the same range taking into account the standard deviation of the tests. Finally, the ACTISILANE composites showed the highest maximum stress for all treatments and lower elongation than aminosilane.

As previously explained, the composites were synthesized and tested under the same conditions and the specimens showed homogeneous distribution of strain on the sample surface, as proved by the DIC measurements. From that, it can be assumed a homogeneous particle distribution within specimens during the tensile test. Therefore, the effect of particle distribution on the mechanical properties could be neglected, allowing to focus on the effects of the interfacial interactions at short and long ranges. In our case, the tensile strength and the maximum strain are characteristic of the adhesion influence through long range interaction between the particles and the matrix. On the other hand, the tensile modulus characterizes the overall cohesion of the material due to short range interactions including chemical bonds stretching and interfacial phenomena. In the next section, we discuss the different behaviors obtained according to the applied treatments and the type of the interfacial interactions.

(a)

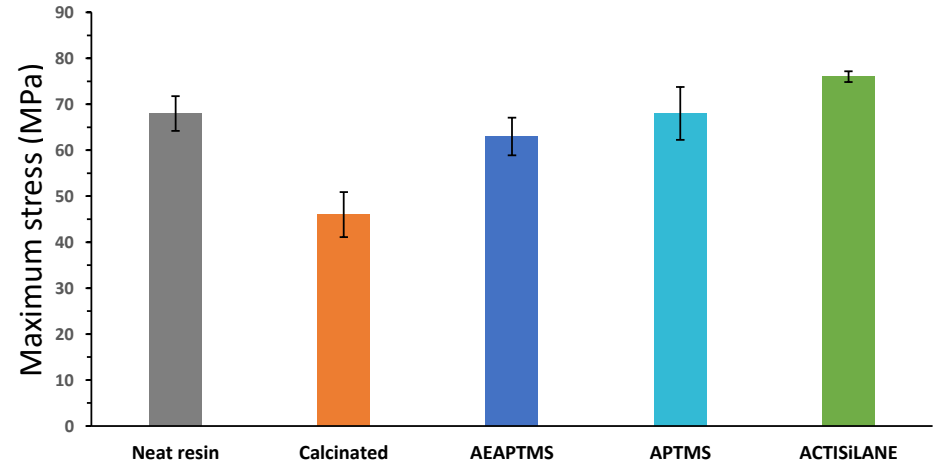

(b)

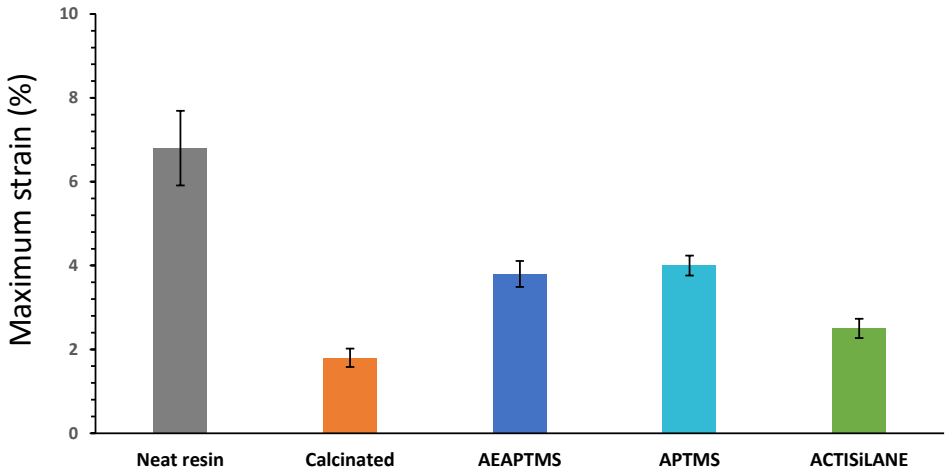

Figure 4.31: Average (a) maximum stress and (b) elongation at break of PA6 specimens and PA6/glass particles composites with different types of particles surface treatment

4.3.3.2 Relationship between the particles surface chemistry and the macroscopic behavior of the resulting composites

The tensile properties of composites depend on particle surface treatments. In particular, the thermodynamic compatibility of the particle surface with the matrix, and consequently, the level of the resulting interfacial interaction as well as the length of the grafted chains govern the overall behavior of the material.

The modulus values presented were obtained at low strains and were dominated by short range interactions. Feng et al. [193] showed that the elastic modulus depends on the chains density, fraction of free volume and chain conformation in the interface region. The polymeric chains located near the interface create the interphase, an area where the macromolecules are disturbed by the presence of fillers. The mobility of chains adsorbed onto the filler surface is greatly limited forming a "dead" zone whose glass transition (T_g)

is high [194]. In other cases, the chain anchoring at the particle surface is sparse resulting in an excess of free volume [193]. Polymer chains adsorbed on an inorganic surface can form "loop" structures [195], which facilitates entanglement with the surrounding polymer chains from the matrix and results in higher polymer mobility within the interphase.

First, the silane chain grafted on the particle surface with aminosilanes causes a decrease in the polymer density near the particle since the surface is occupied by the anchored silane chains. This also leads to a significant increase of the free volume fraction and the overall polymer mobility, since the chains from the matrix are not able to diffuse into the tethered chains. In this case, a larger gap between the polymer and the particle can result in poor cohesion, which explains the slight decrease in modulus in the case of aminosilane composites compared to composites with calcinated particles. The latter contain mainly Si-OH silanol functions and Si-O-Si siloxane functions on their surface. These functions have a very short length and the matrix chains are closer to the particle surface. A scheme explaining this hypothesis is shown in Figure 4.32. This significant change in the free volume fraction appears only in the vicinity of the particle surface because the surface interaction has a short-range effect.

Furthermore, the polymer chains can demonstrate larger deformation when increasing the grafted chains length. Indeed, the polymer chains always exhibit structural deformation near the surfaces due to reduced entropy and less conformational freedom at the interface [193]. In the case of calcined particles, the chain density is high in the near-surface region, so there is limited space for each polymer chain to extend (Figure 4.32(a)). This increases the macroscopic rigidity and results in rapid chain slippage on the particle surface. These features could explain the fast loss of elasticity and the dramatic change in slope observed in the tensile curve. However, for aminosilane treated particle, there is more free volume at the interface because of the presence of long silane chains, allowing the polymer chains to completely extend beyond the particles surface vicinity (Figure 4.32(b)). This results in a slight loss in stiffness but logically sharper in the case of AEAPTMS with the longest silane chains. In addition, the particle/matrix interaction is stronger in the case of aminosilane compared to the calcinated particles. Consequently, the slippage of the polymer chains is slighter giving a progressive loss of elasticity at higher deformations.

In the case of ACTISILANE, the conformation of the chains at the interface is different than in the previous cases. Indeed, the polymer chains are chemically bonded to the particle surface, which leads to a better cohesion. Figure 4.32(c) shows the conformation of the initiated chains from the particle surface. It is reflected by an increased elastic modulus due to higher material stiffness.

The maximum stress and strain reflect the particle-matrix adhesion through long range interactions. These properties are strongly influenced by the interface performance. For calcinated particle, they both decreased, in agreement with a weak interfacial adhesion related to low and short range interactions. Indeed, the calcinated particle surface does

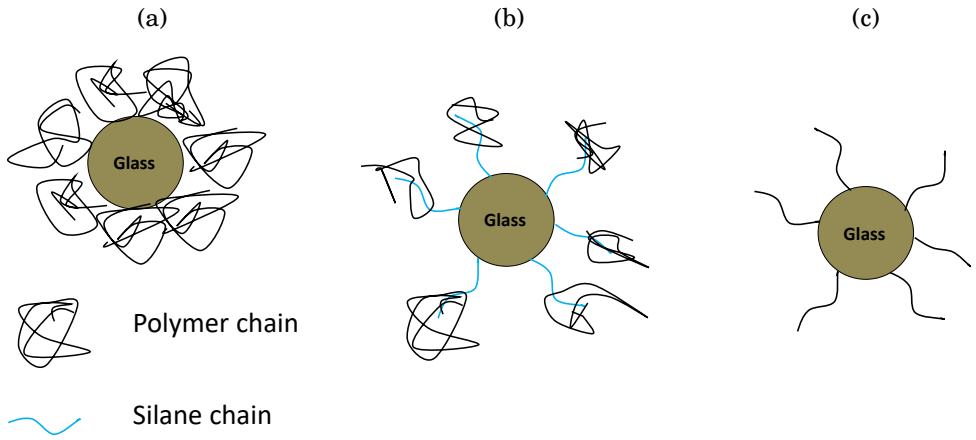

Figure 4.32: Schematic representation of the polymer chains conformation at the PA6/glass particle interface according to the particles surface treatment: (a) Calcinated (b) aminosilane treatment (c) ACTISILANE treatment

not contain any coupling agent. Therefore, only van der Waals type interactions between the particles surface and the PA6 matrix are expected. On the other hand, in the case of aminosilane treated particles, the interpenetration of the grafted chains with the PA6 chains due to the thermodynamic compatibility through hydrogen bonds leads to the creation of a physical interphase. Depending on the grafted/free chains mass ratio R, a wet (R >1) or dry (R<1) conformation is expected. The wet conformation means that the chains from the matrix can penetrate into the corona formed by the grafted chains: the chains from the matrix swell and stretch the grafted chains. Instead, when the chains from the matrix are too long compared to the grafted ones, they cannot enter into the corona formed by the grafted chains (dry configuration). Evidence of these conformations and of the wet/dry transition have been measured on nanosilica/polystyrene [196]. In our case, we assume a wet configuration, involving cooperative movement of the grafted silane chains and the polymer chains within the interphase. This results in increasing the maximum stress and strain compared to the previous cases.

Finally, in the case of ACTISILANE composites, the chains are covalently bonded to the surface. This results in a “perfect” interfacial adhesion and an optimal load transfer from the matrix to the particles which are able to withstand higher stress level due to their greater stiffness. However, the maximum elongation decreased compared to the aminosilane composites. This elongation drop can be explained by extrapolation of the Bueche [197, 198] and Dannenberg [199] models applied to elastomers. The Bueche theory considers that one polymer chain is chemically bound to two particles by its extremities. Therefore, the inter-particle chains reach their extensibility limit under tensile stress and finally fracture occurs (Figure 4.33(a)). In the case of ACTISILANE, the difference from this theory is that a chain can be bonded to only one particle. Therefore, the fracture occurs mainly at the level of polymer chains entanglement between two particules since the interface is very strong. This can be represented by the schematic in Figure 4.33(b) . On the other hand, in the case of aminosilanes, which is consistent with Dannenberg ’s

theory, the interphase formation by the chain interpenetration leads to a slippage of the polymer chains adsorbed at the interface on the particle surface before the fracture occurs. This leads to an increase in the maximum elongation (Figure 4.33(c)).

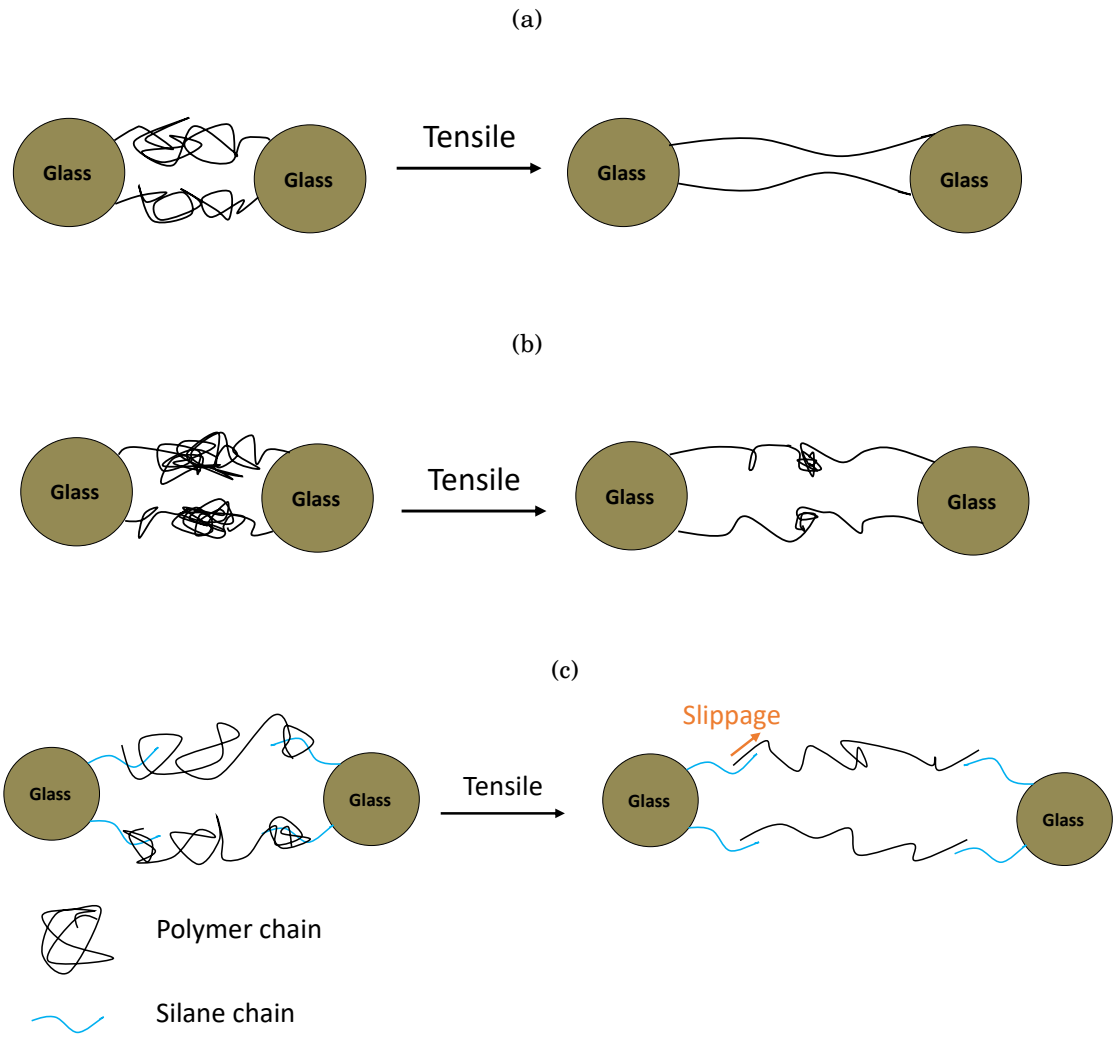

Figure 4.33: Schematic representation of polymer chain conformation at the interface of PA6/glass particle composites under stress as a function of surface treatment (a) Bueche model (b) Case of ACTISILANE treated particle (c) Dannenbergt model (case of aminosilane treted particles

4.3.4 Fracture surfaces analysis

To go further, we investigated the interface quality through observations of the fracture surfaces. Figure 4.34 shows the broken specimens after tensile tests for AEAPTMS composites. We see that the failure did not always occur at the same place and was located almost in the middle of the specimen.



Figure 4.34: AEAPTMS composite specimens after the tensile test

The fractured sections of all the samples were observed by SEM micrographs with various magnifications. The observations were performed by a ZEISS EVO scanning electron microscope (SEM). The following analyses arise of the most representative sample micrographs.

First, Figure 4.35 compares a specimen of the neat resin with that of ACTISILANE composite at low magnification. The distribution of the microparticles within the matrix was homogeneous for all the samples, as seen in Figure 4.35(d). It confirms the homogeneity of the specimens and the reliability of the manufacturing process. The SEM images for the neat resin showed several paths due to the crack propagation (Figure 4.35(a)). The characteristic length of these crack paths decreased significantly with the addition of the particles, as shown in Figure 4.35(c). This can be explained by the "crack-pinning" mechanism described by Lange [200, 201] and refined by Evan [202] for the case of composites reinforced with glass particles. They showed that the crack front changes in length as it interacts with particle due to the difference in toughness between the matrix and the particles. As particles represent an obstacle for the crack propagation, paths length is

reduced.

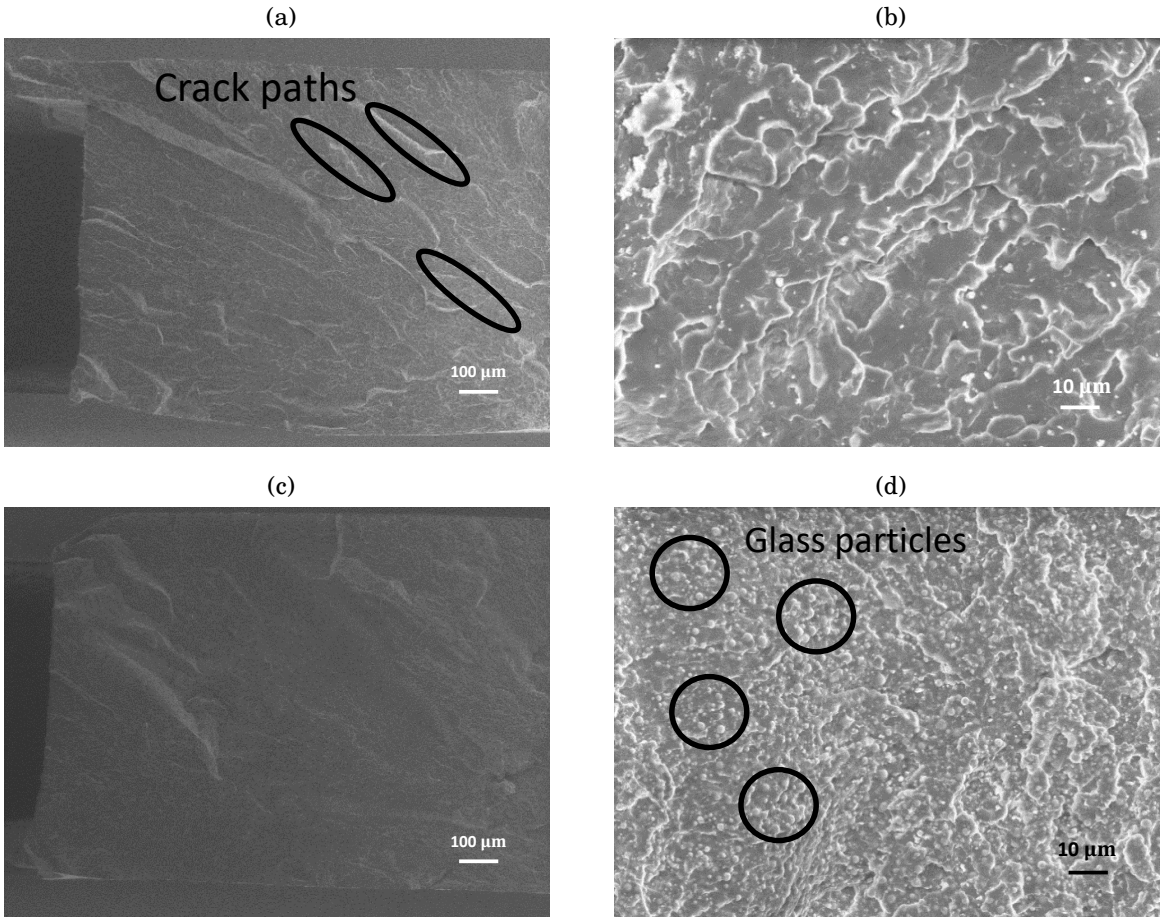

Figure 4.35: SEM images of the fracture surface of (a), (b) PA6 specimens and (c), (d) ACTISILANE composites

The crack propagation mechanisms also allowed to analyze the interface quality in relation with the particle treatment. Figure 4.36 shows SEM images of the calcinated, AEPTMS and ACTISILANE composites representative of respectively, no chemical bond, low interaction and covalent bonds at the glass/matrix interface. For the calcinated-particle composites in Figure 4.36(a), the glass particles were clearly visible. This demonstrates that the crack propagated around the sphere equator. On the other hand, the SEM images of the AEPTMS and ACTSILANE composites (Figure 4.36(b) and 4.36(c)) show that the particles were not distinct and were mainly hidden under the matrix in the AEPTMS composites, or covered by the matrix in the ACTISILANE composites. This demonstrates that the crack has propagated into the matrix above or below the particle poles.

Clearly, the crack propagation path is strongly dependent on the adhesion at the particle-matrix interface. This can be explained as a function of the local stress in a composite under applied stress [203–205], as shown schematically in Figure 4.37. In such a situation, the interface strength has a crucial role on the local stress around the particles. In the case of calcinated particle, the maximum stress is located at the particle equators due to the low interfacial adhesion [205–207]. Therefore, cracks are attracted to

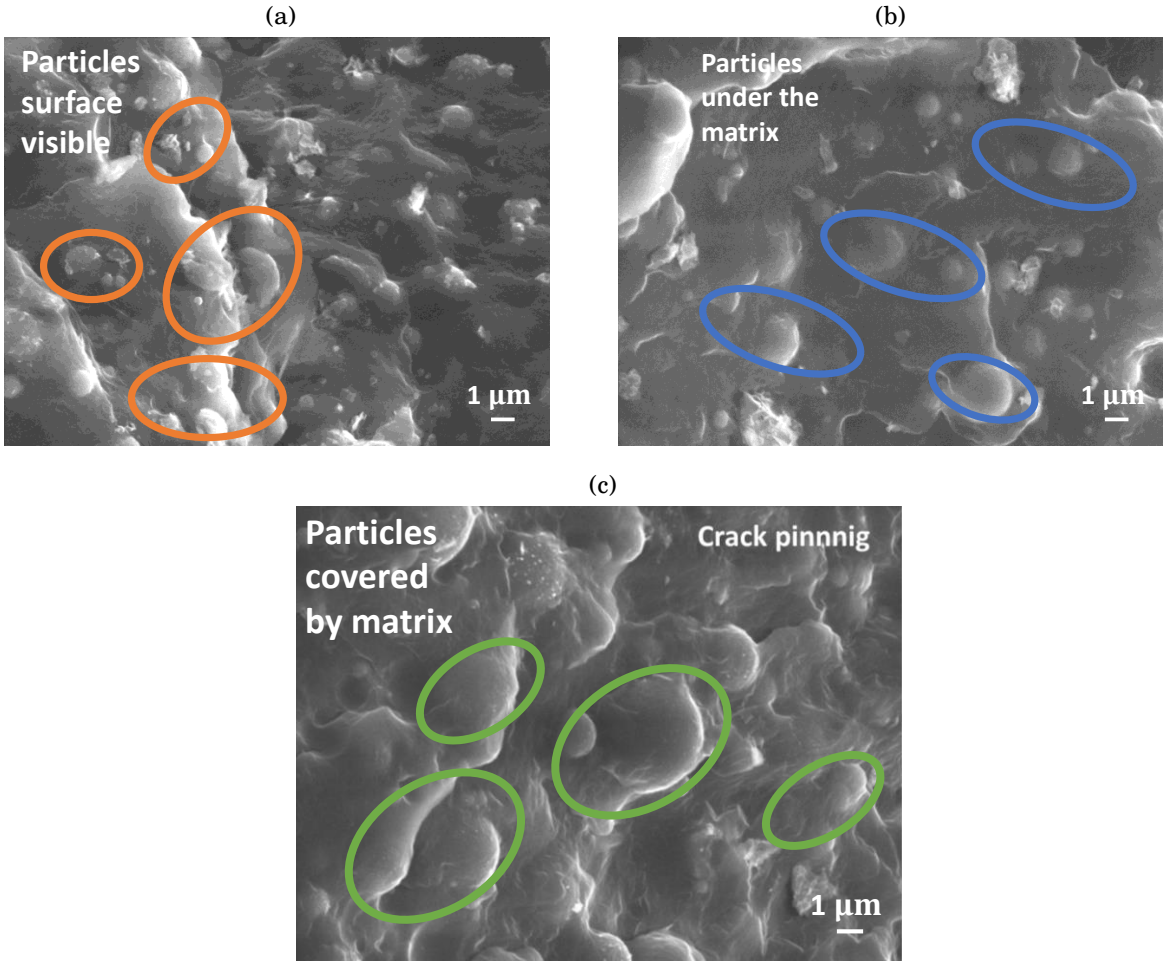

Figure 4.36: SEM images of the fracture surface of composite specimens manufactured with (a) calcinated, (b) AEAPTMS and (c) ACTISILANE particles

the particle equator. Hence, the fracture surface is mainly composed of the upper surface of debonded particles (Figure 4.36(a), Figure 4.37(a), 4.37(b)).

On the other hand, in the case of good interfacial adhesion (AEAPTMS and ACTISILANE composites), the behavior is more complex because the maximum stress location mainly depends on the particles and the matrix elastic constants. Tirosh et al. [208] studied the transverse cracking of well-bonded fibers in composites. Their results can be considered as a two-dimensional analogy of the composites studied in our case. They demonstrated that the maximum stress is in the matrix above and below the poles of the well-bonded fiber cross section in a composite subjected to transverse tensile stress. The exact position of this stress depends on the Poisson's ratio of the matrix. The results can be extrapolated to the composite reinforced with rigid particles [205]. Therefore, in the case of good interfacial adhesion, the maximum stress should be in the matrix above and below the particles poles. This means that the cracks are attracted to the particle poles rather than to their equator (Figure 4.37(a), Figure 4.37(c)). The crack propagation through the matrix above or below the particles leads to locating them under the matrix, as in the case of AEAPTMS composites (Figure 4.36(b)), or to the creation of a matrix layer covering the particles, as in the case of ACTISILANE composites (Figure 4.36(c)). In this last case, the

features can be attributed to crack pinning due to the strong interfacial adhesion. Figure 4.36(c) shows that the glass particles are more firmly bonded to the matrix polymer than the other cases. This demonstrates a very strong adhesion that prevents debonding and increases the effect of the crack pinning mechanism.

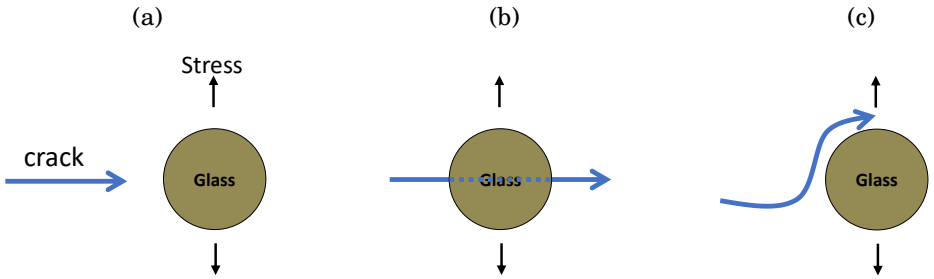

Figure 4.37: Schematic representation of the polymer chains conformation at the PA6/glass particle interface according to the particles surface treatment: (a) Calcinated, (b) aminosilane treatment, (c) ACTISILANE treatment

Accordingly, the previous results demonstrated that the particle treatment with ACTISILANE results in higher composite strength associated to a higher modulus. The creation of covalent bonds at the interface by initiating the polymerization from the particle surface thus induces a significant improvement of adhesion and overall material cohesion.

4.4 Conclusion

In this chapter, an optimized process was developed to manufacture composite specimens with the different treated particles. The physico-chemical characteristics of these composites were analyzed using TGA and DSC. The TGA characterization showed that the particle content corresponds to the targeted one. Moreover, it was demonstrated that all the specimens exhibit a high conversion degree.

DSC analyses showed a crystallinity degree comparable to that of the resin for all the treated composites during the *in situ* synthesis. This crystallinity is strongly affected by the presence of particles which can either disturb the crystallization process (as in the case of calcinated particles), or promote it (as in the case of MONOMSILANE particles). Moreover, it was proved that the particle surface treatment also influences the crystallization after synthesis, especially in the case of ACTISILANE in which the chains mobility is reduced due to their covalent bond with the particles.

Finally, the mechanical properties of the composites were evaluated using tensile tests coupled to kinematic fields measurements. The latter showed a homogeneous deformation for all the specimens. The tensile properties combined with fracture surface analysis concluded that calcinated-particle composites led to low interfacial adhesion. On the other hand, the aminosilane composites demonstrated better adhesion through hydrogen

bonds at the interface. Finally, ACTISILANE treatment provides the best tensile strength combined with an increase in stiffness over a large range interactions. This corresponds to a significant improvement of the interfacial adhesion and the overall cohesion of the material. Therefore, we proved that a covalent bond was formed between the particle and the matrix through the assessment of mechanical properties.

CONCLUSION AND PERSPECTIVES

This PhD thesis work has focused on tailoring the glass surface for the anionic ring-opening polyamide 6 (PA6) synthesis. This resin is a promising choice for the manufacturing of thermoplastic composites by reactive liquid process. In this case, reactive polymerization is a new option to manufacture fiber reinforced composite parts through *in situ* polymerization with equipment similar to Resin Transfer Molding used for thermoset composites.

Polyamide 6 is obtained by anionic ring-opening polymerization (AROP) of its monomer ϵ-caprolactam. During this reaction, the polymerization of the monomers and the crystallization of macromolecules occur simultaneously, which generate a strong coupling between both phenomena. Glass fibers (GF) were chosen for this work because they suit many applications, markets and processes.

The specificity of the *in situ* polymerization reaction during the synthesis of PA6/glass reinforced composites stands in the role of the interface: not only does the reinforcement-matrix adhesion drives the mechanical behavior of the composites, but also the nature of the interface impacts the polymerization and crystallization kinetics. Thus, the objective of this PhD project was to control the interfacial interactions between the reinforcement and the matrix in order to control the reaction kinetics. Besides, the project aimed at enhancing the interfacial adhesion in order to increase the mechanical properties of the resulting composites.

The main original contributions of this work are:

- The development of an optimized grafting protocol that ensures an efficient anionic ring-opening polymerization of ϵ-caprolactam, with high monomer conversion and successful grafting of silanes at the glass surface, while limiting the negative effect of surface bound hydroxyls.

- A broad study of several coupling agents leading to distinct interfacial interactions with the PA6 matrix: no interaction, weak bonds, and strong bonds. In particular, new coupling agents were synthesized from monomers allowing to have covalent bonds at the interface. A systematic and rigorous characterization of the silanized glass surface was performed by several complementary techniques in order to further understand the chemical processes involved.

- A broad understanding of the relationship between the glass surface chemistry, the

polymerization and crystallization kinetics, and the composite properties. These results provide tools to optimize the surface treatment for significant enhancement of the mechanical properties of composites.

In the first chapter, the literature review has explained the mechanism of anionic PA6 synthesis as well as the main factors influencing the reaction. In particular, the addition of glass fibers for the synthesis of composites can influence the polymerization and crystallization kinetics and, thus, the properties of the synthesized PA6 and PA6/GF composites. Therefore, the literature clearly identifies the strong interest in functionalizing the glass reinforcement surface, with a strong emphasis on the negative impact of the surface hydroxyls on the polymerization reaction. Indeed, the -OH groups naturally present on the glass surface deactivate the catalyst and inhibit the reaction. Hence, grafting a silane coupling agent is necessary to substitute the hydroxyls and improve the interfacial adhesion. Finally, the different steps of the glass surface modification with a silane agent are presented. This allowed to identify the impact of each step on the glass surface chemistry, and to underline the factors influencing the silane grafting reaction. To date, very few studies have investigated the interactions between the glass surface and anionic PA6. These studies have mostly focused on a single type of silane: (3-aminopropyl)triethoxysilane (APTES), which is commonly used with conventional polyamides. Accordingly, it is necessary to broaden the study of interfacial interactions with a detailed analysis linking the impact of the modified glass surface on the synthesis kinetics and properties of the resulting composites. This work was carried out with glass micro-particles - comparable in size to the diameter of glass fibers - as a model system in order to avoid the influence of fiber length and orientation on the composite properties and to focus on the role of the interface.

The second chapter of the PhD thesis has demonstrated that the raw glass particles surface is not suitable for the synthesis of PA6 by AROP, and inhibits the reaction due to the catalyst deactivation by surface hydroxyls. Furthermore, the silane grafting protocol described in the literature cannot be extended to the case of anionic PA6. This is due to the high number of residual hydroxyls typically remaining after silane grafting. Therefore, it was necessary to carefully control the hydroxyl density throughout each step of the glass particle surface modification. In order to prevent the inhibition of the polymerization reaction, and to maintain fast polymerization and crystallization kinetics, a careful balance is required between the dehydroxylation process, the simultaneous rehydroxylation and silane grafting processes, and the residual hydroxyl surface density. Accordingly, the evolution of the hydroxyl groups surface density on the glass beads, as a function of calcination time, was monitored by ThermoGravimetric Analysis (TGA) and Fourier Transform InfraRed (FTIR) spectroscopy. Then, the hydroxyl groups surface density was tuned in order to favor the synthesis of anionic polyamide 6, which was monitored by differential scanning calorimetry (DSC). Next, in order to further promote

the polymerization and crystallization of PA6 and to improve interfacial adhesion between the PA6 and glass particles, the grafting process of an amino-silane coupling agent at the glass surface was investigated by TGA and FTIR spectroscopy. The competition between re-hydroxylation and condensation of the silane on the surface during the grafting process was carefully balanced in order to maintain fast polymerization kinetics, as revealed by DSC analysis. Furthermore, both the rehydroxylation and silanization processes could be realized simultaneously without any negative impact on the polymerization reaction, the silane agent gradually replacing the regenerated hydroxyls. To our knowledge, the control of the hydroxyl group density during the complete grafting process of a silane coupling agent on the glass particle surface was not reported until now. In addition, the systematic methodology presented in this part provides a roadmap for the preparation of reinforced reactive thermoplastic materials, including various combinations of reactive resins and reinforcements containing -OH groups on their surface. It can be also adapted for many other applications requiring accurate hydroxyls control and/or silane treatments such as glass coatings for hydrophobic surfaces, antibacterial or antifungal surfaces.

In the third part, various coupling agents were screened to adapt the synthesis of PA6/GF composites with controlled interfacial interactions. The different types of interactions considered offer a large range of possible interactions at the particle-matrix interface: (i) First, a hydrophobic silane minimizing the interfacial interactions; (ii) Second, two aminosilanes forming hydrogen bonds with the PA6 matrix; (iii) Third, a grafted coupling agent generating covalent bonds at the interface. In the latter case, two original approaches were developed. First, a reactive coupling agent with the activator function was synthesized and grafted on the particles surface, in order to initiate the polymerization reaction from the reinforcement surface. Secondly, a reactive coupling agent bearing the covalently linked monomer has allowed the particles to participate in the polymerization reaction. These two coupling agents therefore make it possible for the particles to create covalent bonds with the matrix. After grafting, the treated particle surface was characterized and compared to the untreated particles. A rigorous surface analysis was conducted using several complementary techniques in order to thoroughly investigate the chemical processes involved (FTIR spectroscopy, contact angle measurements, TGA, XPS and confocal microscopy). Then, the PA6 was synthesized *in situ* with glass particles in DSC pans. This work has highlighted the influence of the silane chemical nature on the polymerization and crystallization kinetics, and on the physical and chemical properties of the synthesized anionic PA6/GF composites. For the particles functionalized with the reactive coupling agents, the polymerization and crystallization processes are fast and their kinetics is similar to that of the neat resin. Consequently, this surface treatment has shown full compatibility with the anionic PA6 synthesis, in contrast to the untreated particles which completely inhibited the reaction. In-between, particles treated with a hydrophobic silane agent considerably slow down the polymerization and crystallization

processes of the PA6 matrix, as compared to the pure resin. In addition, particles treated with the aminosilanes, which create weak bonds at the interface with the PA6 matrix, accelerate the polymerization and crystallization processes compared to the hydrophobic silane, but are still slower compared to the neat resin or to the particles grafted with the reactive silanes. Overall, the reactive silane developed in this study results in much shorter synthesis duration. The activator-functionalized silane can also simplify the manufacturing process by eliminating the addition of the activator in the mixture (i.e. eliminating an additional tank containing the activator in the liquid process). Overall, this approach can be applied to any composite reactive system in order to reduce the manufacturing cycle times.

The last part of this study was devoted to evaluate the influence of interfacial interactions on the mechanical properties of the resulting composites. Because of monomer evaporation during the synthesis that induces the formation of voids, different strategies have been tried to manufacture composite samples. After several unsuccessful attempts, the optimization of the manufacturing steps finally resulted in polymerized composites samples which physical and chemical properties were investigated by TGA and DSC. The polymerization and crystallization quality were evaluated through the conversion degree and the degree of crystallinity, respectively. Then, in order to assess the interface performance according to the treatment type, tensile tests coupled to kinematic field measurements were performed. The results demonstrated a satisfying overall homogeneity of the composites during the mechanical tests. This stands in agreement with a successful manufacturing process. Regarding interfacial effects, the properties obtained by tensile tests were consistent with the nature of the bonds associated with the various treatments. Observations of fracture surfaces and crack propagations by scanning electronic microscopy allowed to identify the main phenomena involved in the mechanical behavior according to the treatment type. First, it was shown that the addition of glass particles improved the overall composite stiffness, regardless of the surface treatment type. The analysis of the short range interactions by measuring the elastic moduli at low strains, and the long range interactions through the maximum stress and strain, allowed to compare the interface quality. Calcinated particles lead to poor interfacial adhesion due to the weak interactions involved. In contrast, the formation of hydrogen bonds at the interface by grafting an aminosilane on the particles surface strengthens the interfacial performance. This was demonstrated by the significant increase in the maximum stress and strain compared to the previous case, and by the crack attraction to the particle poles rather than to their equator, as in the case of calcinated particles. Finally, the creation of covalent bonds at the particle-matrix interface, in the case of the ACTISILANE treatment, is reflected by the best interfacial adhesion, combined to an improved cohesion. This is due to the optimal load transfer between the matrix and the particles. Hence, the significant improvement of the composites macroscopic properties is an indirect way to confirm the

efficiency of the developed treatments.

Many perspectives can be stated from this PhD work. Some aspects of the study deserve to be continued to deepen, such as the understanding of the mechanisms governing the interfacial interactions during the anionic PA6/glass synthesis of composites. This will contribute to a global optimization of the manufacturing processes of thermoplastic composites by liquid processes.

In the short term, a study of the molecular architecture of the polymer chains formed during the synthesis by size exclusion chromatography (SEC) is necessary to define the molecular weight, distribution and branching degree of PA6. Indeed, the impact of the glass reinforcement surface chemistry on the architecture of the chains will allow to check the hypotheses put forward to explain the chemical and physical properties observed. Moreover, it would be interesting to study by WAXS the morphology of the PA6 crystals formed in the presence of the treated glass particles. This will provide a better understanding of the impact of the silane surface treatment on the nucleation process.

Then, rheological tests must be carried out to assess the relaxation dynamics and the viscoelastic properties of the composites. Indeed, rheology is a sensitive technique to assess slight morphological changes. Interfacial adhesion, the length of grafted chains, the entanglement degree, the level of particles aggregation, are examples of phenomenon probed by either Dynamic Mechanical Analysis (DMA) in the solid state, or plate/plate configuration dynamic sweeps in the melted state. From these results, it would be interesting to compare the rheological behavior of composites with grafted particles, to the pure resin case. Indeed, the rheological response could indicate whether a filler network is formed, or if glass particles surrounded by a shell of grafted chains are bridged by larger macromolecules from the PA matrix. These observations could then be interpreted by the emulsion model proposed by Palierne [209]. Specially, this would allow to determine the interfacial tension between the matrix and the dispersed phase, the mean radius of the dispersed phase and the interfacial relaxation times.

Considering monomer grafting onto the particles surface, further investigations are necessary. It would be interesting to characterize the synthesized coupling agent before its grafting on the reinforcement surface in order to check the reaction efficiency. Moreover, it is also necessary to carry out a deeper analysis on the particle surface to confirm the monomer grafting on the surface. Then, the evaluation of the mechanical properties of the composites containing the particles treated with this coupling agent must be completed in order to determine the influence of the monomer grafting on the resulting macroscopic properties.

Tensile tests should be supplemented with other mechanical tests for a better evaluation of the reinforcement-matrix interface performance. Short beam shear test seems to be a good test to characterize the interfacial adhesion of composites. This method gives a

suitable indication of the combined performance of the matrix, reinforcement and interface. It consists in calculating the inter-laminar shear strength through the maximum force measured by three-point bending tests performed on a sample positioned between close supports. The main advantage of this method is that the fiber/matrix interface can be evaluated (albeit indirectly) using a composite specimen with representative reinforcement content. From these results, a model predicting the mechanical behavior of composites could be developed by considering a gradient of properties at the particle-matrix interface. Indeed, combining local and global characterizations would provide significant elements for the modeling of these heterogeneous materials. Specially, micromechanical approaches taking into account spherical inclusions with different assumptions regarding their surrounding interphase would be relevant to estimate the effective rigidity of the resulting PA6/GF composites. A calibrated model would ultimately guide the manufacturing process through an appropriate choice of grafting.

Finally, the treatments developed on microparticles must be transposed to glass fibers. The polymerization and crystallization kinetics in the presence of treated fibers are expected to be similar to the model glass particles. The properties of composites reinforced with treated glass fibers must be evaluated. Specific tests characterizing more accurately the interfacial adhesion can be performed, for example the pull-out test. It consists in embedding a fiber or a filament in a matrix block or a thin disk normal to the polymer surface. The force is progressively applied to the free end of the fiber, and gradually increased to pull it out of the matrix. The load and displacement are monitored as the fiber is pulled axially until pull-out occurs or the fiber fractures. Thus, the strength of the fiber/matrix interface can be calculated through the tensile stress on the fiber and the shear stress related to the interface. Again, the mechanical resistance of the interface is expected to be different according to the surface treatment.

To a longer-term view, the silane grafting process must be upscaled. Larger volumes are different to manage compared to the laboratory scale, so that it will be necessary to check whether the grafting reaction is modified. Fiber reinforced composites, containing fibers modified with the surface treatments developed in this study, could be manufactured to get standard specimens. Their mechanical characterization would help to conclude whether the surface treatment is efficient on a larger scale. In addition, measuring the manufacturing cycle times is crucial to know if this reactive pathway is worthy of competing with current manufacturing processes. To make such upscaling, a RTM-like equipment at the pilot scale will be necessary: it requires two heated tanks and a mixing head in the reactive mixture preparation unit, before impregnation.

At last, it should be underlined that the developed treatments can be extended to other types of reinforcements presenting hydroxyl groups on their surface, such as carbon fibers, nanotubes or natural fibers. Moreover, it would be interesting to apply these treatments to other types of reactive matrices such as PA12 or PMMA.

APPENDIX: ANALYSIS TECHNIQUES

Differential Scanning Calorimetry (DSC)

DSC analysis allows to identify thermal transitions and to measure the heat flows involved. A sample and a reference pans are both submitted to the same thermal cycle. Hence, the apparatus measures the energy required to keep the temperature nearly equal between the two pans throughout the experiment. Transitions are then detected and quantified by measuring the the heat released or absorbed during the state transformation.

The DSC apparatus used in this work is a Perkin-Elmer 8500 apparatus based on power compensation. It consists of two ovens: the first one contains the reference (empty pan) and the second one contains the sample (Figure .38(a)). Both ovens are calibrated and heated independently in order to have the same temperature. The power applied to each oven allows to compensate the evolution of the heat flow released or absorbed by the sample at each moment. The power difference between both ovens is thus directly proportional to this flow.

This technique differs from the heat flow DSC which contains only one oven for the sample and the reference .38. In this case, the temperature difference is measured and converted into heat flow.

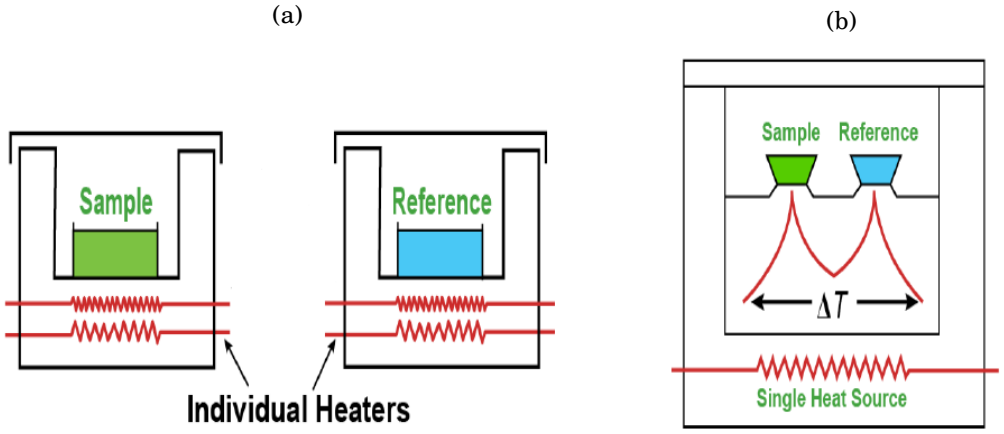

Figure .38: Schematic of a DSC with (a) power compensation and (b) heat flow

A blank was performed for each sample to improve the baseline. It consists in applying the same thermal cycle as that used for the tested sample to an empty capsule. The result is then subtracted from the sample's raw signal

Thermogravimetric analysis (TGA)

Thermogravimetric analysis (TGA) measures the mass evolution of a material as a function of temperature (or time) under a controlled atmosphere. Its principle uses include measurement of a material's thermal stability and its composition.

A TGA analysis is performed by applying a temperature ramp to a sample in a furnace while its mass is measured on an analytical balance. Hence, the sample mass evolution is plotted as a function of temperature or time to illustrate thermal transitions in the material. During the TGA analysis, a loss of mass is observed if a thermal transformation involves a loss of volatile component. Chemical reactions, such as degradation, involve mass loss, while physical changes, such as melting, do not. Therefore this technique is often coupled with the DSC analysis to investigate both chemical and physical transformation of the material as a function of temperature.

The TGA used in this work is a TGA1 STARe System-METTLER TOLEDO whose components are shown schematically in Figure .39.

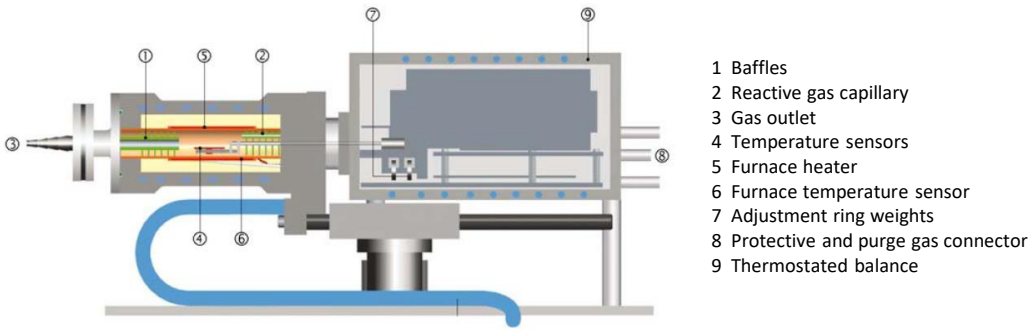

Figure .39: Scheme of the Mettler Toledo TGA

Fourier Transform InfraRed (FTIR) spectroscopy

In a molecule, the atoms are in permanent vibration to each other. These vibrations are divided into two types: (i) valence vibrations, which are in the bond axis; (ii) deformation vibrations, which are outside the bond axes, either in the plane or out of the plane. These vibrations have frequencies that depend on the bonded atoms and the other atoms that constitute the molecule. These vibrations frequencies are located in the mid-infrared region ($2 < \lambda < 30$ μm).

When the frequency of an incident radiation corresponds to the vibration frequency, its amplitude increases due to resonance. Thus, the energy of the incident wave is attenuated. When the frequency of an incident radiation corresponds to the vibration frequency, its amplitude increases due to resonance. Thus, the energy of the incident wave is attenuated. On this basis, the technique consists in exposing a sample to radiation in the IR region. Each couple of atoms and bonds absorbs the radiation at different frequencies. This results in a spectrum as a digital representation of the molecules that constitute the sample. The current spectrometers are Fourier transform devices.

The spectrometers used in this study are Fourier transform spectrometers. They use a Michelson interferometer. The signal transmitted by the detector (IR sensor) is converted into an interferogram (a temporal spectrum). Then, the Fourrier transform allows, by computer calculation, to get the frequency spectrum. The principle of the measurement is schematically shown in Figure .40.

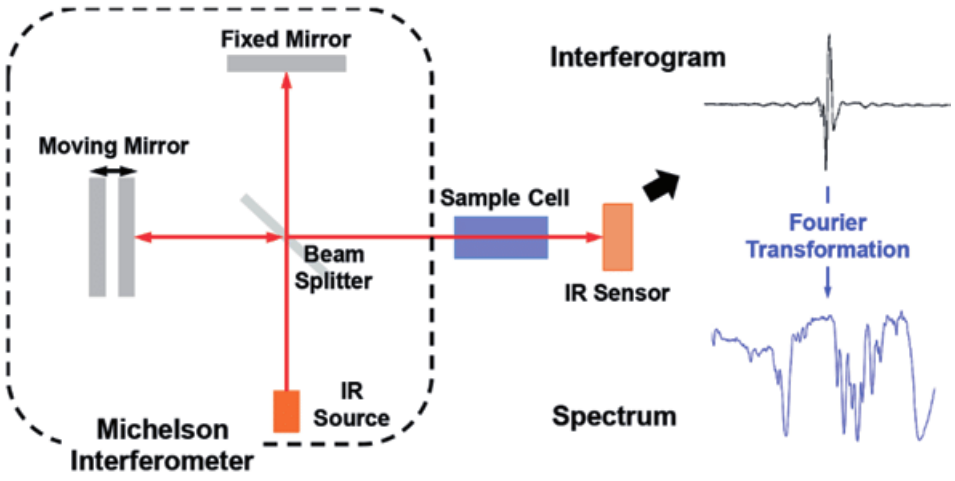

Figure .40: Principle of FTIR spectroscopy measurement

X-ray Photoelectron Spectroscopy (XPS)

X-ray Photoelectron Spectroscopy (XPS) is a surface characterization technique. It consists in the analysis of the kinetic energy distribution of photoelectrons ejected from a sample under X-ray radiation of known energy. This analysis allows to determine the electronic structure and the chemical environment of the atoms present in the sample and to

quantify the elements present on its surface. After X-rays penetrate into the sample, only the electrons ejected from the first 10 nanometers have enough energy to reach the XPS detector (Figure .41). Therefore, this technique is only suitable for surface analysis with a depth not exceeding 10 nm.

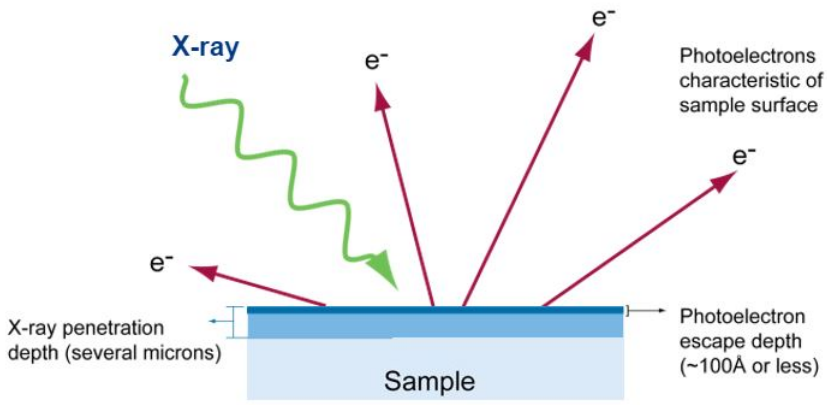

Figure .41: Surface analysis by X-ray Photoelectron

LIST OF FIGURES

1.1 Chemical structure of (a) ϵ-caprolactam monomer and (b) polyamide 6 9
1.2 Reaction mechanism using hexamethylene-1,6-dicarbamoylcaprolactam as activator and caprolactam magnesium bromide as catalyst [10] 10
1.3 Chemical structure of (a) ϵ-caprolactam, (b) N-acetylcaprolactam (N-ACL), (c) hexamethylene-1,6-dicarbamoylcaprolactam (HDCL), (d) caprolactam sodium (NaCL), (e) caprolactam magnesium bromide (MgBrCL) [15] 11
1.4 (a) Crystallization curves from the molten state for different temperatures, (b) Comparison of crystallization from the molten state at 180°C with that obtained by AROP during isothermal synthesis in DSC at the same temperature (from [21]) 12
1.5 Catalyst deactivation by moisture 13
1.6 Degree of conversion as a function of time for four activator (0.6 mol.%)-catalyst (0.6 mol %) couples synthesized in the same conditions [24] 14
1.7 (a) Conversion degree as a function of time - Influence of the reagent concentrations on the reaction rate of the MgBrCL/HDCL system at 150°C, (b) Maximum conversion degree as a function of the reagent concentrations of the MgBrCL/HDCL system at 150°C [15] 14
1.8 Degree of conversion as a function of time at various polymerization temperature [24] 15
1.9 Temperature evolution during the anionic polymerization of PA6 in an adiabatic reactor [38] 16
1.10 DSC thermograms of isothermal syntheses of PA6 with the MgBrCl /HDCL system at (a) 150-160-170°C and (b) 180°C-190°C [17] 17
1.11 Typical TGA curve of a PA6 synthesized by anionic polymerization (ramp from 25 to 600°C at 10°C/min) [45] 18
1.12 Schematic representation of the α and γ crystal lattice structure of PA6 [65] . . 20
1.13 WAXS scans of anionic PA6 samples synthesized under isothermal conditions between 130 and 180°C [17] 21
1.14 Schematic representation of RIM process (from [2]) 24
1.15 Schematic representation of VI process (from [2]) 25
1.16 Schematic representation of RIM process (from [24]) 26
1.17 Schematic representation of RRIM process (from [24]) 27

1.18 Comparison of the Inter-Laminar Shear Stress (ILSS) of reactively processed anionic PA-6 composites and melt processed PA-6 composites and effect of moisture absorption [101] 28
1.19 Deactivation of the catalyst by hydroxyl groups on the glass surface [10] 29
1.20 Unreacted monomer trapped between untreated glass fibers [10] 30
1.21 Chemical structure of an organosilane coupling agent 30
1.22 Grafting mechanism of an organosilane on the glass surface 31
1.23 Interaction between the grafted aminosilane on the surface of glass reinforcement and the PA6 matrix by transamidification reaction [101] 32
1.24 Activator deblocking. Step 1: Deblocking, Step 2a: Branching formation, Step 2b: Formation of the covalent bond between fiber and matrix through the urea bond [101] 33
1.25 (a) Flexural modulus and (b) flexural strength versus silica particle content for Nylon 6/SiO2 nanocomposites: (Δ) untreated and (◇) silanized particles [107] . 35
1.26 Effect of calcination temperature on neighboring silanol groups condensation according to (a) mechanism 1 and (b) mechanism 2 [109] 38
1.27 Evolution of the number of condensed hydroxyl groups that could be regenerated [109] 39
1.28 : APTES-derived layers with structural irregularities: individual silane molecules can be included in the layer via (a) hydrogen bonds, (b) electrostatic attraction, (c) covalent bonds with the substrate and (d) horizontal and (e) vertical polymerization with neighboring silanes; (f) the silane oligomers/polymers created can react and/or interact with functionalities present at the fiber/matrix interface [127] 41
1.29 Mechanism for grafting the activator to the surface of glass reinforcements using Toluene DiIsocyanate (TDI) 43

2.1 SEM observation of as-received glass micro-particles 48
2.2 Percentage by volume of particles as a function of diameter 49
2.3 DSC curves of isothermal syntheses at 180°C of PA6 and PA6-glass particles composites synthesized with pristine particles 52
2.4 Schematic of the surface modification steps of glass particles with AEAPTMS silane with the effect of each step on the surface chemistry 53
2.5 SC curves of isothermal syntheses at 180°C of PA6 and PA6-glass particles composites synthesized with AEAPTMS-1 particles 55
2.6 Thermogram of the normalized mass of the fully rehydroxylated particles in acid, heated at 150°C for 2 h. The mass loss corresponds only to the physically adsorbed water at the surface of the particles, since the onset of dehydroxylation has not been reached yet 58

2.7 (a) TGA thermogram of the normalized mass of fully rehydroxylated particles heated and maintained at 450°C for 24 h, (b) Evolution of the hydroxyl groups surface density as a function of calcination time, for the fully rehydroxylated particles (logarithmic scale). The dotted blue line is a linear regression 59
2.8 Thermogram of the normalized mass of the fully rehydroxylated particles in acid, heated at 150°C for 2 h. The mass loss corresponds only to the physically adsorbed water at the surface of the particles, since the onset of dehydroxylation has not been reached yet 59
2.9 (a) Infrared spectra of initially rehydroxylated glass particles, as a function of the subsequent calcination time at 450°C, (b) Evolution of the transmittance peak T as a function of calcination time at 450°C. The dotted blue line corresponds to the linear regression of the Transmittance as a function of log(t) for the peak located in-between 3430 and 3500 cm^{-1} 60
2.10 DSC thermograms of PA6/glass particles composites in isothermal syntheses at 180°C, for the particle calcination time ranging from 0 h (fully rehydroxylated) to 24 h, compared to the neat resin 62
2.11 Comparison of FTIR spectra for the glass particles calcinated for 24 h, and particles rehydroxylated respectively in the silanization solution (aqueous solution adjusted at pH 4-5 with acetic acid, without the silane), and in 10% HCl, for 3 h 64
2.12 (a) FTIR spectra of glass particles calcinated for 10 h and subsequently partially rehydroxylated in the silanization solution (without the silane) for different durations, (b) DSC curves of isothermal syntheses at 180°C of PA6-glass particles composites, synthesized with partially rehydroxylated particles for 2 h, 3 h and 6 h in the silanization solution (without the silane agent), compared to the DSC curves of the pure resin and PA6-glass particles composites synthesized with the calcinated particles 66
2.13 (a) FTIR spectra of calcinated particles and calcinated + 2 h-silanized particles 67
2.14 (b) DSC curves of isothermal syntheses at 180°C of PA6 and PA6-glass particles composites synthesized with calcinated particles, rehydroxylated particles for 2 h in the silanization solution (without silane) and calcinated + 2 h-silanized particles 68
2.15 (a) FTIR spectra of 2 h and 6 h silanized particles. (b) DSC curves of isothermal syntheses at 180°C for composites synthesized with 2 h and 6 h silanized particles 70

3.1 Grafting of TMPS on the glass particle surface 77
3.2 Grafting mechanism of aminosilanes on the surface of glass particles. (a) APTMS (b) AEAPTMS 78
3.3 Grafting mechanism of ACTISILANE on the surface of glass particles 78
3.4 Reaction mechanism for the synthesis of the ACTISILANE coupling agent . . . 79

3.5 FTIR spectra of (a) ϵ-caprolactam (monomer) and synthesized ACTISILANE (b) 3-isocyanatopropyltriethoxysilane 81
3.6 FTIR spectra of untreated particles compared to the spectra of particles treated with (a) TMPS, (b) APTMS and AEAPTMS, and (c) ACTISILANE 83
3.7 Survey scan of particles treated with ACTISILANE 85
3.8 High resolution scans of N 1s for particles treated with (a) ACTISILANE (b) APTMS 87
3.9 Confocal fluorescence microscopy images of (a) untreated particles, compared to particles treated with (b) TMPS, (c) Raw glass particles not treated with FITC, (d) APTMS, (e) AEAPTM and (f) ACTISILANE 91
3.10 Average maximum fluorescence intensity of untreated particles, compared to particles treated with APTMS, AEAPTMS, and the ACTISILANE 92
3.11 Contact angle images of (a) untreated particles, compared to particles treated with (b) TMPS, (c) APTMS and (d) ACTISILANE 95
3.12 Water drop contact angle as a function of time for the different silane treatments 96
3.13 DSC thermograms of isothermal syntheses at 180°C of PA6 and PA6-glass particles composites synthesized with (a) untreated particles, and particles treated with (b) TMPS, (c) APTMS/AEAPTMS, and (d) ACTISILANE. The neat resin polymerization thermogram is illustrated for a comparison purpose . . . 98
3.14 DSC curves of PA6 and PA6-glass particle composite synthesized with untreated and ACTISILANE treated particles: (a) cooling cycle from 180°C to 0°C at -10 °C/min (b) heating cycle from 0°C to 270°C at 10°C/min 99
3.15 chemical structure of (a) 3-glycidoxypropyltrimethoxysilane GLYMO (b) 3-amino-2-azepanone 103
3.16 Reaction mechanism for the synthesis of the MONOMSILANE coupling agent 104
3.17 Grafting mechanism of MONOMSILANE on the surface of glass particles . . . 105
3.18 FTIR spectra of untreated particles and particles treated with MONOMSILANE105
3.19 FTIR spectra of untreated particles and particles treated with MONOMSILANE107
3.20 DSC thermograms of isothermal syntheses at 180°C of PA6 and PA6-glass particles composites synthesized with MONOMSILANE particles 109
3.21 DSC curves of PA6 and PA6-glass particle composite synthesized with MONOMSILANE treated particles (a) cooling cycle at -10 °C.min^{-1} from 180°C to 0°C (b) heating cycle from 0°C to 270°C at 10°C.min^{-1} 110

4.1 Turbine stirrer with vertical blades 115
4.2 Mold preparation for the CSM process 116
4.3 Composite manufactured by the CSM process 117
4.4 CSM process with rotational system: (a) rotational system during curing, (b) manufactured composite 118
4.5 Mold preparation for VIC process 119
4.6 Installation of the VIC process 119

4.7 Manufactured composites with VIC process 120
4.8 Mold preparation for COM process 122
4.9 Installation of the VIC process 123
4.10 Glove box pollution by the evaporated monomer during TMPS composites manufacturing 124
4.11 TGA curve and its derivative for specimens of (a) neat resin and (b) composites containing calcinated particles 126
4.12 TGA curves and their derivatives of composites containing ACTISILANE treated particles 127
4.13 Effect of increasing initiation points on the length of the formed polymer chains after polymerization 127
4.14 DSC thermograms of the heating cycle from 0°C to 270°C at 10°C/min of the neat resin specimens and the composites synthesized with calcinated and ACTISILANE treated particles 130
4.15 Trapping of the reactive chain ends inside the crystals [26] 132
4.16 DSC thermograms of neat resin specimens and the composites synthesized with calcinated and ACTISILANE treated particles: (a) cooling cycle from 270°C to 0°C at -10°C/min, (b) 2nd heating cycle from 0°C to 270°C at 10 °C/min. Other samples displayed thermograms very similar to those of the composites with calcinated particles 132
4.17 Sample measurements of tensile specimens in mm (in.), ASTM D638 Type I [186]134
4.18 SEM images of the fracture surface of MONOMSILANE composites 135
4.19 Typical experimental setup of the 2D DIC method [187] 137
4.20 Reference square subset before and after deformation [187] 137
4.21 Example of a speckle pattern 137
4.22 Speckle characterization : distribution of the grey levels 138
4.23 Setup of 2D DIC measurements 138
4.24 DIC calculation parameters 139
4.25 Kinematic fields of APTMS composites during a tensile test at 20% maximum loading 140
4.26 Kinematic fields of APTMS composites during a tensile test at 50% maximum loading 141
4.27 Kinematic fields of APTMS composites during a tensile test at 80% maximum loading 141
4.28 Typical stress-strain curve of (a) anionic PA6 and PA6-glass particle composites manufactured with (b) calcinated particles, (c) aminosilane treated particles and (d) ACTISILANE treated particles 142
4.29 Average modulus of PA6 specimens and PA6/glass particles composites with different types of particles surface treatment 143

4.30 Comparaison of the stress-strain curves of PA6-glass particle composites manufactured with calcinated particles, aminosilane treated particles and ACTISILANE treated particles 144
4.31 Average (a) maximum stress and (b) elongation at break of PA6 specimens and PA6/glass particles composites with different types of particles surface treatment 145
4.32 Schematic representation of the polymer chains conformation at the PA6/glass particle interface according to the particles surface treatment: (a) Calcinated (b) aminosilane treatment (c) ACTISILANE treatment 147
4.33 Schematic representation of polymer chain conformation at the interface of PA6/glass particle composites under stress as a function of surface treatment (a) Bueche model (b) Case of ACTISILANE treated particle (c) Dannenbergt model (case of aminosilane treted particles 148
4.34 AEAPTMS composite specimens after the tensile test 149
4.35 SEM images of the fracture surface of (a), (b) PA6 specimens and (c), (d) ACTISILANE composites 150
4.36 SEM images of the fracture surface of composite specimens manufactured with (a) calcinated, (b) AEAPTMS and (c) ACTISILANE particles 151
4.37 Schematic representation of the polymer chains conformation at the PA6/glass particle interface according to the particles surface treatment: (a) Calcinated, (b) aminosilane treatment, (c) ACTISILANE treatment 152
.38 Schematic of a DSC with (a) power compensation and (b) heat flow 161
.39 Scheme of the Mettler Toledo TGA 162
.40 Principle of FTIR spectroscopy measurement 163
.41 Surface analysis by X-ray Photoelectron 164
.42 Mécanisme réactionnel utilisant le hexamethylene-1,6-dicarbamoylcaprolactam ((HDCL)) comme activateur et le bromure de magnésium de caprolactame (MgBrCL) comme catalyseur 177
.43 Schematic representation of RIM process 179
.44 Comparaison de la contrainte de cisaillement interlaminaire (ILSS) de composites à matrice PA6 anionique et de composites à matrice de PA6 commerciale - Influence de l'absorption d'humidité 179
.45 Désactivation du catalyseur par les groupes hydroxyle de la surface du verre . 180
.46 Structure chimique d'un agent de couplage organosilane 181
.47 Mécanisme de greffage d'un organosilane sur la surface du verre 181
.48 Thermogrammes DSC des composites PA6/particules de verre lors de la synthèse isotherme à 180°C, pour le temps de calcination des particules allant de 0 h (entièrement réhydroxylé) à 24 h, comparés à la résine pure 186
.49 Thermogrammes DSC de la synthèse isotherme à 180°C du PA6 et des composites PA6/particules de verre synthétisés avec les particules traitées avec (a) APTMS /AEAPTMS, (b) ACTISILANE/MONOMSILANE 189

List of Tables

1.1 Mechanical properties of PA6 synthesized by AROP [15] 21

1.2 Mechanical properties of the anionic PA6/GF composites and effect of different post-heat treatments on the properties [99] 27

2.1 Description and values of the diameters obtained by laser granulometry 49

2.2 TGA mass loss of AEAPTMS-1 particles compared to the mass loss of pristine particles 54

2.3 TGA mass loss and hydroxyl surface density for glass particles calcinated for 24 h, and calcinated particles subsequently rehydroxylated in the silanization solution (aqueous solution adjusted at pH 4-5 with acetic acid, without the silane), or in 10% HCl, for 3 h 63

2.4 Evolution of TGA mass loss and hydroxyl surface density, for particles calcinated for 10 h, and then partially rehydroxylated in the silanization solution (without the silane) for 2 h, 3 h and 6 h. 65

2.5 TGA mass loss relative to the hydroxyls and silanes, for particles initially calcinated then silanized for 2 h, compared to strictly calcinated particles . . . 68

2.6 Crystallization peak, melting temperature (T_m) and melting enthalpy (ΔH_m) of PA6-glass particles composites synthesized with calcinated particles and calcinated + 2h-silanized particles 69

3.1 Name and structure of the considered silanes and related interfacial interactions expected with the anionic PA6 matrix 76

3.2 Identification and quantification of elements from XPS analysis for the untreated particles, and particles treated with APTMS and ACTISILANE 85

3.3 Atomic concentrations relative to silicon and calcium, for untreated particles and particles treated with APTMS and ACTISILANE 86

3.4 Identification and quantification of chemical bonds from high-resolution scans of C 1s and N 1s for the untreated particles and particles treated with APTMS and ACTISILANE 88

3.5 TGA mass loss of silanized particles compared to the mass loss of untreated particles. The mass loss related to silane and the silane surface density are noted Δm_{silane} and the d_{silane} respectively 93

3.6 Contact angle values of untreated and treated particles according to the type of treatment and expected type of interaction with the PA6 matrix ± 1 95
3.7 Melting temperature (T_m), melting enthalpy (ΔH_m), total enthalpy (Q_{tot}), polymerization enthalpy (ΔH_p^∞) and degree of conversion (X_p^∞) of PA6 after the synthesis of PA6/glass particles composites with different types of grafted silanes 100
3.8 TGA mass loss of silanized particles with the MONOMSILANE compared to the mass loss of untreated particles. The mass loss related to silane and the silane surface density are noted Δm_{silane} and the d_{silane} respectively 106
3.9 Contact angle images of particles treated with MONOMSILANE 106
3.10 Identification and quantification of elements from XPS analysis for the untreated particles and particles treated with MONOMSILANE (analysis carried out on another batch of glass particles) 108
3.11 Melting temperature (T_m), melting enthalpy (ΔH_m), total enthalpy (Q_{tot}), polymerization enthalpy (ΔH_p^∞) and degree of conversion (X_p^∞) of PA6 after the synthesis of PA6/glass particles composites with MONOMSILANE treated particles 110

4.1 Conversion degree of the neat resin specimens and the composite specimens containing the different types of particles 128
4.2 Melting temperatures and enthalpies and crystallinity degree of PA6 specimens and PA6/glass particles composites with different types of particles surface treatment. The results are obtained after a 1st heating cycle from 0°C to 270°C at 10°C/min 130
4.3 Crystallization temperature (T_c) and enthalpy (ΔH_c) measured on DSC curves obtained upon cooling from 270°C to 0°C at -10°C/min, melting temperature (T_m) and enthalpy (ΔH_m) on the curve of 2nd heating cycle from 0°C to 270°C at 10°C/min and Crystallinity degree (X_c^∞) for PA6 specimens and PA6/glass particles composites with different types of particles surface treatment 133
.4 Propriétés mécaniques des composites PA6 anionique/GF - Influence du traitement post-chauffage 179
.5 Nom et structure des silanes considérés et interactions interfaciales correspondantes avec la matrice PA6 anionique 188
.6 Identification et quantification des éléments à partir de l'analyse XPS des particules non traitées et traitées avec l'APTMS et l'ACTISILANE 189

RÉSUMÉ ÉTENDU

Introduction générale

La haute température de fusion des polymères thermoplastiques limite encore leur utilisation. Leur forte viscosité à l'état fondu nécessite en outre des pressions très importantes pour leur mise en œuvre. Ainsi, l'imprégnation du renfort fibreux reste difficile à contrôler et homogénéiser. L'utilisation de résines thermoplastiques réactives à faible viscosité associées à un procédé de fabrication liquide (infusion, RTM) présente une piste prometteuse pour pallier ces problèmes. Dans ces matériaux, la polymérisation est obtenue *in situ* après l'imprégnation du renfort, ce qui améliore l'adhésion renfort-matrice, et requiert un temps de cycle de fabrication relativement court.

Parmi les polymères à basse température de synthèse qui sont adaptés pour ce type de procédé, le polyamide 6 (PA6) obtenu par ouverture de cycle du ϵ-caprolactame (ϵ -CL, T_m = 69°C) présente la plus faible viscosité, ce qui permet une imprégnation homogène du renfort fibreux. De plus, sa polymérisation est rapide et présente un degré de conversion élevé, ce qui conduit à de bonnes propriétés mécaniques du matériau synthétisé. Ce système réactif peut être associé à plusieurs matériaux de renfort pour améliorer les propriétés mécaniques, surtout les fibres longues de carbone ou de verre mais aussi les nanotubes de carbone ou du graphène par exemple. Les fibres de carbone, certes au coût élevé, sont souvent choisies pour des applications avancées car elles présentent la plus grande rigidité et résistance à la traction relativement à leur densité. Les fibres de verre (FV) offrent quant à elles un bon compromis entre les propriétés mécaniques et les coûts de fabrication, ce qui explique leur utilisation très répandue dans plusieurs domaines applicatifs.

Une des problématiques mises à jour avec les composites FV/PA6 anionique synthétisé par procédé réactif est l'interaction entre l'ensimage des fibres de verre et la polymérisation/cristallisation de la matrice PA6. En effet, toutes les fibres commerciales sont ensimées, c'est-à-dire recouvertes d'une couche de polymère de quelques nanomètres. Cet ensimage facilite la manipulation des renforts et permet de favoriser l'adhésion fibre-matrice. L'adhésion gouverne le transfert des contraintes de la matrice vers la fibre et, par conséquent, les propriétés mécaniques des matériaux composites. La nature de l'ensimage et sa composition chimique sont très peu documentées dans la littérature, le plus souvent pour des raisons de confidentialité. Parmi les composants de l'ensimage, l'agent de couplage est considéré comme le principal élément responsable de l'adhésion interfa-

ciale, notamment lorsqu'il interagit à la fois avec la matrice et les renforts. Alors que les agents de couplage industriels sont généralement bien adaptés à la plupart des matrices polymères commerciales, le traitement de surface des renforts de verre doit encore être adapté pour convenir à des polymères spécifiques ou nouveaux. Un cas typique nécessitant un contrôle précis des traitements de surface est celui du PA6 anionique. En effet, un agent de couplage inadéquat peut ralentir la cinétique de polymérisation, voire l'inhiber et/ou affecter le processus de cristallisation. De plus, les groupes hydroxyles naturellement présents à la surface du verre désactivent le catalyseur, ce qui perturbe également la réaction de polymérisation et peut finalement conduire à une réduction significative des propriétés du polymère synthétisé. Par conséquent, le contrôle de la chimie de surface des FV est crucial car il influence non seulement le processus de polymérisation mais aussi l'adhésion fibre-matrice à l'interface, ces deux aspects ayant des conséquences majeures sur le comportement mécanique résultant du composite.

Cette étude vise à développer un traitement de surface des fibres de verre à la fois compatible avec le procédé réactif du PA6 et permettant également de maîtriser les interactions à l'interface renforts/matrice. L'idée est de favoriser les processus de polymérisation et de cristallisation du PA6 et, ainsi, d'améliorer les propriétés finales du composite. Ce travail a été réalisé avec des microparticules de verre comme système modèle afin de se concentrer sur l'effet de l'interface et éviter l'influence combinée de la longueur et de l'orientation des fibres sur les propriétés du matériau.

Le premier chapitre est une revue de la littérature qui présente la synthèse du PA6 anionique et les principaux facteurs influençant la réaction et les propriétés finales. Une attention particulière est accordée aux composites PA6 anionique renforcés de verre. Comme la polymérisation se déroule autour du renfort, différentes interactions peuvent se produire pendant la synthèse. La description de ces interactions permet d'identifier un traitement de surface compatible avec le PA6, en particulier le greffage d'organosilanes. Les différentes étapes et stratégies de la modification de la surface du verre par ces agents de couplage sont précisées ainsi que leurs facteurs influents.

Le deuxième chapitre porte sur le contrôle de la densité des groupes hydroxyles à la surface des particules de verre. Le processus complet de silanisation est analysé, et l'influence du temps et des conditions de calcination est étudiée par analyse thermogravimétrique (ATG) et par spectroscopie infrarouge à transformée de Fourier (IRTF). L'impact de la chimie de surface des particules sur la polymérisation et la cristallisation des composites à base de PA6 est évalué à l'aide de la calorimétrie différentielle à balayage (DSC).

Dans le troisième chapitre, différents agents de couplage à base de silane sont greffés et comparés. La surface des particules de verre est caractérisée par IRTF, spectroscopie photoélectronique à rayons X (XPS), ATG, microscopie confocale ainsi que par des mesures d'angle de contact. Ensuite, la synthèse de composites particules de verre/PA6 anionique est étudiée par DSC pour évaluer l'influence de la nature chimique de l'agent de couplage sur la cinétique de polymérisation/cristallisation et sur les propriétés du polymère

synthétisé.

Dans le dernier chapitre, un procédé est développé pour fabriquer des composites PA6 anionique renforcés par des particules de verre. Après avoir caractérisé les propriétés physico-chimiques des composites fabriqués, l'effet des interactions interfaciales entre le renfort et la matrice sur les propriétés mécaniques est évalué par des essais de traction couplés à la corrélation d'images.

Les résultats importants de ce travail sont récapitulés en conclusion ainsi que certaines des perspectives envisagées pour compléter ce travail.

Etat de l'art

Ce chapitre fournit une revue bibliographique de la synthèse du PA6 par polymérisation anionique par ouverture de cycle (AROP), de ses facteurs d'influence et des propriétés résultantes de la matrice et du composite associé. Les traitements de surface, en particulier le greffage des silanes, et les améliorations qu'ils apportent sont également abordés.

Chimie du PA 6 obtenue par polymérisation anionique et propriétés des composites PA6/verre

Le mécanisme de réaction de polymérisation par ouverture de cycle a attiré l'attention depuis quelques années et demeure la technique la plus adaptée pour la fabrication des composites par voie liquide. Cette technique présente plusieurs avantages. Premièrement, elle ne génère pas de sous-produits nécessitant des étapes de purification. De plus, les masses moléculaires obtenues par la polymérisation anionique par ouverture de cycle sont généralement plus élevées que celles obtenues par polycondensation. Cela est dû à l'étape de purification de la polycondensation durant laquelle les chaînes sont cassées. Ces faibles masses moléculaires en polycondensation sont également maintenues afin d'avoir une viscosité du matériau basse à l'état fondu de sorte à être compatible avec son utilisation ultérieure.

La polymérisation anionique peut être initiée uniquement par un catalyseur mais ce mode de polymérisation génère une période d'induction. Le recours à un activateur permet d'éliminer cette étape et d'accélérer la réaction. De ce fait, la polymérisation nécessite trois composants : le monomère, le catalyseur et l'activateur. Le processus de polymérisation anionique comprend trois étapes principales : (i) la dissociation de l'initiateur et la formation de l'anion lactame, (ii) la formation d'un complexe entre le catalyseur et l'activateur (cette réaction dépendra du type du couple catalyseur-activateur choisi) et (iii) la polymérisation à travers l'anion lactame au cours de laquelle un anion est régénéré après chaque addition de monomère.

Plusieurs mécanismes réactionnels sont décrits dans la littérature. La figure .42 montre le mécanisme réactionnel en utilisant le hexamethylene-1,6-dicarbamoylcaprolactam (HDCL) comme activateur et le bromure de magnésium de caprolactame (MgBrCL) comme catalyseur. La température de synthèse se situe entre 130°C et 170°C. Les taux de conversion peuvent être supérieurs à 97% pour des temps de réaction entre 3 et 60 min selon les types de catalyseur et d'activateur utilisés et selon la concentration des réactifs. Dans ce mécanisme, la polymérisation débute par la dissociation du catalyseur en anion lactame. Cet anion réagit ensuite avec le carbonyle de l'activateur (diisocyanate bloqué) par attaque nucléophile. Cette première attaque se fait sur le carbonyle endocyclique de l'activateur, celui-ci étant plus réactif. Un anion imide est alors formé. Grâce à un échange d'hydrogène entre l'anion imide et le monomère, un anion lactame est régénéré. Ainsi, l'accroissement de la chaîne se poursuit par répétition de l'attaque nucléophile sur le

centre de croissance jusqu'à consommation du monomère. A cause de sa nature anionique, la réaction peut facilement s'arrêter en présence d'humidité ou d'oxygène. Par conséquent, le traitement et le stockage doivent se faire dans un environnement inerte.

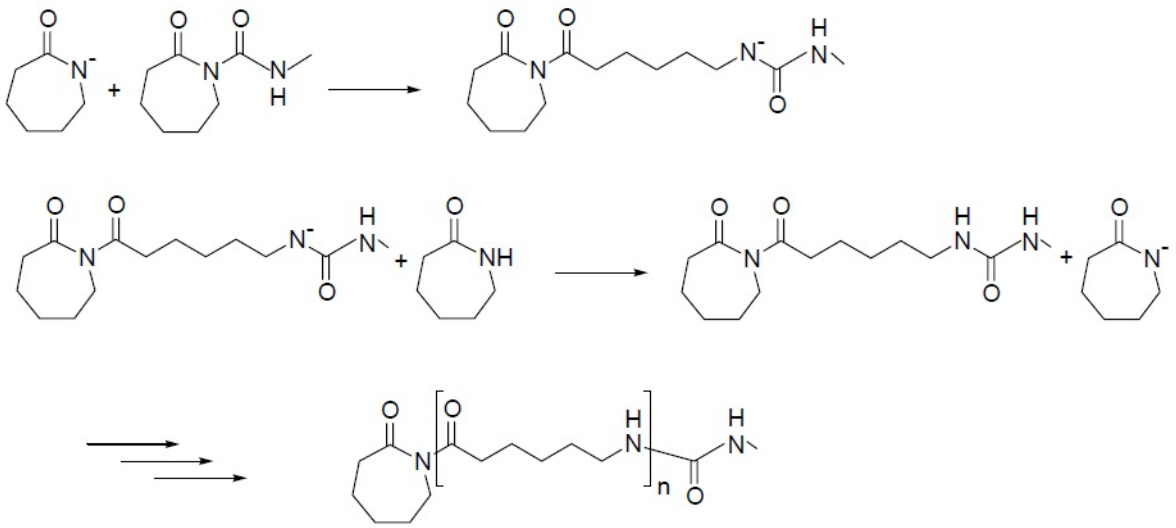

Figure .42: Mécanisme réactionnel utilisant le hexamethylene-1,6-dicarbamoylcaprolactam ((HDCL)) comme activateur et le bromure de magnésium de caprolactame (MgBrCL) comme catalyseur

La polymérisation anionique par ouverture de cycle est soumise à une thermodépendance inversée entre la polymérisation et la cristallisation. En effet, dès que les chaînes atteignent une taille critique, la cristallisation commence dans l'intervalle de température de synthèse (140°C à 180°C). La cristallisation aura une grande influence sur la viscosité, le taux de conversion, la cinétique de réaction, les masses molaires et leur distribution. La cinétique de polymérisation, la vitesse de réaction et les taux de conversion dépendent principalement de la nature et concentration des réactifs et de la température de synthèse. La polymérisation/cristallisation simultanée induit également un couplage fort entre les deux mécanismes.

Il existe principalement trois méthodes pour suivre les cinétiques de polymérisation et de cristallisation lors de la synthèse anionique du PA6 : le suivi du degré de conversion, le suivi *in situ* de la température en réacteur adiabatique et le suivi *in situ* du flux de chaleur. En raison du fort couplage et de la simultanéité des deux phénomènes, leur séparation lors de la caractérisation reste le principal défi de chaque technique. Parmi ces méthodes de caractérisation, le suivi *in situ* du flux de chaleur en Calorimétrie différentielle à balayage (DSC) présente plusieurs avantages en permettant de suivre la synthèse *in situ* du PA6. En effet, la chaleur dégagée par la polymérisation/cristallisation est mesurée en continu en fonction du temps et de la température, puis compensée par l'appareil pour rester à la température de consigne. Ceci permet de mesurer l'exothermie de la réaction. Au contraire des autres techniques, la synthèse isotherme peut être réalisée en DSC, ce qui permet de suivre les cinétiques de polymérisation et et de cristallisation séparément et étudier la

thermodépendance des deux phénomènes.

La maîtrise des propriétés du PA6 synthétisé par AROP constitue également une problématique cruciale. En effet, les conditions de polymérisation conditionnent les propriétés du matériau final. La chimie complexe l'AROP impose de choisir les conditions appropriées de polymérisation afin d'améliorer les propriétés finales du matériau. Typiquement, ces dernières dépendent de la manière dont les chaînes sont formées. Au cours de la synthèse, les propriétés physico-chimiques du matériau évoluent, la nature de cette évolution étant elle-même conditionnée par plusieurs critères. Tout d'abord, la création des chaînes polymères et leur accroissement sont définis par le taux de conversion et la masse molaire. Ces chaînes en cours de croissance peuvent d'autre part cristalliser. Cette cristallinité est quant à elle décrite par le taux de cristallinité et la morphologie cristalline.

Composites PA6 anionique renforcés de verre

La fabrication de composites PA6/renforts en verre à l'aide d'un procédé réactif présente plusieurs enjeux. Les procédés réactifs sont basés sur l'imprégnation des fibres par le mélange réactif qui polymérise ensuite autour d'elles. L'utilisation du système réactif du PA6 dans un procédé liquide nécessite dès lors quelques adaptations par rapport aux composites thermodurcissables. En effet, les résines thermodurcissables ne nécessitent généralement qu'un seul réservoir avant imprégnation car la réaction est essentiellement initiée par la température. Cependant, le système réactif du PA6 anionique nécessite deux réservoirs chauffés et une tête de mélange dans l'unité de préparation du mélange réactif avant imprégnation (Figure .43). Le premier réservoir contient le monomère ϵ-CL et le catalyseur et le second contient le monomère et l'activateur. Cela permet la fusion séparée des réactifs et évite ainsi toute polymérisation prématurée. Un environnement inerte est nécessaire dans les deux réservoirs pour éviter la désactivation de la réaction par l'humidité. Le dosage des deux solutions (généralement 1:1) est effectué à l'aide de pompes à haute pression. La tête de mélange est ensuite utilisée pour mélanger et homogénéiser le système réactif et l'injecter dans le moule. Par ailleurs, les outils doivent également être compatibles avec la chimie du mélange réactif afin d'éviter les réactions parasites et la perturbation du processus de polymérisation.

A notre connaissance, très peu d'études ont porté sur les propriétés mécaniques des composites à base de PA6 anionique renforcé par des fibres de verre. Le tableau .4 résume les propriétés mécaniques des composites obtenus ainsi que l'effet des différents traitements post-chauffage sur les propriétés. Les composites ont été fabriqués par infusion de résine assistée sous vide (VARI). Le PA6 anionique a été synthétisé en utilisant le NaCL comme catalyseur et le HDCL comme activateur, le renfort en verre étant un tissu uni.

La figure .44 présente l'effet de la température du moule sur les propriétés mécaniques des composites PA6 anionique/GF fabriqués par infusion sous vide. Les résultats montrent que la contrainte de cisaillement interlaminaire (ILSS) des composites à base de PA6 anionique est supérieure à celle des composites commerciaux à base de PA6 (même

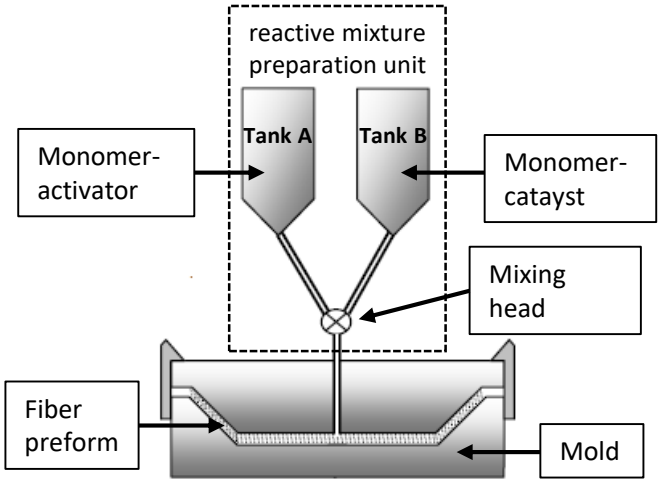

Figure .43: Schematic representation of RIM process

épaisseur, même type de renfort et même taux de fibres) et présente un maximum à une température de synthèse de 180°C.

Table .4: Propriétés mécaniques des composites PA6 anionique/GF - Influence du traitement post-chauffage

	Tensile strength (MPa)	Tensile modulus (GPa)	Flexural strength (MPa)	Flexural modulus (GPa)	ILSS (MPa)
Untreated	433.5 ± 10.0	22.0 ± 1.2	396.4 ± 29.4	23.5 ± 1.2	43.3 ± 1.9
Quenched	330.3 ± 13.5	17.0 ± 1.3	330.7 ± 31.8	20.0 ± 0.5	38.3 ± 2.2
Annealed	442.8 ± 24.0	22.1 ± 1.6	402.9 ± 28.5	21.5 ± 0.8	51.5 ± 2.0

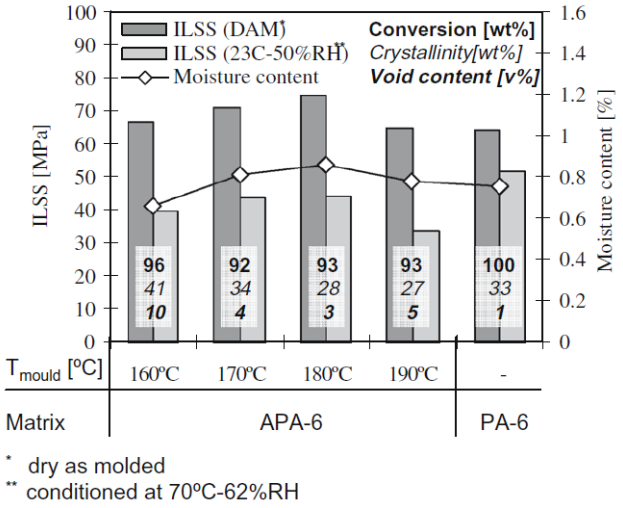

Figure .44: Comparaison de la contrainte de cisaillement interlaminaire (ILSS) de composites à matrice PA6 anionique et de composites à matrice de PA6 commerciale - Influence de l'absorption d'humidité

Interaction entre les renforts de verre et le système réactif lors de la synthèse de composites PA6 anionique/verre

Lors de la fabrication de composites PA6 anionique renforcés de verre, la réaction de synthèse de la résine se produit autour des renforts. En raison de l'extrême sensibilité du PA6 aux protons labiles, la polymérisation anionique par ouverture de cycle peut être affectée par les fonctions chimiques en contact avec le mélange réactif. Comme le renfort représente une surface importante, il peut interagir avec la réaction de synthèse. Par conséquent, le contrôle de la chimie de surface du renforcement est crucial car il influence non seulement les processus de polymérisation et de cristallisation, mais il contrôle également l'adhésion fibre-matrice et les propriétés mécaniques qui en résultent.

Dans le cas de la polymérisation anionique par ouverture du cycle, il est nécessaire de traiter les renforts de verre avant utilisation. En effet, les groupes hydroxyles en surface du verre présentent des protons labiles qui réagissent avec le catalyseur et le désactivent, entraînant une réduction importante du degré de conversion. Cette désactivation est illustrée sur la figure .45 où les anions se transforment en monomère et les cations (charge positive) demeurent au voisinage de la surface du verre (charge négative). Par conséquent, il est nécessaire de contrôler la quantité de groupes hydroxyles afin de réduire leur effet négatif sur la réaction de polymérisation pendant la synthèse et ainsi éviter la diminution des propriétés mécaniques du composite.

La modification de la surface des renforts permet de réduire la quantités des groupes silanols et la désactivation associée. Dans ce cas, le traitement de surface des renforts de verre le plus adapté à la mise en œuvre des composites est le greffage d'un agent de couplage de type organosilane. La grande variété des silanes impose une étude approfondie sur leurs interactions durant et à l'issue de la réaction de synthèse du PA6 obtenu par voie anionique afin de proposer un traitement adapté à la chimie du système réactif.

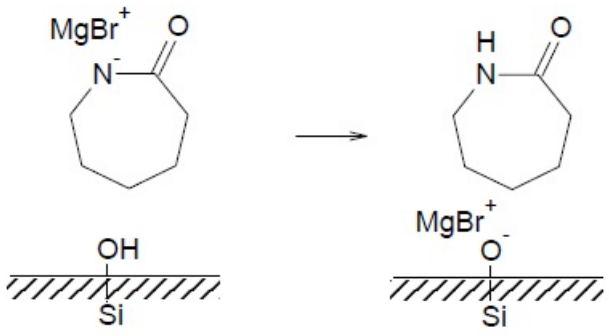

Figure .45: Désactivation du catalyseur par les groupes hydroxyle de la surface du verre

Les organosilanes sont composés d'une chaîne de carbone avec une fonction " R " à une extrémité et une fonction " silane " à l'autre extrémité, comme l'illustre la figure .46. Le mécanisme de greffage d'un silane sur la surface du verre est similaire à celui de l'interaction entre le silane et la silice car dans les deux cas, les fonctions réactives de la

surface sont les groupes hydroxyles. Ce mécanisme est illustré dans la figure .47. Une solution aqueuse permet l'hydrolyse du silane et la formation de groupes silanols. Dans un premier temps, ces groupes interagissent avec les groupes hydroxyles de la surface du verre par des liaisons hydrogènes. Ensuite, la condensation de ces derniers génère des liaisons siloxanes.

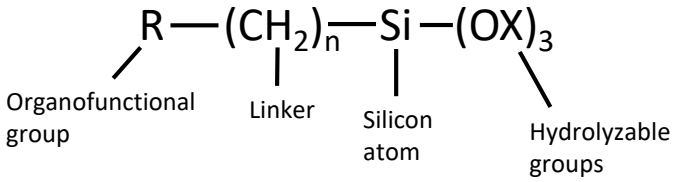

Figure .46: Structure chimique d'un agent de couplage organosilane

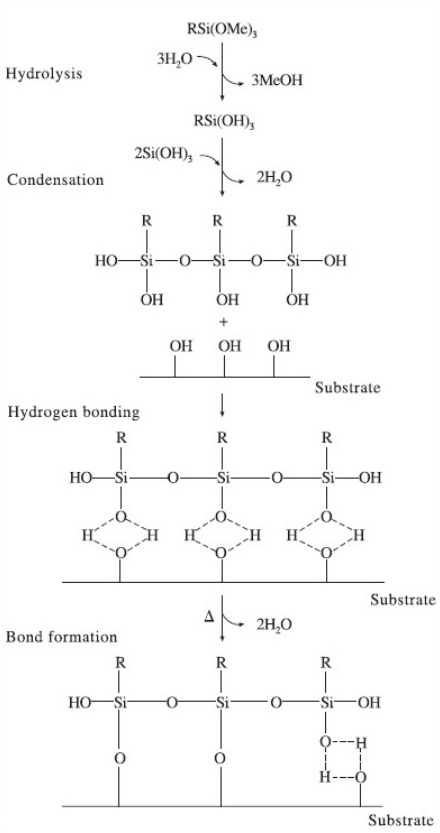

Figure .47: Mécanisme de greffage d'un organosilane sur la surface du verre

Le greffage des silanes à la surface des renforts de verre a pour objectif de créer une liaison entre la fibre et la matrice sans avoir une influence négative sur la réaction de polymérisation et/ou de cristallisation. Comme dans le cas général des PA6, les silanes avec une terminaison amine représentent des bons candidats pour l'amélioration de l'adhésion. Dans le cas de la polymérisation anionique par ouverture de cycle, les amines primaires ou secondaires des aminosilanes réagissent avec le carbonyle du PA6 par des liaisons hydrogènes. A une température élevée (>160°C) et pendant un certain temps

(>30min), une réaction de transamidification est observée entre l'aminosilane et la matrice PA6 durant la polymérisation anionique. Cette transamidifaction permet de former des liaisons covalentes entre l'aminosilane et la matrice qui améliorent l'adhésion de l'interface. Cependant, elle a aussi pour effet de casser les chaînes du PA6, donc d'entraîner une diminution de la masse molaire de celui-ci et ainsi fragiliser la matrice dans cette zone.

Pour remédier à ce problème, les traitements réactifs permettent d'amorcer la réaction de polymérisation anionique par ouverture du cycle du caprolactame à partir d'un composé greffé sur la fibre. La technique la plus utilisée est de greffer l'activateur sur la fibre de verre, ce qui permet de créer une liaison covalente entre la fibre et la matrice. Cette approche présente plusieurs avantages. D'abord, la polymérisation amorcée par la fibre se déroule autour de cette dernière et améliore ainsi l'adhésion en liant la fibre et la matrice d'une manière covalente. Ceci permet un meilleur transfert de charge de la matrice à la fibre lors d'une sollicitation mécanique et, par conséquent, des meilleures propriétés. De plus, l'utilisation d'un activateur greffé sur la fibre permet une simplification du procédé en passant d'un tri-composant à un bi-composant. Cependant, la difficulté de cette technique réside en la maîtrise des quantités de l'activateur lors du greffage afin de garder la stœchiométrie du mélange réactionnel.

En ce qui concerne le protocole de greffage d'un silane à la surface du verre, il commence par un traitement de calcination qui nettoie la surface des contaminants organiques et conduit à la condensation des groupes hydroxyles. Bien que les groupes -OH influencent négativement la synthèse du PA6 anionique, ils représentent les sites réactifs de la surface indispensables à la réaction avec le silane. Par conséquent, une activation de la surface est nécessaire pour régénérer les groupes hydroxyles. En dernier lieu, le silane est condensé sur la surface après son hydrolyse.

Afin d'optimiser ce protocole, il est important de contrôler séparément chaque étape de la modification de la surface. De plus, la condensation du silane en présence d'eau entraîne une perte de sa réactivité. Ainsi, la compréhension des phénomènes d'hydrolyse et de condensation est nécessaire pour améliorer la cinétique de greffage du silane à la surface du verre.

Conclusion

Cette revue de la littérature met en évidence l'intérêt du système réactif PA6 pour la fabrication de composites thermoplastiques par voie liquide. Cependant, le couplage fort entre polymérisation et cristallisation et la sensibilité de la réaction à l'environnement induisent une complexité pour contrôler la synthèse. L'un des paramètres clés de cette synthèse lors de la fabrication du composite est l'interaction avec le renfort. En effet, la difficulté d'adapter la chimie de surface des renforts en verre à la synthèse du PA6 anionique est probablement la raison majeure pour laquelle peu de recherches ont été consacrés au rôle de l'interaction interfaciale sur la polymérisation anionique et sur les propriétés des composites PA6 anionique/verre.

A ce jour, les quelques travaux qui ont étudié le rôle de la chimie de surface du verre sur le PA6 AROP se sont concentrés sur un seul type de silane, à savoir l'aminosilane. Ce dernier est largement utilisé avec les polyamides conventionnels. Pourtant, la nature des agents de couplage silane est un paramètre crucial pour optimiser les propriétés du composite. Elle contrôle les liaisons interfaciales entre la matrice et le renfort, et donc l'adhésion renfort-matrice et les propriétés du composite qui en résultent. De plus, le contrôle des groupes hydroxyles présents à la surface du verre est également un paramètre important pour l'optimisation de la synthèse car ils perturbent la réaction. Malgré son intérêt indéniable, l'influence de la chimie de surface sur les propriétés des composites renforts de verre/PA6 obtenus par polymérisation anionique doit encore être approfondie.

Adaptation de la densité des groupes hydroxyles de la surface du verre à synthèse du PA6 anionique

La surface brute des renforts de verre n'est pas adaptée à la polymérisation anionique par ouverture de cycle. Les groupes hydroxyles présents à la surface du verre perturbent la réaction de polymérisation en raison de la désactivation du catalyseur. L'utilisation d'un agent de couplage organosilane est une bonne option pour éliminer ces groupes hydroxyles tout en améliorant l'adhésion à l'interface renforts-matrice lorsque l'extrémité de l'organosilane est bien adaptée. Les silanes forment en effet des liaisons covalentes en réagissant avec les groupes hydroxyles de la surface du verre, via des réactions de condensation. Dès lors, il est essentiel de contrôler soigneusement le protocole de greffage d'un silane à la surface du verre, avant la fabrication du composite.

Les agents de couplage alcoxysilane sont généralement greffés à la surface du verre à partir d'une solution aqueuse. Le traitement dans cette solution peut donc conduire également à la réhydroxylation des groupes siloxanes de la surface et à la régénération des hydroxyles. Ainsi, la réhydroxylation augmente la densité des groupes hydroxyles, influence le degré de greffage des organosilanes et, finalement, augmente la densité des groupes hydroxyles résiduels. Ceci montre que le greffage des silanes à la surface des renforts de verre est un processus dynamique et complexe résultant d'une compétition entre la condensation des silanes à la surface, qui diminue le nombre de groupes -OH, et la réhydroxylation, qui entraîne une régénération et une augmentation de la concentration de ces groupes. Cette compétition dépend de plusieurs facteurs, notamment le temps de silanisation. Afin d'améliorer les propriétés des composites à base de PA6 anionique, l'optimisation du traitement de surface des renforts doit donc être combinée à un contrôle adéquat du processus de polymérisation de la matrice.

L'étude menée dans ce chapitre visait à adapter le protocole de modification de la surface des renforts de verre grâce à un suivi rigoureux et précis de la densité de surface -OH pendant toutes les étapes de la silanisation. La méthodologie employée repose sur l'utilisation de l'ATG et de la spectroscopie IR. L'impact du protocole de greffage des silanes sur la cinétique de polymérisation et de cristallisation du système modèle, composé d'une matrice PA6 anionique renforcée par des microparticules de verre silanisées, a également été évalué par des mesures de DSC.

Effet du temps de calcination initial sur la densité de surface de -OH et sur la cinétique de polymérisation du PA6

Les particules de verre utilisées comme renfort présentent un diamètre moyen de 4 μm. La densité des groupes hydroxyles présents à la surface des particules a été quantifiée à l'aide de l'ATG. Ceci permet notamment de déterminer l'évolution de la densité des hydroxyles en fonction du temps de calcination à 450°C. Cet effet du temps de calcination sur les groupes hydroxyles a également été caractérisé par spectroscopie IR. Les spectres IRTF

des particules entièrement réhydroxylées et des particules ayant subi une calcination ultérieure ont montré que l'intensité du pic diminue progressivement en augmentant le temps de calcination et disparaît quasiment après 24 heures de calcination. Une telle diminution confirme la déhydroxylation progressive de la surface, ce qui est cohérent avec la perte de masse progressive observée par ATG.

Dans un second temps, une synthèse *in situ* des composites a été réalisée en DSC avec les particules entièrement réhydroxylées et avec les particules calcinées ultérieurement de 2 h à 24 h, l'objectif étant de déterminer l'effet du temps de calcination sur la cinétique de polymérisation et de cristallisation du PA6. Les résultats ont été comparés à ceux de la résine pure. Les thermogrammes DSC des composites présentés dans la figure .48 montrent deux pics : le premier est lié à la polymérisation des monomères et le second est lié à la cristallisation du PA6. Par rapport à la résine pure, les particules entièrement réhydroxylées inhibent complètement la réaction. Le même résultat a été obtenu avec les particules brutes (état de réception et sans traitement ultérieur), ce qui confirme l'incompatibilité de la surface brute du verre avec la synthèse du PA6 anionique en raison de la présence significative de groupes -OH. En revanche, les cinétiques de polymérisation et de cristallisation augmentent significativement en augmentant le temps de calcination jusqu'à 8 h, puis se stabilisent pour des temps de calcination plus longs. Cette amélioration est due à la déhydroxylation de la surface et à l'élimination partielle des groupes hydroxyles pendant la calcination, ce qui limite la désactivation du catalyseur. La stabilisation de la cinétique de polymérisation/cristallisation après 8 h de calcination indique que la densité de surface -OH restante n'a pas d'influence significative sur les phénomènes de polymérisation/cristallisation. Après une calcination de 10 h, la densité des groupes hydroxyles résiduels représente un compromis adéquat qui permet d'assurer une certaine marge, compte tenu de l'inévitable réhydroxylation associée au processus postérieur de greffage de silane en solution aqueuse.

Contrôle de la quantité de -OH régénérée durant le traitement de silanisation

Le processus de réhydroxylation dans la solution aqueuse de silanisation et la réhydroxylation dans une solution de HCl à 10 % (généralement utilisée avant la silanisation) ont d'abord été comparés. La solution aqueuse de silanisation offre un meilleur contrôle de la réhydroxylation car elle évite une régénération excessive de -OH pour les mêmes temps de traitement. Par conséquent, les deux processus de réhydroxylation et de silanisation peuvent être réalisés simultanément. De plus, cette nouvelle approche permet d'éliminer une étape supplémentaire du processus de traitement de surface (pas d'étape de réhydroxylation acide).

Toutefois, lorsque la silanisation est effectuée dans une solution aqueuse et que les processus de réhydroxylation et de silanisation se produisent simultanément, la régénération des hydroxyles pourrait être excessive. En effet, la concentration du silane pourrait

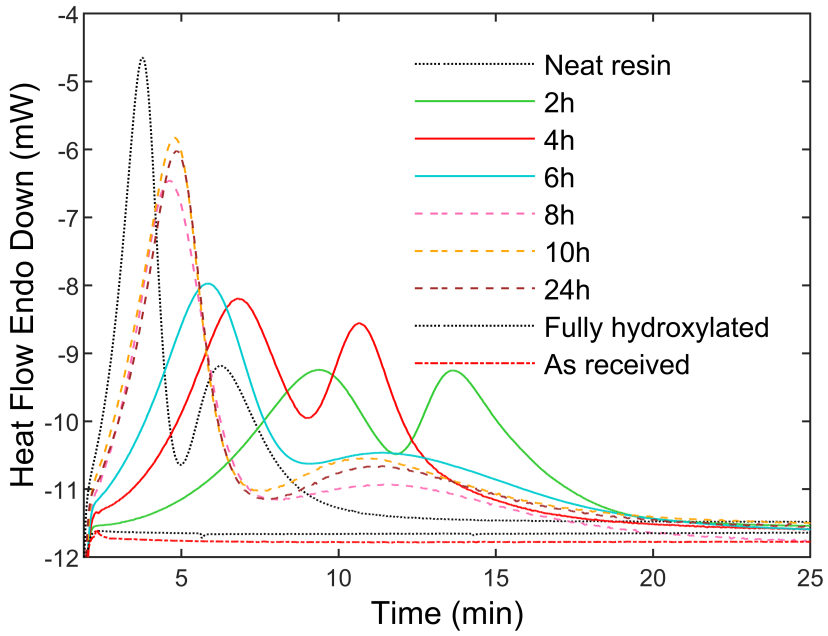

Figure .48: Thermogrammes DSC des composites PA6/particules de verre lors de la synthèse isotherme à 180°C, pour le temps de calcination des particules allant de 0 h (entièrement réhydroxylé) à 24 h, comparés à la résine pure

diminuer considérablement en cas de réaction avec la surface des particules. Ces -OH régénérés et non réagis pourraient alors rester à la surface et ralentir ou inhiber la polymérisation du PA6. Par conséquent, l'effet du temps de traitement sur cette compétition entre la condensation et la réhydroxylation pendant le greffage des silanes à partir d'une solution aqueuse a été identifié. Cette analyse a montré qu'un temps de traitement de 2 h présente un bon compromis entre le nombre d'hydroxyles régénérés et qui réagissent pendant le traitement, ceci sans un impact négatif majeur sur la cinétique de polymérisation/cristallisation.

Conclusion

Le contrôle de la densité des groupes hydroxyles lors de la calcination ou du greffage d'un agent de couplage silane à la surface de particules de verre n'a pas été abordé dans la littérature jusqu'à présent. Dans cette étude, ce contrôle a permis d'améliorer les cinétiques de polymérisation et de cristallisation lors de la synthèse *in situ* des composites à base de PA6 anionique. La suite de l'étude repose sur le protocole de greffage développé dans ce chapitre. On notera que ce meilleur contrôle des groupes -OH trouve également un intérêt essentiel dans de nombreuses autres applications telles que la fabrication de matériaux composites, de revêtements de verre pour les surfaces hydrophobes, de surfaces antibactériennes et antifongiques et, plus généralement, toute application nécessitant un traitement silane.

Impact de la chimie des silanes sur les interactions interfaciales lors de la synthèse des composites PA6 anionique/verre

Le contrôle du type d'interaction renfort-matrice à l'interface en fonction du traitement de surface et du type du silane greffé à la surface des particules de verre est un facteur fondamental pour la cinétique de polymérisation et de cristallisation du PA6 anionique. En effet, la nature des interactions conditionne directement les propriétés résultantes du matériau composite. Par conséquent, avant d'étudier le rôle du silane greffé sur les propriétés mécaniques des composites PA6/particules de verre, l'impact de la chimie du silane sur la polymérisation et la cristallisation de la matrice PA6 doit être analysé.

Ce chapitre est dedié à la compréhension de l'impact de la chimie du silane sur la polymérisation et la cristallisation des composites PA6/particules de verre. L'approche adoptée repose sur un protocole de greffage optimisé qui assure une polymérisation anionique par ouverture de cycle efficace de l'ϵ-caprolactame, avec des degrés de conversion des monomères et de greffage des silanes élevés, comme décrit dans le chapitre précédent. Trois types de chimies de silane différentes, conduisant à des interactions interfaciales distinctes avec la matrice PA6, ont été considérés :(i) un silane hydrophobe (TMPS) minimisant les interactions interfaciales ; (ii) deux aminosilanes (APTMS, AEAPTMS) formant des liaisons hydrogènes avec la matrice PA6 ; (iii) deux silanes greffés contenant l'activateur (ACTISILANE) et le monomère (MONOMSILANE) respectivement permettant d'impliquer la surface du verre dans la réaction de polymérisation et, ainsi, générer des liaisons covalentes à l'interface. Une caractérisation complète et rigoureuse de la surface des particules silanisées a été réalisée par des techniques complémentaires d'analyse de surface. Enfin, l'impact de la nature chimique du silane sur la cinétique de polymérisation et de cristallisation a été évalué par des mesures DSC.

Traitement et caractérisation de la surface des particules

Les structures chimiques des quatre types de silanes et les interactions interfaciales respectivement envisagées avec la matrice PA6 anionique sont présentées dans le tableau .5.

Après traitement, les surfaces des particules de verre ont été caractérisées par IRTF, spectroscopie photoélectronique à rayons X (XPS), ATG, microscopie confocale et par mesures d'angle de contact. Les résultats de la caractérisation ont confirmé que les silanes ont été greffés à la surface des particules avec succès. Par exemple, le tableau .6 présente une comparaison des résultats XPS des billes de verre non traitées et des billes de verre modifiées avec l'APTMS et l'ACTISILANE. Ces résulats montrent que l'azote (N 1s) n'est pas présent à la surface des particules non traitées, mais qu'il apparaît à la surface des particules silanisées. Ceci démontre non seulement la présence des silanes à la surface

Table .5: Nom et structure des silanes considérés et interactions interfaciales correspondantes avec la matrice PA6 anionique

Nom du silane	Structure chimique	Interaction avec le PA6 anionique
3-Aminopropyl)trimethoxysilane (APTMS, 97%)	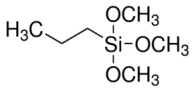	Low interactions
3-Aminopropyl)trimethoxysilane (APTMS, 97%)	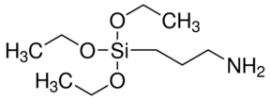	Weak hydrogen bonds
3-(2-Aminoethylamino)-propyltrimethoxysilane (AEAPTMS, 96%)	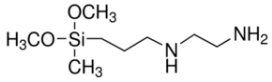	Weak hydrogen bonds
2-oxo-azepane-1-carboxamide-N-[3-(propyl)]-trimethoxysilane (ACTISILANE)	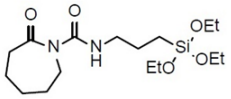	Strong covalent bonds
MONOMSILANE	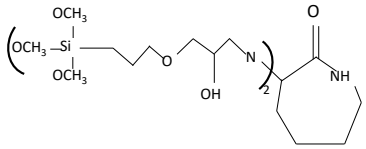	Strong covalent bonds

des particules traitées, mais aussi la conservation des fonctions amines après le greffage.

Influence du traitement de surface sur la polymérisation et la cristallisation du PA6

Après avoir démontré la modification réussie de la surface des particules, la synthèse de composites particules de verre/PA6 anionique a été étudiée par DSC afin d'examiner l'influence de la nature chimique du traitement sur la cinétique de polymérisation/cristallisation. Les résultats de la DSC montrent que les traitements appliqués à la surface des billes sont compatibles avec la réaction de synthèse. Contrairement aux billes non traitées, les billes traitées permettent la polymérisation de la matrice et n'inhibent pas la réaction. A

Table .6: Identification et quantification des éléments à partir de l'analyse XPS des particules non traitées et traitées avec l'APTMS et l'ACTISILANE

Atomes	Énergie de liaison (BE)	Pourcentage atomique (%)		
		Non traitées	APTMS	ACTISLANE
Si 2p	103.1	16.0	16.7	12.3
C 1s	285.0	35.4	41.0	43.2
O 1s	532.0	38.6	34.0	32.5
N 1s	400.0	-	2.4	2.7
Na 1s	1701.4	6.1	3.7	6.5
Ca 2p3/2	346.2	1.9	1.4	1.5
Mg 1s	1303.1	Traces	Traces	Traces

titre d'exemple, la figure .49(a) montre que la cinétique de polymérisation/cristallisation avec les billes traitées avec l'APTMS et l'AEAPTMS est proche de celle de la résine pure. De plus, ces aminosilanes greffés à la surface des billes permettent une interaction de type liaison faible à l'interface entre l'amine primaire du silane et le carbonyle du PA6. Ces interactions pourraient améliorer l'adhésion interfaciale et, par conséquent, les propriétés mécaniques des composites. Les traitements mettant en jeu des liaisons covalentes (ACTISILANE, MONOMSILANE) accélèrent quant à eux encore davantage la polymérisation jusqu'à atteindre une cinétique de synthèse quasi identique à celle de la résine pure comme le montre la figure .49(b).

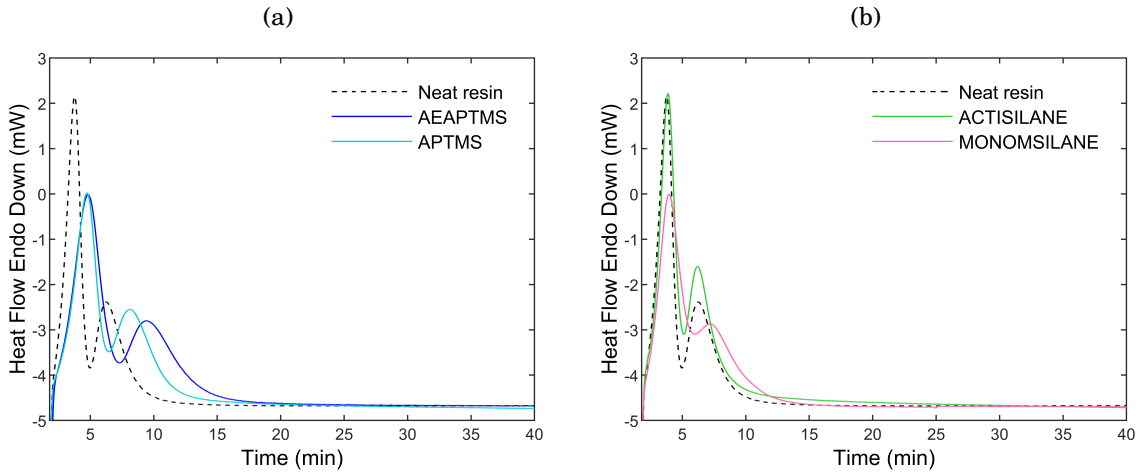

Figure .49: Thermogrammes DSC de la synthèse isotherme à 180°C du PA6 et des composites PA6/particules de verre synthétisés avec les particules traitées avec (a) APTMS /AEAPTMS, (b) ACTISILANE/MONOMSILANE

Enfin, les degrés de conversion et de cristallinité de la matrice PA6 ont également été mesurés. Ces résultats ont montré que, quel que soit le type de silane, le degré de conversion obtenu est supérieur à 95 %. Le processus de cristallisation et le degré de

cristallinité sont aussi affectés par le type du traitement de surface. A titre d'exemple, le traitement MONOMSILANE augmente le degré de cristallinité d'une manière significative comparée à la résine pure et aux autres traitements.

Conclusion

Ce chapitre a mis en évidence l'impact significatif de la chimie de surface des particules de verre sur la polymérisation et la cristallisation de la matrice PA6 anionique. En effet, l'interaction du mélange réactif avec la surface du verre affecte le processus de synthèse. Pour cette raison, un traitement de surface approprié est nécessaire pour assurer la compatibilité entre les réactifs et la surface du verre et, à terme, améliorer les propriétés mécaniques des composites. La démarche utilisée a consisté à adapter la chimie de la surface du verre pour créer trois types d'interactions à l'interface particule-matrice. Premièrement, les particules ont été traitées avec un silane qui empêche les interactions entre les particules et la matrice PA. Ensuite, les aminosilanes sélectionnés ont permis de créer des liaisons faibles à l'interface. Enfin, des agents de couplage réactifs ont été spécifiquement synthétisés dans cette étude en proposant une nouvelle approche pour la création de liaisons covalentes à l'interface. A partir de ces résultats, l'enjeu du prochain chapitre est d'identifier l'influence de la chimie de surface des particules sur les propriétés mécaniques macroscopiques des composites élaborés.

Etude des propriétés des composites à base de PA6 anionique en fonction des traitements de surface des particules de verre

Ce chapitre vise à valider un processus de fabrication des matériaux composites à partir de particules traitées. Différents procédés de fabrication ont été testés et optimisés pour fabriquer des éprouvettes de matériaux composites qui ont ensuite été analysés afin d'évaluer la qualité de la polymérisation et de la cristallisation au cours de cette synthèse à grande échelle. Dans un second temps, les matériaux fabriqués ont été caractérisés par des essais de traction suivis par corrélation d'images numériques afin d'évaluer à la fois les propriétés mécaniques et l'homogénéité des éprouvettes en fonction du type d'interaction interfaciale créée par le silane greffé. Enfin, la pertinence des traitements développés dans le cas d'une mise en œuvre pour des composites massifs PA6 anionique/verre a été examinée et discutée.

Caractérisation physico-chimique des composites fabriqués

Après l'optimisation du processus et la fabrication des éprouvettes, les caractéristiques physico-chimiques des composites fabriqués ont été analysées par ATG et DSC afin d'évaluer le taux de particules et les degrés de conversion et de cristallinité. Les résultats de l'analyse ATG ont montré que le taux de particules de tous les échantillons est très proche du taux de particules ciblé à savoir 50 wt%. Cela confirme l'homogénéité de la distribution des particules dans les éprouvettes composites. De plus, les éprouvettes de résine pure et de composites, quel que soit le type de particules, présentent des degrés de conversion supérieurs à 95%. Ceci est donc cohérent avec les degrés de conversion obtenus par la synthèse en DSC et démontre la réussite de la polymérisation de la matrice pendant le processus de fabrication à grande échelle.

Les analyses DSC ont également mis en évidence un degré de cristallinité ayant un ordre de grandeur comparable à celui de la résine pour tous les échantillons de composite. Toutefois, les différences observées entre les taux sont liées à la présence de particules qui peuvent soit perturber le processus de cristallisation (comme dans le cas des particules calcinées), soit le favoriser (comme dans le cas des particules MONOMSILANE). De plus, il a été démontré que le traitement de surface des particules influence également la cristallisation depuis l'état fondu (après synthèse), notamment dans le cas de l'ACTISILANE où la mobilité des chaînes est réduite en raison de leur liaison covalente avec les particules.

Propriétés mécaniques des composites et analyse des interfaces

Les propriétés mécaniques des composites ont été évaluées à l'aide d'essais de traction suivis par des mesures de champs cinématiques. Ces dernières ont montré des déformations homogènes pour tous les échantillons. Les propriétés de traction combinées à

l'analyse des surfaces de rupture ont montré que les composites contenant des particules calcinées conduisent à une faible adhésion interfaciale. En revanche, les composites contenant les particules traitées avec les aminosilanes présentent une meilleure adhésion grâce aux liaisons hydrogènes qui se forment à l'interface. Enfin, le traitement ACTISILANE fournit la meilleure résistance à la traction combinée à une augmentation de la rigidité. Cela correspond à une augmentation importante de l'adhésion interfaciale et de la cohésion globale du matériau. Par conséquent, la formation des liaisons covalentes entre les particules et la matrice a été prouvé grâce à l'amélioration significative des propriétés mécaniques.

Conclusion

Dans ce chapitre, un procédé optimisé a été développé pour fabriquer des éprouvettes composites avec les différentes particules traitées. Les caractéristiques physico-chimiques de ces composites ont été analysées à l'aide de l'ATG et de la DSC. Ceci a permis de démontrer la réussite de la polymérisation et de la cristallisation lors de la fabrication de composites massifs. Enfin, l'impact de la chimie de surface des particules de verre sur les propriétés mécaniques a été évalué sous sollicitation de traction et au travers de l'analyse des surfaces de rupture. Parmi les traitements considérés dans cette étude, le recours à l'ACTISILANE permet typiquement d'atteindre les meilleures propriétés mécaniques des composites PA6 anionique/verre.

Conclusion générale et perspectives

Cette thèse a porté sur l'adaptation de la surface du verre pour la synthèse du polyamide 6 (PA6) anionique par ouverture de cycle. Cette matrice représente une solution prometteuse pour la fabrication de composites thermoplastiques par procédé liquide réactif. Dans ce cas, la polymérisation réactive permet de fabriquer des pièces composites renforcées de fibres par polymérisation *in situ* avec un procédé similaire au moulage par transfert de résine (RTM) utilisé pour les composites thermodurcissables.

Le polyamide 6 est obtenu par polymérisation anionique par ouverture de cycle (AROP) de son monomère ϵ-caprolactam. Lors de cette réaction, la polymérisation des monomères et la cristallisation des macromolécules se produisent simultanément, ce qui génère un fort couplage entre les deux phénomènes. Les fibres de verre ont été choisies comme renforts des composites car elles conviennent à de nombreuses applications et offrent un bon compromis entre les propriétés mécaniques et les coûts de fabrication.

La particularité de la réaction de polymérisation *in situ* lors de la synthèse des composites PA6 anionique/verre réside dans le rôle de l'interface : l'adhésion renfort-matrice conditionne non seulement le comportement mécanique des composites, mais la nature de l'interface a également un impact sur les cinétiques de polymérisation et de cristallisation. Ainsi, l'objectif de cette thèse était de contrôler les interactions interfaciales entre le renfort et la matrice afin d'améliorer la cinétique de réaction. En outre, ce travail de thèse visait également à améliorer l'adhésion interfaciale afin d'augmenter les propriétés mécaniques résultantes des composites.

Les principales contributions originales de ce travail sont :

- Le développement d'un protocole de greffage optimisé qui assure une polymérisation anionique par ouverture de cycle efficace du ϵ-caprolactam, avec une conversion élevée des monomères et un greffage réussi des silanes à la surface du verre; parallèlement, ce protocole limite l'effet négatif des groupes hydroxyles présents à la surface sur la réaction de synthèse.

- Une étude approfondie de plusieurs agents de couplage conduisant à des interactions interfaciales distinctes avec la matrice PA6 : interactions limitées, liaisons faibles et liaisons fortes. Plus particulièrement, de nouveaux agents de couplage ont été synthétisés à partir du monomère permettant la création de liaisons covalentes à l'interface. Une caractérisation méthodique et rigoureuse de la surface des particules de verre silanisées a été réalisée par plusieurs techniques complémentaires afin de mieux comprendre les processus chimiques mis en jeu.

- Une compréhension approfondie de la relation entre la chimie de la surface des renforts de verre, la cinétique de polymérisation et de cristallisation et les propriétés mécaniques macroscopiques des composites. Ces résultats fournissent une analyse pertinente pour optimiser le traitement de surface des renforts et, ainsi, améliorer considérablement les propriétés mécaniques des composites.

De nombreuses perspectives peuvent être envisagées à partir de ce travail. Certains aspects de l'étude méritent d'être poursuivis et approfondis, tels que l'étude de l'architecture moléculaire des chaînes polymères lors de la synthèse par chromatographie d'exclusion stérique (SEC). Ceci permettra de définir la masse molaire, la distribution et le degré de ramification du PA6 et, par conséquent, déterminer l'impact de la chimie de surface du renfort de verre sur l'architecture des chaînes polymères formées. Il serait également intéressant d'étudier la morphologie des cristaux de PA6 formés en présence des particules de verre traitées par WAXS. Ceci permettra une meilleure compréhension de l'impact du traitement de surface silane sur le processus de nucléation.

Par ailleurs, les traitements appliqués aux microparticules doivent être transposés aux fibres de verre. Les cinétiques de polymérisation et de cristallisation en présence de fibres traitées devraient être similaires à celles des particules de verre modèles. Les propriétés des composites renforcés par les fibres de verre traitées doivent être évaluées. Dans ce cas, des tests spécifiques caractérisant plus précisément l'adhésion interfaciale peuvent être réalisés, tel que le test de déchaussement.

Enfin, il est important de noter que les traitements développés dans cette thèse peuvent être étendus à d'autres types de renforts présentant des groupements hydroxyles à leur surface, tels que les fibres ou les nanotubes de carbone, ainsi que les fibres naturelles.

BIBLIOGRAPHY

[1] A. Shojaei, S. R. Ghaffarian, and S. M. H. Karimian, "Modeling and simulation approaches in the resin transfer molding process: A review," *Polymer Composites*, vol. 24, no. 4, pp. 525–544, 2003.
_eprint: https://onlinelibrary.wiley.com/doi/pdf/10.1002/pc.10050.

[2] K. Van Rijswijk and H. E. N. Bersee, "Reactive processing of textile fiber-reinforced thermoplastic composites – An overview," *Composites Part A: Applied Science and Manufacturing*, vol. 38, pp. 666–681, Mar. 2007.

[3] D. A. Jesson and J. F. Watts, "The Interface and Interphase in Polymer Matrix Composites: Effect on Mechanical Properties and Methods for Identification," *Polymer Reviews*, vol. 52, pp. 321–354, July 2012.

[4] X. Ji, Y. Xu, W. Zhang, L. Cui, and J. Liu, "Review of functionalization, structure and properties of graphene/polymer composite fibers," *Composites Part A: Applied Science and Manufacturing*, vol. 87, pp. 29–45, aug 2016.

[5] R. Pratyush Behera, P. Rawat, S. Kumar Tiwari, and K. Kumar Singh, "A brief review on the mechanical properties of Carbon nanotube reinforced polymer composites," *Materials Today: Proceedings*, vol. 22, pp. 2109–2117, jan 2020.

[6] M. Altin Karatas and H. Gökkaya, "A review on machinability of carbon fiber reinforced polymer (CFRP) and glass fiber reinforced polymer (GFRP) composite materials," *Defence Technology*, vol. 14, pp. 318–326, aug 2018.

[7] U. K. Vaidya and K. K. Chawla, "Processing of fibre reinforced thermoplastic composites," *International Materials Reviews*, vol. 53, pp. 185–218, July 2008.

[8] C. Giori and B. T. Hayes, "Hydrolytic polymerization of caprolactam. I. Hydrolysis—polycondensation kinetics," *Journal of Polymer Science Part A-1: Polymer Chemistry*, vol. 8, pp. 335–349, Feb. 1970.

[9] S. Mochizuki and N. Ito, "The hydrolytic polymerization kinetics of ϵ-caprolactam," *Chemical Engineering Science*, vol. 28, pp. 1139–1147, May 1973.

[10] K. v. Rijswijk, J. Teuwen, H. Bersee, and A. Beukers, "Textile fiber-reinforced anionic polyamide-6 composites. Part I: The vacuum infusion process," *Composites Part A: Applied Science and Manufacturing*, vol. 40, pp. 1–10, Jan. 2009.

[11] K. Hashimoto, "Ring-opening polymerization of lactams. Living anionic polymerization and its applications," *Progress in Polymer Science*, vol. 25, no. 10, pp. 1411 – 1462, 2000.

[12] G. B. Gechele and G. Stea, "Heterogeneous polymerization of ϵ-caprolactam," *European Polymer Journal*, vol. 1, pp. 91–102, May 1965.

[13] N. Barhoumi, A. Maazouz, M. Jaziri, and R. Abdelhedi, "Polyamide from lactams by reactive rotational molding via anionic ring-opening polymerization: Optimization of processing parameters," *Express Polymer Letters*, vol. 7, no. 1, pp. 76–87, 2013.

[14] G. V. den Broek d'Obrenan, *Adaptation du procédé RTM (Moulage par Transfert de Résine) à la mise en œuvre de matériaux composites à matrice thermoplastique*. Thèse, L'Institut National des Sciences Appliquées de Lyon, 2011.

[15] K. Van Rijswijk, H. Bersee, W. Jager, and S. Picken, "Optimisation of anionic polyamide-6 for vacuum infusion of thermoplastic composites: choice of activator and initiator," *Composites Part A: Applied Science and Manufacturing*, vol. 37, pp. 949–956, June 2006.

[16] K. Udipi, R. S. Davé, R. L. Kruse, and L. R. Stebbins, "Polyamides from lactams via anionic ring-opening polymerization: 1. Chemistry and some recent findings," *Polymer*, vol. 38, no. 4, pp. 927 – 938, 1997.

[17] C. Vicard, O. De Almeida, A. Cantarel, and G. Bernhart, "Experimental study of polymerization and crystallization kinetics of polyamide 6 obtained by anionic ring opening polymerization of ϵ-caprolactam," *Polymer*, vol. 132, pp. 88–97, Dec. 2017.

[18] A. Y. Malkin, V. G. Frolov, A. N. Ivanova, and Z. S. Andrianova, "The nonisothermal anionic polymerization of caprolactam," *Polymer Science U.S.S.R.*, vol. 21, pp. 691–700, Jan. 1979.

[19] A. Y. Malkin, S. L. Ivanova, V. G. Frolov, A. N. Ivanova, and Z. S. Andrianova, "Kinetics of anionic polymerization of lactams. (Solution of non-isothermal kinetic problems by the inverse method)," *Polymer*, vol. 23, pp. 1791–1800, Nov. 1982.

[20] C. Vicard, O. De Almeida, A. Cantarel, and G. Bernhart, "Modeling of the polymerization and crystallization kinetic coupling of polyamide 6 synthesized from ϵ-caprolactam," *Polymer*, vol. 180, p. 121681, Oct. 2019.

[21] C. Vicard, O. de Almeida, A. Cantarel, and G. Bernhart, "Ttt diagram of the anionic polymerization pa6 from ϵ-caprolactam," in *ICCM 21-21th International Conference on Composite Materials*, pp. 10–p, 2017.

[22] K. Khodabakhshi, M. Gilbert, P. Dickens, R. Hague, and S. Fathi, "Optimised polymerization conditions for inkjetting of caprolactam to produce polyamide parts," *19th Annual International Solid Freeform Fabrication Symposium, SFF 2008*, pp. 668–675, 01 2008.

[23] C. Vicard, *Étude et modélisation de la synthèse du polyamide 6 pour la mise en œuvre de composites thermoplastiques par voie liquide réactive*.
PhD thesis, Ecole nationale des Mines d'Albi-Carmaux, 2018.

[24] V. Rijswijk, *Thermoplastic composite wind turbine blades: vacuum infusion technology for anionic polyamide-6 composites*.
Thesis, S.l., 2007.

[25] K. Khodabakhshi, M. Gilbert, P. Dickens, and R. Hague, "Optimizing conditions for anionic polymerization of caprolactam for inkjetting," *Advances in Polymer Technology*, vol. 29, no. 4, pp. 226–236, 2010.

[26] V. Rijswijk, H. E. N. Bersee, A. Beukers, S. J. Picken, and A. A. v. Geenen, "Optimisation of anionic polyamide-6 for vacuum infusion of thermoplastic composites: Influence of polymerisation temperature on matrix properties," *Polymer Testing*, vol. 25, no. 3, pp. 392 – 404, 2006.

[27] R. Greenley, J. Stauffer, and J. Kurz, "The kinetic equation for the initiated, anionic polymerization of η-caprolactam," *Macromolecules*, vol. 2, no. 6, pp. 561–567, 1969.

[28] J. Merna, D. Chromcová, J. Brožek, and J. Roda, "Polymerization of lactams: 97. anionic polymerization of ε-caprolactam activated by esters," *European polymer journal*, vol. 42, no. 7, pp. 1569–1580, 2006.

[29] R. Mateva and P. Petrov, "On the activating anionic polymerization of ε-caprolactam in bulk caused by bis carbamyl derivatives," *European polymer journal*, vol. 35, no. 2, pp. 325–333, 1999.

[30] K. J. Kim, D. S. Hong, and A. R. Tripathy, "Kinetics of adiabatic anionic copolymerization of ε-caprolactam in the presence of various activators," *Journal of applied polymer science*, vol. 66, no. 6, pp. 1195–1207, 1997.

[31] P. Sibal, R. Camargo, and C. Macosko, "Designing nylon-6 polymerization systems for rim.," *Polymer process engineering*, vol. 1, no. 2, pp. 147–169, 1983.

[32] G. C. Alfonso, G. Bonta', S. Russo, and A. Traverso, "Adiabatic polymerization of ε-caprolactam in presence of lithium chloride, 1. thermodynamic and kinetic aspects," *Die Makromolekulare Chemie: Macromolecular Chemistry and Physics*, vol. 182, no. 3, pp. 929–939, 1981.

[33] S. Russo, A. Imperato, A. Mariani, and F. Parodi, "The fast activation of ε-caprolactam polymerization in quasi-adiabatic conditions," *Macromolecular chemistry and physics*, vol. 196, no. 10, pp. 3297–3303, 1995.

[34] R. Camargo, V. Gonzalez, C. Macosko, and M. Tirrell, "Bulk polymerization kinetics by the adiabatic reactor method," *Rubber Chemistry and technology*, vol. 56, no. 4, pp. 774–783, 1983.

[35] K. J. Kim, Y. Y. Kim, B. S. Yoon, and K. J. Yoon, "Mechanism and kinetics of adiabatic anionic polymerization of ϵ-caprolactam in the presence of various activators," *Journal of applied polymer science*, vol. 57, no. 11, pp. 1347–1358, 1995.

[36] J.-L. Yeh, J.-F. Kuo, and C.-Y. Chen, "Adiabatic anionic polymerization of caprolactam in the presence of n-acylated caprolactam macroactivator: Kinetic study," *Journal of applied polymer science*, vol. 50, no. 10, pp. 1671–1681, 1993.

[37] V. Korshak, T. Frunze, S. Davtyan, V. Kurashev, T. Volkova, V. Kot'elnikov, and R. Shleifman, "Kinetics of activated anionic polymerization of ε-caprolactam under non-isothermal conditions," *Polymer Science USSR*, vol. 21, no. 9, pp. 2161–2169, 1979.

[38] J. J. Teuwen, A. A. van Geenen, and H. E. Bersee, "Novel reaction kinetic model for anionic polyamide-6," *Macromolecular Materials and Engineering*, vol. 298, no. 2, pp. 163–173, 2013.

[39] S. Bolgov, V. Begishev, A. Y. Malkin, and V. Frolov, "Role of the functionality of activators during isothermal crystallization accompanying the activated anionic polymerization of ε-caprolactam," *Polymer Science USSR*, vol. 23, no. 6, pp. 1485–1492, 1981.

[40] A. Rigo, G. Fabbri, and G. Talamini, "Kinetic study of anionic polymerization of 6-caprolactam by differential calorimetry," *Journal of Polymer Science: Polymer Letters Edition*, vol. 13, no. 8, pp. 469–477, 1975.

[41] J. Karger-Kocsis and L. Kiss, "Dsc studies on the activated anionic polymerization of ε-caprolactam in the presence of crown compounds," in *Journal of Polymer Science: Polymer Symposia*, vol. 69, pp. 67–71, Wiley Online Library, 1981.

[42] A. Y. Malkin, V. Beghishev, and S. Bolgov, "The exothermal effects of superimposed processes of activated anionic polymerization of ε-caprolactam and crystallization of the polymer formed," *Polymer*, vol. 23, no. 3, pp. 385–390, 1982.

[43] D. Wilfong, C. Pommerening, and Z. Gardlund, "Separation of polymerization and crystallization processes for nylon-6," *Polymer*, vol. 33, no. 18, pp. 3884–3888, 1992.

[44] K. Khodabakhshi, M. Gilbert, S. Fathi, and P. Dickens, "Anionic polymerisation of caprolactam at the small-scale via dsc investigations," *Journal of Thermal Analysis and Calorimetry*, vol. 115, no. 1, pp. 383–391, 2014.

[45] C.-L. Zhang, L.-F. Feng, and G.-H. Hu, "Anionic polymerization of lactams: A comparative study on various methods of measuring the conversion of ϵ-caprolactam to polyamide 6," *Journal of Applied Polymer Science*, vol. 101, pp. 1972–1981, Aug. 2006.

[46] A.-C. Draye, O. Persenaire, J. Brožek, J. Roda, T. Košek, and P. Dubois, "Thermogravimetric analysis of poly (ε-caprolactam) and poly [(ε-caprolactam)-co-(ε-caprolactone)] polymers," *Polymer*, vol. 42, no. 20, pp. 8325–8332, 2001.

[47] Y. Gong, A. Liu, and G. Yang, "Polyamide single polymer composites prepared via in situ anionic polymerization of ε-caprolactam," *Composites Part A: Applied Science and Manufacturing*, vol. 41, no. 8, pp. 1006–1011, 2010.

[48] S. Pillay, U. K. Vaidya, and G. M. Janowski, "Liquid molding of carbon fabric-reinforced nylon matrix composite laminates," *Journal of Thermoplastic Composite Materials*, vol. 18, no. 6, pp. 509–527, 2005.

[49] K. Pramoda, T. Liu, Z. Liu, C. He, and H.-J. Sue, "Thermal degradation behavior of polyamide 6/clay nanocomposites," *Polymer degradation and Stability*, vol. 81, no. 1, pp. 47–56, 2003.

[50] F. Dabrowski, S. Bourbigot, R. Delobel, and M. Le Bras, "Kinetic modelling of the thermal degradation: of polyamide-6 nanocomposite," *European Polymer Journal*, vol. 36, no. 2, pp. 273–284, 2000.

[51] J. Li, Z. Fang, L. Tong, A. Gu, and F. Liu, "Effect of multi-walled carbon nanotubes on non-isothermal crystallization kinetics of polyamide 6," *European polymer journal*, vol. 42, no. 12, pp. 3230–3235, 2006.

[52] S. M. Aharoni, *n-Nylons: their synthesis, structure, and properties*.
John Wiley & Sons Incorporated, 1997.

[53] K. Khodabakhshi, *Anionic polymarisation of caprolactam: an approach to optimising thr polymerisation condition to be used in the jetting process*.
PhD thesis, Loughborough University, 2011.

[54] W. E. Nelson, *Nylon plastics technology*.
Plastics and Rubber Institute, 1976.

[55] S. M. Aharoni, "Correlations between chain parameters and failure characteristics of polymers below their glass transition temperature," *Macromolecules*, vol. 18, pp. 2624–2630, Dec. 1985.

[56] K. Ueda, K. Yamada, M. Nakai, T. Matsuda, M. Hosoda, and K. Tai, "Synthesis of high molecular weight nylon 6 by anionic polymerization of ε-caprolactam," *Polymer journal*, vol. 28, no. 5, pp. 446–451, 1996.

[57] H. C. Cartledge and C. A. Baillie, "Studies of microstructural and mechanical properties of nylon/glass composite part i the effect of thermal processing on crystallinity, transcrystallinity and crystal phases," *Journal of Materials Science*, vol. 34, no. 20, pp. 5099–5111, 1999.

[58] I. Kolesov, D. Mileva, R. Androsch, and C. Schick, "Structure formation of polyamide 6 from the glassy state by fast scanning chip calorimetry," *Polymer*, vol. 52, no. 22, pp. 5156–5165, 2011.

[59] V. K.-H. Illers and H. Haberkorn, "Schmelzverhalten, struktur und kristallinität von 6-polyamid," *Die Makromolekulare Chemie: Macromolecular Chemistry and Physics*, vol. 142, no. 1, pp. 31–67, 1971.

[60] J. Karger-Kocsis and L. Kiss, "Attempts of separation of the polymerization and crystallization processes by means of dsc thermograms of activated anionic polymerization of ε-caprolactam," *Die Makromolekulare Chemie: Macromolecular Chemistry and Physics*, vol. 180, no. 6, pp. 1593–1597, 1979.

[61] M. Kyotani, "Studies on crystalline forms of nylon 6. iii. crystallization from the glassy state," *Journal of Macromolecular Science, Part B: Physics*, vol. 11, no. 4, pp. 509–525, 1975.

[62] I. Kolesov and R. Androsch, "The rigid amorphous fraction of cold-crystallized polyamide 6," *Polymer*, vol. 53, no. 21, pp. 4770–4777, 2012.

[63] Y. Khanna and W. Kuhn, "Measurement of crystalline index in nylons by dsc: Complexities and recommendations," *Journal of Polymer Science Part B: Polymer Physics*, vol. 35, no. 14, pp. 2219–2231, 1997.

[64] S. Dasgupta, W. B. Hammond, and W. A. Goddard, "Crystal Structures and Properties of Nylon Polymers from Theory," *Journal of the American Chemical Society*, vol. 118, pp. 12291–12301, Jan. 1996.

[65] T. Fornes and D. Paul, "Crystallization behavior of nylon 6 nanocomposites," *Polymer*, vol. 44, pp. 3945–3961, June 2003.

[66] P. R. Hornsby and J. F. Tung, "Characterization of polyamide 6 made by reactive extrusion. II. Analysis of microstructure," *Journal of Applied Polymer Science*, vol. 54, pp. 899–907, Nov. 1994.

[67] T. Kōmoto, M. Iguchi, H. Kanetsuna, and T. Kawai, "Formation of spherulites during polymerization of lactams," *Die Makromolekulare Chemie: Macromolecular Chemistry and Physics*, vol. 135, no. 1, pp. 145–164, 1970.

[68] R. Mateva, O. Delev, and E. Kaschcieva, "Structure of poly (ε-caprolactam) obtained in anionic bulk polymerization," *Journal of applied polymer science*, vol. 58, no. 13, pp. 2333–2343, 1995.

[69] J. Chaichanawong, C. Thongchuea, and S. Areerat, "Effect of moisture on the mechanical properties of glass fiber reinforced polyamide composites," *Advanced Powder Technology*, vol. 27, no. 3, pp. 898–902, 2016.

[70] K. Potter, *Resin transfer moulding*.
Springer Science & Business Media, 2012.

[71] R. S. Davé, R. L. Kruse, K. Udipi, and D. E. Williams, "Polyamides from lactams via anionic ring-opening polymerization: 3. rheology," *Polymer*, vol. 38, no. 4, pp. 949–954, 1997.

[72] P. Sibal, R. Camargo, and C. Macosko, "Designing nylon-6 polymerization systems for rim.," *Polymer process engineering*, vol. 1, no. 2, pp. 147–169, 1983.

[73] K. Taki, N. Shoji, M. Kobayashi, and H. Ito, "A kinetic model of viscosity development for in situ ring-opening anionic polymerization of ε-caprolactam," *Microsystem Technologies*, vol. 23, no. 5, pp. 1161–1169, 2017.

[74] M. Miscevic, I. Catic, and M. Sercer, "Production of nylon-6 castings by anionic polymerisation of epsilon-caprolactam," *International Polymer Science and Technology(UK)*, vol. 20, no. 11, 1993.

[75] M. Worthington, "The many wonders of cast nylon," *IAPD Magazine June*, pp. 32–33, 1996.

[76] M. Rusu, C. Ibanescu, M. Murariu, A. Bordeianu, S. Balint, and E. Andrei, "Centrifugal casting of polyamide 6. i. influence of thermal treatment," *Polymers & polymer composites*, vol. 6, no. 3, pp. 143–146, 1998.

[77] E. Harkin-Jones and R. Crawford, "Rotational moulding of liquid nyrim in biaxially rotating heated moulds," *Plastics, Rubber & Composites Processing and Appl.*, vol. 1, no. 24, pp. 1–6, 1995.

[78] E. Harkin-Jones and R. Crawford, "Mechanical properties of rotationally molded nyrim," *Polymer Engineering & Science*, vol. 36, no. 5, pp. 615–625, 1996.

[79] G. Rusu, K. Ueda, E. Rusu, and M. Rusu, "Polyamides from lactams by centrifugal molding via anionic ring-opening polymerization," *Polymer*, vol. 42, no. 13, pp. 5669–5678, 2001.

[80] P. Ó. Máirtın, P. McDonnell, M. Connor, R. Eder, and C. Ó. Brádaigh, "Process investigation of a liquid pa-12/carbon fibre moulding system," *Composites Part A: Applied Science and Manufacturing*, vol. 32, no. 7, pp. 915–923, 2001.

[81] L. Zingraff, V. Michaud, P.-E. Bourban, and J.-A. Månson, "Resin transfer moulding of anionically polymerised polyamide 12," *Composites Part A: Applied Science and Manufacturing*, vol. 36, no. 12, pp. 1675–1686, 2005.

[82] P. Rosso, K. Friedrich, A. Wollny, and R. Mülhaupt, "A novel polyamide 12 polymerization system and its use for a lcm-process to produce cfrp," *Journal of Thermoplastic Composite Materials*, vol. 18, no. 1, pp. 77–90, 2005.

[83] H. Parton and I. Verpoest, "In situ polymerization of thermoplastic composites based on cyclic oligomers," *Polymer composites*, vol. 26, no. 1, pp. 60–65, 2005.

[84] S. Pillay, U. K. Vaidya, and G. M. Janowski, "Liquid molding of carbon fabric-reinforced nylon matrix composite laminates," *Journal of Thermoplastic Composite Materials*, vol. 18, no. 6, pp. 509–527, 2005.

[85] A. Luisier, P.-E. Bourban, and J.-A. Månson, "Reaction injection pultrusion of pa12 composites: process and modelling," *Composites Part A: applied science and manufacturing*, vol. 34, no. 7, pp. 583–595, 2003.

[86] B.-G. Cho, S. P. McCarthy, J. P. Fanucci, and S. C. Nolet, "Fiber reinforced nylon-6 composites produced by the reaction injection pultrusion process," *Polymer composites*, vol. 17, no. 5, pp. 673–681, 1996.

[87] X. Ning and H. Ishida, "Rim-pultrusion of nylon-6 and rubber-toughened nylon-6 composites," *Polymer Engineering & Science*, vol. 31, no. 9, pp. 632–637, 1991.

[88] R. Mateva, O. Ishtinakova, R. Nikolov, and C. Djambova, "Kinetics of polymerization of ε-caprolactam in the presence of inorganic dispersed additives," *European polymer journal*, vol. 34, no. 8, pp. 1061–1067, 1998.

[89] K. Te Nijenhuis, R. Addink, and A. Van der Vegt, "A study on composites of nylon-6 with hollow glass microspheres," *Polymer Bulletin*, vol. 21, no. 5, pp. 467–474, 1989.

[90] S.-H. Wu, F.-Y. Wang, C.-C. M. Ma, W.-C. Chang, C.-T. Kuo, H.-C. Kuan, and W.-J. Chen, "Mechanical, thermal and morphological properties of glass fiber and carbon fiber reinforced polyamide-6 and polyamide-6/clay nanocomposites," *Materials Letters*, vol. 49, no. 6, pp. 327–333, 2001.

[91] B. S. Yoon, S. H. Lee, and M. H. Suh, "Continuous glass-fiber reinforced nylon 6 by using a new impregnation die," *Polymer composites*, vol. 18, no. 5, pp. 656–662, 1997.

[92] D. Nuruzzaman, A. A. Iqbal, A. Oumer, N. Ismail, and S. Basri, "Experimental investigation on the mechanical properties of glass fiber reinforced nylon," in *IOP Conference Series: Materials Science and Engineering*, vol. 114, p. 012118, IOP Publishing, 2016.

[93] M. Akkapeddi, "Glass fiber reinforced polyamide-6 nanocomposites," *Polymer Composites*, vol. 21, no. 4, pp. 576–585, 2000.

[94] X. Bian, L. Ambrosio, J. Kenny, L. Nicolais, and A. Dibenedetto, "Effect of water absorption on the behavior of e-glass fiber/nylon-6 composites," *Polymer Composites*, vol. 12, no. 5, pp. 333–337, 1991.

[95] Y. Yoo, M. Spencer, and D. Paul, "Morphology and mechanical properties of glass fiber reinforced nylon 6 nanocomposites," *Polymer*, vol. 52, no. 1, pp. 180–190, 2011.

[96] U. Yilmazer and M. Cansever, "Effects of processing conditions on the fiber length distribution and mechanical properties of glass fiber reinforced nylon-6," *Polymer composites*, vol. 23, no. 1, pp. 61–71, 2002.

[97] K.-q. Han, Z.-j. Liu, and M.-h. Yu, "Preparation and mechanical properties of long glass fiber reinforced pa6 composites prepared by a novel process," *Macromolecular Materials and Engineering*, vol. 290, no. 7, pp. 688–694, 2005.

[98] J. Otaigbe and W. Harland, "Studies in the properties of nylon 6–glass fiber composites," *Journal of applied polymer science*, vol. 36, no. 1, pp. 165–175, 1988.

[99] C. Yan, H. Li, X. Zhang, Y. Zhu, X. Fan, and L. Yu, "Preparation and properties of continuous glass fiber reinforced anionic polyamide-6 thermoplastic composites," *Materials & Design*, vol. 46, pp. 688–695, 2013.

[100] K. Chen, M. Jia, H. Sun, and P. Xue, "Thermoplastic reaction injection pultrusion for continuous glass fiber-reinforced polyamide-6 composites," *Materials*, vol. 12, no. 3, p. 463, 2019.

[101] K. Van Rijswijk, A. Van Geenen, and H. Bersee, "Textile fiber-reinforced anionic polyamide-6 composites. part ii: Investigation on interfacial bond formation by short beam shear test," *Composites Part A: Applied Science and Manufacturing*, vol. 40, no. 8, pp. 1033–1043, 2009.

[102] P. K. Jal, S. Patel, and B. K. Mishra, "Chemical modification of silica surface by immobilization of functional groups for extractive concentration of metal ions," *Talanta*, vol. 62, no. 5, pp. 1005–1028, 2004.

[103] R. Kaas and J. Kardos, "The interaction of alkoxy silane coupling agents with silica surfaces," *Polymer Engineering & Science*, vol. 11, no. 1, pp. 11–18, 1971.

[104] Y. Li, J. Yu, and Z.-X. Guo, "The influence of silane treatment on nylon 6/nano-sio2 in situ polymerization," *Journal of Applied Polymer Science*, vol. 84, no. 4, pp. 827–834, 2002.

[105] C.-C. Huang and F.-C. Chang, "Reactive compatibilization of polymer blends of poly (butylene terephthalate)(pbt) and polyamide-6, 6 (pa66): 1. rheological and thermal properties," *Polymer*, vol. 38, no. 9, pp. 2135–2141, 1997.

[106] T. Bessell and J. Shortall, "The crystallization and interfacial bond strength of nylon 6 at carbon and glass fibre surfaces," *Journal of materials science*, vol. 10, no. 12, pp. 2035–2043, 1975.

[107] G. Rusu and E. Rusu, "Nylon 6/sio2nanocomposites synthesized by in situanionic polymerization," *High Performance Polymers*, vol. 18, no. 3, pp. 355–375, 2006.

[108] D. Li, Q. Liu, L. Yu, X. Li, and Z. Zhang, "Correlation between interfacial interactions and mechanical properties of pa-6 doped with surface-capped nano-silica," *Applied Surface Science*, vol. 255, no. 18, pp. 7871–7877, 2009.

[109] G. Young, "Interaction of water vapor with silica surfaces," *Journal of colloid science*, vol. 13, no. 1, pp. 67–85, 1958.

[110] M. L. Hair, "Hydroxyl groups on silica surface," *Journal of Non-Crystalline Solids*, vol. 19, pp. 299–309, 1975.

[111] L. Zhuravlev, "Surface characterization of amorphous silica—a review of work from the former ussr," *Colloids and Surfaces A: Physicochemical and Engineering Aspects*, vol. 74, no. 1, pp. 71–90, 1993.

[112] L. Zhuravlev, "The surface chemistry of amorphous silica. zhuravlev model," *Colloids and Surfaces A: Physicochemical and Engineering Aspects*, vol. 173, no. 1-3, pp. 1–38, 2000.

[113] A. Bertin and H. Schlaad, "Mild and versatile (bio-) functionalization of glass surfaces via thiol- ene photochemistry," *Chemistry of Materials*, vol. 21, no. 24, pp. 5698–5700, 2009.

[114] W. Guo and E. Ruckenstein, "Crosslinked glass fiber affinity membrane chromatography and its application to fibronectin separation," *Journal of Chromatography B*, vol. 795, no. 1, pp. 61–72, 2003.

[115] L. Tzounis, M. Kirsten, F. Simon, E. Mäder, and M. Stamm, "The interphase microstructure and electrical properties of glass fibers covalently and non-covalently bonded with multiwall carbon nanotubes," *Carbon*, vol. 73, pp. 310–324, 2014.

[116] F. N. Mutua, P. Lin, J. K. Koech, and Y. Wang, "Surface modification of hollow glass microspheres," 2012.

[117] J. Baselga, A. Aznar, and J. Gonzalez, "Microstructural and wettability study of surface pretreated glass fibres," *Journal of Materials Processing Technology*, vol. 92, p. 93.

[118] K. Sever, Y. Seki, I. H. Tavman, G. Erkan, and V. Cecen, "The structure of γ-glycidoxypropyltrimethoxysilane on glass fiber surfaces: Characterization by ftir, sem, and contact angle measurements," *Polymer composites*, vol. 30, no. 5, pp. 550–558, 2009.

[119] M.-C. Brochier Salon and M. N. Belgacem, "Hydrolysis-condensation kinetics of different silane coupling agents," *Phosphorus, Sulfur, and Silicon*, vol. 186, no. 2, pp. 240–254, 2011.

[120] K. Sever, M. Sarikanat, Y. Seki, and I. H. Tavman, "Concentration effect of γ-glycidoxypropyltrimethoxysilane on the mechanical properties of glass fiber–epoxy composites," *Polymer composites*, vol. 30, no. 9, pp. 1251–1257, 2009.

[121] J. Iglesias, J. González-Benito, A. Aznar, J. Bravo, and J. Baselga, "Effect of glass fiber surface treatments on mechanical strength of epoxy based composite materials," *Journal of colloid and interface science*, vol. 250, no. 1, pp. 251–260, 2002.

[122] T. Kawaguchi and R. A. Pearson, "The effect of particle–matrix adhesion on the mechanical behavior of glass filled epoxies: Part 1. a study on yield behavior and cohesive strength," *Polymer*, vol. 44, no. 15, pp. 4229–4238, 2003.

[123] J. Thomason and D. Dwight, "The use of xps for characterisation of glass fibre coatings," *Composites Part A: Applied Science and Manufacturing*, vol. 30, no. 12, pp. 1401–1413, 1999.

[124] J. Thomason, "The interface region in glass fibre-reinforced epoxy resin composites: 3. characterization of fibre surface coatings and the interphase," *Composites*, vol. 26, no. 7, pp. 487–498, 1995.

[125] H. N. Petersen, Y. Kusano, P. Brøndsted, and K. Almdal, "Preliminary characterization of glass fiber sizing," in *Proc. 34th Risø Int. Symp. Mater. Sci*, vol. 34, pp. 333–340, Citeseer, 2013.

[126] E. Asenath Smith and W. Chen, "How to prevent the loss of surface functionality derived from aminosilanes," *Langmuir*, vol. 24, no. 21, pp. 12405–12409, 2008.

[127] M. Zhu, M. Z. Lerum, and W. Chen, "How to prepare reproducible, homogeneous, and hydrolytically stable aminosilane-derived layers on silica," *Langmuir*, vol. 28, no. 1, pp. 416–423, 2012.

[128] M. Yang, Y. Gao, H. Li, and A. Adronov, "Functionalization of multiwalled carbon nanotubes with polyamide 6 by anionic ring-opening polymerization," *Carbon*, vol. 45, no. 12, pp. 2327–2333, 2007.

[129] S. Mortazavian and A. Fatemi, "Effects of fiber orientation and anisotropy on tensile strength and elastic modulus of short fiber reinforced polymer composites," *Composites part B: engineering*, vol. 72, pp. 116–129, 2015.

[130] A. Güllü, A. Özdemir, and E. Özdemir, "Experimental investigation of the effect of glass fibres on the mechanical properties of polypropylene (pp) and polyamide 6 (pa6) plastics," *Materials & design*, vol. 27, no. 4, pp. 316–323, 2006.

[131] E. M. Silverman, "Effect of glass fiber length on the creep and impact resistance of reinforced thermoplastics," *Polymer composites*, vol. 8, no. 1, pp. 8–15, 1987.

[132] B. N. Nguyen, S. K. Bapanapalli, J. D. Holbery, M. T. Smith, V. Kunc, B. J. Frame, J. H. Phelps, and C. L. Tucker III, "Fiber length and orientation in long-fiber injection-molded thermoplastics—part i: Modeling of microstructure and elastic properties," *Journal of composite materials*, vol. 42, no. 10, pp. 1003–1029, 2008.

[133] W. Xu, J. Riikonen, T. Nissinen, M. Suvanto, K. Rilla, B. Li, Q. Wang, F. Deng, and V.-P. Lehto, "Amine surface modifications and fluorescent labeling of thermally stabilized mesoporous silicon nanoparticles," *The Journal of Physical Chemistry C*, vol. 116, no. 42, pp. 22307–22314, 2012.

[134] L. T. Zhuravlev, "Concentration of hydroxyl groups on the surface of amorphous silicas," *Langmuir*, vol. 3, pp. 316–318, May 1987.

[135] J. De Boer, M. Hermans, and J. Vleeskens, "The chemisorption and physical adsorption of water on silica," *Proceedings of the Koninklijke Academie van Wetenschappen. Series B, Physical Sciences*, vol. 60, pp. 45–53, 1957.

[136] J. B. Peri and A. L. Hensley, "The surface structure of silica gel," *The Journal of Physical Chemistry*, vol. 72, pp. 2926–2933, Aug. 1968.

[137] R. K. Iler, *The colloid chemistry of silica and silicates*, vol. 80.
LWW, 1955.

[138] J. Erkelens and B. Linsen, "Quantitative determination of hydroxyl groups and water for silica," *Journal of Colloid and Interface Science*, vol. 29, pp. 464–468, Mar. 1969.

[139] G. Wirzing, "Untersuchungen am System SiO 2/H 2 O im nahen Ultrarot," *Naturwissenschaften*, vol. 50, no. 13, pp. 466–469, 1963.

[140] A. A. Christy and P. K. Egeberg, "Quantitative determination of surface silanol groups in silicagel by deuterium exchange combined with infrared spectroscopy and chemometrics," *The Analyst*, vol. 130, no. 5, p. 738, 2005.

[141] C. G. Armistead, A. J. Tyler, F. H. Hambleton, S. A. Mitchell, and J. A. Hockey, "Surface hydroxylation of silica," *The Journal of Physical Chemistry*, vol. 73, pp. 3947–3953, Nov. 1969.

[142] J. J. Fripiat and J. Uytterhoeven, "HYDROXYL CONTENT IN SILICA GEL "AEROSIL"," *The Journal of Physical Chemistry*, vol. 66, pp. 800–805, May 1962.

[143] R. Gilpin, M. Gangoda, and M. Jaroniec, "Preparation and characterization of silica-carbon hybrids," *Carbon*, vol. 35, no. 1, pp. 133–139, 1997.

[144] V. M. Bermudez, "Proton nuclear magnetic resonance technique for determining the surface hydroxyl content of hydrated silica gel," *The Journal of Physical Chemistry*, vol. 74, pp. 4160–4161, Nov. 1970.

[145] G. E. Kellum and R. C. Smith, "Determination of water, silanol, and strained siloxane on silica surfaces," *Analytical Chemistry*, vol. 39, no. 3, pp. 341–345, 1967.

[146] R. Mueller, H. K. Kammler, K. Wegner, and S. E. Pratsinis, "Oh surface density of sio2 and tio2 by thermogravimetric analysis," *Langmuir*, vol. 19, no. 1, pp. 160–165, 2003.

[147] E. F. Vansant, P. Van Der Voort, and K. C. Vrancken, *Characterization and chemical modification of the silica surface*.
Elsevier, 1995.

[148] J. L. Thomason, U. Nagel, L. Yang, and D. Bryce, "A study of the thermal degradation of glass fibre sizings at composite processing temperatures," *Composites Part A: Applied Science and Manufacturing*, vol. 121, pp. 56–63, jun 2019.

[149] A. Labrosse and A. Burneau, "Characterization of porosity of ammonia catalysed alkoxysilane silica," *Journal of Non-Crystalline Solids*, vol. 221, pp. 107–124, Dec. 1997.

[150] A. Legrand, H. Hommel, A. Tuel, A. Vidal, H. Balard, E. Papirer, P. Levitz, M. Czernichowski, R. Erre, H. Van Damme, J. Gallas, J. Hemidy, J. Lavalley, O. Barres, A. Burneau, and Y. Grillet, "Hydroxyls of silica powders," *Advances in Colloid and Interface Science*, vol. 33, pp. 91–330, Oct. 1990.

[151] A. Perro, "Synthèse et valorisation de particules colloidales de morphologie et de fonctionnalité de surface controlées," 2006.

[152] M. Szekeres, I. Dékány, and A. De Keizer, "Adsorption of dodecyl pyridinium chloride on monodisperse porous silica," *Colloids and Surfaces A: Physicochemical and Engineering Aspects*, vol. 141, no. 3, pp. 327–336, 1998.

[153] M. Szekeres, J. Tóth, and I. Dékány, "Specific Surface Area of Stoeber Silica Determined by Various Experimental Methods," *Langmuir*, vol. 18, pp. 2678–2685, Apr. 2002.

[154] J. Wells, L. Koopal, and A. d. de Keizer, "Monodisperse, nonporous, spherical silica particles," *Colloids and Surfaces A: Physicochemical and Engineering Aspects*, vol. 166, no. 1-3, pp. 171–176, 2000.

[155] A. de Keizer, E. van der Ent, and L. Koopal, "Surface and volume charge densities of monodisperse porous silicas," *Colloids and Surfaces A: Physicochemical and Engineering Aspects*, vol. 142, pp. 303–313, Dec. 1998.

[156] E. P. Plueddemann, "Nature of adhesion through silane coupling agents," in *Silane coupling agents*, pp. 115–152, Springer, 1991.

[157] J. Park and R. Subramanian, "Interfacial shear strength and durability improvement by monomeric and polymeric silanes in basalt fiber/epoxy single-filament composite specimens," *Journal of adhesion science and technology*, vol. 5, no. 6, pp. 459–477, 1991.

[158] R. G. Acres, A. V. Ellis, J. Alvino, C. E. Lenahan, D. A. Khodakov, G. F. Metha, and G. G. Andersson, "Molecular structure of 3-aminopropyltriethoxysilane layers formed on silanol-terminated silicon surfaces," *The Journal of Physical Chemistry C*, vol. 116, no. 10, pp. 6289–6297, 2012.

[159] N. Rathor and S. Panda, "Aminosilane densities on nanotextured silicon," *Materials Science and Engineering: C*, vol. 29, no. 8, pp. 2340–2345, 2009.

[160] J. Zhao, Y. Li, H. Guo, and L. Gao, "Relative surface density and stability of the amines on the biochip," *Chinese Journal of Analytical Chemistry*, vol. 34, no. 9, pp. 1235–1238, 2006.

[161] T. S. Zemanian, G. E. Fryxell, J. Liu, S. Mattigod, J. A. Franz, and Z. Nie, "Deposition of self-assembled monolayers in mesoporous silica from supercritical fluids," *Langmuir*, vol. 17, no. 26, pp. 8172–8177, 2001.

[162] R. De Palma, S. Peeters, M. J. Van Bael, H. Van den Rul, K. Bonroy, W. Laureyn, J. Mullens, G. Borghs, and G. Maes, "Silane ligand exchange to make hydrophobic superparamagnetic nanoparticles water-dispersible," *Chemistry of Materials*, vol. 19, no. 7, pp. 1821–1831, 2007.

[163] X.-Y. Wang, D. Mertz, C. Blanco-Andujar, A. Bora, M. Ménard, F. Meyer, C. Giraudeau, and S. Bégin-Colin, "Optimizing the silanization of thermally-decomposed iron oxide nanoparticles for efficient aqueous phase transfer and mri applications," *RSC advances*, vol. 6, no. 96, pp. 93784–93793, 2016.

[164] J. G. Matisons, "Silanes and siloxanes as coupling agents to glass: a perspective," in *Silicone Surface Science*, pp. 281–298, Springer, 2012.

[165] E. P. Plueddemann, *Silane Coupling Agents*.
Boston, MA: Springer US, 1991.

[166] O. Wichterle, J. Králíček, *et al.*, "The anionic polymerization of caprolactam," in *Fortschritte Der Hochpolymeren-Forschung*, pp. 578–595, Springer, 1961.

[167] E. Schulz and B. Wunderlich, "Macromolecular physics, vol. 2 crystal nucleation, growth, annealing," *New York: Academic*, p. 50, 1976.

[168] R. Puffr and V. Kubanek, "Lactam-based polyamides," *Vol. II, CRC Press, Ann Arbor MI*, pp. 145–162, 1991.

[169] Z. Bukač, P. Čefelín, D. Doskočilová, and J. Šebenda, "Alkaline polymerization of 6-caprolactam. xviii. equilibrium between monomer and polymer," *Collection of Czechoslovak Chemical Communications*, vol. 29, no. 11, pp. 2615–2625, 1964.

[170] L. Ricco, S. Russo, G. Orefice, and F. Riva, "Anionic poly (ε-caprolactam): Relationships among conditions of synthesis, chain regularity, reticular order, and polymorphism," *Macromolecules*, vol. 32, no. 23, pp. 7726–7731, 1999.

[171] N. Zaldua, J. Maiz, A. de la Calle, S. García-Arrieta, C. Elizetxea, I. Harismendy, A. Tercjak, and A. J. Müller, "Nucleation and crystallization of pa6 composites prepared by t-rtm: Effects of carbon and glass fiber loading," *Polymers*, vol. 11, no. 10, p. 1680, 2019.

[172] H. Ishida, "Controlled interphases in glass fiber and particulate reinforced polymers: Structure of silane coupling agents in solutions and on substrates," in *The interfacial interactions in polymeric composites*, pp. 169–199, Springer, 1993.

[173] B. Ellis *et al.*, *Chemistry and technology of epoxy resins*.
Springer, 1993.

[174] C. A. May, "Introduction to epoxy resins," *Epoxy Resins Chemistry and Technology*, vol. 1, pp. 1–8, 1988.

[175] J. Fischer and H. Ritter, "Oligomeric epoxide–amine adducts based on 2-amino-n-isopropylacetamide and α-amino-ε-caprolactam: Solubility in presence of cyclodextrin and curing properties," *Beilstein journal of organic chemistry*, vol. 9, no. 1, pp. 2803–2811, 2013.

[176] K. H. Lee and S. C. Kim, "Reaction-induced crystallization kinetics during the anionic polymerization of ϵ-caprolactam," *Polymer Engineering & Science*, vol. 28, no. 1, pp. 13–19, 1988.

[177] D. Kleshchanok, R. Tuinier, and P. R. Lang, "Direct measurements of polymer-induced forces," *Journal of Physics: Condensed Matter*, vol. 20, no. 7, p. 073101, 2008.

[178] S. Adhikari and M. Muthukumar, "Theory of statistics of ties, loops, and tails in semicrystalline polymers," *The Journal of Chemical Physics*, vol. 151, no. 11, p. 114905, 2019.

[179] S. Balijepalli and G. Rutledge, "Conformational statistics of polymer chains in the interphase of semi-crystalline polymers," *Computational and Theoretical Polymer Science*, vol. 10, no. 1-2, pp. 103–113, 2000.

[180] B. P. Calabia, F. Ninomiya, H. Yagi, A. Oishi, K. Taguchi, M. Kunioka, and M. Funabashi, "Biodegradable poly (butylene succinate) composites reinforced by cotton fiber with silane coupling agent," *Polymers*, vol. 5, no. 1, pp. 128–141, 2013.

[181] J. GRENET and B. LEGENDRE, "Analyse calorimétrique différentielle à balayage (dsc)," 2010.

[182] L. Gunaratne and R. Shanks, "Multiple melting behaviour of poly (3-hydroxybutyrate-co-hydroxyvalerate) using step-scan dsc," *European Polymer Journal*, vol. 41, no. 12, pp. 2980–2988, 2005.

[183] N. Ning, S. Fu, W. Zhang, F. Chen, K. Wang, H. Deng, Q. Zhang, and Q. Fu, "Realizing the enhancement of interfacial interaction in semicrystalline polymer/filler composites via interfacial crystallization," *Progress in Polymer Science*, vol. 37, no. 10, pp. 1425–1455, 2012.

[184] Y. Kazemi, A. R. Kakroodi, L. H. Mark, T. Filleter, and C. B. Park, "Effects of polymer-filler interactions on controlling the conductive network formation in polyamide 6/multi-walled carbon nanotube composites," *Polymer*, vol. 178, p. 121684, 2019.

[185] U. A. Handge, K. Hedicke-Höchstötter, and V. Altstädt, "Composites of polyamide 6 and silicate nanotubes of the mineral halloysite: influence of molecular weight on thermal, mechanical and rheological properties," *Polymer*, vol. 51, no. 12, pp. 2690–2699, 2010.

[186] ASTM, "Standard test method fortensile properties of plastics d 638," *ASTM International*, 2014.

[187] B. Pan, K. Qian, H. Xie, and A. Asundi, "Two-dimensional digital image correlation for in-plane displacement and strain measurement: a review," *Measurement science and technology*, vol. 20, no. 6, p. 062001, 2009.

[188] M. Bornert, F. Brémand, P. Doumalin, J.-C. Dupré, M. Fazzini, M. Grédiac, F. Hild, S. Mistou, J. Molimard, J.-J. Orteu, *et al.*, "Assessment of digital image correlation measurement errors: methodology and results," *Experimental mechanics*, vol. 49, no. 3, pp. 353–370, 2009.

[189] H. Kim, K. Oh, and Y. Seo, "Rheological and mechanical properties of a novel polyamide 6 synthesized by anionic polymerization of ε-caprolactam in a twin-screw extruder," *Polymer*, vol. 177, pp. 196–201, 2019.

[190] A. Hendlmeier, Ž. Simon, A. Chutani, and L. C. Henderson, "Generating short carbon fiber polyamide-6 composites from continuous carbon fiber–a preliminary examination of surface treatment and sizing effects," *Composites Part A: Applied Science and Manufacturing*, vol. 138, p. 106058, 2020.

[191] M. Park, J.-u. Jang, J. H. Park, J. Yu, and S. Y. Kim, "Enhanced tensile properties of multi-walled carbon nanotubes filled polyamide 6 composites based on interface modification and reactive extrusion," *Polymers*, vol. 12, no. 5, p. 997, 2020.

[192] T. Liu, I. Y. Phang, L. Shen, S. Y. Chow, and W.-D. Zhang, "Morphology and mechanical properties of multiwalled carbon nanotubes reinforced nylon-6 composites," *Macromolecules*, vol. 37, no. 19, pp. 7214–7222, 2004.

[193] J. Feng, S. R. Venna, and D. P. Hopkinson, "Interactions at the interface of polymer matrix-filler particle composites," *Polymer*, vol. 103, pp. 189–195, 2016.

[194] C. Rotella, M. Wübbenhorst, and S. Napolitano, "Probing interfacial mobility profiles via the impact of nanoscopic confinement on the strength of the dynamic glass transition," *Soft Matter*, vol. 7, no. 11, pp. 5260–5266, 2011.

[195] N. Jiang, J. Shang, X. Di, M. K. Endoh, and T. Koga, "Formation mechanism of high-density, flattened polymer nanolayers adsorbed on planar solids," *Macromolecules*, vol. 47, no. 8, pp. 2682–2689, 2014.

[196] C. Chevigny, F. Dalmas, E. Di Cola, D. Gigmes, D. Bertin, F. Boué, and J. Jestin, "Polymer-grafted-nanoparticles nanocomposites: dispersion, grafted chain conformation, and rheological behavior," *Macromolecules*, vol. 44, no. 1, pp. 122–133, 2011.

[197] F. Bueche, "Molecular basis for the mullins effect," *Journal of Applied Polymer Science*, vol. 4, no. 10, pp. 107–114, 1960.

[198] F. Bueche, "Mullins effect and rubber–filler interaction," *Journal of applied polymer Science*, vol. 5, no. 15, pp. 271–281, 1961.

[199] E. Dannenberg, "The effects of surface chemical interactions on the properties of filler-reinforced rubbers," *Rubber Chemistry and Technology*, vol. 48, no. 3, pp. 410–444, 1975.

[200] F. Lange, "The interaction of a crack front with a second-phase dispersion," *Philosophical Magazine*, vol. 22, no. 179, pp. 0983–0992, 1970.

[201] F. Lange and K. Radford, "Fracture energy of an epoxy composite system," *Journal of Materials Science*, vol. 6, no. 9, pp. 1197–1203, 1971.

[202] A. Evans, "The strength of brittle materials containing second phase dispersions," *Philosophical Magazine*, vol. 26, no. 6, pp. 1327–1344, 1972.

[203] A. K. Khaund and P. S. Nicholson, "Fracture of a brittle composite: Influence of elastic mismatch and interfacial bonding," *Journal of Materials Science*, vol. 15, no. 1, pp. 177–187, 1980.

[204] J. Goodier, "Concentration of stress around spherical and cylindrical inclusions and flaws," 1933.

[205] J. Spanoudakis and R. Young, "Crack propagation in a glass particle-filled epoxy resin," *Journal of Materials Science*, vol. 19, no. 2, pp. 473–486, 1984.

[206] T. Kawaguchi and R. A. Pearson, "The effect of particle–matrix adhesion on the mechanical behavior of glass filled epoxies. part 2. a study on fracture toughness," *Polymer*, vol. 44, no. 15, pp. 4239–4247, 2003.

[207] M. Dekkers and D. Heikens, "Shear band formation in polycarbonate-glass bead composites," *Journal of materials science*, vol. 19, no. 10, pp. 3271–3275, 1984.

[208] J. Tirosh, E. Katz, G. Lifschuetz, and A. Tetelman, "The role of fibrous reinforcements well bonded or partially debonded on the transverse strength of composite materials," *Engineering Fracture Mechanics*, vol. 12, no. 2, pp. 267–277, 1979.

[209] J. Palierne, "Linear rheology of viscoelastic emulsions with interfacial tension," *Rheologica acta*, vol. 29, no. 3, pp. 204–214, 1990.

Controlling glass/matrix interfacial interactions applied to *in situ* anionic PA6 synthesis for composite manufacturing

In situ polymerization is a relevant option for manufacturing thermoplastic composites to overcome the difficulties associated with the high viscosity of their matrices. Therefore, liquid processes such as infusion or RTM, usually used for thermosetting resins, could be applied to thermoplastics. In the case of polyamide 6 (PA6) synthesized by Anionic Ring-Opening Polymerization (AROP), the system composed of monomers, catalyst and activator reacts in contact with the fibers. The surface chemistry is a crucial factor because it not only influences the polymerization and crystallization processes, but it also controls the fiber-matrix adhesion and thus the final properties of the composites.

This PhD thesis aims at tailoring the surface chemistry of glass reinforcements to control the interfacial interactions and promote the polymerization of PA6. Glass microparticles with representative size of fiber were chosen. First, it was shown that the hydroxyl groups density on the glass surface affects the polymerization kinetics of PA6. A methodology was developed to carefully control this -OH groups density during the complete surface modification sequence. Then, the particles were treated with various silanes to create different types of interactions. A new route consisting in grafting the monomer onto the glass was proposed. Combining the results of the surface characterization and the properties of the composites, we conclude on the effect of the surface treatment on the polymerization and crystallization of PA6. A manufacturing process was developed to upscale specimen preparation. Finally, the mechanical characterization of the composites highlighted the dominating interfacial phenomena. The optimum grafting and surface treatment type were determined from the resulting macroscopic properties.

Keywords : Composite materials, Glass reinforcements, Reactive polyamide 6, Hydroxyl groups, Silane coupling agent, Interface

---

Contrôle des interactions interfaciales verre/matrice appliqué à la synthèse *in situ* du PA6 anionique pour la fabrication des composites

La polymérisation *in situ* est une option pertinente pour la fabrication de composites thermoplastiques pour contourner les difficultés engendrées par la forte viscosité de leurs matrices. Ainsi, les procédés liquides de type infusion ou RTM utilisés habituellement pour les résines thermodurcissables pourraient être appliqués aux thermoplastiques. Dans le cas du polyamide 6 (PA6) synthétisé par polymérisation anionique par ouverture de cycle, le système composé de monomères, de catalyseur et d'activateur réagit au contact des fibres. La chimie de surface des renforts est un paramètre crucial car elle influence non seulement les processus de polymérisation et de cristallisation, mais elle contrôle également l'adhésion fibre-matrice et donc les propriétés finales des composites.

Cette thèse vise à adapter la chimie de surface du verre afin de maîtriser les interactions à l'interface renfort/matrice pour favoriser la polymérisation du PA6. Des microparticules de verre de taille représentative des renforts fibreux ont été choisies. Tout d'abord, il a été montré que la densité des groupes hydroxyles présents à la surface du verre influence la cinétique de polymérisation et de cristallisation du PA6. Une méthodologie a été développée pour contrôler précisément cette densité des groupes -OH tout au long du processus de modification de surface. Ensuite, les particules ont été traitées avec des agents silanes pour créer différents types d'interactions. Une nouvelle approche qui consiste à greffer le monomère sur le verre a été développée. Les résultats de la synthèse *in situ*, combinés à la caractérisation de surface des particules, ont permis de déterminer l'effet des traitements sur la polymérisation et la cristallisation du PA6. Un procédé de fabrication a été mis au point pour élaborer des éprouvettes composites. Enfin, la caractérisation mécanique a mis en évidence les phénomènes aux interfaces, permettant ainsi de mesurer l'influence du greffage et du type de traitement de surface sur les propriétés macroscopiques.

Mots clés : Matériaux composites, Renforts verre, Polyamide 6 réactif, Groupes hydroxyles, Agent de couplage silane, Interface